PhD THESIS CARRIED OUT AT:

Università degli Studi di Torino

Department of Drug Science and Technology

PhD program in Pharmaceutical and Biomolecular Sciences

PhD CYCLE:

XXXVI

TITLE:

"ICOS-Fc, an innovative immune modulator suggested as a new pharmacological strategy in a wide range of pathologies"

THESIS PRESENTED BY:

Chiara Monge

TUTOR: Dr. Chiara Dianzani

PHD COORDINATOR: Prof. Roberta Cavalli

SCIENTIFIC FIELD: Pharmacology

ACADEMIC PERIOD:

2020-2023

"ICOS-Fc, an innovative immune modulator suggested as a new pharmacological strategy in a wide range of pathologies"

CHIARA MONGE

Department of Drug Science and Technology (Turin, Italy)

ABSTRACT

Inducible T-cell costimulator (ICOS) upon binding to its ligand (ICOSL), which was found widely cells expressed, can mediate several immune responses and trigger bidirectional signals on ICOSL expressing cells leading to ICOS/ICOSL targeting in many different pharmacological fields.

The aim of this study was to investigate the therapeutic potentialities of ICOS-Fc, a recombinant form of ICOS, studying its effect upon ICOS/ICOSL system triggering in settings different from the immune system.

Promising results showed that ICOSL has a central role in **tissue repair**. Since it is able to trigger ICOSL, ICOS-Fc showed itself able to improves cutaneous wound healing by increasing angiogenesis, enhancing fibroblasts and reparative macrophages recruitment.

Despite ICOS/ICOSL system has been poorly investigated in **sepsis** context, surprising ICOS-Fc effect emerged on the complex interplay of hyperinflammation and immunosuppression host response developing in septic patients. ICOS-Fc treatment showed to be able to significantly ameliorate the clinical sepsis context and, moreover, the plasma level of ALT, AST, creatinine and urea reported how ICOS-Fc treatment was able to protect from liver and renal injury or dysfunction sepsis caused.

Choosing ICOS/ICOSL pathway as a pharmacological target for antitumor therapies hold a great promise for **cancer therapy** as well. In this regard, ICOSL triggering by ICOS-Fc hampered adhesiveness and migration of dendritic, endothelial, and tumor cells *in vitro* and metastatic dissemination *in vivo*. On the other side, the inhibition of tumor growth was reached only when ICOS-Fc was encapsulated into **nanodelivery system**. All these previous findings were confirmed also in **myeloma multiple** context. Indeed, ICOS-Fc was able to inhibit migratory property of MM cell line expressing high level of ICOSL. Furthermore, when ICOS-Fc was loaded into PLGA, it significantly counteracted tumor growth in MM subcutaneous *in vivo* model.

In addition, the ICOS-Fc antitumor effects were studied more in depth considering the involvement of OPN, another important player in the ICOS/ICOSL axis. Intriguingly, the **OPN or ICOS** different interactions exert opposite ICOSL triggering effects: OPN support metastasis and angiogenesis,

which is dominantly inhibited by ICOS. The *in vitro* migration assay and the *in vivo* evaluation of **melanoma lung metastasis** spreading were performed comparing the metastasizing capability of lower or higher ICOSL expressing melanoma cells. The results confirmed that melanoma cell migration induced by OPN is strictly correlated to ICOSL expression, while ICOS-Fc was significantly able to inhibit it.

The promising ICOS-Fc antitumor effect observed supported its potential application in **combined cancer therapies** and highlighted nanotechnology strategy as a precious tool to improve its therapeutic efficacy. Important findings are here reported regarding the involvement of ICOS-Fc in an innovative drugs combination with SOR and TMZ co-loaded in injectable nanoemulsions for total parental nutrition (Intralipid© – IL) or in β-cyclodextrin based nanosponges (NS) loaded with GEM (NS[GEM+ICOS-Fc]). They were used to optimize melanoma or pancreatic cancer therapy respectively. In both case the results collected highlighted the important ICOS-Fc contribution. For the IL-polychemotherapy proposed, it consisted of an immunostimulatory and antiangiogenic activity with an optimally synergic effect with the other drugs loaded in the nanodelivery system. Compared to free drugs administration, the IL-loading drugs MIX showed an increased inhibition on melanoma cell invasion *in vitro* and significant tumor growth inhibition *in vivo*.

In pancreatic cancer scenario, ICOS-Fc involvement in a combination therapy depicted a promising strategy to overcome pancreatic cancer drug resistance, as a suitable alternative to only GEM standard treatment. The GEM loading into NS functionalized with ICOS-Fc enhanced its cancer cells viability and proliferation inhibition in both 2D and 3D model, depicting a more efficient internalization of the system proposed compared to GEM administered in free form. The migration experiments in both **static** and **dynamic** condition highlighted a significant NS[GEM+ICOS-Fc] anti-invasion effect. These results gained even more weight for GEM resistant cells on with GEM in free form was even able to **induce** cell migration and metastatization. Furthermore, the synergist effect, resulted from the ICOS-Fc anti-invasion with the GEM antiproliferative one, was highly supported by the results collected by the MIVO dynamic migration assay performed. Indeed, it suggested the β-cyclodextrin-NS loaded with ICOS-Fc as a valid strategy that might improve the GEM efficacy in pancreatic cancer treatment.

All these promising findings supported the wide ICOS-Fc pharmacological potentialities and how ICOS/COSL axis represents an important therapeutic target in different pathological scenarios.

LIST OF PUBBLICATIONS

This thesis is based on the work contained in the following published articles:

I. Stoppa, I., Gigliotti, C. L., Clemente, N., Pantham, D., Dianzani, C., **Monge, C.**, Puricelli, C., Rolla, R., Sutti, S., Renò, F., Boldorini, R., Boggio, E., & Dianzani, U. (2022). ICOSL Stimulation by ICOS-Fc Accelerates Cutaneous Wound Healing In Vivo. International Journal of Molecular Sciences, 23(13). https://doi.org/10.3390/ijms23137363

II. Alves, G. F., Stoppa, I., Aimaretti, E., **Monge, C.**, Mastrocola, R., Porchietto, E., Einaudi, G., Collotta, D., Bertocchi, I., Boggio, E., Gigliotti, C. L., Clemente, N., Aragno, M., Fernandes, D., Cifani, C., Thiemermann, C., Dianzani, C., Dianzani, U., & Collino, M. (2022). ICOS-Fc as innovative immunomodulatory approach to counteract inflammation and organ injury in sepsis. Frontiers in Immunology, 13. https://doi.org/10.3389/fimmu.2022.992614

III. Raineri, D., Cappellano, G., Vilardo, B., Maione, F., Clemente, N., Canciani, E., Boggio, E., Gigliotti, C. L., **Monge, C.**, Dianzani, C., Boldorini, R., Dianzani, U., & Chiocchetti, A. (2022). Inducible t-cell costimulator ligand plays a dual role in melanoma metastasis upon binding to osteopontin or inducible t-cell costimulator. Biomedicines, 10(1). https://doi.org/10.3390/biomedicines10010051

IV. Boggio, E., Gigliotti, C. L., Moia, R., Scotta, A., Crespi, I., Boggione, P., De Paoli, L., Deambrogi, C., Garzaro, M., Vidali, M., Chiocchetti, A., Stoppa, I., Rolla, R., Dianzani, C., **Monge, C.**, Clemente, N., Gaidano, G., & Dianzani, U. (2022). Inducible T-cell co-stimulator (ICOS) and ICOS ligand are novel players in the multiple-myeloma microenvironment. British Journal of Haematology, 196(6), 1369–1380. https://doi.org/10.1111/bjh.17968

V. **Monge, C.**, Stoppa, I., Ferraris, C., Bozza, A., Battaglia, L., Cangemi, L., Miglio, G., Pizzimenti, S., Clemente, N., Gigliotti, C. L., Boggio, E., Dianzani, U., & Dianzani, C. (2022). Parenteral Nanoemulsions Loaded with Combined Immuno- and Chemo-Therapy for Melanoma Treatment. Nanomaterials, 12(23). https://doi.org/10.3390/nano12234233

Published articles not included in the thesis:

• Gigliotti CL, Dianzani C, Stoppa I, **Monge C**, Sutti S, Sblattero D, Puricelli C, Rolla R, Dianzani U, Boggio E. Differential Modulation of Human M1 and M2 Macrophage Activity by ICOS-Mediated ICOSL Triggering. Int J Mol Sci. 2023 Feb 2;24(3):2953. doi: 10.3390/ijms24032953. PMID: 36769276; PMCID: PMC9917690

- Dianzani, C., **Monge, C.**, Miglio, G., Serpe, L., Martina, K., Cangemi, L., Ferraris, C., Mioletti, S., Osella, S., Gigliotti, C. L., Boggio, E., Clemente, N., Dianzani, U., & Battaglia, L. (2020). Nanoemulsions as delivery systems for poly-chemotherapy aiming at melanoma treatment. Cancers, 12(5). https://doi.org/10.3390/cancers12051198

- Boggio, E., Gigliotti, C. L., Stoppa, I., Pantham, D., Sacchetti, S., Rolla, R., Grattarola, M., **Monge, C.**, Pizzimenti, S., Dianzani, U., Dianzani, C., & Battaglia, L. (2023). Exploiting Nanomedicine for Cancer Polychemotherapy: Recent Advances and Clinical Applications. In Pharmaceutics (Vol. 15, Issue 3). MDPI. https://doi.org/10.3390/pharmaceutics15030937

- Cucci, M. A., Grattarola, M., **Monge, C.**, Roetto, A., Barrera, G., Caputo, E., Dianzani, C., & Pizzimenti, S. (2023). Nrf2 as a Therapeutic Target in the Resistance to Targeted Therapies in Melanoma. *Antioxidants*, *12*(6). https://doi.org/10.3390/antiox12061313

- Pizzimenti, S., Ribero, S., Cucci, M. A., Grattarola, M., **Monge, C.**, Dianzani, C., Barrera, G., & Muzio, G. (2021). Oxidative stress-related mechanisms in melanoma and in the acquired resistance to targeted therapies. In *Antioxidants* (Vol. 10, Issue 12). MDPI. https://doi.org/10.3390/antiox10121942

- Azzimonti, B., Ballacchino, C., Zanetta, P., Cucci, M. A., **Monge, C.**, Grattarola, M., Dianzani, C., Barrera, G., & Pizzimenti, S. (2023). Microbiota, Oxidative Stress, and Skin Cancer: An Unexpected Triangle. In Antioxidants (Vol. 12, Issue 3). MDPI. https://doi.org/10.3390/antiox12030546

- Ficiarà, E., Ansari, S. A., Argenziano, M., Cangemi, L., **Monge, C.**, Cavalli, R., & D'Agata, F. (2020). Beyond Oncological Hyperthermia: Physically Drivable Magnetic Nanobubbles as Novel Multipurpose Theranostic Carriers in the Central Nervous System. Molecules (Basel, Switzerland), 25(2104), 1–11. https://doi.org/10.3390/molecules25092104

- Bordano, V., Kinsella, G. K., Cannito, S., Dianzani, C., Gigliotti, C. L., Stephens, J. C., **Monge, C.**, Bocca, C., Rosa, A. C., Miglio, G., Dianzani, U., Findlay, J. B. C., & Benetti, E. (2022). G protein–coupled receptor 21 in macrophages: An in vitro study. European Journal of Pharmacology, 926. https://doi.org/10.1016/j.ejphar.2022.175018

ABBREVIATIONS

AML: acute myeloid leukemia

AML-MRC: AML with myelodysplasia-related changes

APCs: antigen presenting cells

B2M: β2-microglobulin

BBB: blood brain barrier

BCBM: breast cancer brain metastasis

BCRP: breast cancer resistance protein

BM: bone marrow

BRAFi: BRAF inhibitors

BTB: blood-brain tumor barrier

BVZ: bevacizumab

CDNS: β-cyclodextrin nanosponges

CIT: chemo-immunotherapy

CLP: cecal ligation and puncture surgery

CNS: central nervous system

CRC: colon rectal cancer

CTLA-4: Cytotoxic T-Lymphocyte Associated Protein 4

CVID: common variable immunodeficiency

DCs: Dendritic cells (immature iDCs; mature mDCs)

DLS: dynamic light scattering

ECs: Vascular Endothelial cells

ECM: extracellular matrix

EMT: epithelial-to-mesenchymal-transition

EPR: enhanced permeability and retention effect

ERK: extracellular signal-regulated kinase

FA: folate acid

FAK: focal adhesion kinase

5-FU: 5-fluorouracile

Frα: FA binding proteins

GEM: gemcitabine

GEMMs genetically engineered mouse models

Hb: haemoglobin

hCNT1: human concentrative nucleoside transporter 1

KO: knockout

ICI: immune checkpoint inhibitor

IDP intrinsically disordered protein

Ig: immunoglobulin

IL: intralipid

LPS: lipopolysaccharides

MDCSs: myeloid-derived suppressor cells

MDOCs: human monocyte-derived OC-like cells

MDR: multidrugresistance

MEK: mitogen-activated protein kinase

MEKi: MEK inhibitors

MFI-R: mean fluorescence intensity ratio

MGUS: monoclonal gammopathy of undetermined significance

MHC: major histocompatibility complex

MM: Myeloma Multiple

MMP: matrix metalloproteinases

MPO: Myeloperoxidase

MRP1: multidrugresistance associated protein

mTOR inhibitor: mammalian target of rapamycin inhibitor

NK: natural killer cells

NPs: nanoparticles

Nrf2: nuclear factor erythroid 2-related factor 2

NSCLC: Non-small-cell lung cancer

NSG: NOD-SCID-IL2R null mice

OBs: osteoblasts

OCs: osteoclasts

OPN: osteopontin

OS: overall survival

PARP: poly (ADP-ribose) polymerase

PCs: plasma cells

PD1: Programmed Cell Death 1

PDAC: pancreatic ductal adenocarcinoma

PDI: polydispersity index

PEG: polyethylene glycol

PFS: progression-free-survival

P-gp: P-glycoprotein

PLA: Proximity Ligation Assay

PLGA: poly lactic-co-glycolic acid nanoparticles

PMN: polymorphonuclear cells

pSS: Primary Sjögren's syndrome

QUR: quercetin

RA: Rheumatoid arthritis

RANK: receptor activator of NF-kB

RANKL: receptor activator of NF-kB ligand

RAP: rapamycin

SLE: Systemic Lupus Erythematosus

SMM: smouldering multiple myeloma

sICOS: soluble ICOS

sICOSL: soluble ICOSL

SLNs: solid lipid nanoparticles

SOR: sorafenib

sRANKL: soluble RANKL

t-AML: therapy-related AML

T1D: type 1 diabetes

TCR: T cell receptor

T_{fh} :T follicular helper cells

$T_{reg:}$ T regulatory cells

TMD: tumor micro-vessel density

TME: tumor microenviroment

TMZ: temozolamide

TNBC: triple negative breast cancer

VEGF: vascular endothelial growth factor

WT: wild type

YAP: yes-associated protein 1

INDEX

1. AIM

My thesis aim was to investigate the therapeutic potentialities of ICOS-Fc, studying its effect through ICOS/ICOSL system triggering in cells not belonging to immune system.

The specific objectives were:

1) Studying ICOS-Fc as a novel player in ICOSL triggering promising pharmacological applications, such as tissue repair, in sepsis and cancer contexts

2) Studying ICOS-Fc different nanoformulations as novel strategies in immune combination cancer therapy

The experiments, whose data are here reported, were performed in the laboratory of Pharmacology in the Department of Drug Science and Technology (University of Turin, Italy), in the laboratory of Immunology in the Department of Health Science (University of Novara, Italy) and in the laboratory of Pathology in the Department of Clinical and Biological Sciences (University of Turin, Italy).

The project I worked on was in collaboration with different research groups, such as those of Prof. Umberto Dianzani (Department of Health Science - University of Novara), Prof. Stefania Pizzimenti (Department of Clinical and Biological Sciences - University of Turin), Prof. Roberta Cavalli (Department of Drug Science and Technology - University of Turin), Prof. Luigi Battaglia (Department of Drug Science and Technology - University of Turin) and Prof. Caterina Guiot (Department of Neurosciences "Rita Levi Montalcini" – University of Turin).

2. BACKGROUND

2.1 ICOS

ICOS is an inducible T-cell co-stimulator receptor, originally discovered in 1999 on the surface of T cells upon T-cell receptor (TCR) stimulation. It is a homodimeric protein, of a molecular weight of 55~60 kD approximately and third member of the CD28 family, next to CD28 and CTLA-4. If CD28 role is enhancing T-cell functions essential for an effective antigen-specific immune response, on the other side a counterbalance, essential to prevent an overstimulation of the lymphoid system, is due to the homologous CTLA-4 mediated signals (Brown, 2012; Liu Jie et al., 2014; Boggio et al., 2016). It has been found involved in several diseases including atherosclerosis, chronic inflammatory diseases, and several autoimmune diseases (Hutloff et al., 1999).

In this regard, CD28 and ICOS share many similarities in structure and function. Indeed, they act likewise during expansion, survival and differentiation of T-cells and they are both necessary for proper IgG responses (van Berkel & Oosterwegel, 2006). The major difference is shown by the fact that ICOS cannot be constitutively expressed on resting T-cells (Li & Xiong, 2020). However, it shares with CD28 the capacity to induce, when highly expressed on activated T-cells, similar amount of cytokines, such as IFNγ, TNFα (Th1) and IL-4, IL-10, IL-5, IL-13 (Th2) and IL-17 (Th17) responsible for T-cell differentiation (Hutloff et al., 1999; Park et al., 2005). Several investigations reported its expression on Th1, Th2, Th17, T follicular helper (Tfh) cells, T follicular regulatory (Tfr) cells, Tregs, type 1 regulatory T (Tr1) cells, and innate lymphoid cells (ILCs) (D. Y. Li & Xiong, 2020b). Its wide distribution on T-cells population highlighted its relevant role in immune responses. Indeed, once triggered, it regulates T-cell activation in lymphoid organs and T-cell function at inflammation sites by supporting the differentiation of regulatory T-cells (Treg) and type 17 T helper cells (Th17). Moreover, it modulates Tfh cells function and CD8+ cell-mediated response to tumors and intracytoplasmic pathogens (Clemente et al., 2020).

ICOS has a unique ligand, ICOSL (also named B7RP-1, B7h, B7-H2, B7-like protein GI50, GL50, KIAA0653, LICOS or CD275), which was firstly detected on a small subset of T-cells, accounting 5% of CD3+ T cells and discovered being expressed on the surface of multiple cells types, such as antigen presenting cells (APCs), B cells, dendritic cells (DCs), macrophages and other cell types from non-lymphoid tissue, including fibroblasts, vascular endothelial cells (ECs) and epithelial cells (Yoshinaga Steven K. et al., 1999; Sharpe & Freeman, 2002; Greenwald et al., 2005).

2.2 ICOS/ICOSL pathway

Considering ICOSL widely distribution, it could be easily explained why ICOS/ICOSL pathway was found involved in mediating several immune responses (Nurieva, 2005; Dianzani et al., 2010) and how much anti-ICOS/ICOSL monoclonal antibodies could show an excellent potential in several clinical applications (D. Y. Li & Xiong, 2020a).

Co-stimulatory pathways were studied as a natural target for immunotherapy in autoimmune diseases. It has been well documented the strict relationship between an increased expression of ICOS bearing Tfh cells and several autoimmune disorders. ICOS ligation induces the expression of numerous cytokines, including IL-21, which is critically required for the Tfh cells formation and function (Gigoux et al., 2009). The abnormal humoral responses caused by ICOS-induced over-release of IL-21 is what detected in Systemic Lupus Erythematosus (SLE) and others autoimmune conditions (Edner et al., 2020). The SLE is a chronic autoimmune disease characterized by multiorgan damage and life-threatening consequences caused by altered production of inflammatory cytokines and autoantibodies. Antagomir-21, niclosamide and prezalumab are examples of potential immunomodulation drugs able to act on Tfh cell-mediated autoimmune response, thus recently proposed as novel pharmacological strategies for SLE treatment (O'Dwyer et al., 2018; Jang et al., 2021; Gao et al., 2022).

Increased ICOS expression has been identify responsible of the pathological synovial inflammation, hyperplasia, and cartilage destruction in multiple joints of patients affected by rheumatoid arthritis (RA) (Lu et al., 2021; Weyand & Goronzy, 2021). The growing understanding of ICOSL biology promoted its use also in RA as a viable therapeutic target next to the commonly used TNFα antagonist therapy. Clear evidence of that is shown by the interesting findings of Ronan O'Dwyer research group, who proved the efficacy of anti-mouse ICOSL domains in a collagen-induced mouse model of RA (O'Dwyer et al., 2018).

Immunotherapy was widely investigated as a potential treatment option for type 1 diabetes (T1D), considered as suitable strategy to forestall or reverse the destruction of β-cells through immune system manipulation. A long time of research was focused on studying the T-cell differentiation involvement in the development of autoimmunity in T1D. The findings highlighted an elevated expression of archetypal Tfh molecules, including CXCR5, IL-21, PD-1, ICOS, and BCL6 in memory T-cells of T1D patients (Kenefeck et al., 2015), which were carefully taken into account as potential pharmacological target (Singh Akash et al., 2023).

Targeting costimulatory molecule was deeply studied also in Primary Sjögren's syndrome (pSS), a systemic autoimmune disease characterized by a lowered salivary secretion, due to an abnormal activation of T and B cells, next to the periductal lymph cells infiltration in the lacrimal and salivary gland tissues (Manoussakis & Moutsopoulos, 2000). The work by Ping Li et al (P. Li et al., 2022) showed how the salivary weight was negatively correlated with the expression of ICOS in patients with pSS. Next to its potential use as pharmacological target, it has been suggested also as an alternative candidate for pSS diagnosis.

On the other side, an ICOS deficiency has been associated with a severe reduction in circulating memory T helper cells, which results in a progressive loss of B cell repertoire and an increased rate of variable immunodeficiency scenario (Grimbacher et al., 2003; Salzer et al., 2004; Bossaller et al., 2006; Warnatz et al., 2006; Yong et al., 2009). The importance of T-cell costimulatory molecules in host defense is highlighted much more when ICOS deficiency promote defective Th1, Th2, and Th17 T-cell cytokine production and/or impaired activation of macrophages, which express ICOS ligand, occurs and is responsible to contribute opportunistic infections. Human ICOS mutations were found involved in antibody deficiency contexts, such as those described in common variable immunodeficiency (CVID). CVID patients are predisposed to recurrent bacterial infections of the respiratory and gastrointestinal tract, due to their markedly reduced serum levels for IgG and IgA or IgM, an impaired ability to specific antibody production after vaccination or exposure, and exclusion of secondary causes for antibody deficiency (Salzer et al., 2004; Warnatz et al., 2006). Indeed, the current therapy preventing most CVID-predisposed infections is the regular administration of Ig (Remiker et al., 2023). However, all findings confirming the critical role of ICOS/ICOSL interaction in germinal center formation, antibody production and B-cell survival encouraged the research for more genetic defects in CVID, both upstream and downstream of the ICOS/ICOSL pathway and beyond (Yong et al., 2009).

2.3 ICOS/ICOSL bidirectional signal

ICOS/ICOSL axis can elicit a bidirectional signal, acting on ICOSL-expressing cells (Mak et al., 2003; Tang et al., 2009).

For instance, it was found playing an important role in the development and biological functions of dendritic cells (DCs). This are the only type of APCs that can transfer information from the outside world to the cells of the adaptive immune system. They play a crucial role not only for inducing

primary immune responses, but also for relevant involvement in immunological tolerance (Banchereau et al., 2000). Indeed, they were found responsible of regulating the type of T cell–mediated immune response, such as the sensitization of MHC-restricted T-cells, the rejection of organ transplants, and the formation of T-dependent antibodies and cytokines release (Banchereau et al., 2000; Tang et al., 2009; Occhipinti et al., 2013).

In this regard, reverse signaling mediated by B7h has been studied as strategy to modulate DCs function with effects on their maturation, adhesiveness and migratory ability, and their recruitment into tissues (Occhipinti et al., 2013).

More recently, ICOS/B7h interaction has been detected in important modulation of OCs functions, which, similarly to DCs, are cells deriving from the monocyte lineage (Boggio et al., 2021). OCs are giant cells formed by cell-cell fusion of monocyte-macrophage precursors playing a crucial role in bone metabolism, acting next to osteoblasts (OBs) and osteocytes. The OCs function and its pathological increased activity was deeply investigated in pathological bone metabolism conditions, such as osteoporosis and RA bone pathologies, and the osteolytic bone metastasis of solid cancers (Myeloma Multiple - MM). As ICOSL expressing cells, OCs were found to be potentially driven by ICOS/ICOSL bidirectional signals, highlighting how much the immune system results involved in the complex bone remodeling process (Gigliotti et al., 2016).

Moreover, recent findings showed how ICOSL expression levels on tumor infiltrating T-cells were correlated with patient survival (Zhang et al., 2016). In addition, both ECs and several kinds of tumor cells lines were found expressing ICOSL and interestingly involved in the ICOS/ICOSL reverse signaling of cancer development. The complex interplay between the tumor and the microenvironment supports cancer progression promoting cancer cells growth, angiogenesis, invasion and dissemination (Weis & Cheresh, 2011; Dianzani et al., 2014). In particular, a successful cancer metastasis spreading appears when tumor cells can invade the extracellular matrix and intravasate taking root into healthy tissues. This is the most dangerous cancer skill, responsible of depicting higher rate of tumor aggressiveness and poor therapy outcomes. In the cells movements across the tissues both ECs, correlated to inflammatory and immune responses leukocyte recruitment into tissues, and tumor cells assume a crucial role.

Studies of ICOS/ICOSL interaction in cancer immune response opened a new field in the pharmacological use of ICOSL as a potential target in antineoplastic therapy as well.

3. ICOS-Fc

In the extensive search of interactors of ICOS/ICOSL system as immunomodulatory drugs, ICOS-Fc stood out with its several promising pharmacological applications. It is a recombinant protein consisting of Fc portion of IgG1 and two molecules of the extracellular portions of ICOS, whose was found able to modulate the function of several human cell types acting on ICOS/ICOSL axis.

In vitro ICOS-Fc showed itself able to modulate human monocyte-derived DCs functions. Occhipinti et al. (2013) demonstrated that ICOS-Fc is capable to substantially block ICOS/ICOSL interaction, resulting in counteracting the adhesion of both iDCs and mDCs (immature and mature respectively) to vascular and lymphoid ECs and their spontaneous and chemokine-driven migration. Dramatically increased migration of DC, due to higher motility and responsiveness to lymph tropic chemoattractant, occurs during infection and inflammation scenarios (Banchereau et al., 2000). In this regard, the inhibition of iDCs migration was found as a relevant ICOS-Fc effect, essential for arresting these cells in the inflamed tissues and in the secondary lymphoid tissues, where they can support the differentiation of Th17 cells and highly inflammatory cytokine release (Occhipinti et al., 2013).

How it has been mentioned, ICOSL has been detected also on OCs (Boggio et al., 2021) and recent findings depicted ICOS-Fc potential pharmacological application in some bone pathologies. The immune system was found involved in the complex bone remodeling process, since it showed itself able to regulate OCs and OBs cells functions through cytokine activity and surface receptors. Several inflammatory cytokines, such as TNFα, IL-1, IL-6 and M-CSF were found able to upregulate the expression of the receptor activator of NF-kB (RANK) ligand (RANKL) and inducing OCs activity. In addition, Th cells were found having a crucial role in the immune control of bone formation. In particular, Th17 cells express high level of RANKL and secrete IL-17, which induces the expression of RANKL and recruitment of inflammatory cytokines. These are some of the key players responsible of the progressive bone loss showed in osteoporosis and RA pathologies and the osteolytic metastasis of MM cancer scenario. Interesting findings showed its capability to inhibit the osteolytic activity of human monocyte-derived OC-like cells (MDOCs) *in vitro*, detected by decreased expression of TRAP, OSCAR, DC-STAMP and NFATc1 in cells ICOS-Fc treated. These data were supported by *in vivo* results showing that treatment with ICOS-Fc strikingly inhibits the systemic bone reabsorption in ovariectomized or soluble RANKL-treated mice. These findings suggested a novel field in the pharmacological use of agonist and antagonist of the ICOS/ICOSL system (Gigliotti et al., 2016).

In addition, ICOS-Fc was proposed as a novel immunomodulatory drug capable to play a large role in the immune inflammatory response and cancer metastasis dissemination as well. Dianzani et al. (2010) demonstrated that ICOS-Fc can significantly counteract the adhesion of ECs to both several tumor cell lines and polymorphonuclear cells (PMNs) (Dianzani et al., 2010). Among the several molecules expressed by ECs and which are involved in T-cell activation, ICOSL is expressed at low level and upregulated upon activation (Khayyamian et al., 2002). The ECs-T cells interaction has been involved in activation of the memory adaptive immune response, graft rejection and even recruitment of Ag-specific effector T-cells in sites of infection.

The promising effect of ICOS-Fc highlighted how ICOSL triggering in ECs is involved in immune and inflammatory response. Upon ICOSL triggering and during their extravasation into inflamed tissue, ICOS+ T-cells may modulate ECs adhesiveness. For instance, the inhibition of PMN adhesiveness switches this interaction on one side promoting an acute-type inflammation driven by PMNs and macrophages, on the other side a chronic-type inflammation driven by lymphocytes and macrophage (Dianzani et al., 2010).

First evidence showing ICOS-Fc potential application against cancer spreading came out by ICOS-Fc *in vitro* activity demonstrated on E-selectin signaling. ICOS-Fc was found able to inhibit ERK and p38 axis activation. Those are key player, induced in ECs trough proadhesive stimuli, responsible of enhancing endothelial permeability and enabling transedothelial migration of cancer cells. Thus, ICOS-Fc showed how ICOSL triggering could result in antiadhesive effects, due to an interference with ERK and p38 signaling pathway (Dianzani et al., 2010).

Subsequently, additional research contributed to describe more ICOS-Fc antitumor effects, supporting its use in novel immunocancer therapies. Striking results showed that ICOS-Fc was capable to inhibit epithelial-to-mesenchymal-transition (EMT) and migration *in vitro*, as well as metastasis *in vivo*. As it is well known EMT is promoted by cancer cells in order to acquire invasive and metastatic proprieties, several reports showed its involvement with epithelial cells disruption of intercellular contacts, induction of cell motility, survival and proliferation ("invasive growth") (Son & Moon, 2010). ICOS-Fc showed itself able to strongly counteract the HGF-induced migration, by preserving the cell epithelial morphology and protecting them from cells scatter HGF-induced (Dianzani et al., 2014).

The ICOS-Fc antimetastatic effect was supported by *in vivo* experiments: mice treated with ICOS-Fc showed lowered lung metastasis formation whether injected with a human (CFPAC-1 Luc) or a

mouse (B16-F10) tumor cell line. This suggested that the effect was ascribable to ICOSL triggering on both kind of tumor cells, as well as ECs (Dianzani et al., 2014).

Moreover, in ECs and tumor cells ICOSL^{high}, ICOSL triggering by ICOS-Fc inhibits the phosphorylation of focal adhesion kinase (FAK), a cytoplasmic tyrosine kinase highly expressed in numerous cancers, regulating several tumorigenic pathways, and is able to promote a downmodulation of β-Pix, which is a Rac-1 activator required by activated integrins and rapid nascent adhesion turnover (Kuo et al., 2011; Dianzani et al., 2014). Considering that the overexpression and activation of both of them are found in several human cancers and have been involved in cancer migration, invasion, EMT and angiogenesis (J. Zhao & Guan, 2009), those findings highlighted more in depth ICOSL triggering by ICOS-Fc immunomodulation potentialities.

With a in depth evaluation of all these data collected, ICOSL-mediated signaling responsible of cell invasion could be analyzed not only in the tumor progression context, but also in physiological processes, such as tissue remodeling during embryonic development and skin wound healing.
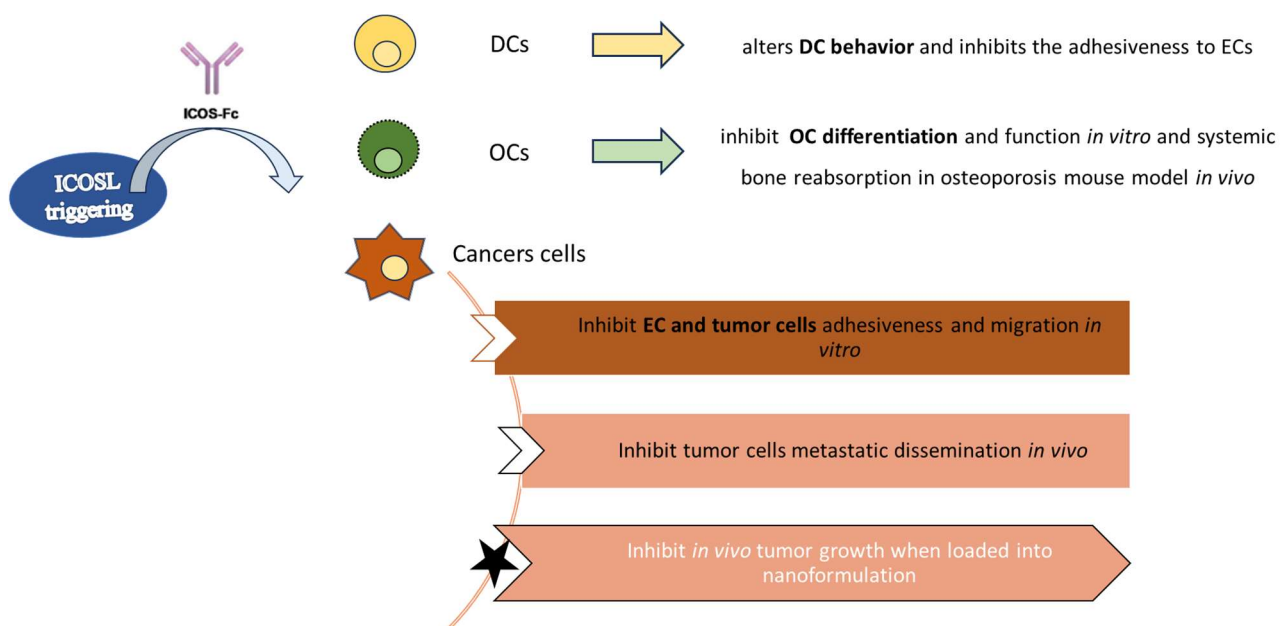

Figure 1: Summary scheme of ICOS-Fc multiple applications

3.1 ICOS-Fc application in wound healing

Skin wound healing starts immediately after injury and involves three phases. The inflammatory phase is the first one, in which platelets tend to aggregate and sequential infiltration of inflammatory cells is induced at the wound site (Guo & DiPietro, 2010). The second proliferative phase, which

generally follows and overlaps with the inflammatory one, consists in the formation of granulation tissue and re-epithelialization. In the reparative dermis, fibroblasts and endothelial cells are the most highly recruited cells, which support capillary growth, collagen and granulation tissue formation at the site of injury. Within the wound bed, fibroblasts produce major components of the extracellular matrix (ECM), like glycosaminoglycans and proteoglycans. Following robust proliferation and ECM synthesis, wound healing enters the final remodeling phase, during which the vascular density of the wound returns to normal and the ECM remodeling ends to an architecture approaching that of normal tissue. This could be achieved allowing the reorganization of the connective tissue in order to promote scar formation (Singampalli et al., 2020; Stoppa et al., 2022).

The immune system plays a central role in orchestrating the tissue healing process (Larouche et al., 2018), this could be confirmed by macrophages, which were found to play multiple roles in wound healing process. In the early wound, they release cytokines promoting inflammatory response by recruiting and activating additional leukocytes. They are responsible for clearing apoptotic cells and promoting successively the tissue regeneration undergoing a phenotypic transition to a reparative state that stimulate keratinocytes, fibroblasts, and angiogenesis (Meszaros et al., 2000; Mosser & Edwards, 2008;).

Upon inflammatory cells and macrophages, T lymphocytes migrate into wounds as well, it is usually registered their peak during the late-proliferative/early-remodeling phase. Hence, in the design of novel therapeutic strategies promoting tissue repair, much more targeting relevance is gifted to the immune system role and the advantage achievable with its modulation (Larouche et al., 2018).

Maeda et al. (2011) demonstrated how important is the role of T-cell costimulatory molecules in wound healing (Maeda et al., 2011). A significant delay in skin wound healing was detected in mice with disruption of the ICOS/ICOSL pathway. The loss of ICOS and/or ICOSL showed to negatively affect the recruitment of all cells types necessary for repairing the wound, such as infiltrating T-cells, macrophages, and neutrophils and was correlated to suppressed keratinocyte migration (epithelial gap), granulation tissue formation, angiogenesis, and myofibroblast proliferation. Several authors demonstrated the key role of ICOS/ICOSL system in lymphocytes migration and how crucial is the cytokines, chemokines, grow factors supplying in handling cell movement in wound healing inflammatory response (Martin, 1997; Kondo & Ishida, 2010; Brancato & Albina, 2011; Maeda et al., 2011).

Prior studies had shown that an IL-6 deficiency resulted in reduced inflammatory cell infiltration, collagen deposition, and angiogenesis at wound site (Maeda et al., 2011; Johnson et al., 2020).

Moreover, an impaired or accelerated wound healing process is correlated to a reduced/absence or increased number of tissue-repairing macrophages respectively (Danon et al., 1989). It has been recently demonstrated how ICOSL activation could modulate human M1 and M2 cells activity and promote tissue repair, thanks to the overall anti-inflammatory effect achieved with the M2-like macrophages recruitment at the wound site (Gigliotti et al., 2023).

Therefore, the local wound inflammatory response could be managed by T-cells not only by producing cytokines but also triggering ICOSL signaling on macrophages. According to the data collected it was suggested that ICOSL-M1 interaction in the first inflammatory phase would induce increased secretion of IL-23, which induces a type 3 response and the neutrophil recruitment, while activating ICOSL on M2 cells would consist in IL-10 and CCL3 increased secretion in the second phase, which again would promote the neutrophils recruitment supporting the removal of tissue debris and the release of pro-angiogenic factors (L. Chen et al., 2018).

Starting from the proved evidence that ICOSL triggering by ICOS drives a "reverse signal", acting on ICOSL-expressing cells, including APC, activated ECs, epithelial cells, fibroblasts and keratinocytes (Sharpe & Freeman, 2002; Yoshinaga Steven K. et al., 1999), ICOS-Fc was proposed and tested as an immunomodulator potentially useful for cutaneous wound healing improvement, since capable of inducing angiogenesis and recruitment of reparative macrophages. During my PhD years promising findings were collected on this research topic, which were performed in collaboration with the laboratory of Professor Umberto Dianzani of the UPO University (Novara).

ICOSL Stimulation by ICOS-Fc Accelerates Cutaneous Wound Healing In Vivo

Background: Wound healing is a complex biological process that consists of hemostasis, inflammation, proliferation, and remodeling phases. A wide numbers of cell types are involved in this process and the immune system is a key player actively participating to reestablish homeostasis following tissue injury via multiple mechanisms. ICOS/ICOSL involvement in tissue repair has been already demonstrated (Maeda et al., 2011), proving that the disruption of the ICOS/ICOSL pathway dramatically delayed skin wound healing in mice, due to a markedly reduced numbers of infiltrating T-cells, macrophages, and neutrophils into wounds and decreased production of IL-6 (Johnson et al., 2020).

Aim: The aim of this work was evaluating the *in vivo* effect of ICOS-Fc, a recombinant soluble form of ICOS, on skin wound healing.

Methods: The effect of human ICOS-Fc on wound healing was previously assessed performing an *in vitro* scratch assay on HaCat human keratinocytes expressing ICOSL, but not ICOS. A linear scratch was performed on a confluent cell monolayer, which was then cultured in serum free medium (to minimize cell proliferation) with or without ICOS-Fc or human ^{F119S}ICOS-Fc, mutant form of ICOS-Fc unable to bind ICOSL. The *in vivo* evaluation of ICOS-Fc effect was conducted performing a wound healing assay firstly on wild type (WT) mice C57BL6/J, evaluating fibroblast migration, the collagen deposition, vessel density and infiltration of inflammatory cells (histological staining and mRNA level through real time PCR).

Successively, the *in vivo* wound healing was performed including ICOS−/− and ICOSL−/− knockout mice and NOD-SCID-IL2R null (NSG) mice, lacking T, B and NK cells. All the animals were wounded on their back using a 4mm puncher, treated daily and monitored for 12d.

Results: *In vitro* treatment of ICOS-Fc significantly enhanced HaCat wound closure in scratch assay, showing a completely opposite effect of ICOS-Fc on cell migration, whose inhibition effect has been previously demonstrated on several kind of cells (ECs and tumor cell lines) (Dianzani et al., 2010; Occhipinti et al., 2013; Dianzani et al., 2014).

ICOS-Fc *in vivo* experiments showed how ICOS-Fc treatment on wild type mice significantly improved wound closure in the first six days of the treatment. In absence of ICOS-Fc treatment all knockout mice showed a substantial healing delay, compared to wild type mice, suggesting the important role of ICOS/ICOSL system and mediated cells recruitment. Moreover, ICOSL triggering relevance in driving tissue repair stood out from the totally negligible ICOS-Fc effect observed in ICOSL -/- treated

animals. On the other side, it significantly improves wound closure in both ICOS-/- and NGS mice and again in the initial part of the healing (1-6d).

The histological staining of fibroblast and collagen showed that ICOS-Fc treatment promote tissue repair, inducing an increased fibroblast migration, but not scar formation suggested by an unchanged collagen deposition.

Moreover, surprising was the enhanced wound angiogenesis found in mice treated with ICOS-Fc, since it previously showed ability to curb neoplastic angiogenesis in several mouse tumor types (Dianzani et al., 2010; Clemente et al., 2020). Differently, in the wound healing scenario, the ICOS-Fc treatment led to an upregulation of CD31 and VEGFα of skin samples with an increased T-cell recruitment.

Likewise intriguing was the increased macrophages wound recruitment, which was detected studying ICOS-Fc effect on *in vitro* migration of M1 and M2 macrophages. Differently from how it inhibited the migration of all cell types analyzed till then (Dianzani et al., 2010; Occhipinti et al., 2013; Dianzani et al., 2014; Raineri et al., 2020; Boggio et al., 2021; Raineri et al., 2022), ICOS-Fc promoted a higher M2-like reparative macrophages migration, compared to M1-like inflammatory macrophages.

On the other side, the ICOS-Fc treatment was correlated to a decreased neutrophils recruitment, confirming its capability to inhibit neutrophil adhesion to ECs, affecting their recruitment to inflamed tissues (Dianzani et al., 2010).

Finally, ICOS-Fc strictly increased IL-6 expression at day 2, supporting the ICOSL-induced IL-6 production, responsible of a substantial improvement of tissue repair.

Conclusion: Promising results showed that ICOSL has a central role in tissue repair. Since it is able to trigger ICOSL, ICOS-Fc showed itself able to improves cutaneous wound healing by increasing angiogenesis, enhancing fibroblasts and reparative macrophages recruitment.

Article

ICOSL Stimulation by ICOS-Fc Accelerates Cutaneous Wound Healing In Vivo

Ian Stoppa [1,2,†], Casimiro Luca Gigliotti [1,2,†], Nausicaa Clemente [1], Deepika Pantham [1,2], Chiara Dianzani [3], Chiara Monge [3], Chiara Puricelli [1,4], Roberta Rolla [1,4], Salvatore Sutti [1], Filippo Renò [1], Renzo Boldorini [1,4], Elena Boggio [1,2,*,‡] and Umberto Dianzani [1,4,‡]

[1] Department of Health Sciences and Interdisciplinary Research Center of Autoimmune Diseases (IRCAD), Università del Piemonte Orientale, 28100 Novara, Italy; ian.stoppa@uniupo.it (I.S.); luca.gigliotti@med.uniupo.it (C.L.G.); nausicaa.clemente@med.uniupo.it (N.C.); deepika.pantham@uniupo.it (D.P.); 20032501@studenti.uniupo.it (C.P.); roberta.rolla@med.uniupo.it (R.R.); salvatore.sutti@med.uniupo.it (S.S.); filippo.reno@med.uniupo.it (F.R.); renzo.boldorini@med.uniupo.it (R.B.); umberto.dianzani@med.uniupo.it (U.D.)

[2] NOVAICOS srls, 28100 Novara, Italy

[3] Department of Scienza e Tecnologia del Farmaco, University of Turin, 10124 Turin, Italy; chiara.dianzani@unito.it (C.D.); chiara.monge@unito.it (C.M.)

[4] Maggiore della Carità University Hospital, 28100 Novara, Italy

* Correspondence: elena.boggio@med.uniupo.it; Tel.: +39-0321660658

† These authors contributed equally to this work.

‡ These authors contributed equally to this work.

Abstract: Background: ICOS and its ligand ICOSL are immune receptors whose interaction triggers bidirectional signals that modulate the immune response and tissue repair. Aim: The aim of this study was to assess the in vivo effects of ICOSL triggering by ICOS-Fc, a recombinant soluble form of ICOS, on skin wound healing. Methods: The effect of human ICOS-Fc on wound healing was assessed, in vitro, and, in vivo, by skin wound healing assay using ICOS$^{-/-}$ and ICOSL$^{-/-}$ knockout (KO) mice and NOD-SCID-IL2R null (NSG) mice. Results: We show that, in wild type mice, treatment with ICOS-Fc improves wound healing, promotes angiogenesis, preceded by upregulation of IL-6 and VEGF expression; increases the number of fibroblasts and T cells, whereas it reduces that of neutrophils; and increases the number of M2 vs. M1 macrophages. Fittingly, ICOS-Fc enhanced M2 macrophage migration, while it hampered that of M1 macrophages. ICOS$^{-/-}$ and ICOSL$^{-/-}$ KO, and NSG mice showed delayed wound healing, and treatment with ICOS-Fc improved wound closure in ICOS$^{-/-}$ and NSG mice. Conclusion: These data show that the ICOS/ICOSL network cooperates in tissue repair, and that triggering of ICOSL by ICOS-Fc improves cutaneous wound healing by increasing angiogenesis and recruitment of reparative macrophages.

Keywords: ICOS:ICOSL system; wound healing; reparative macrophages

1. Introduction

Skin wound healing starts immediately after injury and evolves in three phases. The first one is an inflammatory phase during which platelets tend to aggregate, while inflammatory cells are recruited to the wound site. The second proliferative phase is characterized by the formation of granulation tissue and re-epithelialization due to the migration and proliferation of keratinocytes, fibroblasts, and ECs, and by ECM deposition. The last one is the so-called remodeling phase during which the regenerative process comes to an end and the wound becomes avascular and acellular, thereby allowing the reorganization of the connective tissue to promote scar formation [1,2].

ICOS (CD278) is a T cell co-stimulatory receptor, member of the CD28 family [3], mainly expressed on activated T-cells. ICOS binds ICOSL (CD275, also called B7h, GL50, B7H2), a member of the B7 family. ICOS triggering in T cells promotes not only the

activation of effector T cells in peripheral tissues but also the development of regulatory T cells [4]. ICOSL is expressed on multiple cell types, including antigen presenting cells (APCs), activated ECs, epithelial cells, fibroblasts, and keratinocytes [5,6]. ICOSL triggering mediated by ICOS drives a "reverse signal" that inhibits the migration of endothelial, dendritic, and tumor cells, modulates cytokine secretion while promoting antigen cross-presentation in dendritic cells, and inhibits osteoclast differentiation and functions [7–11].

We have recently shown that ICOSL also binds osteopontin (OPN) at a different site from that used to bind ICOS [12], which suggests that the ICOSL/OPN axis may play a role in wound healing besides tumorigenesis. This hypothesis is also supported by the observation that OPN can act as both an ECM component and a soluble cytokine involved in inflammation and angiogenesis [13,14]. Indeed, ICOSL triggering by OPN induces tumor cell migration and promotes tumor angiogenesis, both of which are counteracted by ICOS-mediated activation of ICOSL [12].

The formal demonstration of a functional role of the ICOS/ICOSL pathway in wound healing comes from the observation that ICOS$^{-/-}$, ICOSL$^{-/-}$, and ICOS/ICOSL$^{-/-}$ mice show delayed wound healing [15] likely due to decreased production of IL-6 [16]. In good agreement with a role of the ICOS/ICOSL dyad in normal tissue repair, we have recently shown that CCl$_4$-induced liver damage, which is dependent on massive recruitment of blood-derived monocytes/macrophages, is dramatically worsened in both ICOS$^{-/-}$ and ICOSL$^{-/-}$ mice [17]. Interestingly, we were able to rescue this impairment by treating mice with ICOS-Fc, a recombinant soluble protein composed of the ICOS extracellular portion fused to the IgG1 Fc portion, which has been previously shown to trigger ICOSL, thereby inhibiting the development of experimental tumor metastases in vitro and tumor angiogenesis in vivo [9,11,17,18].

As the aforementioned findings support a functional role of ICOS/ICOSL in tissue repair, in the present study, we sought to determine the effect of ICOS-Fc in both in vitro and in vivo models of skin wound healing. Our in vivo results show that ICOS-Fc improves would healing likely by increasing angiogenesis and recruitment of reparative macrophages.

2. Results

2.1. ICOSL Activation by ICOS-Fc Increases Keratinocyte Migration In Vitro

To begin to explore the role of ICOSL in tissue repair, we assessed the effect of human ICOS-Fc on keratinocyte wound healing in vitro by scratch assay on HaCat human keratinocytes, which are known to express ICOSL but not ICOS (Figure 1a). For this purpose, we performed a linear scratch on a confluent monolayer of HaCat cells, which were then cultured in serum-free medium to minimize cell proliferation in the presence or absence of human ICOS-Fc or human ^{F119S}ICOS-Fc (2 µg/mL), an ICOS-Fc mutant unable to bind ICOSL. After 24 h, microscopic evaluation revealed that treatment with ICOS-Fc but not ^{F119S}ICOS-Fc led to a substantial increase in the percentage of migrating cells compared to that of the untreated control (Figure 1b,c). This result came as a surprise given that we had previously shown that ICOS-Fc inhibited migration of several cell types and wound closure in scratch assays performed on ECs and several tumor cell lines [8–10].

2.2. ICOS-Fc Treatment Accelerates Skin Wound Healing In Vivo

To assess the effect of ICOS-Fc on skin wound healing in vivo, skin wounds were created on the back of wild-type C57BL/6 mice, which were then daily instilled with 1x PBS with or without mouse ICOS-Fc. Wound healing was then followed up for 10 days. Consistent with our in vitro data, we found that treatment with ICOS-Fc significantly improved wound closure at days 1–6, while the healing curve gradually aligned with control levels at later time points (Figure 2a). Histological staining of fibroblasts and collagen performed at day 3 and 4 by H&E and picrosirius red staining, respectively, revealed that treatment with ICOS-Fc increased fibroblast migration into the wound compared to control at day 3 and, to a higher extent, day 4. In contrast, collagen deposition in ICOS-Fc-treated mice was similar to that of their control counterparts, indicating that treatment with ICOS-Fc

favors repair but not scar formation (Figure 2b–d). Consistently, we observed a dramatic increase in αSMA gene expression, a marker of reparative myofibroblasts [19], at day 2 following treatment with ICOS-Fc, which decreased to control levels in the following days (Figure 2e).
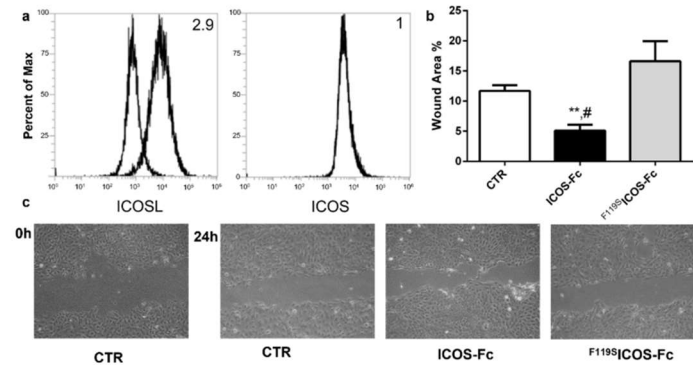

Figure 1. Effect of ICOS-Fc stimulation on the motility of HaCat cells by scratch assay. HaCat cells were cultured to confluence on 6-well plates. A scratch was made through the cell layer using a pipette tip and cells were then cultured in the presence or absence of 2 μg/mL ICOS-Fc or ^{F119S}ICOS-Fc for 24 h. (**a**) ICOS and ICOSL expression in HaCat cells. (**b**) Wound area % after 24 h of treatment as above, calculated as: $1 -$ (scratch width of the treated group/scratch width of the control group) $\times$ 100; results are the means from three independent experiments; ** $p < 0.01$ vs. CTR; # $p < 0.05$ vs. ^{F119S}ICOS-Fc, calculated by paired *t*-test. (**c**) Representative microphotographs of the wounded area taken immediately after the scratch was made 0 h and 24 h later to monitor cell migration into the wounded area (original magnification $10\times$).
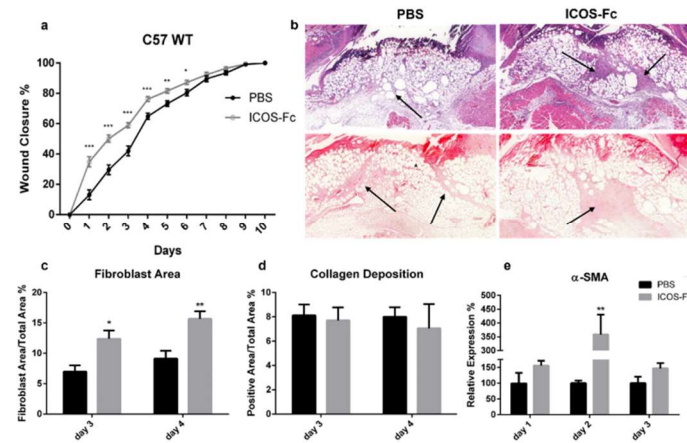

Figure 2. Effect of treatment with ICOS-Fc on wound healing in wild-type C57BL/6 mice. (**a**) Wound healing % in mice treated with PBS (n = 21) or ICOS-Fc (n = 22) calculated as (wound area^{T0}-wound area^{TX})/wound area^{T0} $\times$ 100%; mean $\pm$ SE; (**b**) representative microphotographs of the staining (magnification $200\times$) at day 4; upper panels: Hematoxylin/eosin (H&E) for fibroblast area quantification (black arrows); lower panels: picrosirius red for collagen deposition quantification (black arrows). (**c**,**d**) Wound area % occupied by fibroblasts and collagen as detected by H&E and picrosirius red staining, respectively, at day 3 and day 4. (**e**) αSMA mRNA expression analysis by real time PCR at day 1, day 2, and day 3. Results are expressed as mean $\pm$ SE from 4 independent experiments; * $p < 0.05$; ** $p < 0.005$; *** $p < 0.001$, calculated by Mann–Whitney test.

Next, immunohistochemical staining of vessels with an anti-CD31 antibody revealed a significant increase in CD31^{+} vessels in mice treated with ICOS-Fc at day 3 and 4 compared to their control counterparts (Figure 3a), indicating enhanced wound angiogenesis. This was further supported by augmented CD31 and VEGF mRNA levels at day 1, both of which decreased to control levels in the subsequent days (Figure 3b).
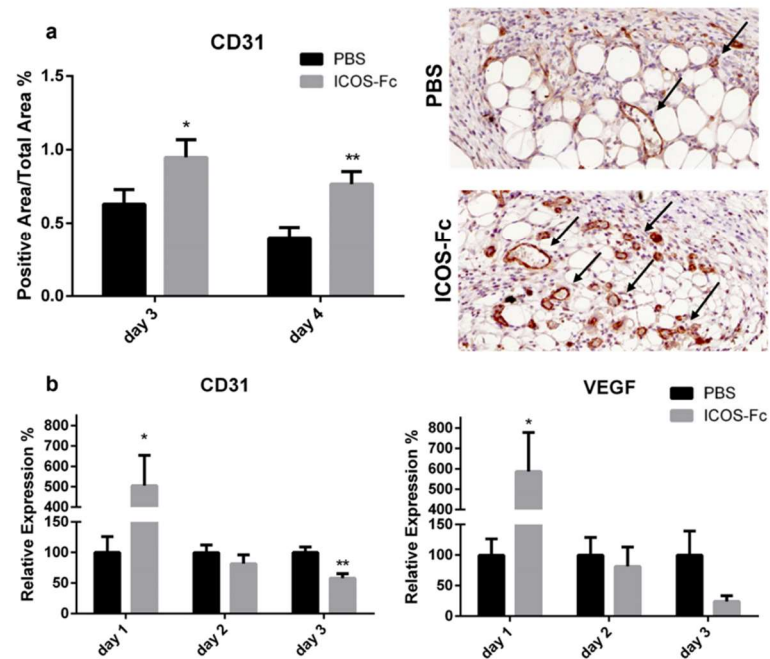

Figure 3. Treatment with ICOS-Fc stimulates angiogenesis during wound healing. (**a**) Wound area occupied by CD31^{+} vessels as detected by immunohistochemistry. Left panel: results at day 3 and day 4 expressed as mean ± SE from four independent experiments. Right panels: Representative microphotographs of CD31 staining (magnification 200×) at day 4. (**b**) Expression of the CD31 (left) and VEGF (right) mRNA levels as assessed by real time PCR at day 3 and day 4 and expressed as mean ± SE from four independent experiments. Results are expressed as % of the mRNA amount detected in PBS-treated mice at each time point; * $p < 0.05$; ** $p < 0.005$; calculated by unpaired Student's *t*-test.

To further characterize the healing process in wounded mice, we next sought to determine the infiltration extent of inflammatory cells by immunohistochemistry using antibodies specific for MPO, CD3, and F4/80. Results showed that treatment with ICOS-Fc decreased MPO^{+} neutrophils at day 3, whereas it increased CD3^{+} T cells at day 3 and 4, and F4/80^{+} monocyte/macrophages at day 3 (Figure 4a–c).

To better characterize the inflammatory microenvironment of the healing wound, we next assessed mRNA expression levels of IL-6, TNF-α, TGF-β, IL-33, IL-10, IL4, IFN-γ, OPN, TREM1, TREM2, ICOS, and ICOSL at day 1 to 3 by real time PCR. We found that treatment with ICOS-Fc strikingly increased expression of IL-6 at day 2, which decreased in the following days (Figure 5a). In contrast, expression of TNF-α was homogeneously decreased at all time points, while expression of TGF-β was moderately decreased at day 3 (Figure 5b,c). Expression of TREM1 and TREM2, respective markers of M1 and M2 macrophages, displayed opposite patterns since treatment with ICOS-Fc downregulated TREM1 and upregulated TREM2 at day 1, so that the TREM2/TREM1 ratio was increased about 5-fold (Figure 5d,e,g). ICOSL gene expression was decreased at day 3 upon ICOS-Fc

treatment (Figure 5f), whereas no differences were detected for IL-10, IL-33, IL-4, IFN-γ, OPN, and ICOS (data not shown).
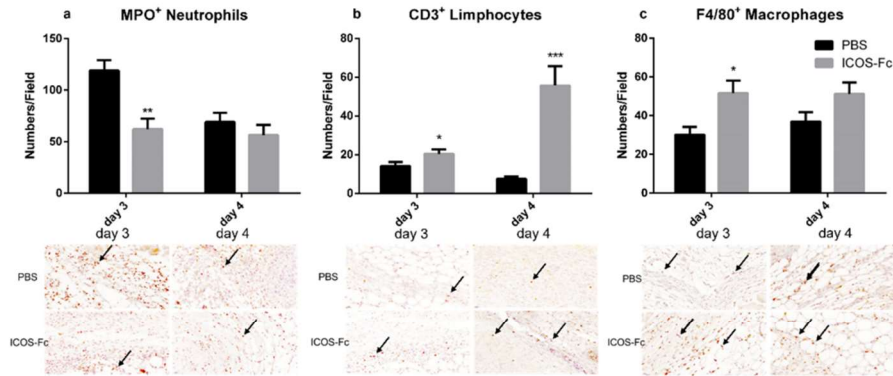

Figure 4. Effect of treatment with ICOS-Fc on the infiltration of inflammatory cells in the wound bed. Infiltration by neutrophils, T cells, and macrophages was assessed by immunohistochemistry using antibodies against MPO (**a**), CD3 (**b**), and F4/80 (**c**), respectively. Upper panels: number of positive cells per field counting 9 fields in each experiment at day 3 and day 4; results are expressed as mean ± SE. Lower panels: representative immunohistochemical staining (magnification 400×) at day 3. Statistical analysis was performed with Mann–Whitney test: * $p < 0.05$; ** $p < 0.01$; *** $p < 0.0005$.
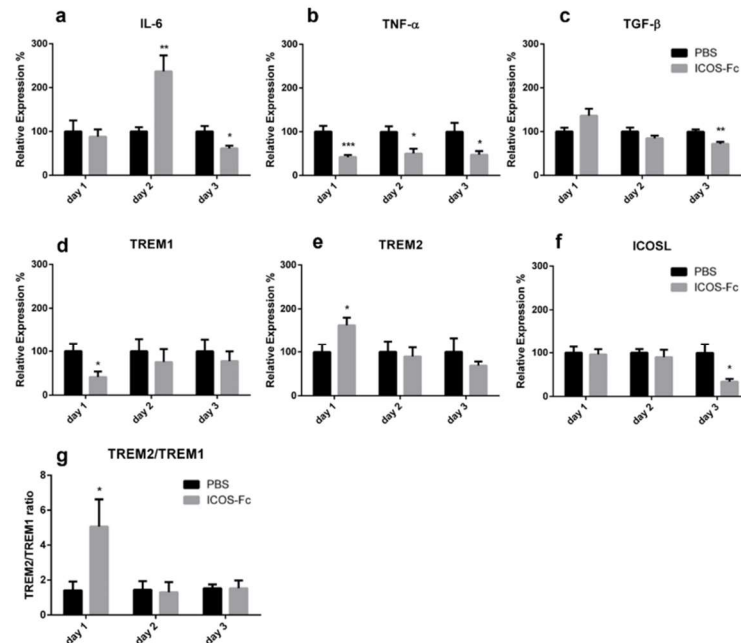
Figure 5. Effect of treatment with ICOS-Fc on the expression of inflammatory molecules in the wound. Expression of IL-6 (**a**), TNF-α (**b**), TGF-β (**c**), TREM1 (**d**), TREM2 (**e**), and ICOSL (**f**) mRNA as assessed by real time PCR at day 1, day 2, and day 3, and expressed as mean ± SE from 3 independent experiments. (**g**) TREM2/TREM1 ratio. Results are expressed as % of the mRNA amount detected in PBS-treated mice at each time point; * $p < 0.05$; ** $p < 0.005$; *** $p < 0.001$, calculated by unpaired Student's *t*-test.

2.3. Effects of ICOSL Triggering on Macrophages

As our results demonstrated that treatment with ICOS-Fc increases the recruitment of macrophages to the healing wound, with apparent predominance of TREM2^{+} M2 macrophages, we sought to determine the effect of ICOS-Fc treatment on the migration of mouse M1 and M2 macrophages differentiated in vitro. To this end, spleen adherent cells were differentiated into macrophages by culturing them for 14 days in the presence of M-CSF. Cells were then cultured for an additional 2 days in the presence of IFN-γ to obtain M1 cells, or with IL-4 to obtain M2 cells; both culture conditions were performed in the presence or absence of LPS. At the end of the culture, differentiation was assessed by evaluating expression of NOS2 and ARG1 mRNA levels, marking M1 and M2 cells, respectively. As expected, M1 cells expressed higher levels of NOS2 and lower levels of ARG1 than M2 cells (Figure 6a). Analysis of ICOS and ICOSL mRNA showed that both M1 and M2 macrophages expressed ICOSL but not ICOS (data not shown), whereas M1 cells expressed higher ICOSL levels than M2 cells (Figure 6b).
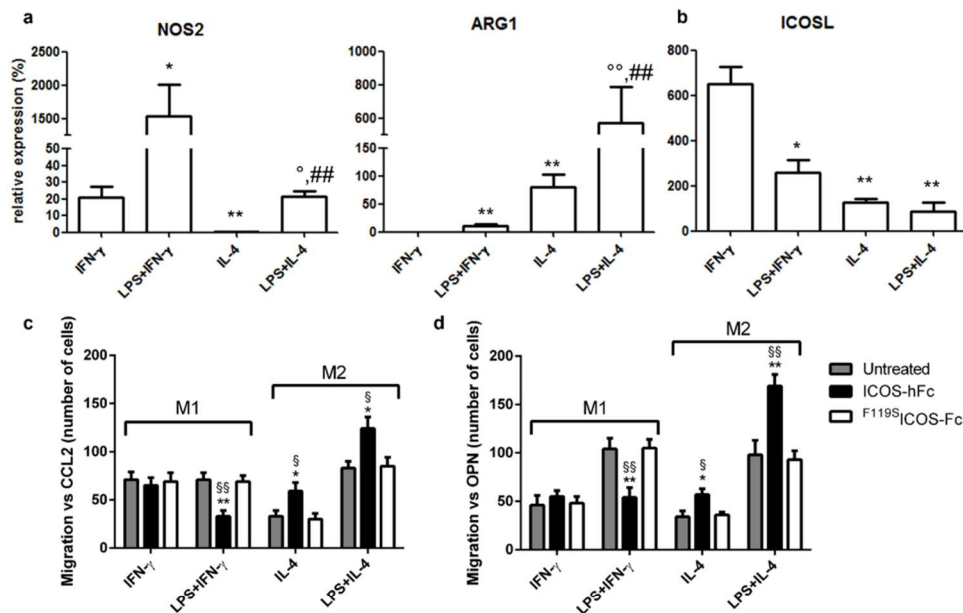

Figure 6. Effect of ICOS-Fc on the migration of murine M1 and M2 macrophages. Macrophages obtained by culturing adherent spleen cells with M-CSF for 14 days (M0) were polarized to M1 or M2 macrophages by culturing them with IFN-γ or LPS + IFN-γ (M1) or with IL-4 or LPS + IL-4 (M2) for 48 h. (**a**) NOS2, ARG1, and (**b**) ICOSL gene expression analysis by real-time PCR. Values are expressed as % of the mRNA detected in M0 macrophages stimulated with LPS for 48 h (* $p < 0.05$, ** $p < 0.01$ vs. IFN-γ, ° $p < 0.05$, °° $p < 0.01$ vs. IL-4, ## $p < 0.01$ vs. LPS + IFN-γ, Mann–Whitney test). (**c**,**d**) Cell migration assay. Murine M1 and M2 macrophages were cultured in the presence and absence of ICOS-hFc or [F119S]ICOS-Fc using either CCL2 (30 nM) (**c**) or OPN (10 μg/mL) (**d**) as chemotactic factors. Values are expressed as number of migrating cells, stimulated with either CCL2 or OPN. The results are expressed as mean ± SE from n = 3–8 experiments; differences versus either [F119S]ICOS-Fc (* $p < 0.05$; ** $p < 0.01$) or the untreated control (§ $p < 0.05$; §§ $p < 0.01$) for each condition are calculated by Dunnett test.

These cells were then used to assess the effect of ICOS-Fc on cell migration induced by either CCL2 or OPN through Boyden chamber assay. To minimize the possible confounding effects due to interactions with Fcγ receptors (FcγRs), we used the recombinant ICOS-hFc,

which consists of the extracellular portion of murine ICOS fused to the Fc of human IgG1. In addition, human ^{F119S}ICOS-Fc, which does not bind to either ICOSL or mouse FcγRs, was used as negative control [8–11]. Consistent with our previous results in vivo, stimulation with ICOS-hFc increased the migration of M2 macrophages—regardless of the presence of LPS in the culture medium—compared to that of ^{F119S}ICOS-Fc-treated cells. In contrast, ICOS-hFc treatment inhibited the migration of M1 macrophages stimulated with LPS, whereas it had no effect on those cultured in the absence of LPS. Similar results were observed by using either CCL2 (Figure 6c) or OPN as chemoattractant stimuli (Figure 6d). On the other hand, treatment with ^{F119S}ICOS-Fc did not show any effect under any experimental conditions when compared to control migration assays performed in the absence of any form of ICOS-Fc.

2.4. Wound Healing in KO Mice

To determine the functional role of ICOS and ICOSL in wound healing in vivo, we investigated the effect of ICOS-Fc treatment in wounded mice deficient for ICOS or ICOSL, and NSG mice, lacking T, B, and NK cells.

Analysis of wound healing in the absence of ICOS-Fc treatment showed that ICOS$^{-/-}$, ICOSL$^{-/-}$, and NSG mice displayed a substantial healing delay, compared to wild type mice, starting from day 4 (Figure 7a). Treatment with ICOS-Fc significantly improved wound closure in ICOS$^{-/-}$ and NSG mice, while it was ineffective in ICOSL$^{-/-}$ mice (Figure 7b–d). Thus, the fact that ICOS-Fc treatment promotes wound healing in all strains expressing ICOSL but fails to do so in ICOSL$^{-/-}$ mice suggests that ICOSL triggering drives tissue repair. Consistent with the data obtained in wild type mice, also in ICOS$^{-/-}$ and NSG mice, ICOS-Fc significantly improved wound closure mainly in the initial part of healing (day 1–6), while the healing curve gradually aligned with control levels at later time points.
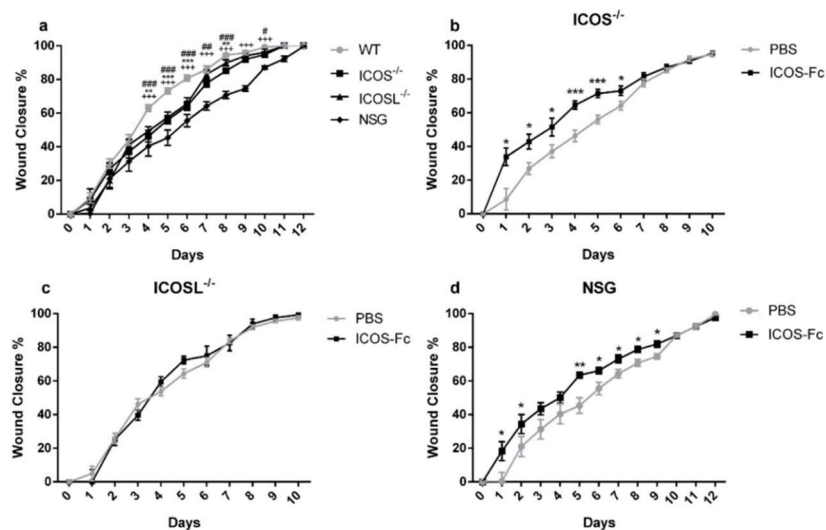
Figure 7. Effect of treatment with ICOS-Fc on wound healing in various KO mice. Wound healing % was calculated as described in the legend to Figure 2. (**a**) Comparison of wound healing in wild-type mice (n = 21), ICOS$^{-/-}$ (n = 16), ICOSL$^{-/-}$ (n = 18), and NSG (n = 15) mice. (**b–d**) Effect of treatment with ICOS-Fc on wound healing in ICOS$^{-/-}$ (PBS: n = 16; ICOS-Fc: n = 11), ICOSL$^{-/-}$ (PBS: n = 9; ICOS-Fc: n = 9), and NSG (PBS: n = 15; ICOS-Fc: n = 16) mice. * $p < 0.05$; ** $p < 0.005$; *** $p < 0.001$; # $p < 0.05$; ## $p < 0.005$; ### $p < 0.001$; +++ $p < 0.001$; calculated by Mann–Whitney test.

3. Discussion

The present study shows that ICOS and ICOSL cooperate in skin wound healing and that triggering of ICOSL by instillation of ICOS-Fc into the wound bed favors tissue repair in vivo. These results extend those obtained by Maeda et al. [15] showing that wound healing is delayed in $ICOS^{-/-}$, $ICOSL^{-/-}$, or $ICOS/ICOSL^{-/-}$ mice, possibly due to defective production of IL-4, IL-10, and, especially, IL-6 at the wound site. Since this defective repair was overcome by adoptive transfer of wild-type T cells (expressing ICOS) in $ICOS^{-/-}$ but not $ICOSL^{-/-}$ mice, the authors concluded that the healing defect in KO mice could be ascribed to the impaired development of T helper type 2 cells due to the lack of ICOS-mediated co-stimulation of T cells.

Even though our findings confirm that wound healing is defective in mice lacking ICOS or ICOSL, the observation that ICOSL stimulation by ICOS-Fc is sufficient to accelerate the early phases of the healing process underscores the importance of ICOSL in ICOS/ICOSL-mediated tissue repair. Indeed, enhanced wound healing in response to ICOS-Fc treatment is readily apparent in both wild-type and $ICOS^{-/-}$ mice, but not in mice lacking ICOSL, which indicates that this effect is not due to the inhibition of ICOS activity in T cells, but it is instead caused by ICOSL-mediated "reverse signaling" in other cell types. The fact that ICOS-Fc treatment is effective also in immunodeficient NSG mice confirms that T cells are not involved in ICOS-Fc-induced wound healing. Moreover, the lack of effect in $ICOSL^{-/-}$ mice rules out possible confounding effects due to the potential interaction of ICOS-Fc with Fcγ receptors.

A key effect of ICOS-Fc is represented by increased angiogenesis and recruitment of fibroblasts at day 3 and 4, as judged by histologic analysis, both of which are preceded by upregulation of CD31 and VEGF-α—two markers of angiogenesis—and αSMA—a marker of reparative myofibroblasts—mRNA expression at day 1 and 2, respectively. Enhanced angiogenesis in response to ICOSL triggering was unexpected since previous works had shown that in vivo treatment with ICOS-Fc curbed neoplastic angiogenesis in several mouse tumor types, and in vitro experiments showed that ICOS-Fc had no effect on angiogenesis induced by VEGF whereas it inhibited that induced by OPN [8,18].

Another interesting observation from our histological analysis is that ICOS-Fc treatment can also modulate the infiltration of inflammatory cells by decreasing neutrophils and increasing T cells and macrophages. The decrease in neutrophils is in line with previous data showing that ICOS-Fc inhibits neutrophil adhesion to ECs, which may affect their recruitment into inflamed tissues [8]. The increase in T cells might be ascribable to the enhanced vascularization of the wound or to the functional antagonism between ICOS-Fc and ICOS expressed on T cells given that, at least in tumors, ICOS-Fc treatment is known to increase effector T cells and decrease regulatory T cells [18,20]. The increase in macrophages is quite intriguing as it is accompanied by a five-fold increase in TREM2/TREM1 expression ratio, which suggests that ICOS-Fc favors recruitment of $TREM2^+$ M2-like reparative macrophages, as compared to $TREM1^+$ M1-like inflammatory macrophages. This possibility is also supported by our cell migration experiments in vitro, showing that ICOS-Fc enhances the migration of M2 macrophages, whereas it inhibits that of M1 macrophages. The increased migration of M2 macrophages was unexpected, since ICOS-Fc had always inhibited the migration response of all cell types analyzed until then [8–10,12,20,21]. The different response of mouse M1 and M2 macrophages may be due to differences in their migration and adhesive properties likely caused by higher expression levels of β2 integrins in M1 vs. M2 cells [22]. Intriguingly, ICOS-Fc treatment also led to increased migration of keratinocytes, as judged by our scratch assay analysis, which could be the result of changes in size, shape, adhesiveness, and organization of keratin intermediate filaments of these cells as shown previously [23].

Overall, the effects of ICOS-Fc on wound healing are in line with our previous work showing that CCl_4-treated $ICOS^{-/-}$ or $ICOSL^{-/-}$ mice develop a more severely acute inflammatory liver damage, along with a reduction of reparative macrophages, compared to their wild-type counterparts. Moreover, treatment with ICOS-Fc protected ICOS-deficient

mice from this increased damage, simultaneously restoring the number of reparative macrophages, whereas it had no effects in ICOSL$^{-/-}$ mice [17]. These findings are also in line with the aforementioned study by Maeda et al. [15], showing that mice lacking ICOS and/or ICOSL display decreased angiogenesis and a reduction of T cells and macrophages at the wound site. Intriguingly, the authors observed decreased IL-6 in the wounds of these mice, and local application of exogenous IL-6 in the initial phase of healing (day 1) led to a substantial improvement of tissue repair. A potential role of ICOSL-induced IL-6 production in wound healing is also supported by our observation that treatment with ICOS-Fc of wounded wild-type mice increases the expression of IL-6 at day 2 [15].

4. Materials and Methods

4.1. Scratch Assay

HaCat cells (human keratinocytes) were purchased from ATCC (Manassas, VN, USA) and grown in DMEM (Life Technologies, Carlsbad, CA, USA) medium plus 10% fetal bovine serum (FBS; Life Technologies). HaCat cells were plated in six-well plates at a concentration of 10^6 cells/well and grown to confluence. To prevent cell proliferation, cells were incubated for 12 h in FBS-free medium. Cell monolayers were wounded by scratching with a sterile plastic pipette tip along the diameter of the well. Cells were then incubated in culture medium in the absence or presence of 2 µg/mL human ICOS-Fc or ^{F119S}ICOS-Fc, an ICOS-Fc mutant unable to bind ICOSL. To monitor cell migration in the wound, five fields of each wound were analyzed and photographed immediately after scratching (0 h) and 24 h later. The wound closure was calculated with the following formula: (1 − (scratch width of the treated group/scratch width of the control group)) × 100%.

ICOS and ICOSL expression was assessed by immunofluorescence and flow cytometry (Attune NxT, Thermo-Fisher, Waltham, MA, USA) using PE-conjugated mAb to ICOS or ICOSL (R&D System, Minneapolis, MN, USA). The mean fluorescence intensity ratio (MFI-R) was calculated according to the following formula: MFI of the stained sample histogram (arbitrary units)/MFI of the control histogram (arbitrary units).

4.2. Mice

C57BL6/J (WT), NOD-SCID-IL2R γ-null mice (NSG) and knockout B6.129P2-Icos^{tm1Mak}/J (ICOS$^{-/-}$) and B6.129P2-Icosl^{tm1Mak}/J (ICOSL$^{-/-}$) mice (The Jackson Laboratory, Bar Harbor, ME, USA) were bred under pathogen-free conditions in the animal facility at Università del Piemonte Orientale, Department of Health Sciences (Authorization No. 217/2020-PR) and treated in accordance with the Ethical Committee and European guidelines.

4.3. In Vivo Wounds

The day before wound induction (day-1), WT, NSG, ICOS$^{-/-}$, and ICOSL$^{-/-}$ mice were anesthetized with 2% isoflurane and their back was shaved. At day 0, mice were anesthetized as above, and wounds were made on their back using a 4 mm puncher (Kai Medical, Solingen, Germany). The wound area was photographed and measured using the following formula: (a/2) × (b/2) × 3.14, where "a" and "b" are the two perpendicular diameters. In the following days, wound closure was calculated using the following formula: (wound area^{T0}-wound area^{TX})/wound area^{T0} × 100. Mice were treated daily with 10 µg/mouse ICOS-Fc in PBS instilled directly into the wound site; controls were treated with an equal volume of PBS. Mice were monitored daily for 12 days, at which point in time the wound was closed. In some experiments, mice were sacrificed at day 1, 2, 3, and 4 to harvest and analyze the healing tissue. Each experiment involved 4–7 mice for each condition tested; each condition was tested in 2–3 independent experiments. Sample size was calculated using G*Power (RRID:SCR_013726) software (Power: 80%; Significance: 95%).

4.4. Real-Time PCR Analysis

Total RNA was isolated from skin samples collected at day 1, 2, and 3 post-injury, or from in vitro-differentiated macrophages using TRIzol reagent (Sigma-Aldrich, St. Louis, MO, USA). RNA (1 µg) was retro-transcribed using QuantiTect Reverse Transcription Kit (Qiagen, Hilden, Germany). Expression of the IL-6, TNF-α, TGF-β, IL-33, IL-10, IL-4, IFN-γ, OPN, TREM1, TREM2, VEGF-α, α-SMA, ICOS, NOS2, ARG1, and ICOSL mRNA were evaluated by real-time PCR (Assay-on Demand; Applied Biosystems, Foster City, CA, USA). The β-actin gene was used to normalize the cDNA amounts. Real-time PCR was performed using the CFX96 System (Bio-Rad Laboratories, Hercules, CA, USA) in duplicate for each sample in a 10 µL final volume containing 1 µL of diluted cDNA, 5 µL of TaqMan Universal PCR Master Mix (Applied Biosystems, Foster City, CA, USA), and 0.5 µL of Assay-on-Demand mix. The results were analyzed with a ΔΔ threshold cycle method.

4.5. Histological Analysis

Skin samples were collected at day 3 and 4 post-injury and processed for paraffin embedding. Samples were cut at 4-µm thickness and stained with hematoxylin and eosin (H&E) (Sigma-Aldrich) for tissue morphology and fibroblast evaluation, or with picrosirius red (Abcam, Cambridge, UK) to evaluate the extent of fibrosis.

Immunohistochemical staining of CD31, MPO, CD3, and F4/80 was performed to detect neo vessel formation and infiltration of immune cells (i.e., neutrophils, T cells, and macrophages). Samples were treated with citrate buffer (Vector Laboratories, Burlingame, CA, USA) for antigen retrieval, and endogenous peroxidases were blocked with 3% H_2O_2 (Sigma-Aldrich). To avoid secondary antibody unspecific binding, samples were pre-incubated with 5% normal goat serum (NGS) (Sigma-Aldrich) for 1 h at room temperature (RT). Samples were stained with rabbit antibodies against CD31 (Abcam, 1:50), MPO (Invitrogen, 1:100), CD3 (Invitrogen, 1:150), or F4/80 (Invitrogen, 1:100) overnight at 4 °C and, then, with a goat anti-rabbit horseradish peroxidase (HRP)-conjugated secondary antibody (Sigma-Aldrich), followed by 3,3′-diaminobenzidine (DAB) (Agilent Dako, Santa Clara, CA, USA). Successively, samples were counterstained with hematoxylin (Sigma-Aldrich), dehydrated, and mounted on cover slips. Slides were acquired using Pannoramic MIDI (3D Histech, Budapest, Hungary) at $200\times$ magnification. The positive areas for CD31, fibroblasts, and collagen were calculated using the following formula: (positive area/total area) $\times$ 100%. MPO, CD3, and F4/80 positive cells were expressed as cell number/field counted in 15 fields for each sample.

4.6. Macrophage Migration Assay

Spleen cells were separated by density gradient centrifugation using the Ficoll-Hypaque reagent (Lympholyte-M, Cedarlane Laboratories, Burlington, ON, Canada) and incubated in tissue culture dishes for 2 h with DMEM supplemented with 10% FBS. Subsequently, supernatants and non-adherent cells were discarded, and the adherent cells were rinsed three times and cultured in DMEM (Life Technologies) medium supplemented with 10% FBS, 1% glutamine, and 1% penicillin/streptomycin plus 20 ng/mL M-CSF (Immunotools, Friesoythe, Germany) for 14 days (normal DMEM medium). At day 14, adherent cells were cultured for additional 48 h with interferon-γ (IFN-γ; 100 U/mL Immunotools) to obtain M1 macrophages, and with interleukin-4 (IL-4; 20 ng/mL Immunotools) to obtain M2 macrophages; each culture condition was performed in the presence or absence of LPS (LPS; 100 ng/mL Sigma).

Macrophage migration was assessed by the Boyden chamber migration assay (BD Biosciences, San Jose, CA, USA). Cells were plated (10^4 cell/well) onto the apical side of 50 µg/mL Matrigel-coated filters in serum-free medium in the presence or absence of msICOS-huFc (2 µg/mL), composed by the extracellular portion of murine ICOS fused to the Fc of human IgG1, or human [F119S]ICOS-Fc (2 µg/mL). Mouse CCL2 (30 nM, Immunotools) or OPN (10 µg/mL) were used as chemoattractants in the bottom chamber. After 6 h, the cells on the apical side were wiped off with Q-tips. Cells on the bottom of the filter

32

were stained with crystal violet and all counted (quadruplicate filter) with an inverted microscope. Data are shown as number of migrating cells [12].

4.7. Statistical Analyses

Statistical analyses were performed using Mann–Whitney U test, Wilcoxon test, Dunnett's test, or Student's *t*-test using GraphPad Instat Software (GraphPad Software, San Diego, CA, USA), as indicated. Data are expressed as mean and standard error of the mean (SEM) and statistical significance was set at $p < 0.05$.

5. Conclusions

In conclusion, this work shows that ICOSL plays a key role in wound healing and that triggering of ICOSL by ICOS-Fc favors healing by increasing angiogenesis and the recruitment of fibroblasts and reparative macrophages. Therefore, ICOS-Fc and other molecules capable of triggering ICOSL might be exploited to improve wound closure in patients with impaired tissue repair.

References

1. Singer, A.J.; Clark, R.A. Cutaneous wound healing. *N. Engl. J. Med.* **1999**, *341*, 738–746. [CrossRef] [PubMed]
2. Singampalli, K.L.; Balaji, S.; Wang, X.; Parikh, U.M.; Kaul, A.; Gilley, J.; Birla, R.K.; Bollyky, P.L.; Keswani, S.G. The Role of an IL-10/Hyaluronan Axis in Dermal Wound Healing. *Front. Cell Dev. Biol.* **2020**, *8*, 636. [CrossRef] [PubMed]
3. Aicher, A.; Hayden-Ledbetter, M.; Brady, W.A.; Pezzutto, A.; Richter, G.; Magaletti, D.; Buckwalter, S.; Ledbetter, J.A.; Clark, E.A. Characterization of human inducible costimulator ligand expression and function. *J. Immunol.* **2000**, *164*, 4689–4696. [CrossRef] [PubMed]
4. Li, D.; Xiong, X. ICOS[+] Tregs: A Functional Subset of Tregs in Immune Diseases. *Front. Immunol.* **2020**, *11*, 2104, Correction in *Front. Immunol.* **2021**, *12*, 701515. [CrossRef]
5. Yoshinaga, S.K.; Whoriskey, J.S.; Khare, S.D.; Sarmiento, U.; Guo, J.; Horan, T.; Shih, G.; Zhang, M.; Coccia, M.A.; Kohno, T.; et al. T-cell co-stimulation through B7RP-1 and ICOS. *Nature* **1999**, *402*, 827–832. [CrossRef] [PubMed]
6. Sharpe, A.H.; Freeman, G.J. The B7-CD28 superfamily. *Nat. Rev. Immunol.* **2002**, *2*, 116–126. [CrossRef]
7. Tang, G.; Qin, Q.; Zhang, P.; Wang, G.; Liu, M.; Ding, Q.; Qin, Y.; Shen, Q. Reverse signaling using an inducible costimulator to enhance immunogenic function of dendritic cells. *Cell. Mol. Life Sci.* **2009**, *66*, 3067–3080. [CrossRef]
8. Dianzani, C.; Minelli, R.; Mesturini, R.; Chiocchetti, A.; Barrera, G.; Boscolo, S.; Sarasso, C.; Gigliotti, C.L.; Sblattero, D.; Yagi, J.; et al. B7h triggering inhibits umbilical vascular endothelial cell adhesiveness to tumor cell lines and polymorphonuclear cells. *J. Immunol.* **2010**, *185*, 3970–3979. [CrossRef]
9. Dianzani, C.; Minelli, R.; Gigliotti, C.L.; Occhipinti, S.; Giovarelli, M.; Conti, L.; Boggio, E.; Shivakumar, Y.; Baldanzi, G.; Malacarne, V.; et al. B7h triggering inhibits the migration of tumor cell lines. *J. Immunol.* **2014**, *192*, 4921–4931. [CrossRef]

10. Occhipinti, S.; Dianzani, C.; Chiocchetti, A.; Boggio, E.; Clemente, N.; Gigliotti, C.L.; Soluri, M.F.; Minelli, R.; Fantozzi, R.; Yagi, J.; et al. Triggering of B7h by the ICOS modulates maturation and migration of monocyte-derived dendritic cells. *J. Immunol.* **2013**, *190*, 1125–1134. [CrossRef]

11. Gigliotti, C.L.; Boggio, E.; Clemente, N.; Shivakumar, Y.; Toth, E.; Sblattero, D.; D'Amelio, P.; Isaia, G.C.; Dianzani, C.; Yagi, J.; et al. ICOS-Ligand Triggering Impairs Osteoclast Differentiation and Function In Vitro and In Vivo. *J. Immunol.* **2016**, *197*, 3905–3916. [CrossRef] [PubMed]

12. Raineri, D.; Dianzani, C.; Cappellano, G.; Maione, F.; Baldanzi, G.; Iacobucci, I.; Clemente, N.; Baldone, G.; Boggio, E.; Gigliotti, C.L.; et al. Osteopontin binds ICOSL promoting tumor metastasis. *Commun. Biol.* **2020**, *3*, 615. [CrossRef] [PubMed]

13. Weber, C.E.; Li, N.Y.; Wai, P.Y.; Kuo, P.C. Epithelial-mesenchymal transition, TGF-β, and osteopontin in wound healing and tissue remodeling after injury. *J. Burn Care Res.* **2012**, *33*, 311–318. [CrossRef] [PubMed]

14. Mori, R.; Shaw, T.J.; Martin, P. Molecular mechanisms linking wound inflammation and fibrosis: Knockdown of osteopontin leads to rapid repair and reduced scarring. *J. Exp. Med.* **2008**, *205*, 43–51. [CrossRef]

15. Maeda, S.; Fujimoto, M.; Matsushita, T.; Hamaguchi, Y.; Takehara, K.; Hasegawa, M. Inducible costimulator (ICOS) and ICOS ligand signaling has pivotal roles in skin wound healing via cytokine production. *Am. J. Pathol.* **2011**, *179*, 2360–2369. [CrossRef]

16. Johnson, B.Z.; Stevenson, A.W.; Prêle, C.M.; Fear, M.W.; Wood, F.M. The Role of IL-6 in Skin Fibrosis and Cutaneous Wound Healing. *Biomedicines* **2020**, *8*, 101. [CrossRef]

17. Ramavath, N.N.; Gadipudi, L.L.; Provera, A.; Gigliotti, L.C.; Boggio, E.; Bozzola, C.; Albano, E.; Dianzani, U.; Sutti, S. Inducible T-Cell Costimulator Mediates Lymphocyte/Macrophage Interactions During Liver Repair. *Front. Immunol.* **2021**, *12*, 786680. [CrossRef]

18. Clemente, N.; Boggio, E.; Gigliotti, L.C.; Raineri, D.; Ferrara, B.; Miglio, G.; Argenziano, M.; Chiocchetti, A.; Cappellano, G.; Trotta, F.; et al. Immunotherapy of experimental melanoma with ICOS-Fc loaded in biocompatible and biodegradable nanoparticles. *J. Control. Release* **2020**, *320*, 112–124. [CrossRef]

19. Darby, I.A.; Laverdet, B.; Bonté, F.; Desmoulière, A. Fibroblasts and myofibroblasts in wound healing. *Clin. Cosmet. Investig. Dermatol.* **2014**, *7*, 301–311.

20. Raineri, D.; Cappellano, G.; Vilardo, B.; Maione, F.; Clemente, N.; Canciani, E.; Boggio, E.; Gigliotti, C.L.; Monge, C.; Dianzani, C.; et al. Inducible T-Cell Costimulator Ligand Plays a Dual Role in Melanoma Metastasis upon Binding to Osteopontin or Inducible T-Cell Costimulator. *Biomedicines* **2021**, *10*, 51. [CrossRef]

21. Boggio, E.; Gigliotti, C.L.; Moia, R.; Scotta, A.; Crespi, I.; Boggione, P.; De Paoli, L.; Deambrogi, C.; Garzaro, M.; Vidali, M.; et al. Inducible T-cell co-stimulator (ICOS) and ICOS ligand are novel players in the multiple-myeloma microenvironment. *Br. J. Haematol.* **2022**, *196*, 1369–1380. [CrossRef] [PubMed]

22. Cui, K.; Ardell, C.L.; Podolnikova, N.P.; Yakubenko, V.P. Distinct Migratory Properties of M1, M2, and Resident Macrophages Are Regulated by αDβ2 and αMβ2 Integrin-Mediated Adhesion. *Front. Immunol.* **2018**, *9*, 2650. [CrossRef] [PubMed]

23. Wang, F.; Chen, S.; Liu, H.B.; Parent, C.A.; Coulombe, P.A. Keratin 6 regulates collective keratinocyte migration by altering cell-cell and cell-matrix adhesion. *J. Cell Biol.* **2018**, *217*, 4314–4330. [CrossRef] [PubMed]

3.2 ICOS-Fc application in sepsis

Although ICOS/ICOSL system has been poorly investigated in sepsis context, surprising data were collected evaluating ICOS-Fc effect on the complex interplay of pro- and anti-inflammatory host response developing in septic patients.

Sepsis is one of the most frequent causes of death worldwide and there is still no specific treatment available (Rudd et al., 2020; Fleischmann-Struzek & Rudd, 2023). It is a life-threatening medical emergency characterized by hyperinflammation, largely driven by innate immune cells, and immunosuppression, mainly affecting adaptive immunity, whose altered interplay results in multiple lethal organ dysfunction (Boomer et al., 2011; Hotchkiss et al., 2013; X. Zhao et al., 2014).

In this context ICOS/ICOSL pathway may play an important role in regulating the hyperinflammation and immunosuppression caused by sepsis. Recent findings reports that septic patients showed reduced ICOS expression in whole blood (Möhnle et al., 2018) and how organ dysfunction is strongly associated with that (Menéndez et al., 2019). Considering the well documented bidirectional signals of ICOS/ICOSL, it has been extensively supported how ICOS triggering modulate cytokine secretion in activated T-cells and how it is able to regulate T-cell function at inflammation sites by supporting the differentiation of Treg and Th17 cells (Dianzani et al., 2010, 2014; Clemente et al., 2020). If on one side, Th17 cells are responsible of amplifying the inflammatory response, through the synthesis of proinflammatory factors (IL-1β, IL-6, and TNFα), on the other side the immune homeostasis is maintained by Tregs secretion of anti-inflammatory factors (TGF-β and IL-10) (L. Chen et al., 2022). Both of them play a crucial role in maintaining immune homeostasis, thus their imbalance is related to the occurrence and development of sepsis (Xia et al., 2020). Considering the high percentage of circulating Treg cells in septic patients and animals (Kurosawa et al., 2008; Leng et al., 2013), could be worth of investigation the ICOS triggering role in the septic immunosuppressive status.

Moreover, ICOSL triggering could be related to the modulation of maturation and migration of macrophage and DCs and the endothelial cell adhesiveness, resulting in an anti-inflammatory effect (Occhipinti et al., 2013). In addition, in the septic patient has been highlighted an increased serum levels of another ligand of ICOSL, osteopontin (OPN), which in normal condition carries out its function acting against virus, bacteria and parasite infections. However, when its protective effects are overweighed by its proinflammatory property, it becomes responsible of greater inflammatory response and increased mortality of severe sepsis (Fortis et al., 2015).

Considering the interesting functional network depicted between ICOS, ICOSL and OPN, ICOS-Fc treatment was proposed as a novel immunomodulatory pharmacological approach, which acts as antagonist of ICOS, agonist of ICOSL and potentially capable of inhibiting proinflammatory activities of OPN.

This work was performed in collaboration with the laboratory of Professor Massimo Collino of the Department of Neurosciences "Rita Levi Montalcini" (University of Turin, Italy).

ICOS-Fc as innovative immunomodulatory approach to counteract inflammation and organ in sepsis

Background: Sepsis results from a disordered infection response of the host, which can pose a threat to life and causes death at intensive care units global. The altered immune homeostasis caused in sepsis context is fostered by an imbalance of Treg and Th17 cells mediated signaling towards an excessive proinflammatory OPN-induced one, responsible of ending in the compromised organ dysfunction (Xia et al., 2020).

Although it is still slightly investigated, recently interesting findings helped to depict more in depth the role of ICOS/ICOSL pathway in sepsis context. Indeed, septic patients showed a reduced ICOS expression in whole blood, an increased percentage of Treg cells explaining the ICOS triggering crucial involvement and an increased serum levels of pro-inflammatory mediator OPN, another ligand of ICOSL.

Starting from the recent findings, ICOS-Fc was proposed as an innovative immunomodulatory drug, capable of modulating cytokine release and cell migration to inflamed tissues by acting on both ICOS and ICOSL, as an antagonist/agonist respectively (Dianzani et al., 2010; Occhipinti et al., 2013; Dianzani et al., 2014; Gigliotti et al., 2016; Ramavath et al., 2021; Stoppa et al., 2022).

Aim: The aim of this research was investigating, in a murine model of sepsis, the potential protective effects of ICOS/ICOSL immunomodulation by administering ICOS-Fc.

Method: A polymicrobial sepsis mouse model was performed by carrying out a cecal ligation and puncture (CLP) surgery on both WT mice and knockout mice (KO) for ICOS, ICOSL and OPN. Administration of ICOS-Fc, ^{F119S}ICOS-Fc, a mutated form uncapable to bind ICOSL, or vehicle was intravenously injected after 1h from the surgical procedure 24h after surgery clinical score and body temperature were recorded; finally, organs (liver and kidney) and plasma were collected for analyses.

Multiplex array was used to evaluate plasma cytokines, systemic levels of AST and ALT (as markers of hepatocellular injury), creatinine and urea (as markers of renal dysfunction). To investigate leukocyte tissue infiltration, myeloperoxidase (MPO) activity analysis was performed on both liver and kidney samples. Western blot analysis was performed to investigate the degree of phosphorylation of FAK/p38 axis, expression of the inflammasome (NLRP3) and cleaved caspase-1 in organs tissues.

Results: ICOS-Fc treatment showed to be able to significantly ameliorate the clinical sepsis context, acting on all the sepsis parameters observed dramatically increased in vehicle-treated septic mice. Indeed, a severe sepsis context is defined by a low body temperature, hepatocellular injury and renal dysfunction correlated to an increase of plasma AST/ALT and creatinine/urea levels respectively.

Compared to the higher clinically score detected in CLP-induced sepsis WT, ICOS-/- and ICOSL-/- KO mice, CLP-OPN-/- mice developed a milder sepsis confirming the OPN crucial role in sepsis pathogenesis.

Intriguingly, ICOS-Fc treatment improved in WT and ICOS-/- mice clinical score and hypothermia, significantly decreased ALT, AST, creatinine and urea levels and reduced specific cytokines release (TNFα, IL-1β, IL-6, IFNγ and IL-10).

The ICOS-Fc effectiveness showed in ICOS-/- mice, compared to the not relevant one found in ICOSL/- mice, suggested how ICOS-Fc protective effect is due to ICOSL triggering. More time confirmed from the evidence that in all animals treated with [F119S]ICOS-Fc was not shown any effect.

The different ICOSL expression in liver and kidney tissues could explain the discrepancy of data collected about organ injury analysis. On one side, ICOS-Fc promoted a decreased levels of ALT, AST, creatinine and urea in both tissues analyzed, while only in kidney a decreased MPO activity. Since hepatocytes did not express ICOSL, the hepatic protection detected after ICOS-Fc administration could be due to a resolution of inflammation rather than a reduction in leukocyte infiltration.

More details about ICOS-Fc immunomodulation molecular mechanism were given studying its effect on crucial inflammatory pathways activated during sepsis (liver and kidney samples of WT mice belonging to Sham, CLP and CLP treated with ICOS-Fc groups). ICOS-Fc significantly attenuated FAK and p38 MAPK phosphorylation, whose activation promote increased expression/secretion of pro-inflammatory cytokines which ends up in the septic cytokine storm and lethal organ failure correlated. Moreover, ICOS-Fc showed itself to interfere with crosstalk linking FAK to NLRP3 activation: both liver and kidney reduced expression of NRLP3 were detected next to its downstream mediator caspase-1.

Conclusion: Collectively, these promising results show the beneficial effects of ICOS-Fc in sepsis mouse model, suggesting ICOS/ICOSL axis as an important target in sepsis-induced inflammation and organ dysfunction.

frontiers | Frontiers in Immunology

ICOS-Fc as innovative immunomodulatory approach to counteract inflammation and organ injury in sepsis

Gustavo Ferreira Alves[1], Ian Stoppa[2], Eleonora Aimaretti[3], Chiara Monge[4], Raffaella Mastrocola[3], Elisa Porchietto[5], Giacomo Einaudi[5], Debora Collotta[1], Ilaria Bertocchi[1], Elena Boggio[2], Casimiro Luca Gigliotti[2], Nausicaa Clemente[2], Manuela Aragno[3], Daniel Fernandes[6], Carlo Cifani[5], Christoph Thiemermann[7], Chiara Dianzani[4], Umberto Dianzani[2†] and Massimo Collino[1*†]

[1]Department of Neurosciences (Rita Levi Montalcini), University of Turin, Turin, Italy, [2]Department of Health Sciences, Università del Piemonte Orientale, Novara, Italy, [3]Department of Clinical and Biological Sciences, University of Turin, Turin, Italy, [4]Department of Drug Science and Technology, University of Turin, Turin, Italy, [5]Pharmacology Unit, School of Pharmacy, University of Camerino, Camerino, Italy, [6]Department of Pharmacology, Federal University of Santa Catarina, Florianópolis, Brazil, [7]William Harvey Research Institute, Bart's and The London School of Medicine and Dentistry, Queen Mary University of London, London, United Kingdom

Inducible T cell co-stimulator (ICOS), an immune checkpoint protein expressed on activated T cells and its unique ligand, ICOSL, which is expressed on antigen-presenting cells and non-hematopoietic cells, have been extensively investigated in the immune response. Recent findings showed that a soluble recombinant form of ICOS (ICOS-Fc) can act as an innovative immunomodulatory drug as both antagonist of ICOS and agonist of ICOSL, modulating cytokine release and cell migration to inflamed tissues. Although the ICOS-ICOSL pathway has been poorly investigated in the septic context, a few studies have reported that septic patients have reduced ICOS expression in whole blood and increased serum levels of osteopontin (OPN), that is another ligand of ICOSL. Thus, we investigated the pathological role of the ICOS-ICOSL axis in the context of sepsis and the potential protective effects of its immunomodulation by administering ICOS-Fc in a murine model of sepsis. Polymicrobial sepsis was induced by cecal ligation and puncture (CLP) in five-month-old male wild-type (WT) C57BL/6, ICOS$^{-/-}$, ICOSL$^{-/-}$ and OPN$^{-/-}$ mice. One hour after the surgical procedure, either CLP or Sham (control) mice were randomly assigned to receive once ICOS-Fc, ^{F119S}ICOS-Fc, a mutated form uncapable to bind ICOSL, or vehicle intravenously. Organs and plasma were collected 24 h after surgery for analyses. When compared to Sham mice, WT mice that underwent CLP developed within 24 h a higher clinical severity score, a reduced body temperature, an increase in plasma cytokines (TNF-α, IL-1β, IL-6, IFN-γ and IL-10), liver injury (AST and ALT) and kidney (creatinine and urea) dysfunction. Administration of ICOS-Fc to WT CLP mice reduced all of these abnormalities caused by sepsis. Similar beneficial effects were not seen in CLP-mice

39

treated with ^{F119S}ICOS-Fc. Treatment of CLP-mice with ICOS-Fc also attenuated the sepsis-induced local activation of FAK, P38 MAPK and NLRP3 inflammasome. ICOS-Fc seemed to act at both sides of the ICOS-ICOSL interaction, as the protective effect was lost in septic knockout mice for the ICOS or ICOSL genes, whereas it was maintained in OPN knockout mice. Collectively, our data show the beneficial effects of pharmacological modulation of the ICOS-ICOSL pathway in counteracting the sepsis-induced inflammation and organ dysfunction.

Introduction

Sepsis is a life-threatening medical emergency characterized by a complex interplay of pro- and anti-inflammatory host responses, resulting in multiple organ dysfunction that can ultimately lead to death (1). Currently, deaths from sepsis correspond to nearly 20% of all deaths worldwide, and there is still no specific treatment available (2). The inducible T cell co-stimulator (ICOS, also known as CD278) belongs to the CD28 family of co-stimulatory immunoreceptors. It is a type I transmembrane glycoprotein whose expression is rapidly upregulated upon T cells activation (3). ICOS binds to its unique ligand (ICOSL, also known as CD275 or B7h), a member of the B7 family highly expressed on antigen-presenting cells (APCs) and non-hematopoietic cells under inflammatory stimuli (4–5). Thus far, the role of ICOS-ICOSL interaction has been poorly investigated in sepsis, although recent findings report that ICOS expression is reduced in whole blood of septic patients (6), and that reduced ICOS levels are strongly associated with organ dysfunction (7). To date, it is very well documented that the ICOS-ICOSL axis may display bidirectional effects. On the one hand, ICOS triggering modulates cytokine production in activated T cells and contributes to T regulatory (Treg) cells differentiation and survival (8–9). Given the fact that both animals and septic patients have an increased percentage of circulating Treg cells (10–12), it is suggestive that ICOS triggering may play a role in the septic immunosuppressive status. On the other hand, ICOSL triggering by ICOS may exert anti-inflammatory effects *via* responses, such as modulating the maturation and migration of macrophage and dendritic cells and the endothelial cell adhesiveness (13).

Recently, another ligand for ICOSL has been identified, osteopontin (OPN), an inflammatory mediator that binds to ICOSL in an alternative binding domain to that used by ICOS. Intriguingly, ICOS and OPN exert different and often opposite effects upon ICOSL triggering since OPN stimulates, whereas ICOS inhibits, migration of several cell types and tumor angiogenesis (14–16). Conventionally, a soluble recombinant form of ICOS (ICOS-Fc) has been designed by fusing a cloned extracellular portion of human or mouse ICOS with an Fc IgG1 portion and this molecule has been shown to trigger ICOSL thus promoting down-stream responses (17).

In vitro, ICOS-Fc inhibits adhesiveness of endothelial cells toward polymorphonuclear cells and tumor cells and migration of endothelial cells and tumor cells (15). These ICOS-Fc effects can also be recorded in dendritic cells (DC), along with modulated cytokine release and antigen cross-presentation in class I major histocompatibility complex molecules (13), while in osteoclasts, ICOS-Fc inhibits differentiation and function (18). *In vivo*, ICOS-Fc inhibits tumor growth and metastasis, development of osteoporosis, liver damage induced by acute inflammation following treatment with CCl4, and it favors skin wound healing (18–21). Nevertheless, little is known about the molecular mechanism(s) involved in ICOSL-mediated inflammatory response. The p38 MAPK, a well-known mediator that drives inflammation through upregulation of several pro-inflammatory cytokines such as TNF-α and IL-6 (22), and the NOD-like receptor protein 3 (NLRP3) inflammasome, able to induce the release of IL-1β and IL-18 and promote cell death by pyroptosis (23), are two of the most well characterized signaling pathways involved in the activation of the cytokine storm that contributes to organ dysfunction during sepsis. Furthermore, their pharmacological or genetic inhibition has been shown to reduce sepsis-related mortality (22–24). Finally, a non-receptor protein kinase namely Focal adhesion kinase (FAK) has been recently reported to signal inflammation downstream of the Toll-like receptor 4 upon lipopolysaccharide (LPS) challenge in macrophages and lung tissues (25). Therefore, here we investigated, for the first time, the pathological role of ICOS-ICOSL axis in the context of sepsis, its impact on selective inflammatory pathways and the potential protective effects of its

40

immunomodulation by administering ICOS-Fc in an experimental model of sepsis.

Material and methods

Animals and ethical statement

Inbred wild-type (WT, C57BL/6) mice, ICOSL knockout mice (ICOSL$^{-/-}$, B6.129P2-$Icosl^{tm1Mak}$/J), ICOS knockout mice (ICOS$^{-/-}$, B6.129P2-$Icos^{tm1Mak}$/J) and OPN knockout mice (OPN$^{-/-}$, B6.129S6(Cg)-$Spp1^{tm1Blh}$/J) were purchased from Envigo laboratories, (IT) and The Jackson Laboratory (Bar Harbor, ME, USA). Mice were housed under standard laboratory conditions, such as room temperature (25 ± 2°C) and light-controlled with free access to water and rodent chow for four weeks prior starting the experimental procedures. All animal protocols reported in this study followed the ARRIVE guidelines [26] and the recommendations for preclinical studies of sepsis provided by the MQTiPSS [27] The procedures were approved by the University's Institutional Ethics Committee as well as the National Authorities (Protocol number: 855/2021).

Cecal ligation and puncture (CLP)-induced sepsis model

Polymicrobial sepsis was carried out by CLP surgery in male, five-month-old mice. Mice were initially placed in an anesthetisia chamber (3% isoflurane -IsoFlo, Abbott Laboratories – delivered in oxygen 0.4 L/min), then kept under anaesthesia throughout surgery with 2% isoflurane delivered in oxygen 0.4 L/min *via* a nosecone. The body temperature was maintained at 37 °C through a homoeothermic blanket and constantly monitored by a rectal thermometer. Briefly, a mid-line laparotomy (~1.0 cm) was performed in the abdomen, exposing the cecum. The cecum was then totally ligated just below the ileocecal valve and a G-21 needle was used to puncture the ligated cecum in a single through-and-through manner. A small amount (droplet, ~3mm) of fecal content was released from the cecum which was carefully relocated into the peritoneum. Sham mice underwent the same surgical procedure, but without CLP. All animals received Carprofen (5 mg/kg, s.c.) as an analgesic agent and resuscitation fluid (0.9% NaCl, 50 mL/kg, s.c.) at 37°C. Mice were constantly monitored post-surgical and then placed back into fresh clean cages.

At 24 h, body temperature and a clinical score to assess symptoms consistent with murine sepsis were recorded blindly. The following 6 criteria were used for the clinical score: lethargy, piloerection, tremors, periorbital exudates, respiratory distress and diarrhea. An observed clinical score >3 was considered as severe sepsis, while a score between 3 and 1 was considered as moderate sepsis [28].

Study design

Seventy-two mice were randomized into eight groups (9 mice per group): Sham + Vehicle, CLP + Vehicle, CLP + ICOS-Fc, CLP + ^{F119S}ICOS-Fc, CLP ICOSL$^{-/-}$ + Vehicle, CLP ICOS$^{-/-}$ + Vehicle, CLP ICOS$^{-/-}$ + ICOS-Fc and OPN$^{-/-}$ + Vehicle. Treatment was given once one hour after surgery, where mice received either ICOS-Fc (100 µg each), ^{F119S}ICOS-Fc (100 µg each) or Vehicle (PBS, pH 7.4, 100 µl each) by intravenous injection (Figure 1).

Blood collection and organ harvesting

Twenty-four h after surgery all mice were anesthetized with isoflurane (3%) delivered in oxygen (0.4 L/min) and euthanized by cardiac exsanguination. Whole blood was withdrawn from each mouse in vials (EDTA 17.1 µM/mL) and plasma content was obtained after centrifugation (13,000 g, 10 min at R.T.). Organ samples (liver and kidney) were harvested and placed in cryotubes which were snap frozen in liquid nitrogen for storage at freezer -80°C. The samples were then analyzed in a blinded fashion (Figure 1).

Biomarkers of organ injury and systemic inflammation

Plasma samples were used to measure systemic levels of aspartate aminotransferase (AST) (#7036) and alanine aminotransferase (ALT) (#7018) (as markers of hepatocellular injury), creatinine (#7075) and urea (#7144) (as markers of renal dysfunction) using colorimetric clinical assay kits (FAR Diagnostics, Verona, Italy) according to the manufacturer's instructions. Systemic cytokine levels were determined in plasma using the Luminex suspension bead-based multiplexed Bio-Plex Pro™ Mouse Cytokine Th17 Panel A 6-Plex (#M6000007NY) assay (Bio-Rad, Kabelsketal, Germany). The cytokines (IL-1β, IL-6, TNF-α, IFN-γ, IL-17 and IL-10) were measured following the manufacturer's instructions.

Myeloperoxidase (MPO) activity analysis

MPO activity analysis was carried out in liver and kidney samples as previously described [29]. Tissue samples (~100 mg) were homogenized (1:5 w-v) in 20 mM PBS (pH 7.4) and then centrifuged at 4°C (13,000 g, 10 min). Pellets were resuspended in

41

FIGURE 1
Timeline of the experimental design to investigate the role of ICOS-Fc in sepsis. Wild-type mice and/or ICOSL, ICOS and OPN knockout mice were randomly selected to undergo either Sham or CLP surgery. One hour later, mice received once either Vehicle (PBS, 100 μL), ICOS-Fc (100 μg) or [F119S]ICOS-Fc (100 μg) intravenously. At 24 h all parameters were analyzed.
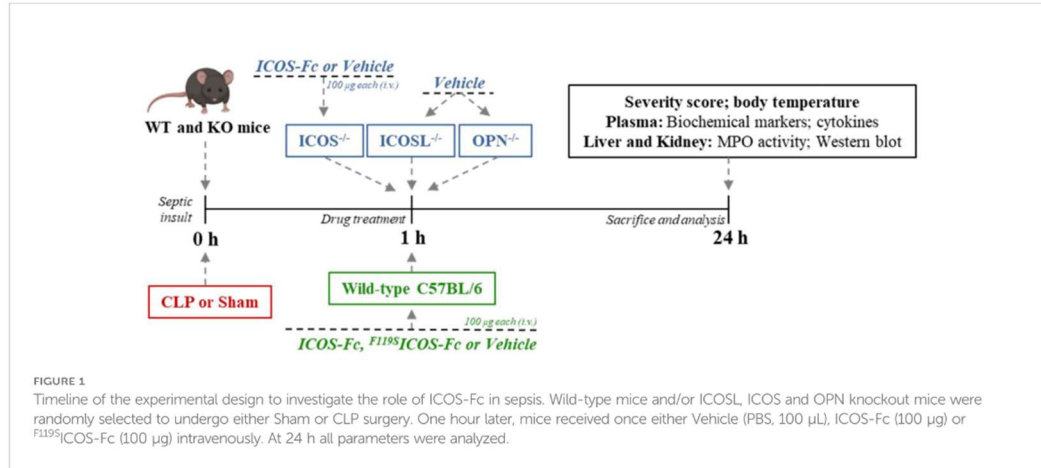
500 μL of hexadecyltrimethylammonium bromide buffer (0.5% HTAB in 50 mM PBS, pH 6.0). A second centrifugation at 4°C (13,000 g, 10 min was performed and the supernatants (30 μL) were assessed for MPO activity by measuring spectrophotometrically (650 nm) the H_2O_2-dependent oxidation of 3,3′,5,5′-tetramethylbenzidine (TMB). Bicinchoninic acid (BCA) protein assay (Pierce Biotechnology Inc., Rockford, IL, USA) was used to quantify the protein content in the final supernatant. MPO activity was expressed as optical density (O.D.) at 650 nm per mg of protein.

Western blot analysis

Semi-quantitative immunoblot technique was carried out in hepatic and renal tissue samples as previously described (30). Total proteins were extracted from 50 mg of each tissue and the total content was quantified using BCA protein method following the manufacturer's instructions. Briefly, total proteins (50 μg/well) were separated by 8 and 10% sodium dodecyl sulphate-polyacrylamide gel electrophoresis (SDS-PAGE) and transferred to a polyvinylidene difluoride (PVDF) membrane, which was then blocked with 5% non-fat dry milk prepared in TBS-T buffer for 1 h at RT, followed by incubation with primary antibodies at the dilution 1:1000., rabbit anti-Thr[180]/anti-Tyr[182] p38 (Cell Signaling #9211); rabbit anti-total p38 (Cell Signaling #9212); mouse anti-NRLP3 (Adipogen- AG-20B-0014-C100); rabbit anti-Caspase-1 (Cell Signaling #24232); rabbit anti-Tyr[397] FAK (Cell Signaling #3283); rabbit anti-total FAK (Cell Signaling #3285). The membranes were then incubated with a secondary antibody conjugated with horseradish peroxidase (HRP) at the dilution 1:10000 for 1 h at RT (anti-mouse or anti-rabbit, Cell Signaling #7076 and #7074, respectively). Afterwards, the membranes were stripped and incubated with rabbit anti-β-actin (Cell Signaling #4970). Immune complexes were visualized by chemiluminescence and the densitometric analysis was performed using Bio-Rad Image Lab Software 6.0.1. Results were normalized to sham bands.

Statistical analysis and data presentation

Sample size was determined on the basis of prior power calculations using G-Power 3.1™ software (31). Data are expressed as dot plots (for each mouse) and as mean ± S.E.M of 9 mice per group. Shapiro-Wilk and Bartlett tests were used to verify data distribution and the homogeneity of variances, respectively. The statistical analysis was performed by one-way ANOVA, followed by Bonferroni's *post-hoc* test. Data not normally distributed, a non-parametric statistical analysis was applied through Kruskal-Wallis followed by Dunn's *post hoc*-test as indicated in the figure legends. Statistical significance was set at $P < 0.05$. Statistical analysis was performed using GraphPad Prism® software version 7.05 (San Diego, California, USA).

Materials

Unless otherwise stated, all reagents were purchased from the Sigma-Aldrich Company Ltd. (St. Louis, Missouri, USA).

42

Results

ICOS-Fc-mediated immunomodulation attenuates clinical status and organ injury/dysfunction triggered by sepsis

Sepsis was induced by CLP in WT mice treated with vehicle, ICOS-Fc or [F119S]ICOS-Fc (unable to bind ICOSL) and clinical scores and body temperature were recorded after 24 h. Moreover, sepsis was induced in mice deficient for ICOS, ICOSL, or OPN to assess the role the endogenous molecules of the ICOS/ICOSL/OPN system. Finally, a group of ICOS-deficient mice received ICOS-Fc treatment to evaluate the effect of the drug in the absence of the endogenous ICOS.
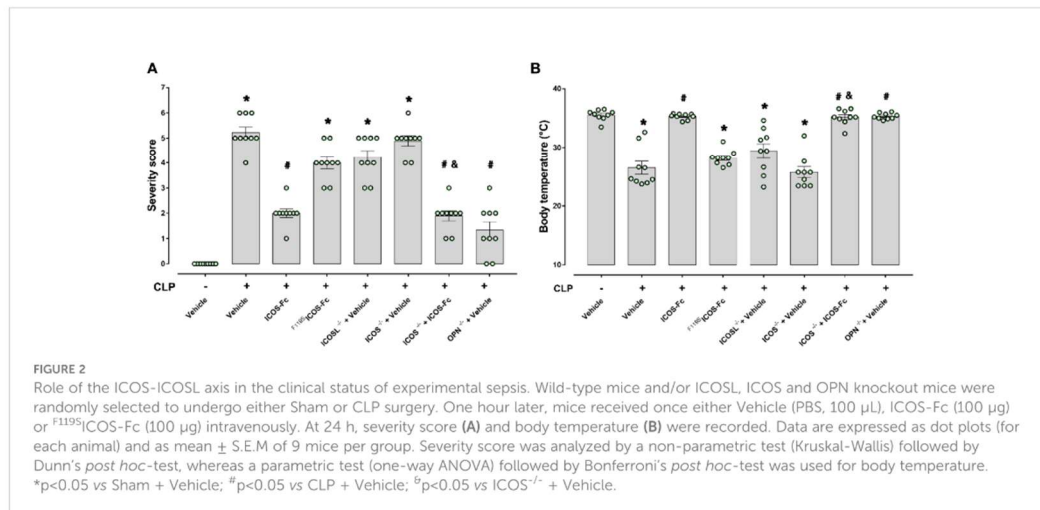
Results showed that, as expected, CLP-induced sepsis in WT mice led to a higher clinical severity score (Figure 2A) when compared to Sham WT mice, which was also associated with lower body temperature (Figure 2B). Intriguingly, treatment with ICOS-Fc improved both clinical score and hyphotermia in WT septic mice, whereas treatment with [F119S]ICOS-Fc had no effect (Figures 2A, B). Analysis of CLP knockout mice showed that ICOS^{-/-} and ICOSL^{-/-} mice showed similar clinical scores and decreased body temperatures as WT mice, whereas OPN^{-/-} mice developed milder sepsis, with lower clinical scores and higher body temperature than WT mice. In ICOS^{-/-} mice, treatment with ICOS-Fc induced similar positive effects as in WT mice (Figures 2A, B).

To investigate organ injury or dysfunction, plasma levels of ALT, AST, creatinine and urea were evaluated in these mice. Figure 3 shows that results mirrored those shown in Fig.2: CLP-induced sepsis caused striking increase of ALT, AST, creatinine and urea levels in WT type mice, and these levels were decreased by treatment with ICOS-Fc, but not [F119S]ICOS-Fc. Levels of these markers were increased also in CLP ICOS^{-/-} and ICOSL^{-/-} mice and urea levels were even higher in ICOS^{-/-} than in WT mice. In CLP ICOS^{-/-} mice, treatment with ICOS-Fc significantly decreased all these markers. In CLP OPN^{-/-} mice, levels of these markers were significantly lower than in CLP WT mice.

ICOS-Fc administration modulates experimental sepsis-induced cytokine storm

The 6 cytokines were measured systemically in plasma samples by using a multiplex array. Figure 4 shows that, in WT mice, CLP-induced sepsis led to a cytokine storm with significant increase of levels of IL-1β, IL-6, IL-10, TNF-α, IFN-γ and a slight not significant increase of IL-17 compared to Sham mice. Administration of ICOS-Fc to WT CLP mice induced a significant decrease of IL-1β and TNF-α, whereas [F119S]ICOS-Fc had no effect. Levels of IL-1β, IL-6, IL-10, TNF-α, and IFN-γ were also increased in CLP ICOS^{-/-} and ICOSL^{-/-} mice at levels similar to those observed in CLP WT mice. Moreover, CLP ICOSL^{-/-} mice showed higher levels of IL-17 than Sham mice, and CLP ICOS^{-/-} mice displayed higher levels of TNF-α and, especially, IL-10 than CLP WT mice. The CLP ICOS^{-/-} mice treated with ICOS-Fc significantly decreased levels of IL-1β, IL-6 and IL-10 compared to the untreated counterparts. In CLP OPN^{-/-} mice, the increase of these cytokines was in general

FIGURE 2
Role of the ICOS-ICOSL axis in the clinical status of experimental sepsis. Wild-type mice and/or ICOSL, ICOS and OPN knockout mice were randomly selected to undergo either Sham or CLP surgery. One hour later, mice received once either Vehicle (PBS, 100 µL), ICOS-Fc (100 µg) or [F119S]ICOS-Fc (100 µg) intravenously. At 24 h, severity score **(A)** and body temperature **(B)** were recorded. Data are expressed as dot plots (for each animal) and as mean ± S.E.M of 9 mice per group. Severity score was analyzed by a non-parametric test (Kruskal-Wallis) followed by Dunn's *post hoc*-test, whereas a parametric test (one-way ANOVA) followed by Bonferroni's *post hoc*-test was used for body temperature. *p<0.05 *vs* Sham + Vehicle; #p<0.05 *vs* CLP + Vehicle; ᵇp<0.05 *vs* ICOS^{-/-} + Vehicle.

43

FIGURE 3

Effect of ICOS-ICOSL axis immunomodulation on sepsis-induced organ damage biomarkers. Wild-type mice and/or ICOSL, ICOS and OPN knockout mice were randomly selected to undergo either Sham or CLP surgery. One hour later, mice received once either Vehicle (PBS, 100 µL), ICOS-Fc (100 µg) or ^{F119S}ICOS-Fc (100 µg) intravenously. At 24 h, blood samples were withdrawn from each mouse and plasma levels of alanine transaminase (ALT) **(A)**, aspartate transaminase (AST) **(B)**, creatinine **(C)** and urea **(D)** were determined. Data are expressed as dot plots (for each animal) and as mean $\pm$ S.E.M of 9 mice per group. Statistical analysis was performed by one-way ANOVA followed by Bonferroni's *post hoc* test. *p<0.05 *vs* Sham + Vehicle; #p<0.05 *vs* CLP + Vehicle; $^{\&}$p<0.05 *vs* ICOS$^{-/-}$ + Vehicle.

moderate, with levels of IL-6, IL-10, TNF-α and IFN-γ higher than in Sham mice, and levels of IL-1β and IL-6 lower than in CLP WT mice.
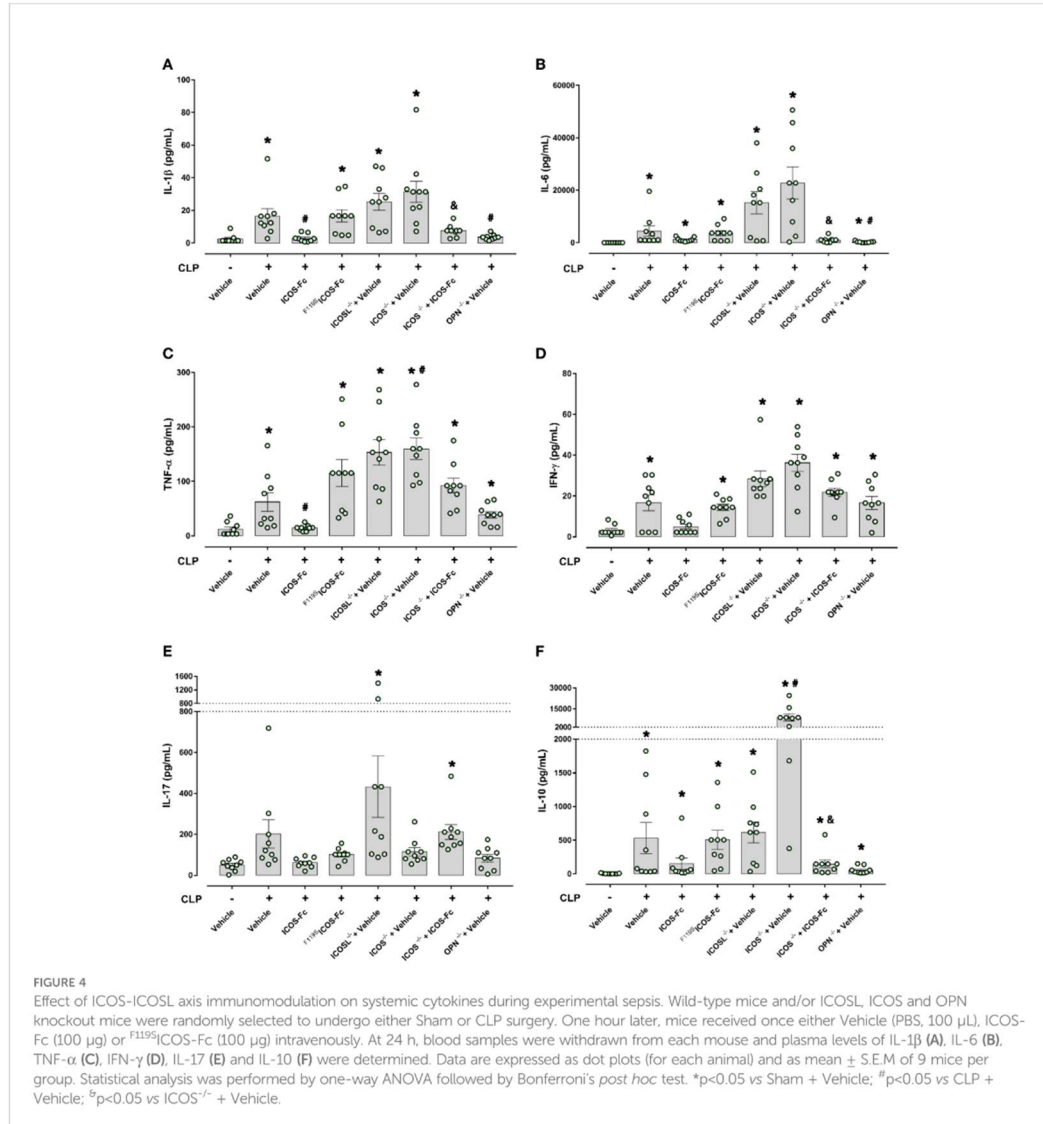
ICOS-Fc treatment reduces sepsis-induced increase in MPO activity in the kidney

MPO activity was assessed in the liver and kidney, as an indirect biomarker of leukocyte tissue infiltration (Figure 5). When compared to Sham mice, CLP WT mice had increased MPO activity in both liver and kidney samples, and MPO activity was significanly decreased by ICOS-Fc (but not ^{F119S}ICOS-Fc treatment) in the kidney, but not in the liver. In the liver, MPO activity was similarly increased also in CLP ICOS$^{-/-}$, ICOSL$^{-/-}$, and OPN$^{-/-}$ mice, and it was not modified by ICOS-Fc treatment in CLP ICOS$^{-/-}$ mice. In the kidney, MPO activity was increased in CLP ICOS$^{-/-}$ and ICOSL$^{-/-}$ mice, and treatment with ICOS-Fc decreased MPO activity in CLP ICOS$^{-/-}$ mice. By contrast, CLP OPN$^{-/-}$ mice showed lower MPO levels in the kidney than CLP WT mice.

ICOS-Fc treatment reduces local FAK/p38 signalling and NLRP3 inflammasome activation in septic mice

In order to better elucidate the molecular mechanism underlying the beneficial effects evoked by ICOS-Fc administration, we focused on WT mice investigating the changes in some signaling cascades, previously documented to be affected by the ICOS-ICOSL axis and, at the same time, known to exert key role in sepsis pathogenesis. Western blot analysis showed that CLP mice showed significant increase of the phosphorylation of FAK at Tyr^{397} and p38 MAPK at Thr^{180}/Tyr^{182} in both hepatic (Figures 6A, C) and renal (Figures 6B, D) tissues, when compared to Sham mice. Interestingly, mice treatment with ICOS-Fc significantly attenuated the degree of phosphorylation of FAK/p38 axis in both tissues, thus suggesting reduced activation of these signaling pathways (Figures 6A–D).

We then assessed the activation of the inflammasome, by evaluating the expression of NLRP3 and cleaved caspase-1 in both liver and kidney samples (Figures 6E–H). Results showed that, in both tissues, CLP-induced sepsis significantly increased both
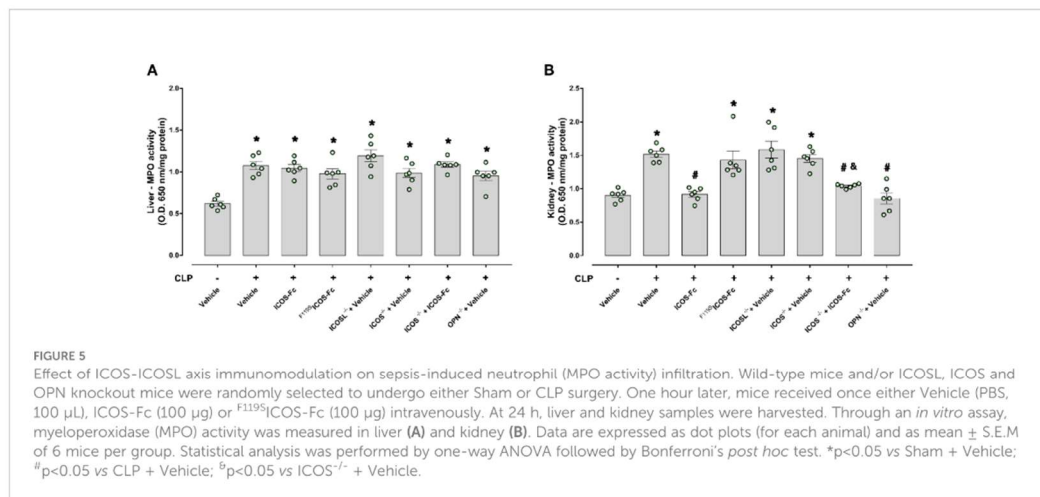
44

FIGURE 4

Effect of ICOS-ICOSL axis immunomodulation on systemic cytokines during experimental sepsis. Wild-type mice and/or ICOSL, ICOS and OPN knockout mice were randomly selected to undergo either Sham or CLP surgery. One hour later, mice received once either Vehicle (PBS, 100 µL), ICOS-Fc (100 µg) or ^{F119S}ICOS-Fc (100 µg) intravenously. At 24 h, blood samples were withdrawn from each mouse and plasma levels of IL-1β **(A)**, IL-6 **(B)**, TNF-α **(C)**, IFN-γ **(D)**, IL-17 **(E)** and IL-10 **(F)** were determined. Data are expressed as dot plots (for each animal) and as mean ± S.E.M of 9 mice per group. Statistical analysis was performed by one-way ANOVA followed by Bonferroni's *post hoc* test. *p<0.05 *vs* Sham + Vehicle; $^{#}$p<0.05 *vs* CLP + Vehicle; $^{&}$p<0.05 *vs* ICOS$^{-/-}$ + Vehicle.

molecules, and the increase was inhibited by mice treatment with ICOS-Fc (Figures 6E–H).

Discussion

Currently, most research on sepsis is focused on blocking the initial hyperinflammation, which in turn has resulted in promising outcomes. However, recent reports showed that both pro- and anti-inflammatory responses occur immediately and simultaneously after the onset of sepsis and most patients who survive this initial hyperinflammatory phase develop an immunosuppressive phase that can progress to late deaths (1, 32 and 33). Among the main causes of death in this immunosuppressive phase, the failure to control a primary infection and/or secondary hospital-acquired infections stands out (34). In the present study we report for the first time

45

FIGURE 5
Effect of ICOS-ICOSL axis immunomodulation on sepsis-induced neutrophil (MPO activity) infiltration. Wild-type mice and/or ICOSL, ICOS and OPN knockout mice were randomly selected to undergo either Sham or CLP surgery. One hour later, mice received once either Vehicle (PBS, 100 µL), ICOS-Fc (100 µg) or [F119S]ICOS-Fc (100 µg) intravenously. At 24 h, liver and kidney samples were harvested. Through an *in vitro* assay, myeloperoxidase (MPO) activity was measured in liver **(A)** and kidney **(B)**. Data are expressed as dot plots (for each animal) and as mean ± S.E.M of 6 mice per group. Statistical analysis was performed by one-way ANOVA followed by Bonferroni's *post hoc* test. *$p < 0.05$ *vs* Sham + Vehicle; [#]$p < 0.05$ *vs* CLP + Vehicle; [δ]$p < 0.05$ *vs* ICOS$^{-/-}$ + Vehicle.

that ICOS-ICOSL axis may play a role in regulation of uncontrolled inflammation and organ injury induced by sepsis and that treatment of septic mice with ICOS-Fc may represent a novel immunomodulatory pharmacological approach that can simultaneously counteract both sepsis-induced hyperinflammation and immunosuppression.

These findings were obtained by evoking polymicrobial sepsis in either WT mice and knockout mice for ICOS, ICOSL and OPN genes. As expected, severe sepsis (score ≥3) was observed in vehicle-treated septic mice, suggesting potential late deaths, since the clinical scoring system is used as a surrogate marker of mortality. This detrimental effect was also associated with low body temperature (~27°C), as similarly, hypothermia is another surrogate marker of mortality, as a 5°C decrease over time or <30°C has also been shown to predict death in CLP-induced septic mice (35). Moreover, septic mice showed liver and kidney damage, displayed by increase of plasma AST/ALT and creatinine/urea levels, respectively, which is in line with the notion that sepsis can cause multiple organ failure including hepatocellular injury and renal dysfunction.

Intriguingly, treatment with ICOS-Fc substantially ameliorated the clinical picture by significantly decreasing all these parameters of sepsis. The effect was specific since no protection was detected following administration of [F119S]ICOS-Fc (a mutated form of ICOS-Fc carrying a phenylalanine-to-serine substitution at position 119).

Theoretically, the protective activity of ICOS-Fc might be ascribed to a twofold mechanism, i.e. on the one hand to the inhibition of the endogenous ICOS activity and, on the other hand, to triggering of the endogenous ICOSL. However, the effectiveness of ICOS-Fc not only in WT mice but also in ICOS$^{-/-}$

mice, lacking the endogenous ICOS, strongly suggest that the main protective effect on sepsis is due to triggering of ICOSL, which is in line with previous works showing that ICOSL triggering by ICOS-Fc elicits several anti-inflammatory activities both *in vitro* and *in vivo* (13, 15, 16, 19).

These results are in keeping also with recent findings showing that ICOS-Fc protects against liver damage through a shift of pro-inflammatory monocyte-derived macrophages to an anti-inflammatory phenotype (20). In parallel, the direct renoprotective effect triggered by ICOS-Fc treatment is supported by a recent study showing a key role of ICOSL in preventing early kidney disease, possibly through a selective binding to podocyte αvβ3 integrin, in which ICOSL serves as an αvβ3-selective antagonist that maintains adequate glomerular filtration (36).

The use of knockout mice highlighted that, in sepsis, a key role may be played by OPN as all the above septic parameters were significantly decreased in OPN$^{-/-}$ mice, so that OPN deficiency mirrored the effect of ICOS-Fc in WT mice. This finding is in line with data showing that, in humans, OPN levels are increased in sepsis (37) and OPN might be involved in the sepsis pathogenesis, possibly by supporting IL-6 secretion (38). Moreover, several reports showed that ICOS-Fc inhibits several proinflammatory activities of OPN *in vitro* and *in vivo* (16, 37, 39 and 40). Our findings are in keeping also with recent data showing that macrophage-derived OPN promotes glomerular injury in an experimental model of inflammatory and progressive kidney disease (41). OPN is an heavily phosphorylated extracellular protein, expressed and secreted by several cell types, including macrophages,
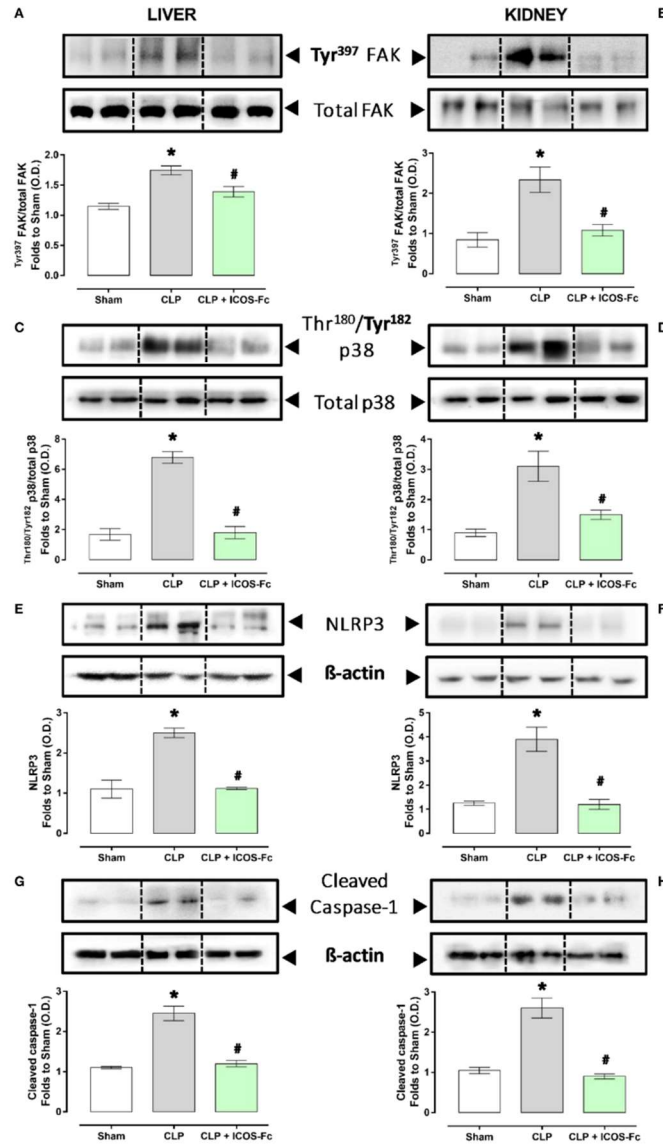
46

FIGURE 6

Effect of ICOS-ICOSL axis immunomodulation on tissue inflammatory pathways during experimental sepsis. Wild-type mice and/or ICOSL, ICOS and OPN knockout mice were randomly selected to undergo either Sham or CLP surgery. One hour later, mice received once either Vehicle (PBS, 100 μL), ICOS-Fc (100 μg) or ᶠ¹¹⁹ˢICOS-Fc (100 μg) intravenously. At 24 h, liver and kidney samples were harvested, and total proteins were extracted from them. Western blotting analysis for phosphorylation of Tyr³⁹⁷ on FAK in the liver **(A)** and kidney **(B)** were normalized to total FAK; Phosphorylation of Thr¹⁸⁰/Tyr¹⁸² on p38 in the liver **(C)** and kidney **(D)** were normalized to total p38; NLRP3 expression in the liver **(E)** and kidney **(F)** were corrected against β-actin and normalized using the Sham related bands; Cleaved caspase-1 expression in the liver **(G)** and kidney **(H)** were corrected against β-actin and normalized using the Sham related bands. Densitometric analysis of the bands are expressed as relative optical density (O.D.). Data are expressed as dot plots (for each animal) and as mean ± S.E.M of 4-5 mice per group. Statistical analysis was performed by one-way ANOVA followed by Bonferroni's *post hoc* test. *p<0.05 *vs* Sham + Vehicle; #p<0.05 *vs* CLP + Vehicle.

47

endothelial cells, dendritic cells and T-cells. It can act as a cytokine mediating several biological functions, including cell migration, adhesion, activation of inflammatory cells, and modulation of T cell activation supporting differentiation of proinflammatory type 1 (Th1) and type 17 (Th17) Th cells (42).

Analysis of plasmatic cytokines showed that, in all mouse strains, sepsis was accompanied by increase of IL-1β, IL-6, IL-10, TNF-α and IFN-γ. Moreover, increase of TNF-α and, especially, IL-10 was particularly striking in ICOS$^{-/-}$ mice, which may point out that ICOS deficiency causes a dysregulation of activation of M1 and M2 macrophages. However, treatment with ICOS-Fc significantly decreased IL-1β and TNF-α in WT mice and IL-1β, IL-6 and IL-10 in ICOS$^{-/-}$ mice indicating that ICOS-Fc substantially downmodulates the cytokine storm in sepsis. In OPN$^{-/-}$ mice, increase of these cytokines was in general moderate, with a significant decrease of IL-1β and IL-6, in line with the mild sepsis developed by these mice.
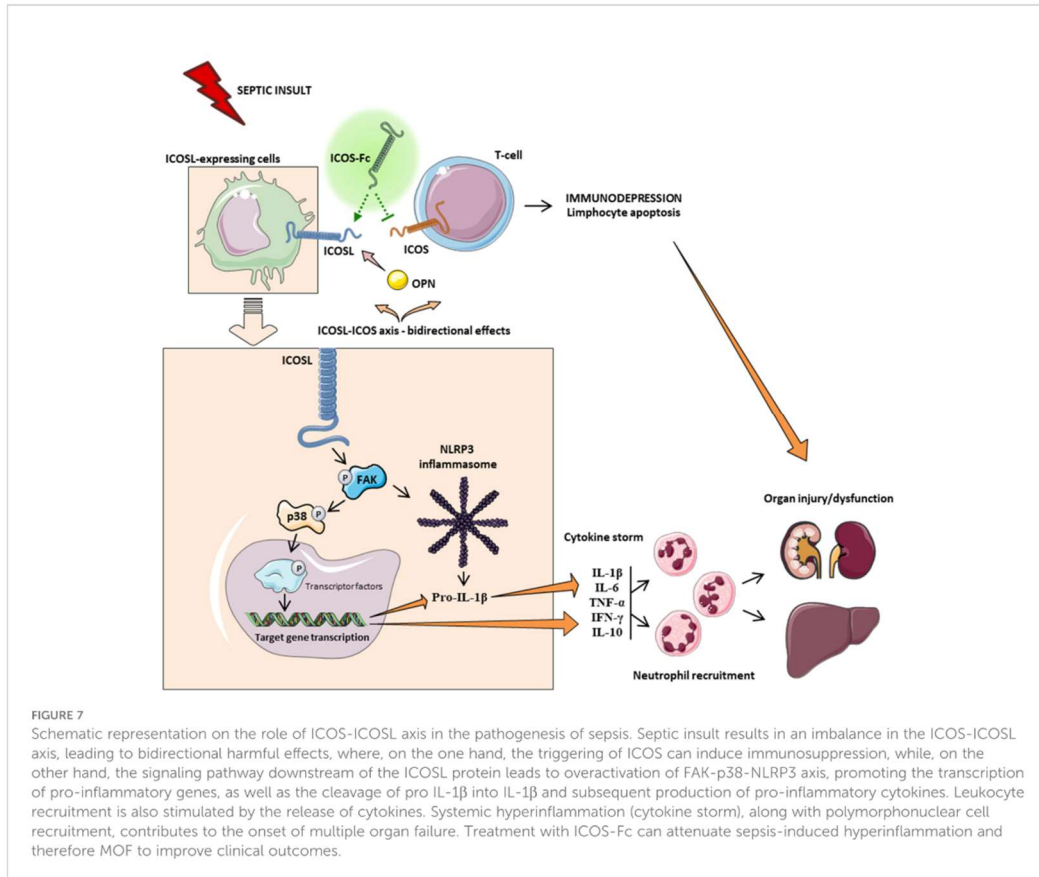
Among the main inflammatory pathways activated during sepsis, we report a local (liver and kidney) overactivation of the FAK and p38 MAPK pathways in CLP mice. Previously, we have shown that the FAK pathway mediates inflammation through p38 MAPK and that this inflammatory axis plays a role in exacerbating inflammation (28). Activation of this axis promotes increased expression/secretion of pro-inflammatory cytokines such as TNF-α, IL-6, IL-1β and IL-17, which in turn contribute to the cytokine storm and multiple organ failure (MOF) associated with sepsis (43). Intriguingly, treatment of septic mice with ICOS-Fc significantly attenuated FAK and p38 MAPK phosphorylation, thus reducing their activation during septic insult, with a following impact on the development of the above-mentioned cytokine storm. These findings are in accordance with previous studies focused on tumor cell migration, whose treatment with ICOS-Fc reduces FAK and p38 MAPK activation both *in vitro* and *in vivo* (15, 19). As we and other have recently shown, FAK activation may also affect the overexpression and activation of another peculiar inflammatory pathway, NLRP3 inflammasome complex (28, 44). Thus, we wondered here whether ICOS-Fc could also infer with this cross-talk mechanism linking FAK to NLRP3 activation within the septic context. We report here that experimental sepsis led to an overactivation of the NLRP3 complex and consequent activation of its downstream mediator caspase-1, which were significantly reduced by treatment with ICOS-Fc, thus leading to reduced systemic release of IL-1β. In addition to the impact on the aforementioned inflammatory pathways, ICOS-Fc administration seems to directly affect leukocyte migration in CLP mice, as documented by the changes in MPO activity, a well-known biomarker of neutrophil infiltration, in both liver

and kidney homogenates (45). Specifically, we documented that the sepsis-induced increase in MPO activity in renal tissues, was significantly counteracted by ICOS-Fc treatment. This effect, on the other hand, was absent when CLP mice were treated with ^{F119S}ICOS-Fc. Intriguingly, increased MPO activity was recorded in liver homogenates from septic mice, regardless of drug treatment or genetic intervention, when compared to Sham mice. Despite ICOS-Fc has been shown to reduce the migration of polymorphonuclear cells into inflamed tissues (15), these discrepant events observed in liver and kidney tissue may be the result of different levels of ICOSL expression. This finding corroborates a previous study reporting that hepatocytes did not express ICOSL, when compare to other organs, such as the kidney (46). Thus, suggesting that the hepatic protection induced by ICOS-Fc in septic mice is mainly due to a local and systemic resolution of inflammation rather than a reduction in leukocyte infiltration. A schematic representation summarizing the role of ICOS-ICOSL axis in the pathogenesis of sepsis and the protective effects of ICOS-Fc following sepsis-induced multiple organ failure is shown in Figure 7.

Despite the originality of our findings, we are aware of several limitations of our study, including the lack of extension of these findings to other important functional organs related to MOF during sepsis, such as the lungs and the cardiac tissue, along with the lack of analysis suggestive of the direct effect of ICOS-Fc treatment in preventing immunosuppression. Albeit the *in vivo* protocol described here is in accordance with the main recommendations provided by MQTiPSS consensus guidelines (27), we are not authorized to perform a survival study to assess the long-term effect of ICOS-Fc due to ethical reasons. Thus, further studies are needed to extend the clinical relevance of our findings as well as to gain a better insight into the safety profile of the proposed drug treatment.

Conclusions

In conclusion, we demonstrate here, for the first time, that the ICOS-ICOSL axis plays a crucial role in the development of systemic inflammation and organ damage induced by a clinically relevant sepsis model. These findings were confirmed by an exacerbation of septic injury in mice knockout for the ICOS and ICOSL genes. Interestingly, we also documented its draggability by showing protection when ICOS-Fc, a recombinant protein which act as an antagonist of ICOS and an agonist of ICOSL, was administered during sepsis. The beneficial effects of this innovative pharmacological approach are likely due to a potential cross-talk mechanisms involving the FAK-p38-NLRP3 inflammasome axis. A greater

48

FIGURE 7
Schematic representation on the role of ICOS-ICOSL axis in the pathogenesis of sepsis. Septic insult results in an imbalance in the ICOS-ICOSL axis, leading to bidirectional harmful effects, where, on the one hand, the triggering of ICOS can induce immunosuppression, while, on the other hand, the signaling pathway downstream of the ICOSL protein leads to overactivation of FAK-p38-NLRP3 axis, promoting the transcription of pro-inflammatory genes, as well as the cleavage of pro IL-1β into IL-1β and subsequent production of pro-inflammatory cytokines. Leukocyte recruitment is also stimulated by the release of cytokines. Systemic hyperinflammation (cytokine storm), along with polymorphonuclear cell recruitment, contributes to the onset of multiple organ failure. Treatment with ICOS-Fc can attenuate sepsis-induced hyperinflammation and therefore MOF to improve clinical outcomes.

understanding of the molecular basis of ICOS-Fc-mediated effects is needed to harness its actions as a potentially powerful immunomodulatory tool for countering inflammation and organ injury in sepsis.

Data availability statement

The raw data supporting the conclusions of this article will be made available by the authors, without undue reservation.

Ethics statement

The animal study was reviewed and approved by Ethical committee OPBA University of Turin and Italian Ministry of Health, Italy.

Author contributions

GA, CD, UD, and MC conceived and designed the experiments. GA, IS, EA, CM, RM, EP, GE, DC, and NC performed the experiments. GA, EA, CM, RM, IB, EB, CG, NC, MA, DF, CT, CC, CD, UD, and MC analyzed the data. GA, CD, UD, CT, and MC, writing - review and editing. All authors have read and agreed to the published version of the manuscript.

Funding

The Università degli Studi di Torino has supported and funded this work (Ricerca Locale 2020 and 2021) and by the Associazione Italiana Ricerca sul Cancro (IG20714), Milan Italy.

Acknowledgments

Parts of the Figure 7 were drawn by using pictures from Servier Medical Art. Servier Medical Art by Servier is licensed

under a Creative Commons Attribution 3.0 Unported License (https://creativecommons.org/licenses/by/3.0/).

Conflict of interest

The authors declare that the research was conducted in the absence of any commercial or financial relationships that could be construed as a potential conflict of interest.

Publisher's note

All claims expressed in this article are solely those of the authors and do not necessarily represent those of their affiliated organizations, or those of the publisher, the editors and the reviewers. Any product that may be evaluated in this article, or claim that may be made by its manufacturer, is not guaranteed or endorsed by the publisher.

References

1. Hotchkiss RS, Monneret G, Payen D. Sepsis-induced immunosuppression: From cellular dysfunctions to immunotherapy. *Nat Rev Immunol* (2013) 13:862–74. doi: 10.1038/nri3552

2. Rudd KE, Johnson SC, Agesa KM, Shackelford KA, Tsoi D, Kievlan DR, et al. Global, regional, and national sepsis incidence and mortality, 1990 – 2017 : analysis for the global burden of disease study. *Lancet* (2020) 395:200–11. doi: 10.1016/S0140-6736(19)32989-7

3. Hutloff A, Dittrich AM, Beier KC, Eljaschewitsch B, Kraft R, Anagnostopoulos I, et al. ICOS is an inducible T-cell co-stimulator structurally and functionally related to CD28. *Nature* (1999) 100:263–6. doi: 10.1038/16717

4. Yoshinaga SK, Whoriskey JS, Khare SD, Sarmiento U, Guo J, Horan T, et al. T-Cell co-stimulation through B7RP-1 and ICOS. *Nature* (1999) 1:827–32. doi: 10.1038/45582

5. Swallow MM, Wallin JJ, Sha WC. B7h, a novel costimulatory homolog of B7.1 and B7.2, is induced by TNFa. *Immunity* (1999) 11:423–32. doi: 10.1016/s1074-7613(00)80117-x

6. Möhnle P, Hirschberger S, Hinske LC, Briegel J, Hübner M, Weis S, et al. MicroRNAs 143 and 150 in whole blood enable detection of T-cell immunoparalysis in sepsis. *Mol Med* (2018) 24:1–14. doi: 10.1186/s10020-018-0056-z

7. Menéndez R, Méndez R, Almansa R, Ortega A, Alonso R, Suescun M, et al. Simultaneous depression of immunological synapse and endothelial injury is associated with organ dysfunction in community-acquired pneumonia. *J Clin Med* (2019) 8:1–10. doi: 10.3390/jcm8091404

8. Burmeister Y, Lischke T, Dahler AC, Mages HW, Lam K-P, Coyle AJ , et al. ICOS controls the pool size of effector-memory and regulatory T cells. *J Immunol* (2008) 180:774–82. doi: 10.4049/jimmunol.180.2.774

9. Chen Q, Mo L, Cai X, Wei L, Xie Z, Li H, et al. ICOS signal facilitates Foxp3 transcription to favor suppressive function of regulatory T cells. *Int J Med Sci* (2018) 15:666–73. doi: 10.7150/ijms.23940

10. Luan Y, Yin C, Qin Q, Dong N, Zhu X, Sheng Z. Effect of regulatory T cells on promoting apoptosis of T lymphocyte and its regulatory mechanism in sepsis. *J Interf Cytokine Res* (2015) 35:969–80. doi: 10.1089/jir.2014.0235

11. Saito K, Wagatsuma T, Toyama H, Ejima Y, Hoshi K, Shibusawa M, et al. Sepsis is characterized by the increases in percentages of circulating CD4 + CD25 + regulatory T cells and plasma levels of soluble CD25. *J Exp Med* (2008) 216:61–8. doi: 10.1620/tjem.216.61

12. Leng F, Liu J, Liu Z, Yin J, Qu H-P. Increased proportion of CD4 d CD25 d Foxp3 d regulatory T cells during early-stage sepsis in ICU patients. *J Microbiol Immunol Infect* (2013) 46:338–44. doi: 10.1016/j.jmii.2012.06.012

13. Occhipinti S, Dianzani C, Chiocchetti A, Boggio E, Clemente N, Gigliotti CL, et al. Triggering of B7h by the ICOS modulates maturation and migration of monocyte-derived dendritic cells. *J Immunol* (2013) 190:1125–34. doi: 10.4049/jimmunol.1201816

14. Lund SA, Giachelli CM. The role of osteopontin in inflammatory processes. *J Cell Commun Signal* (2009) 3:311–22. doi: 10.1007/s12079-009-0068-0

15. Dianzani C, Minelli R, Mesturini R, Chiocchetti A, Barrera G, Boscolo S, et al. B7h triggering inhibits umbilical vascular endothelial cell adhesiveness to tumor cell lines and polymorphonuclear cells. *J Immunol* (2010) 185:3970–9. doi: 10.4049/jimmunol.0903269

16. Raineri D, Dianzani C, Cappellano G, Maione F, Baldanzi G, Iacobucc I, et al. Osteopontin binds ICOSL promoting tumor metastasis,". *Commun Biol* (2020) 3:1–15. doi: 10.1038/s42003-020-01333-1

17. Di Niro R, Ziller F, Florian F, Crovella S, Stebel M, Bestagno M, et al. Construction of miniantibodies for the *in vivo* study of human autoimmune

diseases in animal models. *BMC Biotechnol* (2007) 7:1–10. doi: 10.1186/1472-6750-7-46

18. Gigliotti CL, Boggio E, Clemente N, Shivakumar Y, Toth E, Sblattero D, et al. ICOS-ligand triggering impairs osteoclast differentiation and function *In vitro* and *In vivo*. *J Immunol* (2016) 197:3905–16. doi: 10.4049/jimmunol.1600424

19. Dianzani C, Minelli R, Gigliotti CL, Occhipinti S, Giovarelli M, Conti LM, et al. B7h triggering inhibits the migration of tumor cell lines. *J Immunol* (2014) 192:4921–31. doi: 10.4049/jimmunol.1300587

20. Ramavath NN, Gadipudi LL, Provera A, Gigliotti LC, Boggio E, Bozzola C, et al. Inducible T-cell costimulator mediates Lymphocyte/Macrophage interactions during liver repair. *Front Immunol* (2021) 12:786680. doi: 10.3389/fimmu.2021.786680

21. Stoppa I, Gigliotti CL, Clemente N, Pantham D, Dianzani C, Monge C, et al. ICOSL stimulation by ICOS-fc accelerates cutaneous wound healing *In vivo*. *Int J Mol Sci* (2022) 23:1–12. doi: 10.3390/ijms23137363

22. O'Sullivan AW, Wang JH, Redmond HP. NF-κB and P38 MAPK inhibition improve survival in endotoxin shock and in a cecal ligation and puncture model of sepsis in combination with antibiotic therapy. *J Surg Res* (2009) 152:46–53. doi: 10.1016/j.jss.2008.04.030

23. Cornelius DC, Travis OK, Tramell RW, Borges-Rodriguez M, Baik CH, Greer M, et al, et al. NLRP3 inflammasome inhibition attenuates sepsis-induced platelet activation and prevents multi-organ injury in cecal-ligation puncture. *PLoS One* (2020) 15:1–15. doi: 10.1371/journal.pone.0234039

24. Lee S, Nakahira K, Dalli J, Siempos II, Norris PC, Colas RA, et al. NLRP3 inflammasome deficiency protects against microbial sepsis *via* increased lipoxin B4 synthesis. *Am J Respir Crit Care Med* (2017) 196:713–26. doi: 10.1164/rccm.201604-0892OC

25. Chen X, Zhao Y, Wang X, Lin Y, Zhao W, Wu D, et al. FAK mediates LPS-induced in fl ammatory lung injury through interacting TAK1 and activating TAK1-NF κ b pathway. *Cell Death Differ* (2022) 13:1–12. doi: 10.1038/s41419-022-05046-7

26. du Sert NP, Hurst V, Ahluwalia A, Alam S, Avey MT, Baker M, et al. The arrive guidelines 2.0: Updated guidelines for reporting animal research. *PloS Biol* (2020) 18:1–12. doi: 10.1371/journal.pbio.3000410

27. Osuchowski MF, Ayala A, Bahrami S, Bauer M, Boros M, Cavaillon J-M, et al. Minimum quality threshold in pre-clinical sepsis studies (mqtipss): An international expert consensus initiative for improvement of animal modeling in sepsis. *Shock* (2018) 50:377–80. doi: 10.1097/SHK.0000000000001212

28. Alves GF, Aimaretti E, Einaudi G, Mastrocola R, Oliveira JG, Collotta D, et al. Pharmacological inhibition of FAK-Pyk2 pathway protects against organ damage and prolongs the survival of septic mice. *Front Immunol* (2022) 13:837180. doi: 10.3389/fimmu.2022.837180

29. Kovalski V, Prestes AP, Oliveira JG, Alves GF, Colarites D, El Mattos J, et al. Protective role of cGMP in early sepsis. *Eur J Pharmacol* (2017) 807:174–81. doi: 10.1016/j.ejphar.2017.05.012

30. Nandra KK, Collino M, Rogazzo M, Fantozzi R, Patel NSA, Thiemermann C. "Pharmacological preconditioning with erythropoietin attenuates the organ injury and dysfunction induced in a rat model of hemorrhagic shock,". *DMM Dis Model Mech* (2013) 6:701–9. doi: 10.1242/dmm.011353

31. Faul F, Erdfelder E, Lang A-G, Buchner A. G*Power 3: A flexible statistical power analysis program for the social, behavioral, and biomedical sciences. *Behav Res Methods* (2007) 39:175–91. doi: 10.3758/bf03193146

32. Tsirigotis P, Chondropoulos S, Gkirkas K, Meletiadis J, Dimopoulou I. "Balanced control of both hyper and hypo-inflammatory phases as a new treatment paradigm in sepsis,". *J Thorac Dis* (2016) 8:E312–6. doi: 10.21037/jtd.2016.03.47

33. Boomer JS, To K, Chang KC, Takasu O, Osborne DF, Walton AH, et al. Immunosuppression in patients who die of sepsis and multiple organ failure. *J Am Med Assoc* (2011) 306:2594–605. doi: 10.1001/jama.2011.1829

50

34. Otto GP, Sossdorf M, Claus RA, Rödel J, Menge K, Reinhart K, et al. The late phase of sepsis is characterized by an increased microbiological burden and death rate. *Crit Care* (2011) 15:1–8. doi: 10.1186/cc10332

35. Mai SHC, Sharma N, Kwong AC, Dwivedi DJ, Khan M, Grin PM, et al. Body temperature and mouse scoring systems as surrogate markers of death in cecal ligation and puncture sepsis. *Intensive Care Med Exp* (2018) 6:1–14. doi: 10.1186/s40635-018-0184-3

36. Koh KH, Cao Y, Mangos S, Tardi NJ, Dande RR, Lee HW, et al. Nonimmune cell–derived ICOS ligand functions as a renoprotective αvβ3 integrin–selective antagonist. *J Clin Invest* (2019) 129:1713–26. doi: 10.1172/JCI123386

37. Castello LM, Baldrighi M, Molinari L, Salmi L, Cantaluppi V, Vaschetto R, et al. The role of osteopontin as a diagnostic and prognostic biomarker in sepsis and septic shock. *Cells* (2019) 8:1–12. doi: 10.3390/cells8020174

38. Uchibori T, Matsuda K, Shimodaira T, Sugano M, Uehara T, Honda T. IL-6 trans-signaling is another pathway to upregulate osteopontin. *Cytokine* (2017) 90:88–95. doi: 10.1016/j.cyto.2016.11.006

39. Hirano Y, Aziz M, Yang W-L, Wang Z, Zhou M, Ochani M, et al. Neutralization of osteopontin attenuates neutrophil migration in sepsis-induced acute lung injury. *Crit Care* (2015) 19:1–15. doi: 10.1186/s13054-015-0782-3

40. Fortis S, Khadaroo RG, Haitsma JJ, Zhang H. Osteopontin is associated with inflammation and mortality in a mouse model of polymicrobial sepsis. *Acta Anaesthesiol Scand* (2015) 59:170–5. doi: 10.1111/aas.12422

41. Trostel J, Truong LD, Roncal-Jimenez C, Miyazaki M, Miyazaki-Anzai S, Kuwabara M, et al. Disease different effects of global osteopontin and macrophage osteopontin in glomerular injury. *Am J Physiol - Ren Physiol* (2018) 315:F759–68. doi: 10.1152/ajprenal.00458.2017

42. Boggio E, Dianzani C, Gigliotti CL, Soluri MF, Clemente N, Cappellano G, et al. Thrombin cleavage of osteopontin modulates its activities in human cells *in vitro* and mouse experimental autoimmune encephalomyelitis *in vivo*. *J Immunol Res* (2016) 2016:1–13. doi: 10.1155/2016/9345495

43. Chaudhry H, Zhou J, Zhong Y, Ali MM, Mcguire F, Nagarkatti PS, et al. Role of cytokines as a double-edged sword in sepsis. *In Vivo (Brooklyn)* (2013) 27:669–84.

44. Chung IC, OuYang C-N, Yuan S-N, Li H-P, Chen J-T, Shieh H-R, et al. Pyk2 activates the NLRP3 inflammasome by directly phosphorylating ASC and contributes to inflammasome-dependent peritonitis. *Sci Rep* (2016) 6:1–13. doi: 10.1038/srep36214

45. Yu H, Liu Y, Wang M, Restrepo RJ, Wang D, Kalogeris TJ, et al. Myeloperoxidase instigates proinflammatory responses in a cecal ligation and puncture rat model of sepsis. *Am J Physiol - Hear Circ Physiol* (2020) 319:H705–21. doi: 10.1152/ajpheart.00440.2020

46. Wahl C, Bochtler P, Chen L, Schirmbeck R, Reimann J. B7-H1 on hepatocytes facilitates priming of specific cd8 t cells but limits the specific recall of primed responses. *Gastroenterology* (2008) 135:980–8. doi: 10.1053/j.gastro.2008.05.076

51

3.3 ICOS/ICOSL/OPN important role in tumor development and ICOS-Fc antimetastatic effect

It has been documented how cancer development depends largely on immune dysfunction (Kravchenko et al., 2015; Tsai & Hsu, 2017; Ghahremanloo et al., 2019; Su et al., 2023; Tsai & Hsu, 2017). The characteristics and heterogeneity of cancers are depicted by how tumor cells and immune cells interact in tumor microenviroment (TME) (Farkona et al., 2016; Constantinidou et al., 2019; Khosravi et al., 2020). Several authors demonstrated the adaptive immunity and the anti-tumor response mediated by ICOSL triggering by ICOS (Hutloff et al., 1999; Dianzani et al., 2010, 2014; Solinas et al., 2020). For this reason, choosing ICOS/ICOSL pathway as a pharmacological target for antitumor therapies hold a great promise for cancer therapy (Clemente et al., 2020). For instance, ICOS/ICOSL pathway has been shown to be involved in colorectal cancer (CRC) pathogenesis. Zhang et al. (2016) demonstrated that, being ICOSL mainly expressed on tumor cells, ICOS expression is negatively associated with the progress of CRC and especially with tumor metastasis. Additionally, amount of ICOS+ T-cells in the peripheral blood is significantly higher in CRC patients at stage I and II, compared to late stages and healthy control. This evidence suggested that ICOS expression levels on Th1 cells and other tumor infiltrating T-cells could be associated with patient survival (Zhang et al., 2016).

This was confirmed also by Carthon et al. (2010), who studied if ICOS+ effector T-cells could be considered a valid clinical outcome for melanoma metastatic patients treated with anti-CLTA-4. Once more, improved overall survival of metastatic melanoma patients was correlated with an increased amount of ICOS+ effector T-cells (Carthon et al., 2010; Fu et al., 2011).

Recent findings discovered another important player involved and affecting ICOS/ICOSL axis bidirectional signals. It is a matter of OPN, a phosphoprotein secreted by several cell types, such as macrophages, DCs and Th cells. It is defined as an intrinsically disordered protein (IDP), lacking well-folded crystallizable structure, but showing a flexible and a dynamic one which awards it to adopt different functional structures and interact with several binding partners (Kurzbach et al., 2013; Z. Liu & Huang, 2014). In this regard, it can function both as a matricellular protein and a cytokine mediating several biological functions, such as bone remodeling, macrophage response, cell migration and adhesion, in addition to modulating the activation and differentiation of proinflammatory Th1 and Th17 cells.

It performs additionally a key role in the immune evasion response and crosstalk between cancer cells and its microenvironment. Indeed, it is widely demonstrated to be overexpressed in several

human tumors, in which induces inflammation, tumor invasion and its metastatic dissemination (Castello et al., 2017; Khongsti & Das, 2021). Consequently, it has been emerged as a potential valuable biomarker for diagnosing and treating cancers (Wei et al., 2017).

The interesting functional network between ICOS, ICOSL and OPN was slightly introduced previously talking about OPN proinflammatory activity and its increased level depicted in sepsis context (Alves et al., 2022). However, considering all the functions that they have in common, several are the potential applications of using this trio as a pharmacological target in several human diseases.

In detail, all these molecules support Th17 cell responses and they are involved in the bone metabolism. Indeed, OPN is a key bone component produced by OBs, while ICOSL is expressed by OCs and its triggering by ICOS was shown responsible of inhibiting OCs differentiation *in vitro* and development of osteoporosis *in vivo* (Gigliotti et al., 2016).

The potential crucial role of ICOS/ICOSL/OPN has been highlighted in cancer context as well. For the first time, the groups of research of Prof. Chiara and Umberto Dianzani demonstrated for the first time that ICOSL is a receptor also for OPN and that their interaction take place not overlapping the binding site used by ICOS. The two different interactions exert opposite effects, ICOS/ICOSL mediates inhibition of cell migratory effect, while OPN/ICOSL is correlated to a strong pro-migratory one (Castello et al., 2017; Clemente et al., 2020; Raineri et al., 2020, 2022).

The already demonstrated antimetastatic effect of ICOS-Fc was then exploited to confirm the functional relevance of the OPN/ICOSL interaction in tumor cells migration. The OPN pro-metastatic effect was detected more intense on cells expressing high level of ICOSL, and the cell migration was significantly inhibited when ICOS-Fc was administered. Indeed, both OPN pro-migratory effect and ICOS-Fc effectiveness were negligible in *in vitro* cancer models performed using tumor cells lines expressing low level of B7h (Dianzani et al., 2014; Raineri et al., 2020).

Moreover, *in vivo* 4T1[ICOSL] tumor showed higher levels of OPN and ICOSL expression, associated with a higher density vessel, which depicted the impact of OPN/ICOSL interaction on the TME and tumor angiogenesis (Raineri et al., 2020).

In addition, the role of ICOS/ICOSL/OPN network in tumor cell metastasis was studied in depth comparing the *in vivo* metastasizing capability of two variants of melanoma cells (B16-F10 expressing high or low level of ICOSL), when injected in WT mice or in ICOS, ICOSL and OPN KO mice. Those findings gave the opportunity to explore this immunotherapy outcome either for nonresponding or patients resistant to conventional therapies.

Inducible t-cell costimulator ligand plays a dual role in melanoma metastasis upon binding to osteopontin or inducible t-cell costimulator

Background: Melanoma is a highly immunogenic tumor, alterations in antigen expression or presentation represent its primary immune escape. However, immunosuppression plays another relevant role in supporting this cancer malignancy, as the impairing antitumor response correlated to activated Treg and myeloid-derived suppressor cells (MDCSs) enriched in TME. Studying melanoma progression, OPN was found overexpressed in invasive tumor stages, suppressing Treg proliferation and activation and supporting MDCSs colonization. Highly documented is its wide expression by different component of the TME and its several mediated functions.

As written before, our group of research stood out for finding that ICOS shares its unique ligand with OPN, and that OPN/ICOSL interaction take place at a binding site not overlapping the one used by ICOS. Intriguingly, the OPN or ICOS different interactions exert opposite ICOSL triggering effects, OPN support metastasis and angiogenesis, which is dominantly inhibited by ICOS. Supporting findings were those correlated to ICOS-Fc effectiveness in inhibiting cell migration *in vitro* and cell metastatization *in vivo* melanoma mouse model, added to an antiproliferative and an antiangiogenic activity exerted when encapsulated into nanoparticles (Dianzani et al., 2014; Clemente et al., 2020; Raineri et al., 2020).

Aim: This work was focused in assessing the net effect of ICOSL triggering by this different binding partner in melanoma metastasis formation.

Method: In order to confirm OPN/ICOSL interaction in human melanoma metastasis, a Proximity Ligation Assay (PLA) was performed in human melanoma samples of both primary tumors and corresponding metastasis. B16-F10 cells were used to set up the *in vivo* melanoma model, they do not express ICOS nether OPN, while they were engineered to stably express high (B16$^{ICOSL-high}$) or low (B16$^{ICOSL-low}$) ICOSL level. Their migration response was compared performing an invasion assay (Boyden chamber), putting cancer cells in presence of either OPN or ICOS-Fc, standing opposite effects. Additionally, an anchorage-dependent and independent growth assay were performed to evaluate ICOSL expression role in influencing B16-F10 cells dissemination attitude.

In vivo experiments involved female mice of four different strains: C57BL/6 WT, OPN KO, ICOS KO, ICOSL KO. After 15d from cancer cells i.v. injection (1*10^6 cells/animal), the animals were sacrificed, lung metastases were counted, and organs samples were collected and harvested.

Results: The first part of the project was validating the animal model using two type of cancer cells. It consisted in collecting all preliminary data related to migration and growing behavior of both kind of ICOSL expressing melanoma cells and confirming OPN and ICOS opposite mediated effect. Indeed, the OPN/ICOSL PLA signal was significantly higher in metastases than in primary tumors, confirming also in human melanoma how OPN/ICOSL interaction is increased in metastatic lesions. Moreover, Boyden chamber results confirmed that melanoma cell migration induced by OPN is strictly correlated to ICOSL expression. Indeed, B16$^{ICOSL-low}$ showed a lower OPN-induced migration, compared to that of B16$^{ICOSL-high}$ cells, which was significantly inhibited by ICOS-Fc. However, between them, B16$^{ICOSL-low}$ cells grew more efficiently in the absence of anchorage to the ECM, showing themself as the one kind much more prone to metastasize *in vivo*.

The project proceeded in comparing *in vivo* the metastasizing capability of both variants of melanoma cells, monitoring how OPN and ICOS opposing forces end up in modulating tumor cancer migration by ICOSL triggering.

Melanoma lung metastasis counting values were compared among WT mice, in which all three components of the OPN/ICOS/ICOSL trio are expressed and where every single effect could be masked from another, versus OPN KO, ICOS KO and ICOSL KO mice, lacking one component per time. B16$^{ICOSL-low}$ produced more metastasis than B16$^{ICOSL-high}$ in OPN KO, ICOS KO and ICOSL KO and in WT mice. The differences in lungs metastases counting highlighted how both ICOSL and OPN promote cancer dissemination (decreased metastases were detected in OPN KO and ICOSL KO mice), while ICOS inhibits it. Even if showing a lower metastatic behavior, B16$^{ICOSL-high}$ metastasis formation showed revealing differences among mice strains used. For instance, analyzing ICOS KO mice emerged, as in B16$^{ICOSL-low}$, an increased number of lung metastases confirmed the dominant ICOS-mediated triggering of ICOSL. On the other side, OPN KO mice showed fewer metastases, compared with WT mice, using B16$^{ICOSL-low}$. This evidence supported the effect resulting from a loss of OPN-induced prometastatic effect.

Conclusion: Collectively, these data suggest that OPN induces tumor metastasis by interacting with ICOSL and how ICOS can dominantly inhibit it. Moreover, this model improved current understanding concerning the role of OPN/ICOSL interaction in tumor progression and metastases dissemination. Indeed, it gave the opportunity to study interfering/modulating ICOS/ICOSL/OPN network as potential target for immunotherapy also for patient resistant to conventional therapies.

Article

Inducible T-Cell Costimulator Ligand Plays a Dual Role in Melanoma Metastasis upon Binding to Osteopontin or Inducible T-Cell Costimulator

Davide Raineri [1,2], Giuseppe Cappellano [1,2], Beatrice Vilardo [1,2], Federica Maione [1,2], Nausicaa Clemente [1], Elena Canciani [1,2], Elena Boggio [1], Casimiro Luca Gigliotti [1], Chiara Monge [3], Chiara Dianzani [3], Renzo Boldorini [4], Umberto Dianzani [1,5,*] and Annalisa Chiocchetti [1,2]

[1] Dipartimento di Scienze della Salute, Interdisciplinary Research Center of Autoimmune Diseases-IRCAD, Università del Piemonte Orientale, 28100 Novara, Italy; davide.raineri@uniupo.it (D.R.); giuseppe.cappellano@med.uniupo.it (G.C.); beatrice.vilardo@uniupo.it (B.V.); federica.maione@med.uniupo.it (F.M.); nausicaa.clemente@med.uniupo.it (N.C.); elena.canciani@uniupo.it (E.C.); elena.boggio@med.uniupo.it (E.B.); luca.gigliotti@med.uniupo.it (C.L.G.); annalisa.chiocchetti@med.uniupo.it (A.C.)

[2] Center for Translational Research on Autoimmune and Allergic Diseases, University of Piemonte Orientale, 28100 Novara, Italy

[3] Dipartimento di Scienza e Tecnologia del Farmaco, Università di Torino, 10125 Torino, Italy; chiara.monge@unito.it (C.M.); chiara.dianzani@unito.it (C.D.)

[4] Divisione di Anatomia Patologica, Dipartimento di Scienze della Salute, AOU Maggiore della Carità, Università del Piemonte Orientale, 28100 Novara, Italy; renzo.boldorini@med.uniupo.it

[5] Laboratorio di Biochimica Clinica, Dipartimento di Scienze della Salute, AOU Maggiore della Carità, Università del Piemonte Orientale, Corso Mazzini 18, 28100 Novara, Italy

* Correspondence: umberto.dianzani@med.uniupo.it

Abstract: Recently, we demonstrated that inducible T-cell costimulator (ICOS) shares its unique ligand (ICOSL) with osteopontin (OPN), and OPN/ICOSL binding promotes tumor metastasis and angiogenesis in the 4T1 breast cancer model. Literature showed that OPN promotes melanoma metastasis by suppressing T-cell activation and recruiting myeloid suppressor cells (MDSC). On the opposite, ICOS/ICOSL interaction usually sustains an antitumor response. Here, we engineered murine B16F10 melanoma cells, by transfecting or silencing ICOSL. In vitro data showed that loss of ICOSL favors anchorage-independent growth and induces more metastases in vivo, compared to ICOSL expressing cells. To dissect individual roles of the three molecules, we compared data from C57BL/6 with those from OPN-KO, ICOS-KO, and ICOSL-KO mice, missing one partner at a time. We found that OPN produced by the tumor microenvironment (TME) favors the metastasis by interacting with stromal ICOSL. This activity is dominantly inhibited by ICOS expressed on TME by promoting Treg expansion. Importantly, we also show that OPN and ICOSL highly interact in human melanoma metastases compared to primary tumors. Interfering with this binding may be explored in immunotherapy either for nonresponding or patients resistant to conventional therapies.

Keywords: osteopontin; ICOSL; melanoma; metastasis; tumor microenvironment

1. Introduction

Melanoma is a malignant tumor arising from melanocytes that accounts for only about 1% of skin cancers [1] but it causes the large majority of skin cancer deaths [2]. Indeed, diagnosis is often made at late stages when melanoma cells have already metastasized. Melanoma is a highly immunogenic tumor, and infiltration with cytotoxic CD8^{+} T cells has been associated with a good prognosis, since they can efficiently kill tumor cells [3]. Melanoma immune escape is primarily due to alterations in antigen expression or presentation, but a role has been ascribed also to immunosuppression, mediated in particular regulatory T cells (Tregs) [4,5] and myeloid-derived suppressor cells (MDSCs) [6,7]. Both

Tregs and MDSCs were found to be enriched and activated in the melanoma microenvironment, and are responsible for profound impairment of antitumor immune responses, leading to tumor progression [8].

Melanoma progression is associated with increased expression of osteopontin (OPN), a phosphoprotein acting either as a matricellular protein or as a proinflammatory cytokine [9]: biopsies from different stages of melanoma progression indicate that OPN is specifically overexpressed in invasive tumor stages [10]. Furthermore, high levels of OPN are significantly associated with poor clinical outcome in patients bearing highly metastatic tumors [11]: stromal OPN directly suppresses CD8$^+$ T cell proliferation and activation [12], and in parallel, sustains MDSCs colonization, thus supporting tumor progression [13].

The role of OPN in melanoma metastasis has been demonstrated clearly in animal models. B16-F10 is a murine melanoma cell line used as a model to study metastasis [14]. Injection of B16-F10 melanoma cells in the tail vein of syngeneic mice results in extravasation into the lungs and formation of countable macro-metastases [14]. The intracardiac injection of B16-F10 cells leads to metastasis in the lungs and other organs, such as the liver [15]. Intracardiac injection of B16-F10 cells into OPN knock-out (OPN-KO) mice produces fewer metastases than occur in wild-type mice, whereas no difference is found when injection is intravenous [16].

OPN is expressed by different components of the tumor microenvironment, such as macrophages, dendritic cells (DCs), and activated T cells. Thanks to its multiple adhesion motifs (i.e., calcium-binding sites, heparin-binding domains and integrin domains), OPN is able to interact with different receptors and exerts multiple functions. In particular, two classes of receptors have long been identified for OPN, namely integrins and CD44$_{v6-7}$ [17]. More recently, for the first time, the present group demonstrated that OPN directly binds the immune checkpoint receptor inducible T-cell costimulator ligand (ICOSL) [17], finding that it binds directly to ICOSL at a binding site that is distinct and nonoverlapping compared to that employed by ICOS, which is the conventional partner of ICOSL. The two interactions exert opposing effects on cell migration, which is induced by OPN, but dominantly inhibited by ICOS. Moreover, angiogenesis and tumor metastasis are increased, both in vitro and in vivo, by OPN-mediated triggering of ICOSL, whereas they are inhibited by ICOS-mediated ICOSL triggering [17–19].

ICOSL is a transmembrane receptor belonging to the B7 family that is expressed in B cells, dendritic cells, monocytes, endothelial cells, fibroblasts, epithelial cells, and several types of tumor cells [20]. Its main known function is to trigger ICOS, a costimulatory receptor expressed by activated T cells [21]. Inflammatory signals increase ICOSL expression in several cell types of nonlymphoid tissue, such as the brain, lung, heart, kidney, liver, and gut, which suggests that the ICOS/ICOSL interaction regulates the activity of effector and effector/memory T cells [22]. ICOS is a type I transmembrane glycoprotein belonging to the CD28 family; it acts as a costimulatory immune checkpoint receptor. It is expressed by activated T cells, and its stimulation modulates differentiation and potentiates cytokine production of T helper (Th) cells [21]. Depending on the microenvironment cytokine milieu, ICOS supports differentiation of Tregs: Th17, Th2 (in mouse), and Th1 (in human) cells. Moreover, it is highly expressed by T follicular helper (Tfh), and a deficiency of the ICOS gene causes defective formation of germinal centers in both humans [23]. The ICOS-ICOSL interaction also triggers "reverse signaling" to the cell expressing ICOSL. In DCs, triggering of ICOSL with ICOS-Fc, a recombinant soluble form of ICOS, modulates cytokine secretion, promotes antigen cross-presentation, and inhibits adhesiveness and migration; in endothelial and tumor cells it inhibits adhesion and migration. Moreover, it induces dephosphorylation of ERK and p38 in endothelial cells, dephosphorylation of FAK in tumor cells, and downmodulation of β-PIX in DCs and tumor cells [19,24–26]. The present group employed the B16 mouse melanoma model to demonstrate that ICOS-Fc inhibits cell migration in vitro and the development of metastases in vivo [19,24]. Further, ICOS-Fc encapsulated in nanoparticles inhibits the growth of established subcutaneous B16 tumors by inhibiting tumor angiogenesis and Treg development [18].

Collectively, these data draw a picture in which the triggering of ICOSL by one or other of the binding partners, ICOS and OPN, mediates opposing activities on tumor metastasis, which is promoted by OPN and inhibited by ICOS. Stemming from these findings, the present study aimed to evaluate the net effect of ICOSL binding to OPN and to ICOS on the metastasis potential of the two binding partners in vivo. To this end, B16-F10 melanoma cells, stably silenced for ICOSL, were injected intravenously (i.v.) into either syngeneic wild-type C57BL/6 mice, or mice deficient in one molecule at a time (OPN-KO, ICOS-KO, ICOSL-KO mice). Interestingly, it emerged that OPN, through binding with ICOSL, promotes melanoma metastasis formation.

2. Materials and Methods

2.1. Cell Lines

B16-F10 mouse melanoma cells, purchased from the American Type Culture Collection (ATCC; Manassas, VA, USA), were grown in culture dishes as a monolayer in RPMI 1640 medium plus 10% fetal bovine serum (FBS) (Life technologies, Carlsbad, CA, USA), 100 U/mL penicillin, and 100 μg/mL streptomycin at 37 °C in 5% CO_2-humidified atmosphere.

2.2. ICOSL Cloning

ICOSL was cloned as described elsewhere [17]. Briefly, cDNA derived from RNA extracted from mouse splenocytes was cloned into pcDNA 3.1 vector. The plasmid was then transformed into JM109 bacteria (Promega, Madison, WI, USA) and the resulting colonies were sequenced by Sanger sequencing (Life technologies, Carlsbad, CA, USA).

2.3. Cell Transfection and Cell Silencing

B16-F10 cells were transfected as reported elsewhere [17]. Briefly, 2×10^6 B16-F10 cells were transfected with 10 μg of a DNA plasmid (pcDNA3.1) carrying the ICOSL cDNA, using lipofectamine™ 3000 (Life technologies, Carlsbad, CA, USA). The endogenous ICOSL gene was siRNA-silenced using lipofectamine™ RNAiMAX transfection reagent (Life technologies, Carlsbad, CA, USA) as reported elsewhere [17]. Real-time PCR was used to evaluate the expression of ICOSL in the transfected (B16-ICOSL-high) and silenced (B16-ICOSL-low) cells, 48 h after transfection and silencing. Next, 1 μg of RNA was retrotranscribed to cDNA using the QauntiTect Reverse Transcription Kit (Qiagen, Hilden, Germany). Real-time PCR was performed using CFX96 System (Bio-Rad Laboratories) in duplicate for each sample, in a 10 μL final volume containing 1 μL of diluted cDNA, 5 μL of TaqMan Universal PCR Master Mix (Life technologies, Carlsbad, CA, USA), and 0.5 μL of Assay-on-Demand mix. The results were analyzed with a ΔΔ threshold cycle method using *GAPDH* as housekeeping gene. Surface expression of ICOSL was evaluated by flow cytometry using anti-ICOSL PE mAb (Catalog number #107405, clone HK5.3, Biolegend, San Diego, CA, USA).

2.4. Invasion Assays

In the Boyden chamber (BD Biosciences) invasion assay, 1×10^3 cells of B16-ICOSL-high and B16-ICOSL-low were plated onto the apical side of 50 μg/mL Matrigel-coated filters (8.2 mm diameter and 0.5 mm pore size; Neuro Probe; BIOMAP snc, Milan, Italy) in serum-free medium with or without 2 μg/mL ICOS-Fc. Medium containing 20% FBS, as control, or 10 μg/mL of OPN (Bio-techne, Minneapolis, MN, USA) were placed in the basolateral chamber as chemoattractants for the tumor cells. The chamber was incubated at 37 °C under 5% CO_2. After 6 h, the cells on the apical side were wiped off with Q-tips. The cells on the bottom of the filter were stained with crystal violet and all counted with an inverted microscope (magnification ×40). The results are expressed as the number of migrated cells per high-power field.

2.5. Anchorage-Dependent Growth Assay

For the anchorage-independent growth assay, 1.6×10^3 cells were plated in RPMI (Life technologies, Carlsbad, CA, USA) plus 10% FBS in a 96-well plate. From day 1 to day 4 cells were counted daily using trypan blue. For the anchorage-independent growth assay, a 12-well plate was coated with RPMI 3% agar. After solidification, 5×10^3 cells were plated over the 3% agar bottom layer, in RPMI 1% agar. Cells were grown at 37 °C for 14 days. 1 mg/mL of 3-(4,5-dimethylthiazol-2-yl)-2,5-diphenyltetrazolium bromide (MTT) was then added and the plate incubated for 3 h at 37 °C. The colony images were taken using Chemidoc (Biorad, Hercules, CA, USA).

2.6. In Vivo Experiments

Eight-to-ten-week-old adult female mice of the following 4 standard inbred strains were used: C57BL/6, B6.129S6(Cg)-Spp1tm1Blh/J, also known as OPN KO, B6.129P2-Icostm1Mak/J, also known as ICOS KO, and B6.129P2-Icosltm1Mak/J, also known as ICOSL KO (all mice were purchased from The Jackson Laboratory, Bar Harbor, ME, USA). Animals were maintained under pathogen-free conditions in the animal facility of Università del Piemonte Orientale; they were fed ad libitum on rodent chow, and water was freely available in the home cages; the ambient temperature was maintained at 21 ± 1 °C. All experimental procedures were conducted during the light phase of a 12:12 h light:dark cycle. One million cells were i.v. injected and after 15 days the mice were sacrificed and lung metastases counted by two operators working blind. The lungs were cut into small pieces and incubated at 37 °C for 30 min with 0.5 mg/mL of Collagenase type IV (Merck, Darmstadt, Germany). After neutralization of the enzyme with 2 mM of EDTA (Merck, Darmstadt, Germany), the tissue was crushed and passed through a 100 μm filter. Red blood cells were lysed by osmotic shock. Aliquots of one million cells were stained with mAb as follows. Myeloid MDSC (M-MDSC) (CD11b$^+$, Ly6C^{high} and Ly6G^{low}) with anti-CD11b Percp-Cy5.5 (Catalog number #101228, clone M1/70, Biolegend, San Diego, CA, USA), anti-Ly6C APC (Catalog number #128016, clone HK1.4, Biolegend, San Diego, CA, USA), and anti-Ly6G APC-Cy7 (Catalog number #127624, clone 1A8, Biolegend, San Diego, CA, USA) Treg cells (CD4$^+$, CD25$^+$ and Foxp3$^+$) with anti-CD4 FITC (Catalog number #100406, clone GK1.5, Biolegend, San Diego, CA, USA) and anti-CD25 PE (Catalog number #12-0251-83, clone PC61.5, Life Technologies, Carlsbad, CA, USA); cells were then permeabilized and stained with anti-Foxp3 APC antibody (Catalog number #17-5773-82, clone FJK-16s, Life Technologies, Carlsbad, CA, USA). Cells were acquired using Attune flow cytometry (Thermo Fisher Scientific, Waltham, MA, USA) and data analyzed using FlowJo Software (Becton and Dickinson, Franklin Lakes, NJ, USA). The results are expressed as % of Ly6C^{high} in CD11b$^+$ cells (M-MDSC) and as % of Treg in CD4$^+$ cells (Treg).

2.7. Proximity Ligation Assays (PLA)

PLA technology is based on the detection of protein interactions. This technique uses one pair of primary antibodies that target the proteins of interest with the aim of studying the interaction. PLA was carried out with Duolink® In Situ Red Starter Kit Goat/Rabbit (Merck, Darmstadt, Germany). Additional reagents used were Duolink® In Situ PLA® Probe Anti-Goat MINUS (# DUO92006) and Duolink® In Situ PLA® Probe Anti-Rabbit PLUS (#DUO92002). Antibody concentrations were optimized using immunofluorescence prior to PLA experiments. Human melanocytic skin lesions or metastatic tissue have been removed based on the clinical suspicion/confirmation of melanoma, accordingly to the best clinical practices (study approved by the Ethical Committee of AOU Maggiore della Carità di Novara, 14 December 2012, CE 166/12). The origin of the tumor biopsy (i.e., primary tumor or metastasis) was confirmed by the pathologist. Each primary tumor was paired with its lymph node metastasis. No clinical data are provided in the manuscript because samples were anonymized. Paraffin-embedded primary tumor or metastasis tissues from patients were deparaffinized and subjected to graded rehydration through an alcohol series (xylene; 100, 95, and 70% ethanol) before immersion in PBS 1×. Heat-induced epitope

retrieval was performed using a microwave. Tissue samples were then blocked with protein block serum-free (Dako) for 1 h at room temperature. Tissues were incubated with primary antibodies (diluted 1:100 in blocking solution) overnight at 4 °C. The In Situ Red Starter Kit Goat/Rabbit was used following the manufacturer's protocol. The sections were observed by Leica TCS SP2 AOBS confocal laser-scanning microscope (Leica Microsystems, Wetzlar, Germany) and analyzed with the Image Pro Plus Software for micro-imaging 5.0 (Meyer Instruments, Houston, TX, USA).

2.8. Statistics

The number of metastases, the infiltrate among the mouse groups, and migrations were analyzed using one-way ANOVA; in all other cases the Mann–Whitney *t*-test was used as indicated. *p* values below 0.05 were considered statistically significant. The statistical analyses were performed with GraphPad Instat software (Prism 8 version 8.4.3) (GraphPad Software, San Diego, CA, USA).

3. Results
3.1. OPN and ICOSL Highly Interact in Human Melanoma Metastases

Recently, in a murine breast cancer model, we showed that OPN interacts with ICOSL, and that this binding sustains the angiogenic process. To characterize the role of OPN-ICOSL in patient-derived tumors more precisely, human melanoma samples were here scored for mutual OPN/ICOSL interactions. To this end, the proximity ligation assay (PLA) technology was employed, as it is a highly specific and sensitive tool for the in situ detection of protein-protein interactions [17]. By means of immunofluorescence (IF) analysis, human specimens of primary melanomas (*n* = 10) and their matched lymph node metastases (*n* = 10) were screened; OPN/ICOSL interactions were found in both primary tumor and metastatic tissues. Quantification of the OPN-ICOSL PLA signal showed this was higher in metastases than in primary tumors (Figure 1A,B).
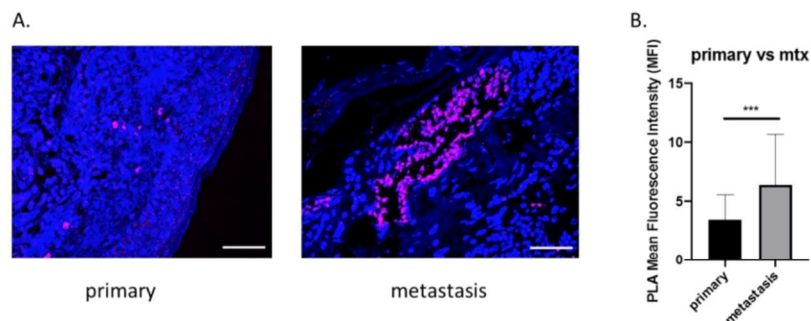

Figure 1. Increased OPN-ICOSL interaction in primary and its paired metastatic human melanoma. (**A**) Proximity Ligation Assay (PLA) in primary tumor and corresponding metastasis. The merged PLA signal (violet) shows ICOSL and OPN interaction, while nuclei are labeled with DAPI (blue). Images were quantified using ImageJ software in order to calculate the ratio between red (OPN) and green (ICOSL) channels; values are shown as percentage of red–green co-staining. Scale bar 50 µm. Four images were analyzed for each sample at a magnification of 40×. (**B**) The histograms quantify OPN-ICOSL PLA in signals of primary and metastatic tumors, expressed as MFI (mean ± SEM). Mann–Whitney statistical test was used, *** *p* < 0.001.

These findings suggest that the simultaneous presence of OPN and ICOSL is relevant in human melanomas, and that binding between these two molecules increases in metastatic lesions.

3.2. ICOSL Expression Modulates In Vitro Growth and In Vivo Metastasis of B16-F10 Melanoma Cells

Since OPN/ICOSL were observed to increase in human metastatic melanomas, it was decided to investigate whether the interaction between these two molecules could also play a role in a preclinical B16 mouse model. To this end, B16-F10 cells were injected i.v. into syngeneic mice to generate black countable lung colonies.

Of note, B16-F10 parental cells express ICOSL, as shown by RT-PCR (Figure 2A) and flow cytometry (Figure 2B), but do not express ICOS or OPN (data not shown). Since surface expression of ICOSL was variable in different cell batches, and was closely dependent on cell culturing conditions (not shown), cells were engineered to stably express high (B16-ICOSL-high) or low (B16-ICOSL-low) levels of ICOSL. B16-ICOSL-high cells were obtained by transfecting B16-F10 cells with a plasmid encoding the entire murine ICOSL cDNA, and B16-ICOSL-low by transfecting B16-F10 cells with a siRNA targeting ICOSL. Both cell lines showed stable expression levels of ICOSL mRNA and protein, which were consistently higher in B16-ICOSL-high than in B16-ICOSL-low cells (Figure 2A,B). A previous study having found that melanoma cell migration in response to OPN depends on ICOSL expression, the migration response to OPN of the two cell lines was compared (Figure 2C). B16-ICOSL-high cells were seen to migrate toward OPN, whereas B16-ICOSL-low cells did not. As expected, ICOS-Fc was able to interfere and block this migration (Figure 2C).
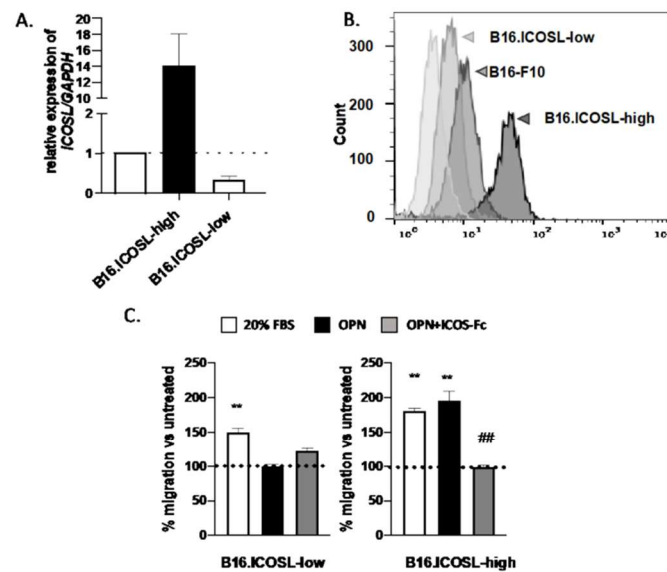
Figure 2. Engineering of B16-F10 melanoma cell lines expressing stable levels of ICOSL. (**A**) Relative quantification of *ICOSL* RNA in B16-ICOSL-high and B16-ICOSL-low cells; the dotted line shows B16-F10 parental cells. Data are shown as means $\pm$ SEM gene expression relative to expression of the endogenous control *GAPDH* ($2^{-\Delta Ct}$ method). One representative experiment is shown ($n = 3$ biological replicates); (**B**) representative histogram showing surface expression of ICOSL in B16-ICOSL-high (dark gray), B16-ICOSL-low (gray), and parental B16-F10 cells (light gray); (**C**) migration of B16-ICOSL-high and B16-ICOSL-low cells in response to 10 μg/mL of rhOPN or 20% FBS as chemotactic stimulus. The gray column shows inhibition of OPN-induced migration by ICOS-Fc. The dotted line shows the migration of control cells, set at 100% in the absence of chemotactic stimuli. Data are expressed as means $\pm$ SEM ($n = 5$) of the number of migrated cells per high-power field, ** $p < 0.01$ refers to baseline, ## $p < 0.01$ refers to OPN-induced migration, one-way ANOVA test was used.

In previous work, it was found that ICOSL expression inhibits the growth of mammary carcinoma cells in anchorage-independent but not in anchorage-dependent conditions, thus the in vitro growth of B16-ICOSL-high and of B16-ICOSL-low cells in these culture conditions was compared. B16-ICOSL-high and B16-ICOSL-low displayed comparable anchorage-dependent growth, as assessed by culturing cells in standard culture plates in the presence of FBS (Figure 3A). However, anchorage-independent growth in soft agar was lower in B16-ICOSL-high cells than in B16-ICOSL-low cells (Figure 3B).
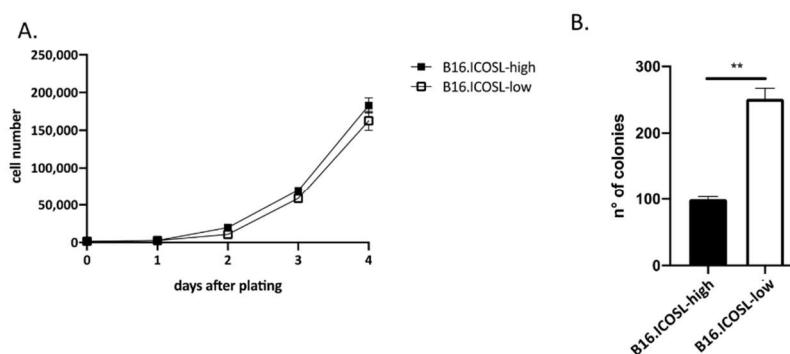
Figure 3. ICOSL expression inhibits anchorage-independent tumor cell growth. (**A**) Kinetic growth assay of B16-ICOSL-low and B16-ICOSL-high cells in the presence of 10% FBS ($n = 2$). Cells were counted following trypan blue staining; (**B**) the soft agar colony formation assay was run to estimate anchorage-independent growth of B16-ICOSL-low and B16-ICOSL-high cells. Colonies were counted digitally using ImageJ software. Data are expressed as means $\pm$ SEM. The Mann–Whitney statistical test was used, ** $p < 0.01$.

The finding that tumor cells expressing low levels of ICOSL grow efficiently in the absence of anchorage to the extracellular matrix suggests that they may be prone to metastasize in vivo. To assess this possibility, the metastatic potentials of B16-ICOSL-high and B16-ICOSL-low cells were compared, injecting them into the tail vein of C57BL/6 mice and counting lung metastases after 15 days: B16-ICOSL-low cells produced more metastases than B16-ICOSL-high cells (Figure 4A,B). In order to exclude any nonlung metastatic spread, we macroscopically analyzed all the available organs comprising liver, omentum and gut, lymph nodes, muscles, bone and brain: no metastases were found (data not shown). The TME of the metastases was characterized by analyzing the infiltrating leukocytes of the metastatized lung, focusing on M-MDSC and Tregs, which are known to be supported by OPN and ICOS, respectively, and are key components of the immune suppressive TME [13,27–29]. M-MDSC were evaluated as percentage of $CD11b^+/Ly6C^+/Ly6G^-$ cells among total $CD11b^+$ cells, and Treg cells as percentage of $CD4^+CD25^+Foxp3^+$ among total $CD4^+$ cells (the gating strategy and the fluorescence minus controls (FMOs) are shown in Supplementary Figures S1 and S2). Similar amounts of both cell types were detected in lungs metastasized with either B16-ICOSL-low or B16-ICOSL-high cells (Figure 4C), suggesting that the metastasis process, in this setting, is not influenced by recruitment of M-MDSC and Tregs in premetastatic niches and finally, the percentages are in line with those detected in the lungs of tumor-free mice (Supplementary Figure S3).
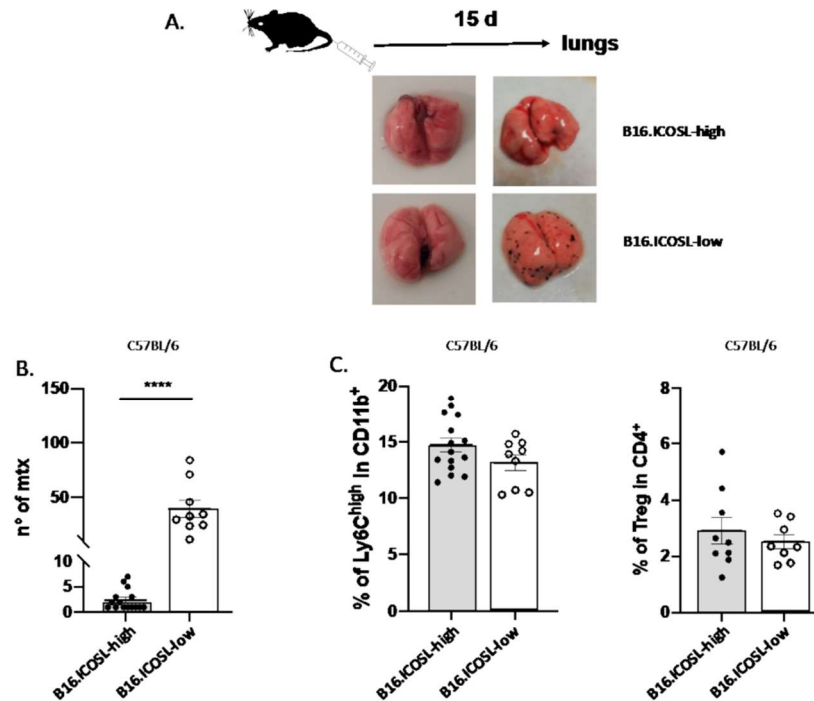
Figure 4. Role of ICOSL expression in B16-F10 cell metastasis. (**A**) Schematic illustration of experimental in vivo approach (top) and representative images of metastatic lung (bottom) from B16-ICOSL-high and B16-ICOSL-low injected mice, at baseline (left) and after 15 days (right). (**B**) The graph shows the number of lung metastases in B16-ICOSL-high and B16-ICOSL-low C57BL/6-injected mice ($n = 9$–15 mice). Data are shown as means $\pm$ SEM. The Mann–Whitney statistical test was used, **** $p < 0.0001$ (**C**) Left: bar graph showing the percentage of M-MDSC among total CD11b$^+$ cells in the lung of C57BL/6 mice injected with B16-ICOSL-high and B16-ICOSL-low cells. Right: bar graph showing the percentage of Treg among total CD4$^+$ cells in the lung of C57BL/6 mice injected with B16-ICOSL-high and B16-ICOSL-low cells.

3.3. ICOSL Mediates Different Metastatic Effects When Binding to OPN or to ICOS

With C57BL/6 mice it is not possible to model the net OPN/ICOSL interaction in the tumor context, since these mice fully express all three molecules (OPN, ICOS, and ICOSL) and thus the effect of each may be masked by an opposing action of the others. Thus, in order to gain in-depth understanding of the roles of ICOSL's two binding partners, and to elucidate their mechanisms, the metastasis of B16-ICOSL-high and B16-ICOSL-low cells was examined in wild-type mice compared to OPN-, ICOS-, or ICOSL-KO mice; these are mice in which either OPN or ICOS or ICOSL is lacking. ICOSL-KO mice were included to examine the role of stromal ICOSL in comparison to tumor ICOSL. When necessary, ICOSL expression was silenced in tumor cells to eliminate its interference, using B16-ICOSL-low cells. For comparison purposes, ICOSL was also transfected into B16-F10 cells, so as to overexpress it and evaluate its role when expressed by tumor cells, using B16-ICOSL-high cells. Of note, these engineered cell models are only capable of addressing OPN produced by stromal cells (B16-F10 cells do not secrete OPN; data not shown) whereas they can address ICOSL expressed either by tumor cells or by the stromal compartment.

The first comparison between B16-ICOSL-low and B16-ICOSL-high cells showed that the former produced more metastases than did the latter, in OPN-KO, ICOS-KO, and ICOSL-KO strains, and in wild-type mice (Figure 5A).
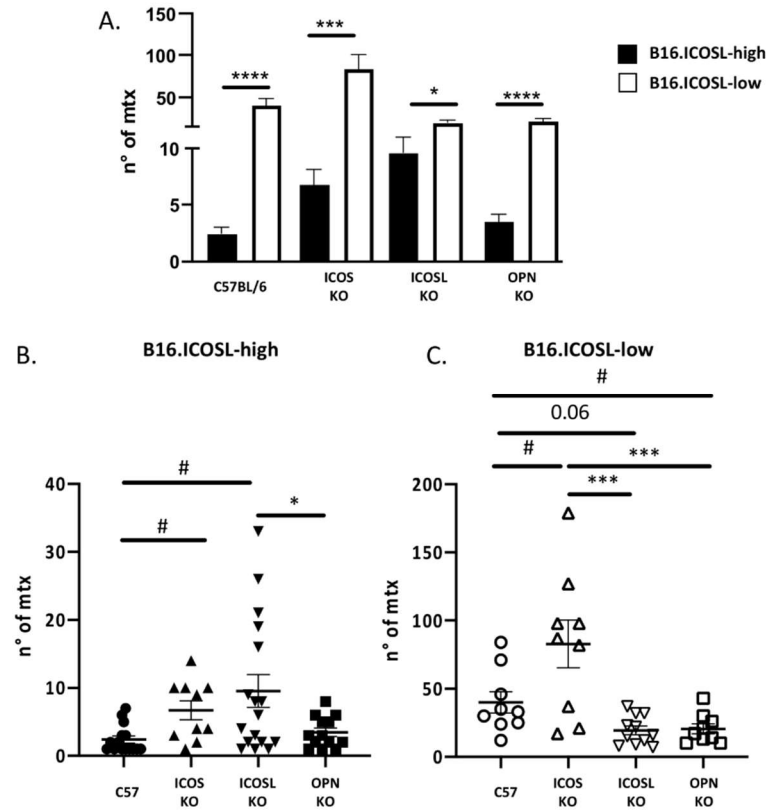
Figure 5. ICOSL mediates different metastasizing effects when binding to OPN and ICOS. (**A**) The histogram shows the number of metastases in each genotype (C57BL/6, OPN-KO, ICOSL-KO and ICOS-KO) of B16-ICOSL-high and B16-ICOSL-low injected mice (n = 9–17 mice). (**B**) The histogram shows the number of metastases in different genotypes (C57BL/6, OPN-KO, ICOSL and ICOS-KO) in B16-ICOSL-high injected mice (n = 9–17 mice). (**C**) The histogram shows the number of metastases within genotypes (C57BL/6, OPN-KO and ICOS-KO) of B16-ICOSL-low injected mice (n = 9–11 mice). One-way ANOVA test was used, * $p < 0.05$, *** $p < 0.001$, **** $p < 0.0001$ and # $p < 0.05$ refers to C57 mouse background.

The second analysis compared the metastases formed by B16-ICOSL-high, displaying low metastatic behavior, in the different mouse strains. Results showed that metastases were higher in ICOSL-KO mice and ICOS-KO mice than in wild-type mice. In addition, ICOSL-KO mice displayed an increased amount of metastasis compared to OPN-KO mice (Figure 5B). The results of ICOS-KO mice confirm that ICOS inhibits metastasis. By contrast, the results of ICOSL-KO and OPN-KO were unexpected and indicated that expression of high levels of ICOSL in the tumor cells increases the system complexity.

The third analysis compared the metastases formed by B16-ICOSL-low, displaying high metastatic behavior, in the different mouse strains. Results showed that, compared to wild-type mice, metastases were decreased in OPN-KO mice and ICOSL-KO mice, and increased in ICOS-KO mice (Figure 5C). These results are in line with the model that OPN and ICOSL promote, whereas ICOS inhibits metastasis.

To assess the effects of ICOS, OPN and ICOSL expressed by the TME on the B16-F10 metastasis microenvironment, the lung-infiltrating m-MDSC and Treg cells in wild-type

mice were compared with those in the different KO mice (the gating strategy is shown in Supplementary Figures S1 and S2).

As in wild-type C57BL/6 mice also in ICOS-KO, OPN-KO and ICOSL-KO mice, m-MDSC and Treg were not significantly different in lungs metastasized by B16-ICOSL-high versus B16-ICOSL-low cells (Figure 6). On the contrary, comparison of wild-type mice with each KO strain showed that: (1) M-MDSC were significantly increased in ICOS-KO and a trend ($p = 0.07$) was found in ICOSL-KO mice when injected with B16-ICOSL-low, but not with B16-ICOSL-high cells (Figure 6A,B); (2) Tregs were decreased in ICOSL-KO mice injected with both B16-ICOSL-high -low cells, and increased in OPN-KO mice with B16-ICOSL-low cells, but not in those injected with B16-ICOSL-high cells (Figure 6C,D). All the other comparisons showed no statistically relevant difference.
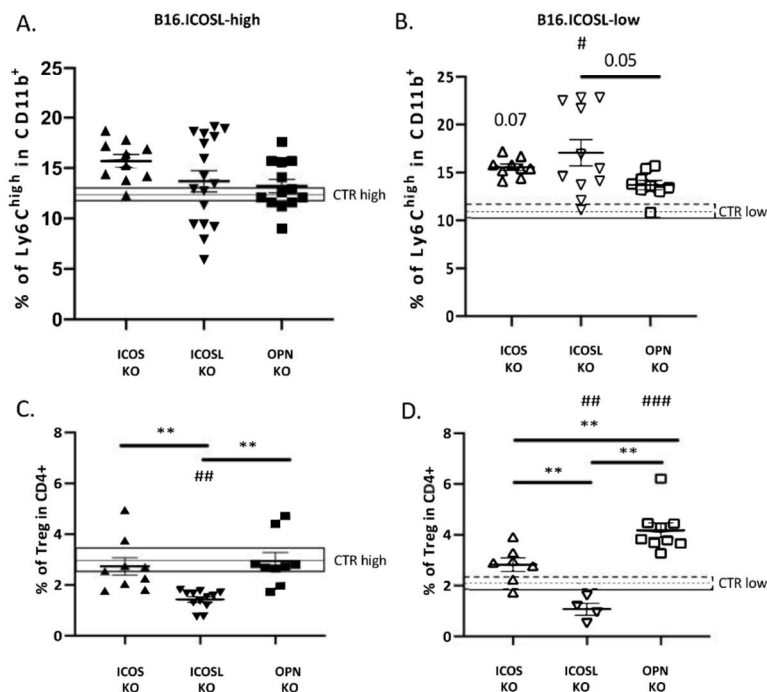
Figure 6. Percentage of Treg and M-MDSC infiltrating B16.ICOS-high/low tumors in C57BL/6 and KO mice (**A**) M-MDSC as % of CD11b$^+$ cells in lungs of C57BL/6, OPN-KO, ICOSL-KO and ICOS-KO mice injected with B16-ICOSL-high cells; the gray rectangle shows the percentage of M-MDSC in C57 mice. Data are means $\pm$ SEM (n = 10–17 mice). (**B**) M-MDSC as % of CD11b$^+$ cells in lungs of C57BL/6, OPN-KO, ICOSL-KO and ICOS-KO mice injected with B16-ICOSL-low cells; the gray rectangle shows the percentage of M-MDSC in C57 mice. Data are means $\pm$ SEM (n = 9–11 mice). (**C**) Treg as percentage of CD4$^+$ in lungs of C57BL/6, OPN-KO and ICOS-KO mice injected with B16-ICOSL-high cells; the gray rectangle shows the percentage of Tregs as percentage of CD4$^+$ in C57BL/6 mice. Data are means $\pm$ SEM (n = 9–12 mice). (**D**) Treg as percentage of CD4$^+$ in lungs of C57BL/6, OPN-KO and ICOS-KO mice injected with B16-ICOSL-low cells; the gray rectangle shows the percentage of Tregs in C57BL/6 mice. Data are means $\pm$ SEM (n = 4–9 mice). One-way ANOVA test was used, ** $p < 0.01$; # $p < 0.05$, ## $p < 0.01$ and ### $p < 0.001$ refer to C57BL/6 mouse background.

The amounts of M-MDSCs and Tregs obtained from the lungs of control tumor-free mice were similar in wild type and each KO strain (Supplementary Figure S3).

4. Discussion

This study investigates the role in tumor cell metastasis of the ICOS/ICOSL/OPN network, comparing the metastasizing capability of two variants of melanoma B16-F10 cells, respectively expressing high and low levels of ICOSL. The study used wild-type mice and three strains of KO mice, lacking either ICOS, or OPN, or ICOSL. It emerged that the three members of the ICOS/ICOSL/OPN network play distinct and differing roles, possibly acting both at the tumor cell level and at that of the TME. These differing effects may be ascribed to the complexity of the ICOS/ICOSL/OPN network, in which (1) both ICOS and OPN bind to ICOSL, but exert different, often opposing, effects on the cell that expresses ICOSL; (2) OPN also binds other surface receptors, such as integrins and CD44; (3) OPN and its ligands (ICOSL, integrins, and CD44) can be expressed by tumor cells and by several cell types of the TME, influencing tumor cell survival, proliferation, and metastasis; (4) ICOS can be expressed by different types of T cells, including effector and Treg cells, and also by some other cell types in the TME, such as DCs and macrophages. Moreover, OPN produced by tumor cells may lack important domains and may carry different post-translational modifications, making it structurally and functionally different from that produced by other cell types [30].

The first part of the study validates the model employing two types of B16-F10 cells, and confirms the results of previous work on different tumor cell types [17]. That prior study showed that expression of high levels of ICOSL promotes cell migration in response to OPN, which is inhibited by ICOS-mediated triggering of ICOSL, and that it inhibits tumor cell growth in anchorage-independent, but not in anchorage-dependent, conditions. The effect on anchorage-independent growth suggests that expression of ICOSL may increase tumor cell anoikis, which is a cell-death process whereby cells undergo apoptosis after they lose contact with the extracellular matrix (ECM) [31]. Acquisition of anoikis resistance is necessary for tumor cells to survive while traveling through the circulation [32].

Since the triggering of ICOSL by OPN, or alternatively by ICOS, exerts opposing effects on tumor cell migration, metastasis of B16-ICOSL-high and of B16-ICOSL-low cells in wild-type mice was compared, to assess the net effect of these opposing forces in vivo. Expression of high levels of ICOSL was found to substantially decrease metastasis, suggesting that the inhibitory effect of ICOS-mediated triggering of ICOSL is dominant over the promoting effect mediated by OPN; this is in line with previous work showing that treatment of mice with ICOS-Fc inhibits tumor cell metastasis [18].

To dissect the role of each member of the ICOS/OPN/ICOSL network expressed in the TME, the metastasis ability of B16-ICOSL-high was compared with that of B16-ICOSL-low cells, using KO mice lacking one network member at a time. B16-ICOSL-high and B16-ICOSL-low cells express neither OPN nor ICOS, so that the only source of the two ligands of ICOSL was in the TME. Importantly, removing each molecule of the trio, one at a time, is useful at a twofold level: on one hand it allows evaluation of the effect of the absence of the knocked-out molecule itself, but on the other hand it sets the conditions to evaluate, without any interference, the residual activity of the other two interactors, as depicted for better clarity in Figure 7. Analysis of ICOS-KO mice showed that, compared to wild-type mice, they undergo increased metastasis formation, whether using B16-ICOSL-high or B16-ICOSL-low cells. This effect is in line with the loss of the dominant ICOS-mediated triggering of ICOSL both on tumor or stromal cells. Indeed, in B16-ICOSL-low metastases, the increased numbers of M-MDSC cells might play a role in the increased metastasis, and help tumor cells (not expressing ICOSL) to elude the immune system. On the contrary, M-MDSC were not increased in B16-ICOSL-high metastases, suggesting that expression of high levels of ICOSL on tumor cells might inhibit the development of M-MDSC, possibly by sequestering OPN, known to support M-MDSC development. In line with this hypothesis, the same increase in M-MDSC displayed by B16-ICOSL-low, (and not by B16-ICOSL-high metastases), was also detected in ICOSL-KO mice, (and not in OPN-KO mice). Since C57BL/6 mice did not show any increase in M-MDSC, these data collectively suggest that

such an increase requires both the availability of OPN and absence of the ICOS/ICOSL interaction at the TME level.
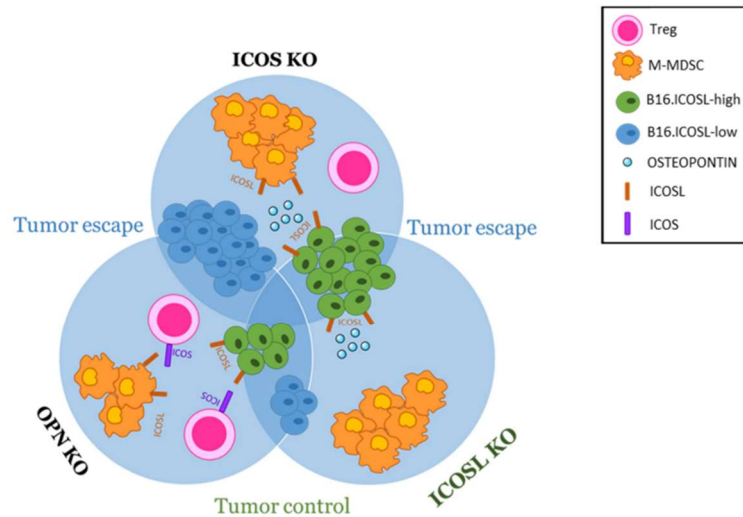

Figure 7. The metastatic niche model at a glance. The melanoma metastatic niche contains malignant cells towards which immune suppressive cells are recruited and corrupted. Tumor and stromal cells produce the ECM proteins that regulate cell function, and their interaction is also relevant for tumor progression and metastasis. The model used here was implemented to investigate metastasis, Tregs and M-MDSC-infiltrating metastatic melanoma, induced by ICOSL binding to ICOS or to OPN. Melanoma cells, expressing ICOSL (green) or not expressing it (blue), were used to induce metastases in scenarios lacking one of the three molecules of the trio. By removing one molecule at a time, the effect of each molecule expressed can be observed without interference from the other two. The results on the three strains of KO mice were then compared to each another and to those on wt mice. Using this model, it was shown that OPN/ICOSL promote metastasis.

Analysis of OPN-KO mice showed that, when compared to wild-type mice, they developed fewer metastases using B16-ICOSL-low. This effect is in line with a loss of the prometastatic effect exerted by OPN. Interestingly, this model shows that B16-ICOSL-low metastases contained increased numbers of Treg cells compared to C57BL/6 mice, suggesting that OPN may inhibit development of these cells; this effect would be reversed by the expression of high levels of ICOSL in B16-ICOSL-high cells, which is in line with the notion that ICOS triggering in T cells supports Tregs.

Lastly, through analysis of ICOSL-KO, the role played by ICOSL—expressed by either the tumor or the TME cells—was elucidated. Compared to C57BL/6, ICOSL-KO mice displayed more B16-ICOSL-high metastases and fewer B16-ICOSL-low metastases, which runs counter to the dominant negative effect exerted by ICOS on adhesion and migration of ICOSL-expressing tumor cells. One possible explanation for this disparity is that, in ICOSL-KO mice, the lack of endogenous ICOSL makes large amounts of OPN available to the tumor cells, an abundance that might promote metastasis of B16-ICOSL-high cells by overcoming the dominant negative effect exerted by ICOS. Importantly, low numbers of B16-ICOSL-low metastases, which were comparable in number to those occurring in OPN-KO mice, suggest that the metastasis process is closely related to the simultaneous expression and interaction of OPN and ICOSL. In ICOS-KO mice, OPN has no competitor for ICOSL in the TME in promoting M-MDSC recruitment. Moreover, the observation that both B16-ICOSL-high and B16-ICOSL-low metastases displayed lower numbers of Treg cells in ICOSL-KO mice than they did in wild-type mice is in line with the notion that the

triggering of ICOS by microenvironmental ICOSL plays a key role in the development of these cells.

Collectively, these data suggest that OPN produced by TME favors tumor metastasis by interacting with stromal ICOSL; these activities are dominantly inhibited by ICOS. At the light of the important role played by both host OPN and ICOSL in metastasis development, further experiments using double OPN-KO and ICOSL-KO mice would be useful to sustain our findings.

The multiple interaction spots of OPN/ICOSL detected by PLA in human melanoma metastases, compared to those in primary tumors, support the hypothesis the binding between these two molecules plays a role in metastasis, but appears to contradict our in vitro finding that melanoma cells expressing low levels of ICOSL are prone to survive in attachment-independent conditions and display increased metastatic capacity. We can speculate that low expression of ICOSL in the primary tumor might favor detachment of tumor cells, their survival in the blood stream, and their extravasation at the metastatic site, since these cells would be less sensitive to the dominant negative inhibition triggered by ICOS. At the metastasis site, the ICOSL/OPN interaction might thus be crucial for engraftment of the metastasis, possibly taking advantage of a positive feedback loop, since previous findings show that boosting ICOSL expression in 4T1 cells increases their expression of OPN [17]. This opens an opposite scenario, not mutually exclusive with the previous one, in which OPN, which is one of the most abundantly expressed genes in melanoma metastases, acts as a chemoattractant for circulating ICOSL-positive tumor cells, and thus promotes development of the premetastatic niche by interacting with its multiple receptors [33,34]. Beside its effect on tumor cell migration and survival, the network also plays a role in tumor neoangiogenesis, since OPN induces—while ICOS inhibits—angiogenesis.

Targeting this network may exert an antitumor effect by acting at multiple levels and addressing important unmet clinical needs, since approximatively 60% of patients do not achieve any significant therapeutic response, and a substantial proportion of responders relapse within 2 years [35].

ICOS-Fc treatment of mice carrying established primary melanomas decreases infiltrating Treg cells [36,37]. Anti-PD1 and anti-CTLA4 treatments are effective in melanoma immune therapy and, intriguingly, their effectiveness is marked by increased expression of ICOS [38]. Therefore, ICOS itself may play a role as an effector molecule recruited by this therapy, possibly by acting at several levels in the ICOS/ICOSL/OPN network. Recently, OPN has been shown to act as an immune checkpoint that negatively regulates T-cell activation and decreases the effectiveness of anti-PD-1-based immune therapy [39]. OPN neutralization may thus be another approach to increasing the efficacy of PD-1-based immune checkpoints blockade (ICB) immunotherapy in responding patients, and to overcome resistance to ICB immunotherapy in nonresponding patients [40].

Finely tuning/interfering with the OPN/ICOS/ICOSL network may represent a next-generation immunotherapy either for patients resistant to conventional therapies (i.e., ICB).

This model may be relevant for other cancer types too. Accumulative evidence suggests that OPN is one of the most potent metastasis-associated proteins during the progression of other cancer types such as breast, colon, lung, pancreatic, renal, and esophageal cancer [33]. Cancer is often linked to an expansion of MDSCs/Tregs [41,42], in which OPN/ICOSL/ICOS trio may be involved. Given that the frequencies of MDSCs/Tregs have also been negatively correlated with the response to immunotherapy, targeting these cells in cancer patients may be a viable therapeutic approach to reverse immune escape and to maximize immune-based treatments.

Lastly, many investigations have been performed to decipher the multiple signaling pathways and gene expression profiles induced by OPN by focusing on its binding to integrins and CD44. To the best of our knowledge, no studies have been performed yet investigating OPN/ICOSL intracellular signaling pathways. This research is necessary to improve the current understanding and to unveil the precise role of OPN/ICOSL in-

teraction in tumor microenvironment remodeling, in tumor progression and metastasis development. These studies may be relevant to dissect pathogenetic roles and to identify new therapeutic targets.

References

1. Siegel, R.L.; Miller, K.D.; Jemal, A. Cancer statistics, 2018. *CA Cancer J. Clin.* **2018**, *68*, 7–30. [CrossRef]
2. Liu, Y.; Sheikh, M.S. Melanoma: Molecular Pathogenesis and Therapeutic Management. *Mol. Cell Pharmacol.* **2014**, *6*, 228.
3. Antohe, M.; Nedelcu, R.I.; Nichita, L.; Popp, C.G.; Cioplea, M.; Brinzea, A.; Hodorogea, A.; Calinescu, A.; Balaban, M.; Ion, D.A.; et al. Tumor infiltrating lymphocytes: The regulator of melanoma evolution. *Oncol. Lett.* **2019**, *17*, 4155–4161. [CrossRef] [PubMed]
4. Huang, L.; Guo, Y.; Liu, S.; Wang, H.; Zhu, J.; Ou, L.; Xu, X. Targeting regulatory T cells for immunotherapy in melanoma. *Mol. Biomed.* **2021**, *2*, 11. [CrossRef]
5. Paluskievicz, C.M.; Cao, X.; Abdi, R.; Zheng, P.; Liu, Y.; Bromberg, J.S. T Regulatory Cells and Priming the Suppressive Tumor Microenvironment. *Front. Immunol.* **2019**, *10*, 2453. [CrossRef] [PubMed]
6. De Cicco, P.; Ercolano, G.; Ianaro, A. The New Era of Cancer Immunotherapy: Targeting Myeloid-Derived Suppressor Cells to Overcome Immune Evasion. *Front. Immunol.* **2020**, *11*, 1680. [CrossRef] [PubMed]
7. Talmadge, J.E.; Gabrilovich, D.I. History of myeloid-derived suppressor cells. *Nat. Rev. Cancer* **2013**, *13*, 739–752. [CrossRef]
8. Haist, M.; Stege, H.; Grabbe, S.; Bros, M. The Functional Crosstalk between Myeloid-Derived Suppressor Cells and Regulatory T Cells within the Immunosuppressive Tumor Microenvironment. *Cancers* **2021**, *13*, 210. [CrossRef] [PubMed]
9. Castello, L.M.; Raineri, D.; Salmi, L.; Clemente, N.; Vaschetto, R.; Quaglia, M.; Garzaro, M.; Gentilli, S.; Navalesi, P.; Cantaluppi, V.; et al. Osteopontin at the Crossroads of Inflammation and Tumor Progression. *Mediat. Inflamm* **2017**, *2017*, 4049098. [CrossRef] [PubMed]
10. Yin, M.; Soikkeli, J.; Jahkola, T.; Virolainen, S.; Saksela, O.; Hölttä, E. Osteopontin promotes the invasive growth of melanoma cells by activating integrin $\alpha v \beta 3$ and down-regulating tetraspanin CD9. *Am. J. Pathol.* **2014**, *184*, 842–858. [CrossRef]
11. Kiss, T.; Ecsedi, S.; Vizkeleti, L.; Koroknai, V.; Emri, G.; Kovács, N.; Adany, R.; Balazs, M. The role of osteopontin expression in melanoma progression. *Tumour Biol.* **2015**, *36*, 7841–7847. [CrossRef]

12. Klement, J.D.; Paschall, A.V.; Redd, P.S.; Ibrahim, M.L.; Lu, C.; Yang, D.; Celis, E.; Abrams, S.I.; Ozato, K.; Liu, K. An osteopontin/CD44 immune checkpoint controls CD8^{+} T cell activation and tumor immune evasion. *J. Clin. Invest.* **2018**, *128*, 5549–5560. [CrossRef] [PubMed]

13. Sangaletti, S.; Tripodo, C.; Sandri, S.; Torselli, I.; Vitali, C.; Ratti, C.; Botti, L.; Burocchi, A.; Porcasi, R.; Tomirotti, A.; et al. Osteopontin shapes immunosuppression in the metastatic niche. *Cancer Res.* **2014**, *74*, 4706–4719. [CrossRef]

14. Overwijk, W.W.; Restifo, N.P. B16 as a mouse model for human melanoma. *Curr. Protoc Immunol.* **2001**, *39*, 20–21. [CrossRef]

15. Kumar, S.; Sharma, P.; Kumar, D.; Chakraborty, G.; Gorain, M.; Kundu, G.C. Functional characterization of stromal osteopontin in melanoma progression and metastasis. *PLoS ONE* **2013**, *8*, e69116. [CrossRef]

16. Giopanou, I.; Lilis, I.; Papaleonidopoulos, V.; Agalioti, T.; Kanellakis, N.I.; Spiropoulou, N.; Spella, M.; Stathopoulos, G.T. Tumor-derived osteopontin isoforms cooperate with TRP53 and CCL2 to promote lung metastasis. *Oncoimmunology* **2017**, *6*, e1256528. [CrossRef] [PubMed]

17. Raineri, D.; Dianzani, C.; Cappellano, G.; Maione, F.; Baldanzi, G.; Iacobucci, I.; Clemente, N.; Baldone, G.; Boggio, E.; Gigliotti, C.L.; et al. Osteopontin binds ICOSL promoting tumor metastasis. *Commun. Biol.* **2020**, *3*, 615. [CrossRef] [PubMed]

18. Clemente, N.; Boggio, E.; Gigliotti, L.C.; Raineri, D.; Ferrara, D.; Miglio, G.; Argenziano, M.; Chiocchetti, A.; Cappellano, G.; Trotta, F.; et al. Immunotherapy of experimental melanoma with ICOS-Fc loaded in biocompatible and biodegradable nanoparticles. *J. Control Release* **2020**, *320*, 112–124. [CrossRef] [PubMed]

19. Dianzani, C.; Minelli, R.; Gigliotti, C.L.; Occhipinti, S.; Giovarelli, M.; Conti, L.; Boggio, E.; Shivakumar, Y.; Baldanzi, G.; Malacarne, V.; et al. B7h triggering inhibits the migration of tumor cell lines. *J. Immunol.* **2014**, *192*, 4921–4931. [CrossRef]

20. Yao, S.; Zhu, Y.; Zhu, G.; Augustine, M.; Zheng, L.; Goode, D.J.; Broadwater, M.; Ruff, W.; Flies, S.; Xu, H.; et al. B7-h2 is a costimulatory ligand for CD28 in human. *Immunity* **2011**, *34*, 729–740. [CrossRef]

21. Hutloff, A.; Dittrich, A.M.; Beier, K.C.; Eljaschewitsch, B.; Kraft, R.; Anagnostopoulos, I.; Kroczek, R.A. ICOS is an inducible T-cell co-stimulator structurally and functionally related to CD28. *Nature* **1999**, *397*, 263–266. [CrossRef] [PubMed]

22. Riley, J.L.; Blair, P.J.; Musser, J.T.; Abe, R.; Tezuka, K.; Tsuji, T.; June, C.H. ICOS costimulation requires IL-2 and can be prevented by CTLA-4 engagement. *J. Immunol.* **2001**, *166*, 4943–4948. [CrossRef]

23. Warnatz, K.; Bossaller, L.; Salzer, U.; Skrabl-Baumgartner, A.; Schwinger, W.; van der Burg, M.; van Dongen, J.J.; Orlowska-Volk, M.; Knoth, R.; Durandy, A.; et al. Human ICOS deficiency abrogates the germinal center reaction and provides a monogenic model for common variable immunodeficiency. *Blood* **2006**, *107*, 3045–3052. [CrossRef]

24. Dianzani, C.; Minelli, R.; Mesturini, R.; Chiocchetti, A.; Barrera, G.; Boscolo, S.; Sarasso, C.; Gigliotti, C.L.; Sblattero, D.; Yagi, J.; et al. B7h triggering inhibits umbilical vascular endothelial cell adhesiveness to tumor cell lines and polymorphonuclear cells. *J. Immunol.* **2010**, *185*, 3970–3979. [CrossRef] [PubMed]

25. Nurieva, R.I. Regulation of immune and autoimmune responses by ICOS-B7h interaction. *Clin. Immunol.* **2005**, *115*, 19–25. [CrossRef] [PubMed]

26. Occhipinti, S.; Dianzani, C.; Chiocchetti, A.; Boggio, E.; Clemente, N.; Gigliotti, C.L.; Soluri, M.F.; Minelli, R.; Fantozzi, R.; Yagi, J.; et al. Triggering of B7h by the ICOS modulates maturation and migration of monocyte-derived dendritic cells. *J. Immunol.* **2013**, *190*, 1125–1134. [CrossRef]

27. Busse, M.; Krech, M.; Meyer-Bahlburg, A.; Hennig, C.; Hansen, G. ICOS mediates the generation and function of CD4^{+}CD25^{+}Foxp3^{+} regulatory T cells conveying respiratory tolerance. *J. Immunol.* **2012**, *189*, 1975–1982. [CrossRef]

28. Vocanson, M.; Rozieres, A.; Hennino, A.; Poyet, G.; Gaillard, V.; Renaudineau, S.; Achachi, A.; Benetiere, J.; Kaiserlian, D.; Dubois, B.; et al. Inducible costimulator (ICOS) is a marker for highly suppressive antigen-specific T cells sharing features of TH17/TH1 and regulatory T cells. *J. Allergy Clin. Immunol.* **2010**, *126*, 280–289. [CrossRef]

29. Zheng, J.; Chan, P.L.; Liu, Y.; Qin, G.; Xiang, Z.; Lam, K.T.; Lewis, D.B.; Lau, Y.L.; Tu, W. ICOS regulates the generation and function of human CD4^{+} Treg in a CTLA-4 dependent manner. *PLoS ONE* **2013**, *8*, e82203. [CrossRef] [PubMed]

30. Nakamura, K.D.; Tilli, T.M.; Wanderley, J.L.; Palumbo, A., Jr.; Mattos, R.M.; Ferreira, A.C.; Klumb, C.E.; Nasciutti, L.E.; Gimba, E.R. Osteopontin splice variants expression is involved on docetaxel resistance in PC3 prostate cancer cells. *Tumour Biol.* **2016**, *37*, 2655–2663. [CrossRef] [PubMed]

31. Paoli, P.; Giannoni, E.; Chiarugi, P. Anoikis molecular pathways and its role in cancer progression. *Biochim. Biophys. Acta* **2013**, *1833*, 3481–3498. [CrossRef]

32. Wang, W.C.; Zhang, X.F.; Peng, J.; Li, X.F.; Wang, A.L.; Bie, Y.Q.; Shi, L.H.; Lin, M.B.; Zhang, X.F. Survival Mechanisms and Influence Factors of Circulating Tumor Cells. *Biomed. Res. Int.* **2018**, *2018*, 6304701. [CrossRef]

33. Zhao, H.; Chen, Q.; Alam, A.; Cui, J.; Suen, K.C.; Soo, A.P.; Eguchi, S.; Gu, J.; Ma, D. The role of osteopontin in the progression of solid organ tumour. *Cell Death Dis.* **2018**, *9*, 356. [CrossRef]

34. Zhou, Y.; Dai, D.L.; Martinka, M.; Su, M.; Zhang, Y.; Campos, E.I.; Doricicz, I.; Tang, L.; Huntsman, D.; Nelson, C.; et al. Osteopontin expression correlates with melanoma invasion. *J. Invest. Dermatol.* **2005**, *124*, 1044–1052. [CrossRef]

35. Wolchok, J.D.; Chiarion-Sileni, V.; Gonzalez, R.; Rutkowski, P.; Grob, J.J.; Cowey, C.L.; Lao, C.D.; Wagstaff, J.; Schadendorf, D.; Ferrucci, P.F.; et al. Overall Survival with Combined Nivolumab and Ipilimumab in Advanced Melanoma. *N. Engl. J. Med.* **2017**, *377*, 1345–1356. [CrossRef] [PubMed]

36. Anani, W.; Shurin, M.R. Targeting Myeloid-Derived Suppressor Cells in Cancer. *Adv. Exp. Med. Biol* **2017**, *1036*, 105–128. [CrossRef] [PubMed]

37. Tanaka, A.; Sakaguchi, S. Targeting Treg cells in cancer immunotherapy. *Eur. J. Immunol.* **2019**, *49*, 1140–1146. [CrossRef]

38. Fu, T.; He, Q.; Sharma, P. The ICOS/ICOSL pathway is required for optimal antitumor responses mediated by anti-CTLA-4 therapy. *Cancer Res.* **2011**, *71*, 5445–5454. [CrossRef] [PubMed]

39. Klement, J.D.; Poschel, D.B.; Lu, C.; Merting, A.D.; Yang, D.; Redd, P.S.; Liu, K. Osteopontin Blockade Immunotherapy Increases Cytotoxic T Lymphocyte Lytic Activity and Suppresses Colon Tumor Progression. *Cancers* **2021**, *13*, 1006. [CrossRef] [PubMed]

40. Moorman, H.R.; Poschel, D.; Klement, J.D.; Lu, C.; Redd, P.S.; Liu, K. Osteopontin: A Key Regulator of Tumor Progression and Immunomodulation. *Cancers* **2020**, *12*, 3379. [CrossRef] [PubMed]

41. Halvorsen, E.C.; Mahmoud, S.M.; Bennewith, K.L. Emerging roles of regulatory T cells in tumour progression and metastasis. *Cancer Metastasis Rev.* **2014**, *33*, 1025–1041. [CrossRef] [PubMed]

42. Yin, Z.; Li, C.; Wang, J.; Xue, L. Myeloid-derived suppressor cells: Roles in the tumor microenvironment and tumor radiotherapy. *Int. J. Cancer* **2019**, *144*, 933–946. [CrossRef] [PubMed]

3.4 ICOS-Fc application on Myeloma Multiple

Multiple Myeloma (MM) is a complex and heterogeneous malignant disease of plasma cells (PCs) that are located into the bone marrow (BM) and whose malignancy is exhibited through the production of abnormal immunoglobulin (M protein), mostly IgG and IgA (Michels & Petersen, 2017). Development and progression of MM was found often correlated to chromosomal abnormalities with other genetic mutations. For instance, KRAS and NRAS genes mutations were demonstrated favoring tumor cells survival and proliferation, while treatment resistance and poor prognosis were correlated to TP53 tumor suppressor gene deletion and/or mutations (Hoang et al., 2006; W. Xiong et al., 2008; Jovanović et al., 2019; Yang et al., 2022). The disease tends to progress from a premalignant monoclonal gammopathy of undetermined significance (MGUS), eventually developing through an intermediate stage of smouldering multiple myeloma (SMM). Both do not display the end organ damage typical of MM, whose clinical scenario is commonly described with CRAB acronym. The "C" stands for hyperCalcemia; the "R" for Renal insufficiency; the "A" for Anaemia and the "B" for Bone disease, whose characteristic osteolytic lesions are showed by the majority of MM patients and are considered the MM hallmark (Fairfield Heather et al., 2016; Tomasson et al., 2018).

The MM severe net bone loss and limited bone healing is due to the progressive loss of balanced functional activities of OBs (bone building) and OCs (bone breakdown and resorption). The OCs activity is overstimulated by high levels of RANKL expressed on the surface of myeloma cells, BM stromal cells, Th cells (mainly Th17 cells), and soluble RANKL (sRANKL) in the serum. Moreover, the involvement of BM microenvironment mediated by MM PCs is crucial in fostering cytokines and vascular endothelial growth factor production (IL-6 and VEGF), vascular permeability, angiogenesis and different cells interactions, which all together work for perpetuate uncontrolled tumor growth, bone destruction and immune dysfunction (Fairfield Heather et al., 2016; Bernstein et al., 2022; Schinke et al., 2022; Rafae et al., 2023). Indeed, MM patients show an impaired immunity and a higher susceptibility to infectious diseases. The tumor strategy of promoting a suppressive environment, able to evade immune system response, can affect different immune cell populations. Indeed, MM is characterized by a reduction in the diversity and function of T-cells and natural killer (NK) cells, as well as an increase in Treg cells and MDSC, whose accumulation blocks their differentiation into DCs causing their deficiency and drop of functions (Brimnes et al., 2010; Rafae et al., 2023). As a result, next to the traditional chemotherapy and radiation, in the last two decades

research was extensively focused on MM novel immunotherapy approaches and tremendous advances in outcomes were achieved (Rajkumar, 2022; Morè et al., 2023). Unfortunately, MM remains not only incurable in most patients, but the progressive compromised bone condition daily threatens patients safety and wellbeing, even if a remission was started and ongoing (Roodman, 2011; Bird & Boyd, 2019; Bernstein et al., 2022).

In this scenario, earns more relevance the discovered and well documented involvement of the inducible T-cell co-stimulator (ICOS) and its ligand (ICOSL) in bone metabolism. Their important role in activation of Th cells, Treg differentiation and T-/B-cell interaction was widely demonstrated in osteoporosis context, highlighting how ICOS/ICOSL interaction can modulate OCs function (Gigliotti et al., 2016). The second significant aspect of ICOS/ICOSL system in MM lies in the fact that ICOSL is also bound by OPN, which is not only expressed by MM cells, but found involved also in tumor progression, cancer cell metastatization, angiogenesis and bone destruction (Valković et al., 2014; Castello et al., 2017; Raineri et al., 2022).

The promising inhibitory effect of ICOS-Fc on OCs next to its capability to block OPN-induced cancer cells migration suggested ICOS-Fc as potentially effective immunomodulator drug in MM therapy.

Inducible T-cell co-stimulator (ICOS) and ICOS ligand are novel players in the multiple-myeloma microenvironment

Background: MM is a malignant disease characterized by the accumulation of MM PCs into the bone marrow, which produce abnormal immunoglobulin (M-protein). It usually develops from a premalignant condition MGUS and SMM, which could be asymptomatic and do not achieve the organ damage typical of MM. The acronym CRAB is used to gather its clinical specific hallmarks, such as hyperCalcemia, Renal insufficiency, Anaemia and Bone disease, resulting in severe osteolytic lesions caused by imbalanced functions of OBs and OCs. It has been already documented the relevance of the BM microenvironment involvement led by MM PCs, which promotes tumor growth, bone destruction and immune dysfunction. Interestingly, ICOS/ICOSL system was found involved in the lymphocyte-bone cells interaction, depicting how its mediated signaling could inhibit OCs activity (Gigliotti et al., 2016). Moreover, acquired evidence showed ICOSL triggering anti-tumor effects by acting on tumor cells, TME, DCs, ECs and macrophages (Dianzani et al., 2010; Occhipinti et al., 2013; Dianzani et al., 2014). In this regard, the OPN documented involvement in bone formation and tumor progression achieved much more relevance when it was identified as another ligand for ICOSL. Next to the OPN/ICOSL induced cell migration effect, ICOS-Fc was able to block cancer cell migration induced by OPN. This effect confirmed how ICOS interaction with ICOSL dominantly counteract OPN effect. Since OPN is also expressed on myeloma cells, it is considered another important aspect of targeting the ICOS/ICOSL system for MM.

Aim: The aim of this work was to investigate the expression of ICOS and ICOSL and their soluble form (sICOS and sICOSL) in MM cells and to evaluate the potential ICOS-Fc immunomodulatory role in MM progression.

Method: a cohort of plasma cell dyscrasia patients (MGUS, SSM and MM) were involved to evaluate both serum level of sICOS and sICOSL and MM cells surface expression of ICOS and ICOSL. Migration assay was performed using the murine cell line MOPC-21 and MOPC-21[ICOSL], expressing low and high level of ICOSL respectively, and the human RPMI-8226, which spontaneously express high level of ICOSL.

In order to evaluate the antiproliferative effect of ICOS-Fc, it was performed an *in vivo* MM mouse model, using NSG mice injected subcutaneously with MOPC-21[ICOSL] cells.

Since *in vivo* ICOS-Fc antiproliferative effect was detected only when it was delivered into nanoparticles (Clemente et al., 2020), once again the ICOS-Fc administration was done through

nanodelivery system (PLGA nanoparticles). Tumor samples were harvested and stained with CD31 or Ki67 to assess tumor vessel formation and cancer cell proliferation.

Results: Serum levels of sICOS and sICOSL differed among the different plasma cell disorders considered. They were found to positively correlate with several markers of tumor burden, such as β2-microglobulin (B2M), M protein, BM plasma cells and negatively correlated with haemoglobin (Hb). The results showed that higher were the serum levels of sICOSL and sICOS found in MM patients, compared to MGUS and SMM cases, and massive sICOS level could be associated with worse overall survival (OS) of MM patients.

The flow cytometry results demonstrated that MM cells express both ICOSL, and at lower levels, ICOS. This evidence led to evaluate ICOS-Fc anti-migratory effect on all kind of MM cells (MOPC-21; MOPC-21^{ICOSL}; RPMI-8226). As able to inhibit invasion of different kinds of tumor cells, ICOS-Fc revealed itself capable to significantly counteract migration of both myeloma cells lines expressing high level of ICOSL.

Moreover *in vivo* results already showed that ICOS-Fc nanoencapsulation in poly lactic-co-glycolic acid (PLGA) nanoparticles promoted a better drug tumor targeting and therapy effectiveness optimization, which resulted in ICOS-Fc-PLGA capability to decrease tumor growth of ICOSL+ cells in melanoma mouse model (Clemente et al., 2020). In the MM model scenario, the results showed again how ICOS-Fc-PLGA treatment can counteract tumor growth, compared to control mice. The Ki67 staining of the tumor samples confirmed ICOS-Fc clear effect on cancer cell proliferation rate. Moreover, the resulting therapeutic effect could be correlated to an ICOS-Fc anti-angiogenic effect, supported by a significant decreased of tumor vascular density (CD31 staining of tumor sections).

The NGS mice were chosen to collect clear evidence about ICOS-Fc antineoplastic effect, without any potential effects coming from an immune response involvement. In this regard, ICOS-Fc might boost the anti-tumor immune response helping to overcome immune evasion. Even if in the MM mouse model exploited the immunological effect was underestimated, the promising findings collected with a well-documented immunomodulation potentiality of ICOS-Fc, supported the hypothesis to reach better therapeutical advantages using an immunocompetent *in vivo* model.

Conclusion: These promising results indicated that both sICOS and sICOSL may play a role in myeloma cells growth. They could be considered as valid therapeutic target for MM, since widely distributed within the TME and neoplastic cell surface. Moreover, ICOS/ICOSL axis could be exploited to support anti-tumor immune response, reinforcing the efficacy of immunotherapeutic approaches.

bjh research paper

Inducible T-cell co-stimulator (ICOS) and ICOS ligand are novel players in the multiple-myeloma microenvironment

Elena Boggio,[1,*] Casimiro Luca Gigliotti,[1,*] Riccardo Moia,[2,3,*] Annamaria Scotta,[3] Ilaria Crespi,[3] Paola Boggione,[2,3] Lorenzo De Paoli,[2,3] Clara Deambrogi,[2,3] Massimiliano Garzaro,[1] Matteo Vidali,[3] Annalisa Chiocchetti,[1] Ian Stoppa,[1] Roberta Rolla,[1,3] Chiara Dianzani,[4] Chiara Monge,[4] Nausicaa Clemente,[1] Gianluca Gaidano[2,3] and Umberto Dianzani[1,3]

[1]Department of Health Sciences and Interdisciplinary Research Center of Autoimmune Diseases (IRCAD), Università del Piemonte Orientale, [2]Division of Hematology, Department of Translational Medicine, Università del Piemonte Orientale, [3]Maggiore della Carità University Hospital, Novara, and [4]Department of Scienza e Tecnologia del Farmaco, University of Turin, Turin, Italy

*These authors contributed equally.

Summary

The inducible T-cell co-stimulator (ICOS) is a T-cell receptor that, once bound to ICOS ligand (ICOSL) expressed on several cell types including the B-cell lineage, plays a decisive role in adaptive immunity by regulating the interplay between B and T cells. In addition to its immunomodulatory functions, we have shown that ICOS/ICOSL signalling can inhibit the activity of osteoclasts, unveiling a novel mechanism of lymphocyte–bone cells interactions. ICOS and ICOSL can also be found as soluble forms, namely sICOS and sICOSL. Here we show that: (i) levels of sICOS and sICOSL are increased in multiple myeloma (MM) compared to monoclonal gammopathy of undetermined significance and smouldering MM; (ii) levels of sICOS and sICOSL variably correlate with several markers of tumour burden; and (iii) sICOS levels tend to be higher in Durie–Salmon stage II/III *versus* stage I MM and correlate with overall survival as an independent variable. Moreover, surface ICOS and ICOSL are expressed in both myeloma cells and normal plasma cells, where they probably regulate different functional stages. Finally, ICOSL triggering inhibits the migration of myeloma cell lines *in vitro* and the growth of ICOSL[+] MOPC-21 myeloma cells *in vivo*. These results suggest that ICOS and ICOSL represent novel markers and therapeutic targets for MM.

Keywords: inducible T-cell co-stimulator (ICOS)/ICOS ligand (ICOSL) system, multiple myeloma, sICOS and sICOSL.

Introduction

Multiple myeloma (MM) is a plasma cell neoplasia resulting from monoclonal expansion of long-lived myeloma cells in the bone marrow (BM), leading to production of monoclonal immunoglobulins (M protein), mostly IgG or IgA.

Multiple myeloma tends to develop from premalignant monoclonal gammopathy of undetermined significance (MGUS), possibly going through a stage known as asymptomatic smouldering multiple myeloma (SMM).[1–4] Both MGUS and SMM do not display the end organ damage typical of MM, consisting of osteolytic lesions, anaemia, hypercalcaemia, and renal failure, which constitutes the classical CRAB clinical presentation (hyperCalcaemia, Renal failure, Anaemia, Bone disease).[4,5]

In MM, active osteolytic lesions are promoted by osteoclasts (OC) stimulated by high levels of receptor activator of nuclear factor kappa-B ligand (RANKL) expressed on the surface of myeloma cells, BM stromal cells, T helper (Th) cells (mainly Th-17 cells), and soluble RANKL (sRANKL) in the serum.[6–8]

We have recently shown that novel players in bone metabolism are the inducible T-cell co-stimulator (ICOS) and its ligand (ICOSL), both with a well-established role in activation of Th cells and T-/B-cell interaction.[9] ICOS (CD278)

belongs to the CD28 family and binds ICOSL (also known as B7h, CD275, B7H2, B7-RP1, or GL50), a member of the B7 family.[10–12] ICOS is mainly expressed on activated T cells, but weak levels have been detected also on dendritic cells (DC).[13] ICOSL is expressed not only on a wide variety of cell types, including B cells, macrophages, and DC, but also on non-haematopoietic cells, such as vascular endothelial cells, epithelial cells, fibroblasts, and many cancer cell types.[14–17]

The main biological function of ICOSL is triggering ICOS, which acts as a costimulatory molecule for activated Th cells by modulating their cytokine secretion.[18–21] Moreover, the ICOS/ICOSL axis can elicit a bidirectional signal acting on ICOSL-expressing cells.[22,23] In DC, ICOSL triggering by ICOS-Fc, a recombinant soluble form of ICOS composed of the extra-cellular portion of ICOS fused to the IgG$_1$ Fc portion, modulates cytokine secretion, potentiates cross-presentation of endocytosed antigens on class I MHC molecules, and inhibits cell adhesiveness and migration. Moreover, ICOS-Fc inhibits adhesiveness and migration of endothelial cells and tumour cell lines *in vitro* as well as metastatic dissemination of tumour cells *in vivo*.[24–26] Recently, we have shown that ICOS-Fc encapsulated in biocompatible and biodegradable nanoparticles inhibits the growth of established B16-F10 melanoma by decreasing tumour vascularization and inhibiting regulatory T cells.[27]

Two aspects of the ICOS/ICOSL system are relevant for MM. First, ICOSL is expressed on OC, and ICOS-Fc inhibits RANKL-driven maturation and osteolytic activity of these cells *in vitro*, and the development of RANKL-induced osteoporosis *in vivo*.[9] Second, ICOSL is also bound by osteopontin (OPN), involved in bone formation. OPN is also expressed by myeloma cells where it regulates a number of functions, including adhesion to the extra-cellular matrix and angiogenesis. OPN and ICOS form a complex with ICOSL through different binding sites and elicit different, often opposite, functional effects.[28–30]

ICOS and ICOSL can also be secreted as soluble forms — namely sICOS and sICOSL — which may derive from alternative transcription of the gene, alternative splicing of the mRNA, or proteolytic cleavage of the membrane form.[31,32] Of note, the serum levels of sICOS and sICOSL are increased in some autoimmune diseases.[33–37]

The aim of this study was to assess the expression of ICOS and ICOSL in plasma cell dyscrasias to investigate the role of this receptor system in malignant progression and end organ damages.

Materials and methods

Patients

The study enrolled 204 patients with plasma cell dyscrasias referred to the Hematology Division of the "AOU Maggiore della Carità", Novara, Italy between November 2016 and March 2021. They were grouped in MGUS, SMM, and MM

according to the 2017updated ESMO guidelines, referring to International Myeloma Working Group (IMWG) diagnostic criteria (Table I).[38] All MM patients received therapy, including immunomodulatory agents, proteasome inhibitors, monoclonal antibodies, and chemotherapy. At the time of sampling, the median number of previous lines of therapy was 1 (0–6). Fifty-nine healthy controls (HCs) were matched for gender and age. The protocol was approved by the local Ethics Committee (No. CE 33/17), and all subjects signed an informed consent.

ICOS/ICOSL analysis

Serum levels of sICOS, sICOSL and sRANKL were assessed by enzyme-linked immunosorbent assay (Cloud Clone Corporation, Katy, TX, USA). In two samples, sICOS and sICOSL levels were also measured after ultracentrifugation for 1 h at 4°C at 100.000 g in both the supernatant and the extra-cellular vesicle (EV) pellet.

Surface expression of ICOS and ICOSL was evaluated by flow cytometry (Attune NxT, Thermo-Fisher, Waltham, MA, USA) using fluorescein isothiocyanate (FITC)-conjugated anti-CD38 (eBioscience, San Diego, CA, USA), PE-conjugated anti-ICOS (R&D System, Minneapolis, MN, USA), PE-Cyanine (Cy) 7-conjugated anti-ICOSL (BioLegend, San Diego, CA, USA), PE- or APC-Cy7-conjugated anti-CD45 (eBioscience), and APC-conjugated anti-CD56 (eBioscience) mAb.[39–42]

Cell migration assay

MOPC-21 cells (mouse myeloma) were a gift from Monash University (Clayton, Australia); RPMI-8226 cells (human myeloma) were purchased from ATCC (Manassas, VN, USA).

MOPC-21^{ICOSL} cells were MOPC-21 cells that were transfected with 2·5 μg of plasmid DNA coding for mouse ICOSL, as previously reported.[30]

In transwell plates (Corning Inc., Corning, NY, USA), 1×10^6 cells were plated onto the upper side of each well in serum-free medium with or without 2 μg/ml of ICOS-Fc

Table I. Patients' characteristics.

		MGUS	SMM	MM	Total
Patients	*n* (%)	36 (17·6)	97 (47·5)	71 (34·8)	204
Gender	Female	14 (38·9)	38 (39·2)	36 (50·7)	88 (43·2)
	Male	22 (61·1)	59 (60·8)	35 (49·3)	116 (56·8)
Age (years)	Median	69	72	71	71
	Min	32	38	40	32
	Max	83	90	84	90
	Mean	65·2	69·9	69·6	68·9
	SD	11	11·5	8·3	10·5

MM, multiple myeloma; MGUS, monoclonal gammopathy of undetermined significance; SD, standard deviation; SMM, smouldering multiple myeloma.

1370

(human or murine), that is an agonist of ICOSL, or ^{F119S}ICOS-Fc (human). Twenty percent fetal bovine serum (FBS) was used as a chemoattractant. After 18 h, the cells migrated to the lower chamber were counted with an inverted microscope (magnification ×100).

In vivo experiments

Eight-week-old female NOD-SCID-IL2Rγ–null mice (NSG) (Charles River Laboratories, Wilmington, MA, USA) were injected subcutaneously with 2×10^6 MOPC-21^{ICOSL} cells. When tumours were palpable, mice were treated every four days by intraperitoneal injection of murine ICOS-Fc loaded in poly(lactic-co-glycolic acid) (PLGA) nanoparticles (ICOS/PLGA, 100 μg) or empty PLGA or saline. The tumour size was measured every four days and mice were sacrificed after 20 days.[27]

Mice were bred under pathogen-free conditions in the animal facility of the Department of Health Sciences. The study was approved by Ministero della Salute, Rome (No. 477/2016-PR and No. 849/2016 PR).

Staining of CD31 and Ki67, and tumour microvessel density measurements were performed on tissue sections as previously described.[27,43]

Statistical analyses

Correlations were determined using Spearman's non-parametric test. Comparisons were performed using the Mann–Whitney test, Wilcoxon test, and paired t-test. Survival analysis was performed by the Kaplan–Meier method and compared between strata using the log-rank test. The adjusted association between exposure variables and overall survival (OS) was estimated by Cox regression.

Results

Serum levels of sICOS and sICOSL in patients with plasma cell dyscrasias

Serum levels of sICOS and sICOSL were measured in a cohort of plasma cell dyscrasia patients ($n = 204$) (Table I), and in 59 HCs. MM patients displayed higher sICOS and sICOSL serum levels than those found in MGUS and SMM patients (Fig 1A,B). Of note, the serum levels of sICOS and sICOSL in MGUS and SMM patients were not statistically different from those present in HCs (Fig 1A,B). Stratification of MM patients according to the Durie–Salmon staging system (DS; DS-I: $n = 16$; DS-II: $n = 39$; DS-III: $n = 16$) revealed that sICOS serum concentration was higher in DS-II and DS-III compared to DS-I (Fig 1C,D), whereas no difference was found for sICOSL.

Correlations with disease markers

Spearman's Rho test was performed to evaluate any correlations between sICOSL or sICOS serum levels and other known serum disease markers. These included i) the tumour burden markers β2-microglobulin (B2M), M protein, BM plasma cells, and haemoglobin (Hb); ii) the bone metabolism markers calcium, sRANKL, and OPN.

Analysis of the tumour burden markers showed that, in all patients, sICOS correlated directly with B2M, total M protein, BM plasma cells and inversely with Hb (Fig 2A–D). On the other hand, sICOSL correlated directly with B2M and total M protein (Fig 2E–F). sICOS also showed a positive correlation with BM plasma cells among MM and MGUS patients ($r = 0.731$, $P = 0.02$), whereas sICOSL correlated with total M protein in MM patients ($r = 0.478$, $P = 0.0002$) (data not shown).

Analysis of bone metabolism and kidney injury markers revealed a direct correlation between sICOSL and sRANKL (Fig 2G).

Since MM patients display decreased levels of polyclonal Ig, we also analyzed the correlation of serum sICOS and sICOSL with polyclonal IgM and IgA in 50 MM patients producing IgG M protein (IgG/MM). We found that sICOS, but not sICOSL (data not shown), negatively correlated with polyclonal IgA and IgM (Fig 2H–I).

After a median follow-up period of 37.6 months, 40 patients died, and the 36-month OS was 78.7%. As expected, patients with MM had a worse OS than those with SMM or MGUS. Stratification of all patients for the median value of serum concentration of sICOS (27.9 pg/ml), sICOSL (994.7 pg/ml), or sRANKL (1024.3 pg/ml) showed that patients with sICOS levels above the median value had a worse OS than those below this value (OS-36: 70.1% vs 89.2%, $P = 0.002$). By contrast, levels of sICOSL and sRANKL did not correlate with OS (Figure S1). An optimized sICOS threshold of 40 pg/ml was the best cut-off for OS, which was 67.2% for patients above this cut-off and 89.2% for those below ($P = 0.00017$) (Fig 3A). Multivariate analysis showed that sICOS levels above 40 pg/ml maintained an independent association with an increased risk of death (HR 2.78, 95% CI 1.07–7.2, $P = 0.035$) when adjusted for Durie–Salmon staging. The clinical impact of sICOS was detected in MM, but not in SMM and MGUS (Fig 3B–D).

Surface expression of ICOS and ICOSL

Since serum levels of sICOS and sICOSL correlated with several tumour burden markers, we next assessed the surface expression of these receptors on myeloma cells. Flow cytometry analysis of BM samples from 31 MM patients showed that myeloma cells homogeneously expressed both ICOS (MFI-r 3.6 ± 0.25) and, to a higher extent, ICOSL (MFI-r 7.3 ± 0.66) (Fig 4A).
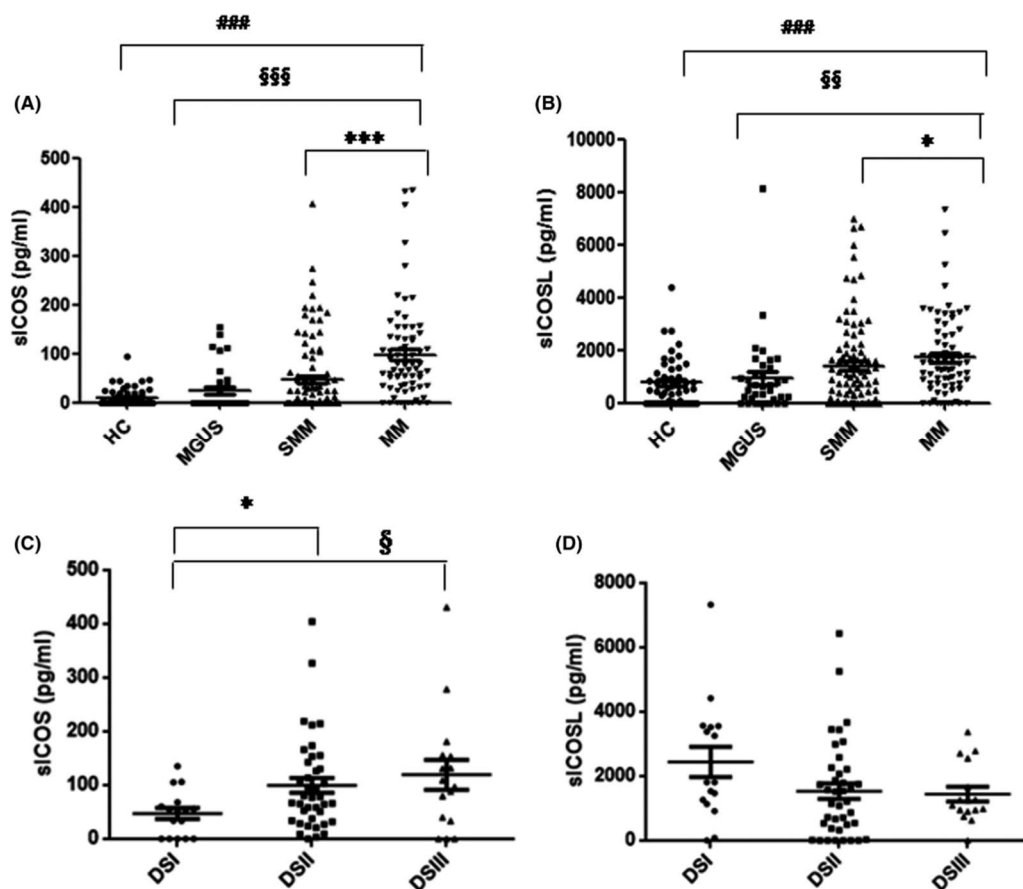
1371

Fig 1. Serum levels of soluble inducible T-cell co-stimulator (sICOS) and sICOS ligand (sICOSL) are increased in multiple-myeloma (MM) patients. (A) sICOS and (B) sICOSL were evaluated in the sera of smouldering MM (SMM) ($n = 97$), MM ($n = 71$) and monoclonal gammopathy of undetermined significance (MGUS) ($n = 36$) patients, and 59 HCs by enzyme-linked immunosorbent assay (ELISA). *, $P < 0.05$, ***, $P < 0.0001$ *versus* SMM; §§, $P < 0.01$, §§§, $P < 0.0001$ *versus* MGUS, ###, $P < 0.0001$ *versus* HC calculated by the Mann–Whitney non-parametric test. (C) sICOS and (D) sICOSL levels in MM patients stratified according to Durie–Salmon staging: DS-I ($n = 16$), DS-II ($n = 39$), and DS-III ($n = 16$). *, $P < 0.05$ *versus* DS-II, §, $P < 0.05$ *versus* DS-III calculated by the Mann–Whitney non-parametric test. Values are represented as mean ± SEM.

To investigate whether ICOS and ICOSL were also expressed on normal plasma cells, we analyzed surface expression of these molecules in BM plasma cells from eight patients affected from immune thrombocytopenia (ITP). We identified two plasma cell subsets, one expressing both ICOS and ICOSL, similar to myeloma cells, and the other expressing ICOSL but not ICOS (Fig 4B). More specifically, the ICOS+ICOSL+ and ICOS−ICOSL+ subsets accounted respectively for 45 ± 8·2% and 55 ± 8·3% (mean ± SEM) of BM plasma cells.

In MM patients ($n = 20$), a correlation was found between sICOS serum concentration and ICOS cell surface expression on myeloma cells, but not between sICOSL serum concentration and ICOSL cell surface expression (Fig 5A,B).

To assess whether serum sICOS and sICOSL were present as free proteins or associated with the EVs, we analyzed sICOS and sICOSL before and after ultracentrifugation of the serum, which is supposed to precipitate EVs. After centrifugation, sICOS and sICOSL were mainly found in the supernatant, whereas only minimal amounts were found in the EV pellet, suggesting that sICOS and sICOSL are present in the serum as free molecules (Fig 5C,D).

Effect of ICOS-Fc on myeloma cells

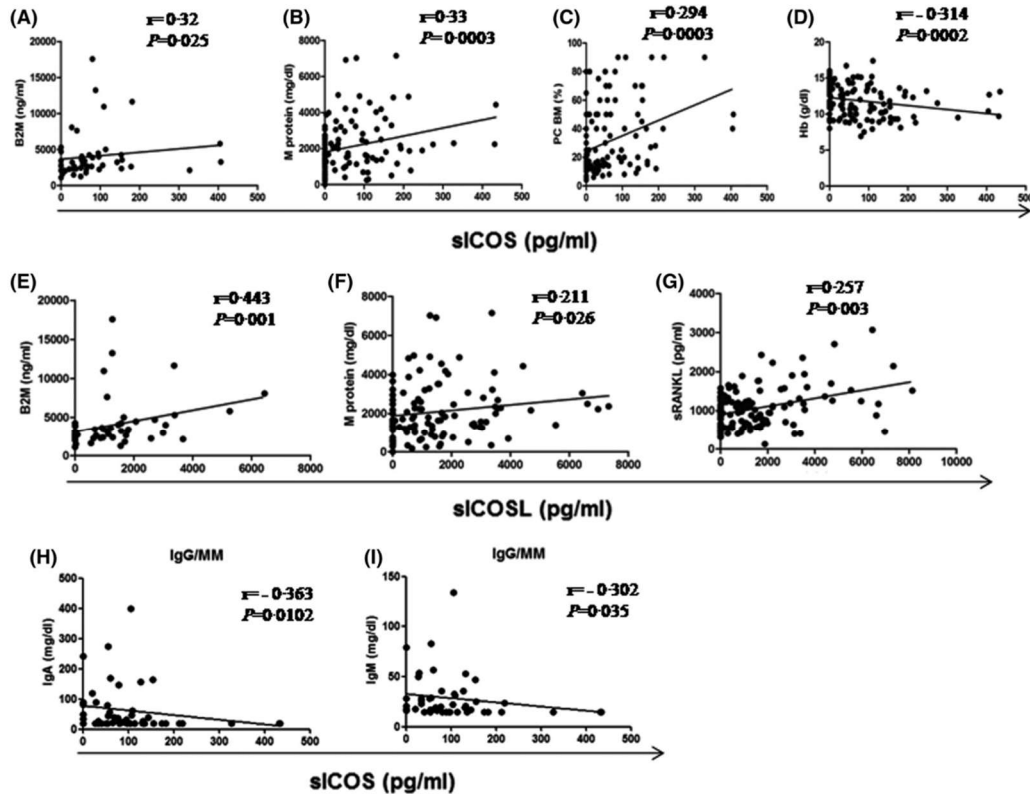As we have previously shown that triggering of ICOSL with ICOS-Fc inhibits migration of several types of tumour

79

Fig 2. Correlation of serum levels of soluble inducible T-cell co-stimulator (sICOS) and sICOS ligand (sICOSL) with disease markers. Correlations detected in total patients between serum levels of (A–D) sICOS and those of (A) β2-microglobulin (B2M), (B) M protein, (C) bone marrow (BM) plasma cells (BM PC), (D) haemoglobin (Hb); and between levels of (E–G) sICOSL and those of (E) B2M, (F) M protein, and (G) sRANKL. Panels H–I show the correlation detected in IgG/multiple myeloma (MM) between sICOS and polyclonal (H) IgA and (I) IgM. Spearman's ρ test.

cells,[25,26] we next asked whether this effect would also be true in myeloma cells. To this end, we performed migration assays using murine myeloma cells expressing either low (MOPC-21) or high levels of ICOSL (MOPC-21^{ICOSL}). In addition, we carried out similar experiments using RPMI-8226 human myeloma cells, which spontaneously express high levels of ICOSL (Fig 6A). Cells were seeded in the upper chamber of a transwell plate in the presence or absence of ICOS-Fc—human or mouse, as appropriate—, and the extent of migration was assessed in the lower chamber after 18 h, using FCS as chemoattractant.^{F119S}ICOS-Fc, a point mutant unable to bind ICOSL, was used as negative control. As shown in Fig 6B, ICOS-Fc inhibited the migration of both RPMI-8226 and MOPC-21^{ICOSL} cells but not that of MOPC-21 cells, which migrated to a much lower extent than MOPC-21^{ICOSL} cells. As expected, ^{F119S}ICOS-Fc had no effect on either cell line.

We previously demonstrated that treatment of mice with ICOS-Fc loaded in poly(d,l-lactide-co-glycolide) (PLGA) nanoparticles (ICOS/PLGA) hampered the growth of established tumours arising upon subcutaneous injection of ICOSL$^+$ melanoma cells.[27] To assess whether this effect would also occur in myeloma cells, we injected subcutaneously MOPC-21^{ICOSL} cells in immunodeficient NSG mice and treated them with ICOS/PLGA as soon as the tumour was palpable. NSG mice were chosen to avoid any potential bias due to the effect of ICOS-Fc on the anti-tumour immune response. Control mice were treated with either saline or empty PLGA nanoparticles. Tumour growth monitoring revealed that treatment with ICOS/PLGA significantly decreased tumour growth compared to control mice (Fig 7A).

We next stained tumour sections for CD31 and Ki-67 to assess tumour vessel formation and cancer cell proliferation,
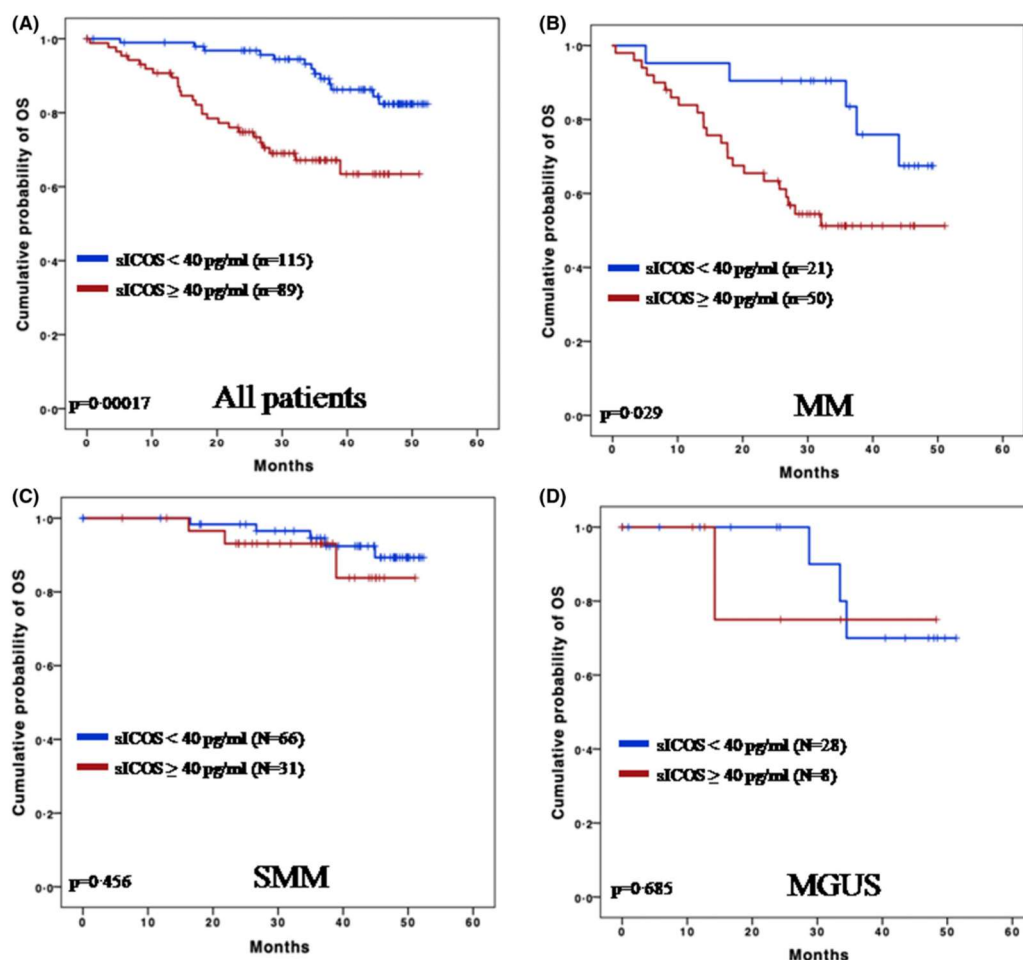
1373

Fig 3. Prognostic impact of of soluble inducible T-cell co-stimulator (sICOS) levels on survival. Kaplan–Meier estimates of overall survival (OS) of patients with sICOS above or below the 40 pg/ml cut-off. (A) All patients [multiple myeloma (MM) + smouldering MM (SMM) + monoclonal gammopathy of undetermined significance (MGUS)]. (B) MM patients. (C) SMM patients. (D) MGUS patients. [Colour figure can be viewed at wileyonlinelibrary.com]

respectively. Tumours from ICOS-Fc-treated mice displayed decreased tumour vascular density (Fig 7B) and cell proliferation rate compared to mice treated with either empty PLGA or saline (Fig 7C). Real-time polymerase chain reaction (PCR) analysis did not reveal any statistically significant differences in mRNA expression levels of ICOSL, IL-10, IFN-γ, IL-6, TNF-α, IL-1β, TGF-β, and OPN among the three groups (data not shown).

Discussion

This study shows that: *i)* sICOSL and sICOS serum levels vary across the spectrum of plasma cell disorders; *ii)* sICOSL

and sICOS serum levels correlate with several markers of tumour burden; *iii)* high serum levels of sICOS but not sICOSL are an independent prognostic factor of shorter survival in patients with plasma cell disorders; *iv)* ICOSL surface expression on neoplastic plasma cells may influence the biological behaviour of MM.

Here, we have applied multiple approaches to investigate the ICOS/ICOSL status in MM, a tumour in which ICOS/ICOSL signalling may exert multiple functions. Our results show that MM patients display higher serum levels of sICOSL and sICOS compared to those observed among MGUS and SMM cases. Moreover, sICOSL and sICOS serum levels positively correlate with the tumour burden markers
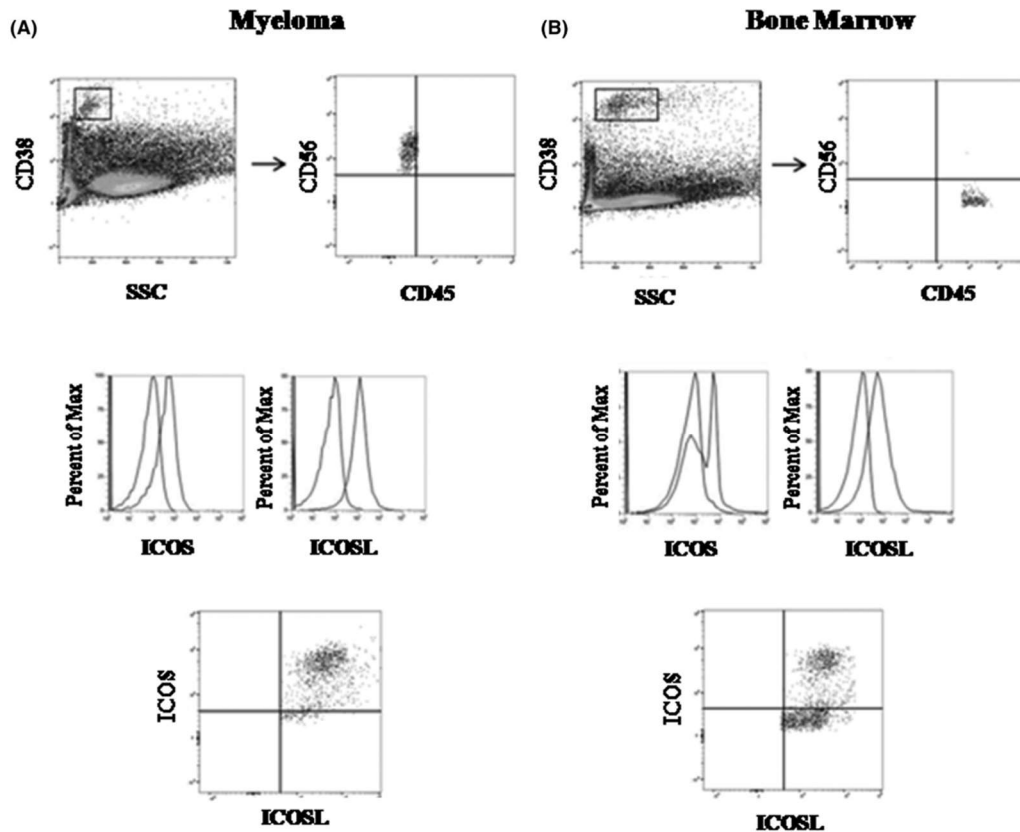
Fig 4. Flow cytometry plots of soluble inducible T-cell co-stimulator (sICOS) and sICOS ligand (sICOSL) expression in bone marrow (BM)-derived myeloma cells and normal plasma cells. Representative dot plots and histograms of (A) myeloma and (B) BM samples. Plasma cells were gated on $CD38^{bright}$ ($CD38^{+++}$) cells displaying the expected side scatter profile. Phenotype of the myeloma cells was $CD38^{+++}/CD45^{-}/CD56^{+}$, that of normal plasma cells was $CD38^{+++}/CD45^{+}/CD56^{-}$. The histograms show the overlay between control staining and ICOSL or ICOS staining.

B2M, M protein, and BM myeloma plasma cell infiltration, whereas they negatively correlate with Hb levels.

From a clinical standpoint, an optimized threshold of 40 pg/ml sICOS emerged as the best cut-off to split patient survival and retain a prognostic value in multivariate analysis. Although these results point to sICOS and sICOSL as potentially useful prognostic markers of plasma cell dyscrasias, they await further validation in prospective cohorts of MM patients.

Flow cytometry analysis shows that ICOSL and, at lower levels, ICOS are expressed as surface receptors on MM cells, confirming recent findings by mass cytometry.[44] The observation that the serum levels of sICOS correlate with surface expression of ICOS in myeloma cells suggests that at least part of sICOS may derive from the neoplastic cell population. This correlation was not detected for sICOSL, possibly due to the fact that its release from myeloma cells might be

hidden by the basally high serum levels of sICOSL, which are approximately one log-level higher than sICOS levels in HCs. Moreover, increased sICOSL levels in MM may also depend on its release from many types of non-neoplastic $ICOSL^{+}$ cells inside and outside of the BM, whereas ICOS expression appears to be restricted to only a few cell types.

The identification of two plasma cell subsets: $ICOS^{+}ICOSL^{+}$ and $ICOS^{-}ICOSL^{+}$ in normal BM plasma cells, indicates that ICOS and ICOSL expression may not represent a specific trait of neoplastic plasma cells. The $ICOS^{+}ICOSL^{+}$ phenotype might comprise long-lived plasma cells, which are the normal counterpart of myeloma cells. Consequently, the $ICOS^{-}ICOSL^{+}$ subset may comprise plasmablasts, which would be in line with the notion that activated B cells express ICOSL but not ICOS.[45]

The possibility that ICOS/ICOSL signalling plays a role in MM development is supported by our *in vivo* experiments
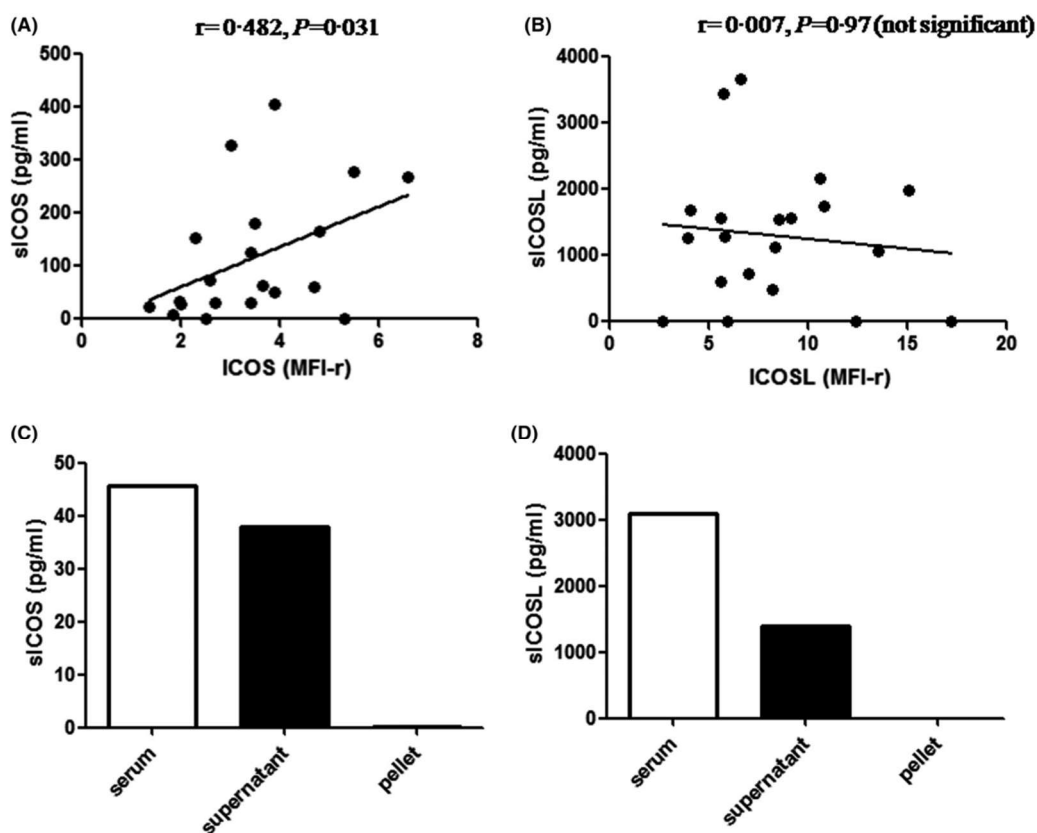
1375

Fig 5. Serum soluble inducible T-cell co-stimulator (sICOS) and sICOS ligand (sICOSL) may be partly released by myeloma cells as free molecules. sICOS serum levels (A) correlate with ICOS surface expression levels on myeloma cells. (B) The correlation between sICOSL and the expression level of ICOSL is not significant in 20 patients with multiple myeloma (MM) (Spearman's ρ test). ICOS and ICOSL expression levels were evaluated as mean fluorescence intensity ratio (MFI-r). Levels of (C) sICOS and (D) sICOSL evaluated in the serum of a patient before (white bars) and after (black bars) ultracentrifugation, which allowed the separation of EVs in the pellet from the supernatant. The graph represents data from one of two experiments performed with sera from two different patients.

showing that treatment with ICOS-Fc significantly inhibits the growth of MOPC-21[ICOSL] tumours in mice. This effect may be due to inhibition of tumour angiogenesis, as documented by the decreased tumour microvessel density displayed by tumours from mice treated with ICOS-Fc. However, ICOS-Fc might also exert direct effects on myeloma cells by inhibiting their migration, since ICOS-Fc inhibits *in vitro* migration of ICOSL^{+} myeloma cells. Moreover, ICOS-Fc might boost the anti-tumour immune response and overcome immune evasion, acting as an immune checkpoint antagonist, as suggested by our previous work on different tumour types[27,46] and several other works showing that inhibition of ICOS function on T cells impairs regulatory T-cell activity.[47] This immunological effect has been underestimated in our experimental model based on subcutaneous tumours in immunodeficient mice, prompting studies in the

immunocompetent BM setting, which might highlight interferences of ICOS-Fc with the complex MM niche, including those with osteoclasts (OC), whose maturation and osteoerosive activity is inhibited by ICOS-Fc.[9]

Survival and growth of plasma and myeloma cells depend on their bidirectional crosstalk with the BM microenvironment through a complex network, also including ICOS and ICOSL, which creates a permissive niche.[48–53] Thus, the functional effects of surface and soluble forms of ICOS and ICOSL are likely to depend on the relative amounts of these molecules in the BM niche. In this regard, our data suggest that ICOS and ICOSL expressed on the cell surface of myeloma cells may transduce signals modulating neoplastic cell behaviour, as supported by the observation that increased ICOSL expression not only correlates with enhanced migration of MOPC-21 cells — possibly due to its interaction with
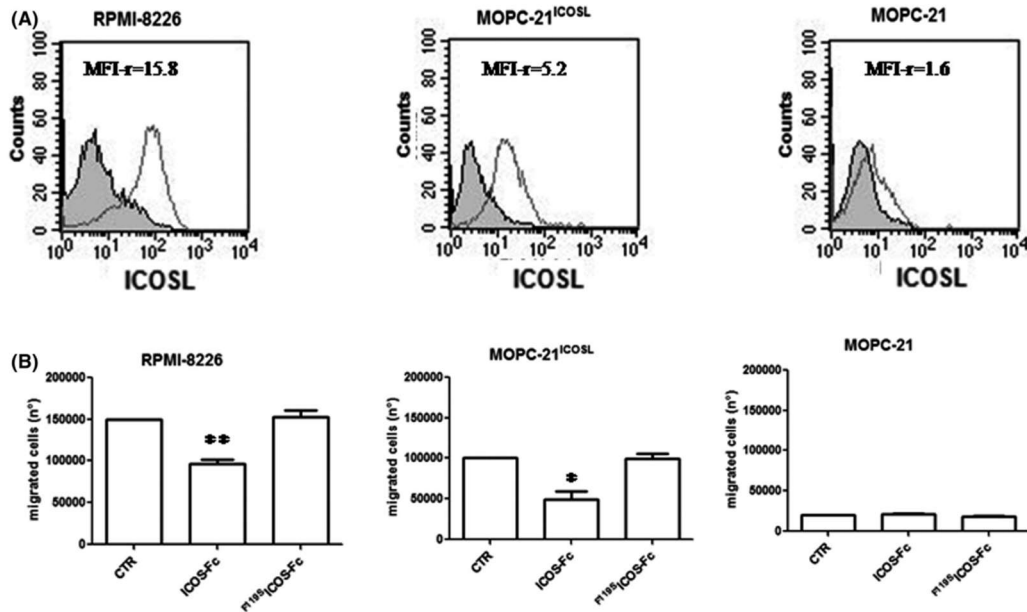
Fig 6. Inducible T-cell co-stimulator (ICOS)-Fc inhibits myeloma cells migration *in vitro*. (A) Representative histograms of ICOS ligand (ICOSL) expression in RPMI-8226, MOPC-21^{ICOSL}, and MOPC-21 cells. Each panel shows the overlay between the negative control and the positive staining. Values of mean fluorescence intensity ratio (MFI-r) are indicated. (B) Treatment with ICOS-Fc inhibits migration of RPMI-8226 (human) and MOPC-21^{ICOSL} (mouse) myeloma cells expressing ICOSL, but not that of MOPC-21 myeloma cells not expressing ICOSL, compared to both untreated cells and cells treated with the inactive mutant ^{F119S}ICOS-Fc. *, $P < 0.05$; **, $P < 0.01$ calculated by paired *t*-test. Values are represented as mean $\pm$ SEM ($n = 3$).
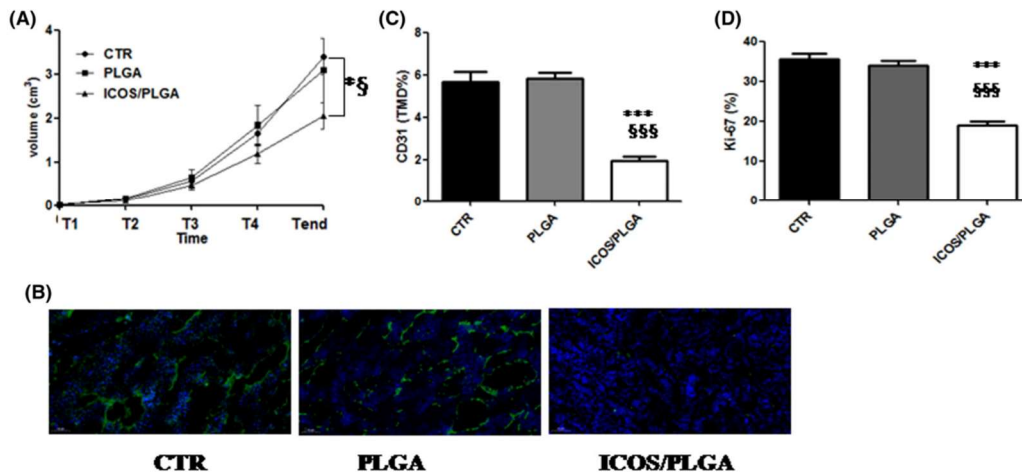
Fig 7. Inducible T-cell co-stimulator (ICOS)-Fc inhibits myeloma cells growth *in vivo*. (A) Treatment with ICOS-Fc loaded in poly(lactic-co-glycolic acid) (PLGA) nanoparticles (ICOS/PLGA, $n = 15$), but not saline [control (CTR), $n = 17$] or empty PLGA nanoparticles ($n = 14$), inhibits subcutaneous growth of MOPC-21^{ICOSL+} cells in NSG mice. (B) CD31 staining and (C) tumour microvessel density (TMD) measured on CD31 expression. (D) Proportion of Ki-67 positive tumour cells. Values are represented as mean $\pm$ SEM; *, $P < 0.05$; ***, $P < 0.0001$ vs CTR; §, $P < 0.05$; §§§, $P < 0.0001$ vs PLGA, calculated by the Mann–Whitney non-parametric test. [Colour figure can be viewed at wileyonlinelibrary.com]

OPN — but also makes these cells susceptible to ICOS-Fc-mediated inhibition of migration. In this context, it is also conceivable that aberrant expression of membrane-bound ICOSL on myeloma cells may antagonize ICOSL expressed on other cell types of the myeloma niche, such as endothelial cells and OC, which would make them resistant to ICOS-mediated inhibition.

It is also unclear what the functional effects of sICOS and sICOSL — present in the serum as free molecules — would be. In general, soluble forms of membrane receptors can act as decoy receptors able to antagonize their membrane-bound counterparts, as shown for several cytokine receptors.[54,55] Alternatively, they may work as agonistic ligands when they are multivalent, as reported for soluble Fas ligand (FasL) trimers, which are capable of inducing cell death upon Fas triggering.[56,57] Both models may apply to sICOSL and sICOS, which can function as either antagonistic monomers or agonistic dimers.[58,59]

Overall, our findings indicate that sICOS and sICOSL may play a role in myeloma cell growth. Furthermore, given their ubiquitous distribution within the tumour microenvironment and neoplastic cell surface, these molecules may also represent attractive therapeutic targets for MM. In this context, the ICOS/ICOSL axis might also be exploited to trigger T-ell immunity to further reinforce the efficacy of novel immunotherapeutic approaches.[47]

Acknowledgements

Conflicts of interest

EB, CLG, and UD are listed as inventors on the patent WO/2016/189428 "Ligands of B7h receptor in the treatment of osteopenia and osteoporosis", and are founders of an UPO Spinoff (NOVAICOS). AC, UD, CD, EB, NC, and CLG are listed as inventors on the patent PCT/IB2019/050154 "Novel anti-tumour therapeutic agents".

Funding information

Author contributions

Supporting Information

Additional supporting information may be found online in the Supporting Information section at the end of the article.

Fig S1. Lack of prognostic impact of sICOS, sICOSL, and sRANKL levels on survival. Kaplan-Meier estimates of overall survival (OS) of patients. (A) MM vs SMM+MGUS. (B–D) All patients (MM+SMM+MGUS) with (B) sICOS, (C) sICOSL, or (D) sRANKL above or below the median level.

References

1. Röllig C, Knop S, Bornhäuser M. Multiple multiple myeloma. *Lancet.* 2015;**385**(9983):2197–208. https://doi.org/10.1016/S0140-6736(14)60493-1

2. Michels TC, Petersen KE. Multiple myeloma: diagnosis and treatment. *Am Fam Physician.* 2017;**95**(6):373–83.

3. Terpos E, Christoulas D, Gavriatopoulou M, Dimopoulos MA. Mechanisms of bone destruction in multiple myeloma. *Eur J Cancer Care (Engl).* 2017;**26**(6):e12761. https://doi.org/10.1111/ecc.12761

4. Tomasson M, Ali M, De Oliveira M, Xiao Q, Jethava Y, Zhan F, et al. Prevention is the best treatment: the case for understanding the transition from monoclonal gammopathy of undetermined significance to myeloma. *Int J Mol Sci.* 2018;**19**(11):1–19. https://doi.org/10.3390/ijms19113621

5. Fairfield H, Falank C, Avery L, Reagan MR. Multiple myeloma in the marrow: pathogenesis and treatments. *Ann N Y Acad Sci.* 2016;**1364**(1):32–51. https://doi.org/10.1111/nyas.13038

6. Tikhonova AN, Dolgalev I, Hu H, Sivaraj KK, Hoxha E, Cuesta-Domínguez Á, et al. The bone marrow microenvironment at single-cell resolution. *Nature.* 2019;**569**(7755):222–8. https://doi.org/10.1038/s41586-019-1104-8

7. Terpos E, Szydlo R, Apperley JF, Hatjiharissi E, Politou M, Meletis J, et al. Soluble receptor activator of nuclear factor kappaB ligand-osteoprotegerin ratio predicts survival in multiple myeloma: proposal for a novel prognostic index. *Blood.* 2003;**102**(3):1064–9. https://doi.org/10.1182/blood-2003-02-0380

8. Buckle CH, de Leenheer E, Lawson MA. Soluble rank ligand produced by myeloma cells causes generalised bone loss in multiple myeloma. *PLoS One.* 2012;**7**(8):e41127. https://doi.org/10.1371/journal.pone.0041127

9. Gigliotti CL, Boggio E, Clemente N, Shivakumar Y, Toth E, Sblattero D, et al. ICOS-ligand triggering impairs osteoclast differentiation and function in vitro and in vivo. *J Immunol.* 2016;**197**(10):3905–16. https://doi.org/10.4049/jimmunol.1600424

10. Hutloff A, Dittrich AM, Beier KC, Eljaschewitsch B, Kraft R, Anagnostopoulos I, et al. ICOS is an inducible T cell co-stimulator structurally and functionally related to CD28. *Nature.* 1999;**397**(6716):263–6. https://doi.org/10.1038/16717

11. Buonfiglio D, Bragardo M, Redoglia V, Vaschetto R, Bottarel F, Bonissoni S, et al. The T cell activation molecule H4 and the CD28-like molecule

ICOS are identical. *Eur J Immunol.* 2000;**30**(12):3463–7. https://doi.org/10.1002/1521-4141(2000012)30:12<3463:AID-IMMU3463>3.0.CO;2-5

12. Redoglia V, Dianzani U, Rojo JM, Portolés P, Bragardo M, Wolff H, et al. Characterization of H4: a mouse T lymphocyte activation molecule functionally associated with the CD3/T cell receptor. *Eur J Immunol.* 1996;**26**(11):2781–9. https://doi.org/10.1002/eji.1830261134

13. Hedl M, Lahiri A, Ning K, Cho JH, Abraham C. Pattern recognition receptor signaling in human dendritic cells is enhanced by ICOS ligand and modulated by the Crohn's disease ICOSLG risk allele. *Immunity.* 2014;**40**(5):734–46. https://doi.org/10.1016/j.immuni.2014.04.011

14. Sharpe AH, Freeman GJ. The B7-CD28 superfamily. *Nat Rev Immunol.* 2002;**2**(2):116–26. https://doi.org/10.1038/nri727

15. Nurieva RI. Regulation of immune and autoimmune responses by ICOS-B7h interaction. *Clin Immunol.* 2005;**115**(1):19–25. https://doi.org/10.1016/j.clim.2005.02.010

16. Swallow MM, Wallin JJ, Sha WC. B7h, a novel costimulatory homolog of B7.1 and B7.2, is induced by TNFalpha. *Immunity.* 1999;**11**(4):423–32. https://doi.org/10.1016/s1074-7613(00)80117-x

17. Greenwald RJ, Freeman GJ, Sharpe AH. The B7 family revisited. *Annu Rev Immunol.* 2005;**23**:515–48. https://doi.org/10.1146/annurev.immunol.23.021704.115611

18. Yagi J, Arimura Y, Dianzani U, Uede T, Okamoto T, Uchiyama T. Regulatory roles of IL-2 and IL-4 in H4/inducible costimulator expression on activated CD4+ T cells during Th cell development. *J Immunol.* 2003;**171**(2):783–94. https://doi.org/10.4049/jimmunol.171.2.783

19. Mesturini R, Nicola S, Chiocchetti A, Bernardone IS, Castelli L, Bensi T, et al. ICOS cooperates with CD28, IL-2, and IFN-gamma and modulates activation of human naïve CD4+ T cells. *Eur J Immunol.* 2006;**36**(10):2601–12. https://doi.org/10.1002/eji.200535571

20. Mesturini R, Gigliotti CL, Orilieri E, Cappellano G, Soluri MF, Boggio E, et al. Differential induction of IL-17, IL-10, and IL-9 in human T helper cells by B7h and B7.1. *Cytokine.* 2013;**64**(1):322–30. https://doi.org/10.1016/j.cyto.2013.05.021

21. Tafuri A, Shahinian A, Bladt F, Yoshinaga SK, Jordana M, Wakeham A, et al. ICOS is essential for effective T-helper-cell responses. *Nature.* 2001;**409**(6816):105–9. https://doi.org/10.1038/35051113

22. Mak TW, Shahinian A, Yoshinaga SK, Wakeham A, Boucher L-M, Pintilie M, et al. Costimulation through the inducible costimulator ligand is essential for both T helper and B cell functions in T cell-dependent B cell responses. *Nat Immunol.* 2003;**4**(8):765–72. https://doi.org/10.1038/ni947

23. Tang G, Qin Q, Zhang P, Wang G, Liu M, Ding Q, et al. Reverse signaling using an inducible costimulator to enhance immunogenic function of dendritic cells. *Cell Mol Life Sci.* 2009;**66**(18):3067–80. https://doi.org/10.1007/s00018-009-0090-7

24. Occhipinti S, Dianzani C, Chiocchetti A, Boggio E, Clemente N, Gigliotti CL, et al. Triggering of B7h by the inducible costimulator modulates maturation and migration of monocyte-derived dendritic cells. *J Immunol.* 2013;**190**(3):1125–34. https://doi.org/10.4049/jimmunol.1201816

25. Dianzani C, Minelli R, Mesturini R, Chiocchetti A, Barrera G, Boscolo S, et al. B7h triggering inhibits umbilical vascular endothelial cell adhesiveness to tumor cell lines and polymorphonuclear cells. *J Immunol.* 2010;**185**(7):3970–9. https://doi.org/10.4049/jimmunol.0903269

26. Dianzani C, Minelli R, Gigliotti CL, Occhipinti S, Giovarelli M, Conti L, et al. B7h triggering inhibits the migration of tumor cell lines. *J Immunol.* 2014;**192**(10):4921–31. https://doi.org/10.4049/jimmunol.1300587

27. Clemente N, Boggio E, Gigliotti LC, Raineri D, Ferrara B, Miglio G, et al. Immunotherapy of experimental melanoma with ICOS-Fc loaded in biocompatible and biodegradable nanoparticles. *J Control Release.* 2020;**10**(320):112–24. https://doi.org/10.1016/j.jconrel.2020.01.030

28. Castello LM, Raineri D, Salmi L, Clemente N, Vaschetto R, Quaglia M, et al. Osteopontin at the crossroads of inflammation and tumor progression. *Mediators Inflamm.* 2017;**2017**:4049098. https://doi.org/10.1155/2017/4049098

29. Clemente N, Raineri D, Cappellano G, Boggio E, Favero F, Soluri MF, et al. Osteopontin bridging innate and adaptive immunity in autoimmune

diseases. *J of Immunol Res.* 2016;**2016**:7675437. https://doi.org/10.1155/2016/7675437

30. Raineri D, Dianzani C, Cappellano G, Maione F, Baldanzi G, Iacobucci I, et al. Osteopontin binds ICOSL promoting tumor metastatization. *Communicat Biol.* 2020;**3**(1):615. https://doi.org/10.1038/s42003-020-01333-1

31. Lownik JC, Luker AJ, Damle SR, Cooley LF, El Sayed R, Hutloff A, et al. ADAM10-mediated ICOSL shedding on B cells is necessary for proper T cell ICOS regulation and TFH responses. *J Immunol.* 2017;**199**(7):2305–15. https://doi.org/10.4049/jimmunol.1700833

32. Lownik JC, Wimberly JL, Conrad DH, Martin RK. B cell ADAM10 controls murine lupus progression through regulation of the ICOS:ICOS-ligand axis. *J Immunol.* 2019;**202**(3):664–74. https://doi.org/10.4049/jimmunol.1801207

33. Iwai H, Abe M, Hirose S, Tsushima F, Tezuka K, Akiba H, et al. Involvement of inducible costimulator-B7 homologous protein costimulatory pathway in murine lupus nephritis. *J Immunol.* 2003;**171**(6):2848–54. https://doi.org/10.4049/jimmunol.171.6.2848

34. Her M, Kim D, Oh M, Jeong H, Choi I. Increased expression of soluble inducible costimulator ligand (ICOSL) in patients with systemic lupus erythematosus. *Lupus.* 2009;**18**(6):501–7. https://doi.org/10.1177/0961203308099176

35. Yu H, Zou X, Peng L, Wang Y, Zhang C, Chen B, et al. Effect of soluble inducible costimulator level and its polymorphisms on age-related macular degeneration. *DNA Cell Biol.* 2013;**32**(12):717–21. https://doi.org/10.1089/dna.2013.2127

36. Wang D, Zhou D, Du Q, Liang QI, Wang Q, Fang LI, et al. Aberrant production of soluble inducible T-cell co-stimulator (sICOS) and soluble programmed cell death protein 1 (sPD-1) in patients with chronic hepatitis C. *Mol Med Rep.* 2013;**7**(4):1197–202. https://doi.org/10.3892/mmr.2013.1326

37. Yanaba K, Asano Y, Noda S, Akamata K, Aozasa N, Taniguchi T, et al. Increased production of soluble inducible costimulator in patients with diffuse cutaneous systemic sclerosis. *Arch Dermatol Res.* 2013;**305**(1):17–23. https://doi.org/10.1007/s00403-012-1292-7

38. Moreau P, San Miguel J, Sonneveld P, Mateos MV, Zamagni E, Avet-Loiseau H, et al. Multiple myeloma: ESMO Clinical Practice Guidelines for diagnosis, treatment and follow-up. *Annals Oncol.* 2017;**28**:iv52–iv61. https://doi.org/10.1093/annonc/mdx096

39. Lin P, Owens R, Tricot G, Wilson CS. Flow cytometric immunophenotypic analysis of 306 cases of multiple myeloma. *Am J Clin Pathol.* 2004;**121**(4):482–8. https://doi.org/10.1309/74R4-TB90-BUWH-27JX

40. Frigyesi I, Adolfsson J, Ali M, Kronborg Christophersen M, Johnsson E, Turesson I, et al. Robust isolation of malignant plasma cells in multiple myeloma. *Blood.* 2014;**123**(9):1336–40. https://doi.org/10.1182/blood-2013-09-529800

41. Flores-Montero J, de Tute R, Paiva B, Perez JJ, Böttcher S, Wind H, et al. Immunophenotype of normal vs. myeloma plasma cells: toward antibody panel specifications for MRD detection in multiple myeloma. *Cytometry B Clin Cytom.* 2016;**90**(1):61–72. https://doi.org/10.1002/cyto.b.21265

42. Arroz M, Came N, Lin P, Chen W, Yuan C, Lagoo A, et al. Consensus guidelines on plasma cell myeloma minimal residual disease analysis and reporting. *Cytometry B Clin Cytom.* 2016;**90**(1):31–9. https://doi.org/10.1002/cyto.b.21228

43. Clemente N, Ferrara B, Gigliotti C, Boggio E, Capuccio M, Biasibetti E, et al. Solid lipid nanoparticles carrying temozolomide for melanoma treatment. preliminary in vitro and in vivo studies. *Int J Mol Sci.* 2018;**19**(2):255. https://doi.org/10.3390/ijms19020255

44. Wang J, Zheng Y, Tu C, Zhang H, Vanderkerken K, Menu E, et al. Identification of the immune checkpoint signature of multiple myeloma using mass cytometry-based single-cell analysis. *Clin Transl Immunol.* 2020;**9**(5):e01132. https://doi.org/10.1002/cti2.1132

45. Zheng J, Chan P-L, Liu Y, Qin G, Xiang Z, Lam K-T, et al. ICOS regulates the generation and function of human CD4$^+$ Treg in a CTLA-4 dependent manner. *PLoS One.* 2013;**8**(12):e82203. https://doi.org/10.1371/journal.pone.0082203

1379

46. Iwata R, Lee JH, Hayashi M, Dianzani U, Ofune K, Maruyama M, et al. ICOSLG-mediated regulatory T-cell expansion and IL-10 production promote progression of glioblastoma. *Neuro Oncol*. 2020;**22**(3):333–44. https://doi.org/10.1093/neuonc/noz204

47. Amatore F, Laurent Gorvel L, Olive D. Role of inducible co-stimulator (ICOS) in cancer immunotherapy. *Expert Opin Biol Ther*. 2020;**20**(2):141–50. https://doi.org/10.1080/14712598.2020.1693540

48. Lightman SM, Utley A, Lee KP. Survival of long-lived plasma cells (LLPC): piecing together the puzzle. *Front Immunol*. 2019;3(10):965. https://doi.org/10.3389/fimmu.2019.00965

49. Winter O, Dame C, Jundt F, Hiepe F. Pathogenic long-lived plasma cells and their survival niches in autoimmunity, malignancy, and allergy. *J Immunol*. 2012;**189**(11):5105–11. https://doi.org/10.4049/jimmunol.1202317

50. Dhodapkar KM, Barbuto S, Matthews P, Kukreja A, Mazumder A, Vesole D, et al. Dendritic cells mediate the induction of polyfunctional human IL17-producing cells (Th17-1 cells) enriched in the bone marrow of patients with myeloma. *Blood*. 2008;**112**(7):2878–85. https://doi.org/10.1182/blood-2008-03-143222

51. Braga WMT, da Silva BR, de Carvalho AC, Maekawa YH, Bortoluzzo AB, Rizzatti EG, et al. FOXP3 and CTLA4 overexpression in multiple myeloma bone marrow as a sign of accumulation of CD4+ T regulatory cells. *Cancer Immunol Immunother*. 2014;**63**(11):1189–97. https://doi.org/10.1007/s00262-014-1589-9

52. Warnatz K, Bossaller L, Salzer U, Skrabl-Baumgartner A, Schwinger W, van der Burg M, et al. Human ICOS deficiency abrogates the germinal center reaction and provides a monogenic model for common variable immunodeficiency. *Blood*. 2006;**107**(8):3045–52. https://doi.org/10.1182/blood-2005-07-2955

53. Dong C, Temann UA, Flavell RA. Cutting edge: critical role of inducible costimulatorin germinal center reactions. *J Immunol*. 2001;**166**(6):3659–62. https://doi.org/10.4049/jimmunol.166.6.3659

54. Bonecchi R, Garlanda C, Mantovani A, Riva F. Cytokine decoy and scavenger receptors as key regulators of immunity and inflammation. *Cytokine*. 2016;**87**:37–45. https://doi.org/10.1016/j.cyto.2016.06.023

55. Mantovani A, Locati M, Vecchi A, Sozzani S, Allavena P. Decoy receptors: a strategy to regulate inflammatory cytokines and chemokines. *Trends Immunol*. 2001;**22**(6):328–36. https://doi.org/10.1016/s1471-4906(01)019 41-x

56. Suda T, Hashimoto H, Tanaka M, Ochi T, Nagata S. Membrane Fas ligand kills human peripheral blood T lymphocytes, and soluble Fas ligand blocks the killing. *J Exp Med*. 1997;**186**(12):2045–50.

57. Schneider P, Holler N, Bodmer JL, Hahne M, Frei K, Fontana A, et al. Conversion of membrane-bound Fas(CD95) ligand to its soluble form is associated with downregulation of its proapoptotic activity and loss of liver toxicity. *J Exp Med*. 1998;**187**(8):1205–13. https://doi.org/10.1084/jem.186.12.2045

58. Levin SD, Evans LS, Bort S, Rickel E, Lewis KE, Wu RP, et al. Novel immunomodulatory proteins generated via directed evolution of variant IgSF domains. *Front Immunol*. 2020;**21**(10):3086. https://doi.org/10.3389/fimmu.2019.03086

59. Chattopadhyay K, Bhatia S, Fiser A, Almo SC, Nathenson SG. Structural basis of inducible costimulator ligand costimulatory function: determination of the cell surface oligomeric state and functional mapping of the receptor binding site of the protein. *J Immunol*. 2006;**177**(6):3920–9. https://doi.org/10.4049/jimmunol.177.6.3920

4. ICOS-Fc nanoformulations

4.1 Cancer drug nanodelivery system

In cancer therapy, nanotechnology-based drug delivery systems arose as effective therapeutic approach able to overcome the challenges and limitations of the old and conventional therapies, such as their high dose and low availability, intolerance, instability, fluctuations in plasma drug levels not providing sustained effect (Pourmadadi et al., 2023).

Next to the severe side effects, the multidrugresistance (MDR) is the ricurrent stumbling block to a positive chemotherapeutic therapy outcome (Boggio et al., 2023). When not already inherent, it consists in a complex and multifactorial process that cancer cells acquire to escape from chemotherapy. In this regard, the reduction in drug cytotoxicity is correlated to functional gene mutations, which are responsible to alter target proteins, to decrease membrane permeability and to modulate drug metabolism. Many forms of drug resistance could be identified, such as the tumor drug accumulation, the prevention of cell drug internalization, the enhanced DNA repair processes and the increased in drug efflux transporters (Z. S. Chen & Tiwari, 2011; Zhang et al., 2017; H. Wang & Huang, 2020). Frequently it is a matter of P-glycoprotein (P-gp), multidrugresistance associated protein (MRP1) and breast cancer resistance protein (BCRP), which belong to the ATP-binding cassette efflux transporters family (Higgins, 2007; Trédan et al., 2007; Prasad Preethy et al., 2013).

In this scenario, nanoparticle formulations stand out for their capability to avoid multiple membrane efflux pumps, promoting drug released into cancer cells via endocytosis uptake mechanism (H. L. Wong, Bendayan, et al., 2006; H. L. Wong, Rauth, et al., 2006; Shuhendler et al., 2010; Prasad P. et al., 2013). This is one of the NPs advantages that fostered their use in anticancer therapy, followed through well documented evidence proving their correlated drug biodistribution optimization, drug cytotoxicity strengthening with the minimization of the free drug adverse effects. Moreover, the drug encapsulation into a protective shell-like structure leads to reduce the potential enzymatic and chemical drug degradation, increasing its bioavailability (Choudhury et al., 2017). In this context, main notable advantages of nano-delivery systems are the tumor targeting and the controlled drug release at the target site. The first one is due to the enhanced permeability and retention effect (EPR), which allows the nanoparticles discharging from vessels and their accumulation inside the tumor. The second one resulted from the improved *in-situ* drug retention, which permits prolonged maintenance of therapeutic drug levels, thus reduced dose frequency administration (Hani et al., 2023). Both effects could be enhanced through active targeting strategies, consisting in the NPs

functionalization with specific ligands targeting receptors or other surface proteins overexpressed on cancer cells (Bazak et al., 2015; Clemente et al., 2020). For instance, whole antibody or antibody fragments, such as single chain fragment variable (scFv), were used to target CD133 or HER2, receptors overexpressed on tumor cells of glioblastoma and breast cancer respectively. RDG peptide has been used to target integrins, overexpressed in the melanoma tumor cells. It was well demonstrated how an integrin-mediated endocytosis resulted in a more efficient intracellular delivery and in a significant reduced tumor growth (Boggio et al., 2023). Furthermore, several publications reported the high versatility of nanocarriers conjugated with folate acid (FA), which promote a selective cells-drug delivering, based on the system high affinity for FA binding proteins (FRα), aberrantly expressed in a wide spectrum of solid tumors (Assaraf et al., 2014; Seidu et al., 2022).

The choice of the drug carrier material is taken among several candidates (inorganic, metal, polymeric, lipid, and surfactant matrixes) and it depends on many factors, starting from the particle size required and the physical properties of the drug, to the surface characteristics, the degree of biodegradability, biocompatibility, toxicity and drug release profile (Felice et al., 2014; Vega-Vásquez et al., 2020).

Furthermore, a surface conjugation with polyethylene glycol (PEG) could be added to NPs which are, due to their charge, their molecular size and their hydrophobicity, highly vulnerable to be opsonized. The "proteic repellent" function of PEG protects the nanodelivery system from the immune system mediated elimination, enhancing NPs longevity within the bloodstream (Veronese & Pasut, 2005; Felice et al., 2014; Mishra et al., 2016).

Thanks to their high biocompatibility, almost all the NPs delivery systems approved by the FDA or currently in clinical trials are based on liposomes or polymers (Acharya & Sahoo, 2011; Boggio et al., 2023; Zeng et al., 2023). Is the matter of Doxil® (PEGylated liposome loaded with doxorubicin) approved in 1995 to be used in advanced-stage breast and ovarian cancer patients and in 2007 for multiple myeloma therapy (Hani et al., 2023). This liposomal anthracycline system stood out for its significant anticancer activity, assisted by a PEG-mediated considerably prolonged drug circulation, and a markable reduced cardiotoxicity. Furthermore, currently available for acute lymphoblastic leukemia are Oncaspar® (polymer protein conjugated with L-asparaginase approved in 2006), and Marqibo® (liposome loaded with vincristine approved in 2012). The first one main advantage consists in reducing the immunogenicity of asparaginase, while the encapsulation of vincristine

allows to ameliorate its restricted pharmacokinetic properties, depicted by its rapid clearance rate and dose-related neurotoxicity (Verhoef et al., 2014; Mao et al., 2019).

As a widely used delivery system, another liposomal drug delivery has been approved by FDA in 2015 (Onivyde®) for pancreatic and CRC. In these disease, the irinotecan liposomal injection offers several advantages, such as favoring the lactone E-ring stabilization, a pharmacokinetics improvement, side effects reduction, a prolonged action and an increased selective tumor uptake (Su et al., 2023).

Beyond the great therapy advantage achieved with drug loading into nanocarrier, the research moved progressively from single-agent therapies towards the combination nanomedicine therapeutic potentialities.

4.2 Combination therapy in cancer nanomedicine

The combination of different anti-tumor drugs and their loading into nanocarriers was proposed as a promising strategy to enhance drug efficacy and reduce life-threatening toxicities keeping the advantages of nanotechnology formulations (Boggio et al., 2023). Indeed, the pharmaceutical relevance of the combined nanomedicines consists in maximizing drugs additive or synergistic effects, allowing to reduce respectively each drug therapeutic dose.

Not few challenges have to be overcome to reach the best co-delivery nanoformulation. Indeed, the drugs can be loaded in a precise, therapeutically synergistic ratio, which not always corresponds to the one needed for synergism. Moreover, the potential interactions among drugs pair and the nanocarrier core could strongly impact on release kinetics and drugs stability, depicting the high synthetic challenge of formulating combined nanomedicine (Bhattacharjee, 2022).

However, once found the suitable drugs match, the co-loaded drugs are then delivered together and targeted to the same tissue, being able to affect cancer development, acting on both cancer cells and tumor microenviroment. What make this system more effective is the capability to perform an anticancer therapy through more and different mechanism of actions (Parhizkar et al., 2020).

This is what depicts them as a more powerful strategy against cancer MDR, whose mechanisms are influenced by both tumor cells and the TME, representing the principal cause of chemotherapy failures in metastatic cancer patients. Next to the cancer cells resistance, the compromised TME play a crucial role by acting as a both physical barrier, decreasing drug intratumor penetration and diffusion, and as a biological barrier by regulating genetic mutations, epigenetic changes with effects on multiple crosstalk networks. An in-depth study of MDR causes, tumor biology, molecular

pathways and tumor-TME interactions suggested co-delivery nanosystems as useful tool to circumvent MDR and ameliorate cancer therapy outcomes.

Thanks to their multiple pharmacologic advantages, the most significant combine nanomedicines applications concern chemoresistant tumors, such as triple-negative breast cancer (TNBC); highly metastasized tumors, such as melanoma; and tumors in which biological barriers hamper successful drug targeting, such as the blood-brain barrier (BBB) crossing challenge in glioblastoma therapy (Boggio et al., 2023).

Drugs combinations can include cytotoxic drugs, such as doxorubicin, vincristine, camptotecin, paclitaxel and temozolamide. Among those, key role is fulfilled by doxorubicin, whose chemoresistance and systemic toxicity were frequently handled through involving it in suitable combined nanomedicine therapy.

Different cytotoxic drugs can be combined together or combined with targeted drugs, such as the tyrosine kinase inhibitors (i.e., erlotinib, lapatinib). Clear antineoplastic effect was found correlated to liposome-based nanocarriers co-loaded with doxorubicin and erlotinib, which significantly reduced tumor growth in a breast xenograft mouse model (Morton et al., 2014). Moreover, Ni et al. (2021), disclosed the effectual synergism of doxorubicin-lapatinib association delivered through a co-functionalized nanoparticle (A-NPs-cT) for breast cancer brain metastases (BCBM) treatment. *In vivo* studies highlighted an improved therapeutic efficacy in BCBM-bearing mice, enhanced by a selective NPs crossing of blood-brain tumor barrier (BTB) (Ni et al., 2021).

Furthermore, promising effects were detected from drugs combination with phytochemicals agents, such as quercetin (QUR). It is a matter of a natural flavonoid compound with extensive bioactivities including anti-inflammatory, antitumor, antioxidation and hyperlipidaemia activities. When combined with different chemotherapeutics, it was found able to produce relevant synergistic effects. Its antineoplastic contribution was reported due to its chemosensitizer function, which allows it to suppress the expression of mutant p53 and Pgp and promote cells apoptosis (X. Wang et al., 2014; Cote et al., 2015; Z. Zhang et al., 2018). Vincristine cytotoxicity and antitumor efficacy was found enhanced through its combination with QUR in a liposome formulation co-delivering. This combination effectively increased the intracellular accumulation of vincristine, supported by the reduced vincristine efflux QUR-mediated, in a trastuzumab-insensitive xenograft breast cancer model (M. Y. Wong & Chiu, 2011).

Nanocarrier ability to deliver nucleic acids (e.g. siRNA) was exploited also in combination therapy. This strategy gives the opportunity to knock down genes involved in MDR, contributing to enhance

the resulting antineoplastic effect. For instance, siRNA targeting P-gp drug exporter, co-delivered with doxorubicin in mesoporous silica NPs, was reported to significantly contribute to inhibit tumor growth and overcoming doxorubicin MDR in both *in vitro* and *in vivo* human breast cancer xenograft model (Meng et al., 2013). Furthermore, the folate-targeted polymeric micelle incorporating temozolamide and anti-BCL-2 siRNA showed striking *in vivo* glioma growth inhibition. BCL-2 belongs to antiapoptotic protein family, whose expression was documented overexpressed in several cancer types. BCL-2 silencing leads to a valid strategy to overcome cancer resistance and hamper tumor apoptosis. Its association with the first-line drug chose in glioma chemotherapy led to enhanced survival rate of rats bearing orthotropic C6 glioma (Peng et al., 2018).

Finally, one major success of combine nanomedicine is highlighted by Vyxeos (CPX-351), approved by both FDA (2017) and by EMA (2018) for the treatment of two types of acute myeloid leukemia (AML): newly diagnosed therapy-related AML (t-AML) or AML with myelodysplasia-related changes (AML-MRC). It is a matter of a liposomal fixed combination of daunorubicin and cytarabine, which co-delivered in a 1:5 molar ratio showed an effective antineoplastic synergistic effect (Krauss et al., 2019; Tzogani et al., 2020).

It is increasingly recognized that for inducing a durable cancer remission, a therapy aiming only at killing cancer cells is not sufficient. In this regard, it is well-documented the cytotoxic chemotherapy immunosuppressive effect and the cancer therapeutic improvement achieved in boosting the immune system's response against cancer progression. These evidence led to a particular kind of combination therapy, define chemo-immunotherapy (CIT), which consist in combining chemotherapy agents with immunomodulatory molecules (Sordo-Bahamonde et al., 2023).

4.3 Chemo-Immunotherapy

In the last cancer therapy decade, positive outcomes were recurring found correlated to host immunity adjuvant involvement. It is well documented how cancer cells evade anti-cancer immunity bypassing cancer-immunity cycle. This starts with the APCs identification of cancer antigens that leads to the naïve T-cells activation via MHC-antigen-T cell receptor (TCR) interaction, along with the costimulatory signals (CD28/B7-1/2- mediated signaling). Successively, once reached the circulation system, the activated immune cells infiltrate the TME and promote target cancer cell death through the interaction between their TCR and antigen presented on MHC of tumor cells. In this regard, the conventional chemotherapy agents act primarily killing the cancer cells, but their cytotoxic and

cytostatic effects is found directed also towards healthy proliferating cells, such as hematopoietic cells. These are the chemotherapy aspects responsible of myelosuppression and patients therapy failures (Zhu et al., 2021).

In the last decade, the immunotherapy, such as immune checkpoint inhibitor (ICI)-based one, revolutionized cancer treatment and became the frontline therapy for many cancers. The success of immunotherapy was reached upon broadening the targeting strategy from only cancer cells to the cancer immune environment. Monoclonal antibodies targeting immune checkpoints, as Programmed Cell Death 1 (PD-1) and Cytotoxic T-Lymphocyte Associated Protein 4 (CTLA-4), stood out for their clinical benefits and better toxic profile, compared to chemotherapy. ICI efficacy was demonstrated for the first time in metastatic melanoma, for which nivolumab and pembrolizumab (anti-PD-1), ipilimumab (anti-CTLA-4) and the association anti-PD-1/ CTLA-4 (nivolumab–ipilimumab) are approved and currently used treatments (Robert Caroline et al., 2015; Larkin et al., 2019). However, T-cell-targeted immunomodulators are now used as single agents or in combination with chemotherapies for the treatment for about 50 cancer types (Xin Yu et al., 2019). Despite their striking clinical results, only a minority of patients experience long-term benefits from ICI monotherapies, treatment failure is often correlated to primary and secondary resistance to single agent immunotherapy (Jenkins et al., 2018). On the other side, several preclinical evidence detected more efficient chemotherapy outcomes in immunocompetent mice, compared to immunodeficient counterparts (Zitvogel et al., 2016). Some chemotherapeutic drugs achieved higher effectiveness mediating an immune stimulatory effect by targeting the immunosuppressive TME. All of these evidence supported the novel CIT strategy, promoted by the opportunity to combine together chemotherapy and immunotherapy advantages (Pol et al., 2015; Kroemer et al., 2022; P. Liu et al., 2022).

Among several CIT successful combinations, the foremost has been achieved in lung cancer, in particular for Non–Small-Cell Lung Cancer (NSCLC). Unprecedented efficacy was observed associating pembrolizumab to a standard chemotherapy, resulting in significantly higher rates of response and longer progression-free survival than chemotherapy alone (Gandhi et al., 2018; Paz-Ares et al., 2018). Improvement of metastatic NSCLC patients' survival was reached also through the administration of atezolizumab with the already approved bevacizumab-chemotherapy association. The promising outcomes correlated to this strategy are due to bevacizumab-chemotherapy immunomodulatory effects that may augment the efficacy of atezolizumab (Socinski et al., 2018). Multiple clinical trials have demonstrated the efficacy of chemo-immunotherapy in digestive tumors,

in advanced biliary tract cancer, and in cervical cancer (Colombo et al., 2021; Sordo-Bahamonde et al., 2023).

Moreover, the NP-loaded drug-containing CIT association will represent the future prospective for reaching more effective anticancer therapy. NPs can encapsulate both agents, and eventually conjugate one of them displaying it on the NPs surface. Usually, it is a matter of the immunotherapeutic agent, such as ICIs, or antibodies, RNAs, and small molecule inhibitors. An example is reported by Ghasemi-Chaleshtari et al. (2020) results, showing that cisplatin NPs labelled with anti-PD-1 are able to infiltrate the tumor site, where they promote cisplatin release and, targeting T-cells, they impact tumor cells simultaneously. Moreover, Hess et al. (2019) results showing a higher tumour regression promoted by nano-liposome containing paclitaxel and decorated with PD-L1 mAb, compared to the respective monotherapy (Hess et al., 2019; Ghasemi-Chaleshtari et al., 2020; ; Kiaie et al., 2023).

All the suggested ICOS-Fc potential therapeutic applications were till now related to its mono-therapeutic effect, delivered in free form or encapsulated into nanodelivery system (Dianzani et al., 2014; Clemente et al., 2020; Boggio et al., 2021). Its involvement in combination therapy nanomedicine was suggested considering the possibility to broaden its therapeutical potentialities, thanks to its cooperative immunomodulant role with other drugs association.

4.3.1   ICOS-Fc in combined immuno chemotherapy for melanoma treatment

According to its high immunogenic feature, melanoma development is strictly correlated to tumor-immune system crosstalk. This explains why next to the dacarbazine or targeted standard chemotherapy, such as BRAF inhibitors (BRAFi), and/or mitogen-activated protein kinase (MEK) inhibitors (MEKi), immunotherapy strategy is progressively arising. The aggressiveness of malignant melanoma is highly due to its MDR and massive metastatization properties responsible of cancer spreading to distal sites, such as lungs, brain and bones (Leonardi et al., 2018). The therapeutic options depend upon disease staging: if not diagnosed on time, it can easily reach advanced and lethal stages characterized by poor patients outcomes even though surgical removal (Atkinson, 2017).

Among the immunotherapy options, both immuno checkpoints inhibitors, such as the CTLA-4 blocker ipilimumab and PD1 blocker pembrolizumab, and several BRAFi/MEK1 combinations (dabrafenib/trametinib; vemurafenib/cobimetinib; encorafenib/binimetinib) are currently available.

Moreover, compared to the administration of BRAFi or MEKi administered alone, their association showed increased progression-free survival (PFS) and OS (Robert, Karaszewska, et al., 2015; Cucci et al., 2023). Their therapeutic effectiveness is linked to tumor-mutation burden and their capacity to unlock anti-tumor immune response, reason why most of this kind of treatment failures happened in patients without pre-existing anti-tumor immunity (Seidel et al., 2018). In this regard, a multi-pronged approach involving both polychemotherapy with immunotherapy in the nanotechnology-based drug delivery scenario has been emerged and is leading to novel therapeutic strategy of improved efficacy.

Beside this kind of immunotherapy, we have recently reported the efficacy of targeting ICOS/ICOSL pathway in melanoma mouse model. ICOS-Fc loaded into both β-cyclodextrin-based NS (CDNS) and PLGA was found able to counteract tumor growth of established s.c. B16-F10 tumors. The antitumor effect observed was correlated to three distinct mechanisms. Firstly, through its NPs encapsulation, ICOS-Fc mediated an immunomodulation effect, resulting in the suppression of anti-tumor immune response. Secondly, it decreased tumor vascularization performing an anti-angiogenic effect. Finally, it may act as an antitumor agent, by acting directly on tumor cells expressing ICOSL, hampering the leading steps of tumor progression, such as the adhesion, migration and EMT of tumor cells. Those findings supported ICOS-Fc potential application in combined cancer therapies and highlighted nanotechnology strategy as a precious tool to improve its therapeutic efficacy. Indeed, the administration of ICOS-Fc in free form repeatedly showed ineffectiveness on tumor growth in several and different transplantable and spontaneous tumor mouse model (Clemente et al., 2020).

The ICOS-Fc addition was suggested to optimize an innovative drugs combination co-loaded in injectable nanoemulsions for total parental nutrition (Intralipid© – IL). It is a matter of a novel polychemotherapy strategy involving an alkylating agent, temozolamide (TMZ), which is usually chosen as a therapeutic alternative to dacarbazine because of its ability to reach the central nervous system (CNS) and affect brain metastasis. According to literature evidence, in order to enhance TMZ effect the association proposed included an mTOR inhibitor (rapamycin – RAP) (Dronca et al., 2014; Dianzani et al., 2020). Additionally, bevacizumab (BVZ) represents the third component of the proposed therapeutic mix (IL MIX). It is a monoclonal antibody characterized by anti-angiogenic activity, due to its VEGF binding interaction. VEGF overexpression is a markable aspect standing out in metastatic melanoma, whose adverse prognostic feature are correlated with high VEGF serum levels. Hainsworth et al. (2010) demonstrated how the combination of BVZ antiangiogenic agent

with a RAP derivative, which mediates a down-regulation of the VEGF receptor, resulted in a well-tolerated therapy in patients with metastatic melanoma (Hainsworth et al., 2010).

Another innovative aspect of this polychemotherapy stands in the nanocarrier choice, the IL exploitation in drug delivery formulations was already investigated (Hippalgaonkar et al., 2010), but its use for delivering a polychemotherapy is innovative. The drugs loading into IL nanoemulsion takes place in the inner oil phase, reason why only lipophilic drug could be delivered. The RAP lipophilic drug was loaded with a "lipophilized" TMZ form, obtained through its conversion to an ester prodrug (TMZ-C12), and BVZ was loaded through an ion pairing strategy, already tested to load antibodies in solid lipid nanoparticles (SLNs) (Battaglia et al., 2015).

The drugs combination in the IL MIX was compared to RAP loaded into IL (IL RAP), TMZ loaded into IL (IL TMZ), blank IL, free RAP, free TMZ and free MIX. Efficient loading of the drugs in the liquid lipid matrix resulted in the anti-tumoral effects measured by *in vitro* cytotoxicity, cell migration and tube formation assays. Moreover, the *in vivo* experiments, performed using female C57BL6/J mice injected subcutaneously with B16-F10 cells, showed a significant reduction of tumor growth, with inhibition of tumor angiogenesis and mitotic index (Dianzani et al., 2020a). Despite the promising data obtained, a strong dependence on RAP dose was detected. In this regard, an optimization of the co-loaded system was suggested and led to focusing on drugs single doses reduction, limiting their correlated side adverse effects.

According to the previous results, IL MIX treatment induced an increased in IL-10 and INFγ secretion. The first one mediates an anti-inflammatory and pro-oncogenic effects, such as increasing Treg population and inducing M2 polarization of tumour associated macrophages. On the other side, INFγ is produced and released by Th1 and NK cells, which are lymphocyte with antitumor and anti-proinflammatory functions (Conciatori et al., 2018). Those findings suggested a potential IL MIX effect in restoring the anti-tumor immune response and supported the further co-delivery optimization. In order to enrich the polychemotherapy system with an immunotherapy contribution, ICOS-Fc was considered and identified suitable for being involved. Its ability to act on both immune response and TME represented an added value for the melanoma therapeutic options.

Parenteral Nanoemulsions Loaded with Combined Immuno and Chemo-Therapy for Melanoma Treatment

Background: Cutaneous melanoma is the 17th most common cancer worldwide (Sung et al., 2021). Although the very high survival rate at early stages (5 years' survival > 99%), the patients with advanced disease show weak treatment responsiveness based on conventional chemotherapy and radiotherapy (5 years survival rate only 15%). Half of the melanoma cases show activating mutations in BRAF, reason why the use of specific inhibitors towards mutant BRAF variants and MEK, a downstream signaling target of BRAF in the MAPK pathway, showed in advanced melanoma patients a significantly improved PFS and OS. Targeted therapies emerged with monoclonal antibodies immunotherapies as a valid alternative to the standard dacarbazine and TMZ options. Despite the significant therapeutic advancements, the induced chemoresistance and the tumour mutation burden, still hamper the therapeutic efficacy of both targeted therapy and immunotherapy. In this regard, the multi-pronged approach of IL co-loading TMZ, BVZ and RAP showed promising effect on *in vivo* melanoma model (Dianzani et al., 2020a). A further optimization of this system was suggested in order to involve the anti-tumour immune system response in the polychemotherapy synergistic effect. The ICOS-Fc was included considering its ability to act on both the immune response and on TME. Due to the loading capacity of this system, the addition of ICOS-Fc led to replace BVZ and RAP with sorafenib (SOR), a multi-kinase inhibitor with anti-proliferative activity (iBRAF), a broader anti-angiogenic activity achieved at lower therapeutic doses and immune response mediating effect. Usefully already tested for melanoma treatment in combination with TMZ (Amaravadi et al., 2009; Y. Q. Xiong et al., 2009; Cao et al., 2011).

Aim: The aim of this project was to evaluate the therapeutic effect of a combined immunochemotherapy consisting in loading of immunotherapeutic (ICOS-Fc), targeted (SOR) and chemotherapeutic (TMZ) agents with IL, in a s.c. melanoma mouse model.

Method: The characterization of the formulations was performed through dynamic light scattering technique (DLS), in order to evaluate mean droplet size, polydispersity index (PDI) and Zeta potential. The preliminary *in vitro* biological investigation consisted in analyzing this nanoformulations effects on cell viability (MTT and Colony forming assays on B16, D4M, M14 and A2058 cell lines) and cell invasion (Boyden chamber invasion assay on B16 and D4M cell lines). SOR release from IL and its internalization by melanoma cells were evaluated through HPLC analysis. Finally, the *in vivo* experiments were performed using female C57BL6/J, injected subcutaneously with 1 x 10^5 B16-

F10 / animal. The treatments were administered through i.v. injection for three times a week, for two weeks. The experimental groups were set to test the effect of IL MIX, MIX free, IL ICOS-Fc and IL MIX without ICOS-Fc. Tumour masses were monitored and measured during the treatment period; the animals were sacrificed three days after last injection. Immunohistochemistry analysis of CD31 and Ki67 were performed to evaluate tumor micro-vessel density (TMD) and cancer cell proliferation rate respectively. Finally, Real Time PCR of tumors were used to investigate expression of INFγ, IL-β, IL-6, IL-10 and TNFα.

Results: all the nanoformulations used for *in vitro* and *in vivo* experiments showed a mean size in the range between 244-350nm, the negative Zeta potential detected are high enough to avoid aggregation phenomena and the PDI values depicted a very homogeneous size distribution of the nanoformulations. Overall, the drugs combination was efficiently loaded into the lipid matrix without *in vitro* relevant changes in mean IL droplet size.

The studies showed that, compared to the free drugs, the IL loading drugs MIX always increased the inhibitory effect on cell invasion. However, the effect depicted on cell toxicity was variable, depending on drugs, cell line chosen (human and murine origine and with or without BRAF^{V600E} mutation) and kind of assay.

On the other side, the *in vivo* results supported the efficacy of the co-delivery system proposed: 1) IL MIX showed promising therapeutic efficacy, significantly reducing tumour growth and mitotic index (Ki67); 2) only IL MIX treatment altered the cytokine expression pattern depicted by an increased INFγ, IL-β, IL-6 and IL-10 expression; 3) the free drugs and IL MIX without ICOS-Fc failed in terms of tumor growth inhibition, angiogenesis inhibition and immunomodulation. Moreover, no relevant signs of toxicity on target organs were detected due to the subtherapeutic doses employed for each compound: in our experiments, TMZ 1,5mg/kg, SOR 1.25mg/kg, and ICOS-Fc 1.25mg/kg were co-administered, while in literature the doses used are of 40mg/kg, 9.0mg/kg and 5.0mg/kg respectively. Furthermore, the therapeutic contribution of ICOS-Fc in the combine therapy was confirmed and more evident when its lacking in the MIX resulted in a lesser effect on tumour growth (mass, volume), cell proliferation (Ki67) and immune modulation (IL-β, IL-6 and IL-10 expression).

In contrast, the immunomodulation observed could be also influenced by the kind of mouse model employed. Indeed, the choice of the immunocompetent B16-F10 model for this work was due to the fact that it expresses a large amount of ICOSL. However, a BRAF-mutated mouse model could be a next project step, considered to confirm the *in vitro* data collected on D4M BRAF-mutated cell line

and to include in the IL MIX combine therapy an BRAFi, such as vemurafenib, to reach advantage from.

Conclusion: This research work showed a novel polychemotherapy, including for the first time ICOS-Fc as an immunotherapeutic drug working on ICOS/ICOSL system. The promising results collected highlighted the important ICOS-Fc contribution, due to its immunostimulatory and antiangiogenic activity with an optimally synergic effect with the other drugs loaded in the nanodelivery system.

Article

Parenteral Nanoemulsions Loaded with Combined Immuno- and Chemo-Therapy for Melanoma Treatment

Chiara Monge [1,†], Ian Stoppa [2,†], Chiara Ferraris [1,3], Annalisa Bozza [1], Luigi Battaglia [1,4,*], Luigi Cangemi [1], Gianluca Miglio [1], Stefania Pizzimenti [5], Nausicaa Clemente [2], Casimiro Luca Gigliotti [2], Elena Boggio [2], Umberto Dianzani [2,6] and Chiara Dianzani [1]

1. Dipartimento di Scienza e Tecnologia del Farmaco, Università degli Studi di Torino, via Pietro Giuria 9, 10125 Torino, Italy
2. Dipartimento di Scienze della Salute, Università del Piemonte Orientale, via Solaroli 17, 28100 Novara, Italy
3. Dipartimento di Scienze Cliniche e Biologiche, Università degli Studi di Torino, Regione Gonzole 10, 10043 Orbassano, Italy
4. Nanostructured Interfaces and Surfaces (NIS) Interdepartmental Centre, Università degli Studi di Torino, 10124 Torino, Italy
5. Dipartimento di Scienze Cliniche e Biologiche, Università degli Studi di Torino, Corso Raffaello 30, 10124 Torino, Italy
6. Azienda Ospedaliero-Universitaria Maggiore della Carità, Corso Giuseppe Mazzini 18, 28100 Novara, Italy
* Correspondence: luigi.battaglia@unito.it; Tel.: +39-011-670-7142
† These authors contributed equally to this work.

Abstract: High-grade melanoma remains a major life-threatening illness despite the improvement in therapeutic control that has been achieved by means of targeted therapies and immunotherapies in recent years. This work presents a preclinical-level test of a multi-pronged approach that includes the loading of immunotherapeutic (ICOS-Fc), targeted (sorafenib), and chemotherapeutic (temozolomide) agents within Intralipid®, which is a biocompatible nanoemulsion with a long history of safe clinical use for total parenteral nutrition. This drug combination has been shown to inhibit tumor growth and angiogenesis with the involvement of the immune system, and a key role is played by ICOS-Fc. The inhibition of tumor growth in subcutaneous melanoma mouse models has been achieved using sub-therapeutic drug doses, which is most likely the result of the nanoemulsion's targeting properties. If translated to the human setting, this approach should therefore allow therapeutic efficacy to be achieved without increasing the risk of toxic effects.

Keywords: Intralipid®; ICOS-Fc; combination therapy; melanoma

1. Introduction

Therapeutic options for melanoma depend upon disease staging. The surgical removal of a primary tumor is normally practiced in the case of early-stage disease (0–IIA). In stage IIB/C (tumor thickness > 2.0 mm) and stage III, adjuvant chemotherapies are practiced following surgery. Dacarbazine, the standard chemotherapy for stage IV (metastatic) melanoma up to 2011, is simply a palliative care treatment [1]. Temozolomide (TMZ) is an alternative treatment as it can reach the central nervous system (CNS) to treat brain metastases [2]. New pharmacological agents have recently been approved. Since half of the total melanomas show the V-raf murine sarcoma viral oncogene homolog B1 (BRAF) mutation, they may respond to targeted therapies with BRAF (vemurafenib, dabrafenib, encorafenib) and/or mitogen-activated protein kinase (MEK) inhibitors (trametinib, cobimetinib, binimetinib). Moreover, melanomas respond to immunotherapy with monoclonal antibodies that block the immune checkpoint receptors cytotoxic T-lymphocyte antigen 4 (CTLA4), such as ipilimumab, and programmed cell death protein 1 (PD1), such as pembrolizumab and nivolumab [1]. Indeed, melanoma is one of the most immunogenic tumors and its relationship with the host immune system is currently under investigation [3].

Besides immunotherapy with CTLA4 and PD1 inhibitors, we have recently reported the efficacy of targeting the inducible T-cell co-stimulator (ICOS)/ICOS ligand (ICOS-L) dyad in mouse models of melanoma [4]. ICOS [5–7] is an immune checkpoint protein, mainly present on activated T cells, that belongs to the cluster of differentiation 28 (CD28) family, with members such as CTLA4 and PD1. ICOS-L (or B7h) is its natural ligand, and is expressed by several cell types, such as B cells, macrophages, dendritic cells (DC), endothelial cells (EC), epithelial cells, fibroblasts, and several types of tumor cells. However, while CTLA4 and PD1 exert inhibitory functions on T cells, CD28 and ICOS trigger co-stimulatory signals. Indeed, the triggering of ICOS by ICOS-L co-stimulates T cells in inflamed tissues by modulating cytokine secretion from T helper cells, the cytotoxic activity of T cells, and the regulatory development of regulatory T cells [8,9]. On the other hand, the triggering of ICOS-L by ICOS inhibits the migration of vascular EC, DC, and tumor cells, as well as tumor metastatization in vivo [10,11]. In the tumor microenvironment, ICOS-L is expressed by several types of immune cells, by EC, and often by tumor cells, whereas ICOS is expressed by infiltrating T cells. We have recently found that the growth of established mouse melanoma is inhibited by treatment with ICOS-Fc, a recombinant water-soluble ICOS protein, when it is loaded into either biocompatible poly(lactic-co-glycolic acid) (PLGA) or cyclodextrin nanoparticles, which are able to target the drug to the tumor mass [4]. The main effect of ICOS-Fc is the inhibition of tumor angiogenesis, which is accompanied by variable immuno-regulatory activities, depending on the nanoparticle vector, and by direct effects on tumor cells, which are mainly detectable in vitro. Intriguingly, ICOS-L can also bind osteopontin (OPN), which is a well-known pro-neoplastic factor. Triggering of ICOS-L by OPN stimulates angiogenesis and tumor cell migration, whereas ICOS exerts a dominant negative effect on these activities [12]. Moreover, the ICOS/ICOS-L dyad may even play a role in anti-CTLA4 monoclonal antibody (mAb) anti-tumor activity, which results in an expansion of ICOS$^+$ effector T cells, while its effect is significantly decreased in ICOS$^{-/-}$ mice [13].

Nonetheless, despite significant therapeutic advancements, malignant melanoma remains an aggressive and resistant tumor with unpredictable responses to chemotherapy, making it a major health challenge [1]. Targeted therapies are hampered by chemoresistance [14], while the response to immunotherapy strictly correlates to tumor-mutation burden [15–17]. Therefore, a multi-pronged approach that can target melanoma proliferation, angiogenesis, and chemoresistance should be practiced, concurrently to immunotherapy, to improve therapeutic efficacy. We have recently shown that combinations of drugs against melanoma can be loaded into nanoemulsions for total parenteral nutrition, namely Intralipid® 10% (IL), and that the combinations are effective in an in vivo mouse model of melanoma [18]. Specifically, a combination of drugs, including tumor proliferation (TMZ), angiogenesis (bevacizumab), and mTOR inhibitors (rapamycin), was loaded into IL and tested on available cell and animal models. Despite the promising results obtained, a strong dependence on rapamycin dose was observed as the relevant in vivo tumor inhibition was only achieved at a high dose of this drug. This poses a concern for human translation. Indeed, besides synergism between drugs, the rationale for anti-cancer drug combinations focuses on reducing the dose of each component to prevent side effects.

Hence, in the present work, we have optimized an innovative drug combination, which, after loading into IL, may be capable of acting at sub-therapeutic doses of each single component. To this aim, while TMZ was maintained as the main cytotoxic agent, the immune system was involved in the drug combination, unlike in our previous study, by including ICOS-Fc, capable to act on both the immune response and the tumor microenvironment. Since ICOS-Fc would not be compatible with the anti-angiogenic monoclonal antibody, bevacizumab, as they would exceed the maximum protein loading in the IL oil droplets, the new formulation included sorafenib (SOR), loaded into IL instead of rapamycin and bevacizumab, to counteract angiogenesis, which plays a key role in melanoma development. Indeed, SOR is a multi-kinase inhibitor that can exert anti-proliferative activity by inhibiting various intracellular, rapidly accelerated fibrosarcoma (RAF) kinases,

including BRAF. As previously mentioned, targeted therapies for melanoma currently make use of selective BRAF inhibitors (such as vemurafenib), due to the specific melanoma mutational burden, but suffer from the significant limitation of chemoresistance. SOR displays broader anti-angiogenic activity than these compounds as it blocks the vascular endothelial growth factor receptor (VEGFR) with high affinity and at low therapeutic doses, as well as activating the immune response. It has also already been tested for melanoma treatment in combination with TMZ [19–21].

2. Experimental

2.1. Materials

2.1.1. Chemicals

IL 10% was obtained from Fresenius Kabi (Bad Homberg, Germany). The 3-(4,5-dimethyl thiazol-2-yl)-2,5-diphenyltetrazolium bromide (MTT), 60,000–90,000 MW dextran, acetonitrile, crystal violet, dichloromethane, dimethylformamide (DMF), dimethylsulfoxide (DMSO), polystyrene sulfonate (PS), TMZ, and the TRIzol reagent were obtained from Sigma-Aldrich (St. Louis, MO, USA). Ethyl acetate, phosphotungstic acid, silica gel, and sodium docusate (AOT) were obtained from Merck (Darmstadt, Germany). Agarose CL 4B, isopropanol, triethylamine, and trifluoroacetic acid (TFA) were obtained from Alfa-Aesar (Haverhill, MA, USA). Acetic acid, bromododecane, and sodium nitrite were obtained from Carlo Erba (Val De Reuil, France). SOR was obtained from LcLabs (Woburn, MA, USA). Sulfuric acid was obtained from Fluka (Buchs, Switzerland). ICOS-Fc was obtained from Novaicos (Novara, Italy). Kolliphor® EL was a kind gift from BASF (Ludwigshafen am Rhein, Germany).

Matrigel was obtained from BD Biosciences (San Jose, CA, USA). Polyclonal rabbit anti-cluster of differentiation 31 (CD31) was obtained from Abcam (Cambridge, UK). Monoclonal mouse anti-human Kiel original clone 67 (Ki-67) antigen was obtained from Thermo Fisher Scientific (Waltham, MA, USA). The QuantiTect Reverse Transcription Kit was obtained from Qiagen (Hilden, Germany). The TaqMan gene expression Assay-on-Demand and TaqMan Universal PCR Master Mix were obtained from Applied Biosystems (Foster City, CA, USA). The CFX96 System was obtained from Bio-Rad Laboratories (Hercules, CA, USA).

2.1.2. Cells

A2058 and M14 human melanoma cells and B16-F10 murine melanoma cells were purchased from the American Type Culture Collection (ATCC; Manassas, VA, USA). D4M cells, a mouse melanoma engineered cell line harboring the BRAFV600E mutation, were a gift from D.W. Mullis, Department of Medicine, Norris Cotton Cancer Center, Geisel School of Medicine at Dartmouth, Lebanon, NH, USA. M14 and B16-F10 cells were cultured in Roswell Park Memorial Institute 1640 medium (RPMI 1640; Sigma-Aldrich, St. Louis, MO, USA), while A2058 and D4M were cultured in Dulbecco's Modified Eagle Medium (DMEM; Sigma-Aldrich, St. Louis, MO, USA). All culture media were supplemented with 10% fetal calf serum (FCS; PAA Laboratories, Pasching, Austria), penicillin/streptomycin (100 units/mL), and L-glutamine (2 mmol/L) (both from Sigma-Aldrich, St. Louis, MO, USA). Cell lines were cultured in a 5% CO_2, 37 °C incubator.

2.1.3. Animals

C57BL/6J mice were obtained from The Jackson Laboratory (Bar Harbor, ME, USA) and were then bred under pathogen-free conditions in the animal facility of the University of Piemonte Orientale, Department of Health Sciences (Authorization No. 61/2005-A—6 May 2005, issued by the General Directorate of Veterinary and Food Health—Italian Ministry of Health). Experiments were performed using female, 6-to-9-week-old C57BL/6J mice that were treated in accordance with the University Ethical Committee and European guidelines (Experimental protocol authorization No. 241/2022-PR, released on the 15-04-2022 by the Italian Ministry of Health for protocol No. DB064.76).

2.2. Preparation of Formulations under Study

2.2.1. Prodrug Synthesis

A lipophilic TMZ dodecyl ester (TMZ-C12) was synthesized, in accordance with the literature [18,22,23].

2.2.2. Formulation of Drug Combination-Loaded IL

The combination of drugs (IL MIX) was loaded into IL 10% in accordance with the following procedure. pH = 3.0 buffer citrate 0.1 M (40 µL) was first added to 1.6 mL of IL. Then, 1.2 mg of TMZ-C12 was dissolved in 80 µL of DMF, together with 0.5 mg of SOR, and this solution was added dropwise to IL. Subsequently, 96 uL of the AOT stock solution (4.5 mg/mL—10.1 mM) and variable amounts of the ICOS-Fc stock solutions (either 286 µL of 1.75 mg/mL human ICOS-Fc, or 302 µL of 1.65 mg/mL mouse ICOS-Fc) were added to IL, forming an ion pair [18,24] at a 1:150 AOT-ICOS-Fc molar ratio. The final drug concentrations in IL were: 0.6 mg/mL (1.65 mM) TMZ-C12, 0.25 mg/mL (0.54 mM) SOR, and 0.25 mg/mL (3.2 µM) ICOS-Fc. PS was used as the de-bridging agent exclusively in the case of the formulation of IL MIX with human ICOS-Fc. To this aim, 100 µL of a 10 mg/mL PS solution in water was added to avoid droplet aggregation (Figure 1). Human ICOS-Fc was used for in vitro studies on human cell lines (M14, A2058). Mouse ICOS-Fc was used for in vitro studies on mouse cell lines (B16, D4M) and for animal experiments.
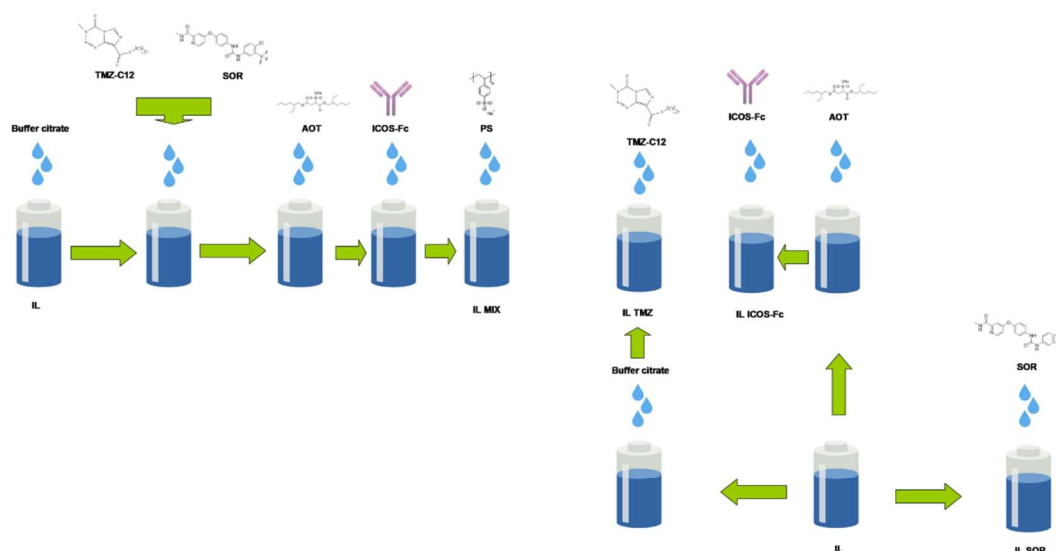
Figure 1. Flowchart of the preparation of the drug-loaded nanoemulsions. Abbreviations: AOT: sodium docusate; IL: Intralipid® 10%; SOR: sorafenib; TMZ-C12: temozolomide dodecyl ester; MIX: drug combination (temozolomide dodecyl ester, sorafenib, ICOS-Fc); PS: polystyrene sulfonate.

2.2.3. Preparation of Control Formulations

The following IL-based controls were used for cell studies: IL TMZ-C12, IL SOR, and IL ICOS-Fc (Figure 1). IL ICOS-Fc was also prepared using a 10-fold lower ICOS-Fc dose (0.025 mg/mL—0.32 µM) for use exclusively in in vitro cell migration experiments. The free-drug solution controls were: free TMZ, dissolved in DMF (6 mg/mL—31.2 mM), free SOR, dissolved in DMSO (5 mg/mL—10.8 mM), and free ICOS-Fc mg/mL, dissolved in water (1.75 mg/mL—22.4 µM for human ICOS-Fc; 1.65 mg/mL—22.1 µM for murine ICOS-Fc). A mixture of the free drugs (MIX) was obtained impromptu from the single stock solutions.

The free MIX for the animal experiments was prepared as follows: SOR (0.25 mg/mL—0.54 mM) was dissolved in Kolliphor® EL/ethanol/normal saline (1:1:6 volume ratio), with mouse ICOS-Fc being added to a final concentration of 0.25 mg/mL (3.2 µM) and TMZ powder being added to the formulation prior to use (0.32 mg/mL—1.65 µM) in order to avoid pH-dependent degradation.

2.3. Characterization of Formulations

2.3.1. Determination of Droplet Size, Morphology, and Zeta Potential

The dynamic light scattering technique (DLS; 90 Plus, Brookhaven, NY, USA) was used to determine the mean droplet size, polydispersity index (PDI), and Zeta potential of the IL-based formulations, at 25 °C and in triplicate. Measurement angles were 90° for particle size and 15° for Zeta potential. Transmission electron microscopy (TEM; High-Resolution JEOL 300 kV) was used via IL-negative staining with 1% phosphotungstic acid [18,25].

2.3.2. Determination of Drug Recovery and Entrapment Efficiency

Drug recovery, defined as the ratio between the actual and theoretical drug concentrations, was determined by high-pressure liquid chromatography (HPLC) [18]. TMZ-C12 and SOR were extracted via the dilution of 50 µL of IL-based formulations in 100 µL of acetonitrile under a vortex, and centrifuging at 14,000 rpm (Allegra 64R centrifuge, Beckman Coulter, Brea, CA, USA). To extract the ICOS-Fc–AOT ion pair, the precipitate obtained in the previous step was dissolved in 100 µL of acetic acid, and lipids were precipitated with 50 µL of water (14,000 rpm centrifugation). Since PS interferes with the HPLC detection of ICOS-Fc, the recovery of IL MIX that was formulated with human ICOS-Fc was determined prior to its addition as the de-bridging agent. Drug entrapment efficiency (EE%), defined as the ratio between the drug amount entrapped in the lipid matrix and the total drug amount in the nanoemulsion, was assessed for each single therapeutic agent either after size exclusion with Agarose CL 4B, or after gradient centrifugation with 30% 60,000–90,000 MW dextran.

2.3.3. HPLC Analysis of MIX

HPLC analyses were performed by modifying a literature method [18,26]. The HPLC system was composed of a YL9110 quaternary pump, a YL9101 vacuum degasser, and a YL9160 photo diode array (PDA) detector, linked to YL-Clarity software for data analysis (Young Lin, Hogyedong, Anyang, Korea). The column was a 300 nm pore size C8 Tracer Excel, 25 × 0.4 cm (Teknokroma, Barcelona, Spain). A gradient was performed at 75 °C and using a 1 mL/min flow rate between eluent A (0.1% TFA) and eluent B (79% isopropanol, 20% acetonitrile, 10% water, 0.1% TFA): 0 min–90% A; 15 min–40% A; 24 min–40% A; 27 min–90% A. The PDA wavelengths were 220 nm (ICOS-Fc), 265 nm (SOR), and 329 nm (TMZ-C12), and the retention times were 11.3 min for ICOS-Fc, 16.2 min for SOR, and 20.6 min for TMZ-C12.

2.4. Cytotoxicity: MTT Assay

Cells (1×10^3/well) were seeded in 96-well plates for 24 h and then treated with the formulations under study. Viability was assessed via an MTT assay at 72 h, according to the manufacturer's instructions. Four replicates were performed in five separate experiments.

2.5. Proliferation: Clonogenic Assay

The B16, D4M, M14, and A2058 melanoma cell lines (8×10^2/well) were seeded into six-well plates. After 24 h, cells were treated with the formulations under study for 3 h. Afterwards, the medium was changed, and cells were cultured in drug-free medium for an additional 7 days. The clonogenic assay was then performed as previously described [18].

2.6. Invasion: Boyden Chamber Assay

Preliminary experiments were performed to identify non-toxic drug concentrations. B16, D4M, M14, and A2058 melanoma cells (8×10^3) were seeded into 96-well plates and treated for 6 h with the formulations under study. Cell viability was assessed using the Crystal Violet assay, as previously described [18]. Melanoma cells (2×10^3) were then plated onto the apical side of a Boyden chamber with filters (0.5 μm pore size and 8.2 mm diameter) that were coated with 50 μg/mL of Matrigel in serum-free medium. The cells were then either treated with non-toxic concentrations (as previously assessed) of the formulations under study or left untreated. The Boyden chamber-invasion assay was performed as previously described [18].

2.7. SOR Release from IL and Internalization into Melanoma Cells

2.7.1. SOR Release from IL

Here, 1 mL of IL SOR was diluted in 4 mL of RPMI under magnetic stirring. At scheduled times, 0.5 mL of the mixture was withdrawn and centrifuged at 25,000 rpm (Allegra 64R centrifuge, Beckman Coulter, Brea, CA, USA), and the obtained supernatant was injected into the HPLC system. The SOR amount that was still present in the lipid matrix at the end of the experiment was assessed via extraction from the centrifuged lipid pellet. Briefly, the pellet was dissolved in 0.5 mL of acetonitrile and the lipid was precipitated with 0.5 mL of water, followed by centrifugation at 25,000 rpm (Allegra 64R centrifuge, Beckman Coulter, Brea, CA, USA).

2.7.2. SOR Internalization in Melanoma Cells

Briefly, 1 μL of free SOR and, separately, 20 μL of IL SOR were diluted in 1 mL of RPMI, with and without FCS, containing 5×10^3 melanoma cells. After 3 h of incubation, the cells were isolated by centrifugation and the pellet obtained was extracted using 50 μL of methanol, prior to injection into the HPLC system.

2.7.3. HPLC Analysis of SOR

A Jasco PU 1580 pump and a C18 Beckmann ODS 25×0.5 cm column were used. The mobile phase, acetonitrile/water 65:35, was delivered at a flow rate of 1 mL/min. The Jasco UV 1575 UV-visible detector was set at λ 264 nm, and the calibration curve ranged between 2.5 and 0.25 ug/mL ($R^2 = 0.9994$, CV = 0.070, LOD = 2.80 ng/mL, LOQ = 9.34 ng/mL).

2.8. Animal Experiments

B16-F10 melanoma cells were injected subcutaneously (1×10^5 in 100 μL/mouse), and tumor growth was monitored every two days. Ten days after tumor induction, the mice were divided into different groups (five mice each; T0) and either treated, via i.v. injection, with the formulations under study, or with the same volume of phosphate-buffered saline (PBS), used as a control. Mice were treated three times a week for two weeks (six i.v./mouse, T1 to T6) and sacrificed three days after the last injection (Tend), or immediately after they displayed suffering. In each treatment, drug doses were: TMZ 1.5 mg/kg, SOR 1.25 mg/kg, and ICOS-Fc 1.25 mg/kg. Tumor volume was monitored over the treatment period and the final tumor mass and volume were measured at the end of the experiment, after animal sacrifice.

2.9. Immunohistochemistry of Tumor Specimens

The immunohistochemical analyses of CD31, an EC marker used to assess tumor micro-vessel density (TMD), and Ki-67, a marker of proliferating cells, were performed in animal-tumor specimens, as previously described [18].

2.10. Real-Time Polymerase Chain Reaction (PCR) of Tumors

Ribonucleic acid (RNA) was obtained from snap-frozen tumors, using the TRIzol reagent. Then, 1 μg of RNA was retrotranscribed to cDNA using the QuantiTect Re-

verse Transcription Kit. Interferon-γ (IFN-γ), interleukin-1β (IL-1β), interleukin-6 (IL-6), interleukin-10 (IL-10), and tumor necrosis factor-α (TNF-α) expression were evaluated using a TaqMan gene expression assay. The complementary deoxyribonucleic acid (cDNA) amounts were normalized using the β-actin gene. Real-time PCR was performed on a CFX96 System and samples were run in duplicate in a 10 μL final volume that contained 1 μL of diluted cDNA, 5 μL of TaqMan Universal PCR Master Mix, and 0.5 μL of Assay-on-Demand mix. Relative gene expression was calculated using the ΔΔ threshold cycle method.

2.11. Statistical Analysis

Data are presented as mean ± SEM. Statistical analyses were performed using Prism 3.0 software (GraphPad Software, La Jolla, CA, USA) by means of one-way ANOVA and the Dunnett's test.

3. Results

3.1. Characterization of Formulations

Table 1 shows the characterization of the IL-based formulations. TMZ was loaded into the lipid matrix by means of its ester prodrug, which also increases its stability in biological fluids, preventing premature imidazotetrazine ring-opening at neutral pH [18,27]. ICOS-Fc is a high-molecular-weight and hydrophilic protein that was associated with the lipid matrix via ion pairing with AOT [18,24]. However, in some cases, the high density of positively charged amino groups on the ICOS-Fc molecule can cause the negatively charged IL droplets to aggregate, especially when the combination of drugs is loaded together with ICOS-Fc in the lipid matrix, meaning that PS was added, as a de-bridging agent, to the IL MIX formulation with human ICOS-Fc.

Table 1. Characterization of Intralipid® (IL)-based formulations. Abbreviations: EE%: % entrapment efficiency; MIX: drug combination (temozolomide dodecyl ester, sorafenib, ICOS-Fc); N.D.: not determined; PS: polystyrene sulfonate; SOR: sorafenib; TMZ-C12: temozolomide dodecyl ester.

	Mean Size (nm)	Polydispersity	Z Potential (mV)	Recovery %	EE %	
					Size Exclusion	Dextran Gradient
IL MIX (human ICOS-Fc)	279.9 ± 3.0	0.146	−28.50 ± 3.35	TMZ-C12: 94.0 ± 8.0 SOR: 96.1 ± 6.0 ICOS-Fc: 106.3 ± 11.7	TMZ-C12: 95.9 SOR: 84.6	TMZ-C12: 94 SOR: 74
IL MIX (human ICOS-Fc low dose)	269.3 ± 10.1	0.025	−29.41 ± 3.06	TMZ-C12: 100 ± 5.1 SOR: 91 ± 6.7 ICOS-Fc: N.D.	N.D.	N.D.
IL MIX (mouse ICOS-Fc)	270.2 ± 2.1	0.099	−39.08 ± 3.69	TMZ-C12: 99 ± 11.1 SOR: 119 ± 11.8 ICOS Fc: 107 ± 21.4	N.D.	N.D.
IL MIX without ICOS-Fc	257.6 ± 5.0	0.129	−33.58 ± 3.03	TMZ-C12: 91 ± 6.5 SOR: 105 ± 6.0	N.D.	N.D.
IL TMZ-C12	275.0 ± 0.7	0.003	−39.52 ± 7.22	68 ± 5.0	N.D.	N.D.
IL SOR	262.6 ± 1.2	0.071	−20.72 ± 1.91	102.7 ± 11.7	N.D.	N.D.
IL mouse ICOS-Fc	348.3 ± 6.1	0.142	−33.17 ± 4.5	116 ± 10.2	47	97
IL human ICOS-Fc	265.6 ± 1.6	0.028	−26.79 ± 3.40	78 ± 9.8	55.4	97
IL human ICOS-Fc (+PS)	262.0 ± 3.7	0.050	−48.08 ± 8.47	88.7 ± 9.3	N.D.	N.D.
IL human ICOS-Fc low concentration	244.6 ± 18.0	0.051	−15.72 ± 1.83	N.D.	N.D.	N.D.
Blank IL	290.0 ± 1.9	0.005	−39.53 ± 2.07	N.D.	N.D.	N.D.

Overall, the drug combination was efficiently loaded into the lipid matrix without relevant changes in mean IL droplet size. The EE% of ICOS-Fc was determined exclusively on IL ICOS-Fc in the absence of PS, which would prevent the HPLC detection of the protein, as previously reported. The loading of SOR, whether alone or used in combination, led to a reduction in the Zeta potential absolute value, and this is probably due to the amino group

present in the compound. The same occurred with ICOS-Fc, and this is probably caused by the excess amino groups of the protein that are exposed on the IL surface. However, the original Zeta potential was restored when the negatively charged PS was added as a de-bridging agent.

The loading of ICOS-Fc was further investigated by TEM (Figure 2). The presence of condensed material on the surface of the IL droplets may be attributed to the ion-paired protein that is loaded into IL, as shown in a previous work by our research group [18].
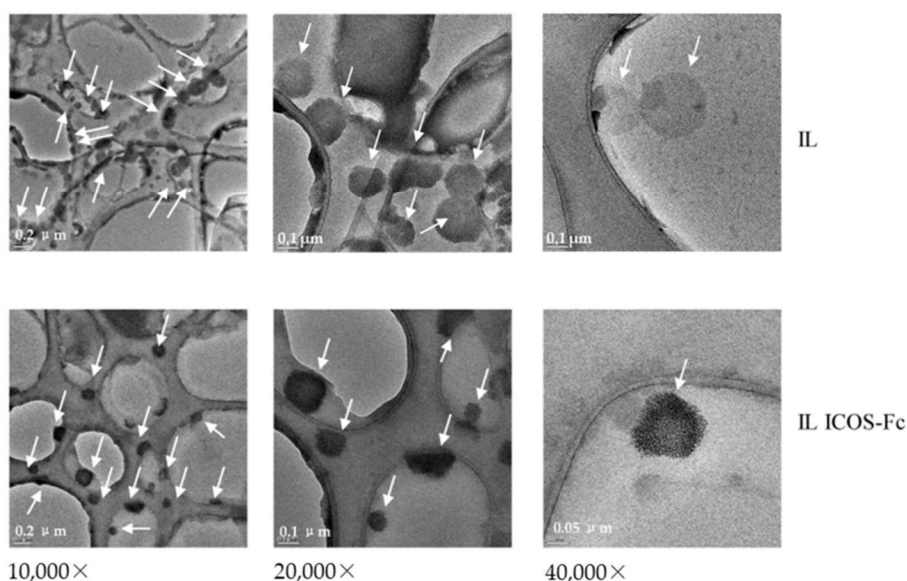

Figure 2. Transmission electron microscopy (TEM) images of Intralipid® (IL) and ICOS-Fc-loaded IL.

3.2. In Vitro Studies

To preliminarily assess the biological effects of the IL formulations, we evaluated the effect on cell viability assessed by the MTT (Figure 3) and clonogenic (Figure 4) assays using the B16, D4M, M14, and A2058 cell lines, and on cell invasion (Figure 5) using B16 and D4M cells. The ICOS-Fc control (low concentration) was only included in the invasion experiments (Figure 5) since it is known not to affect cell viability (MTT—Figure 3, clonogenic assay—Figure 4).

The comparison between the activity of free drugs and that of the corresponding IL-loaded ones showed that IL loading always increased the inhibitory effect on cell invasion. In contrast, the effect on cell toxicity (i.e., inhibition of cell viability) was variable using the different drugs, cell lines, and assays. Compared to free drug, IL SOR decreased the cell toxicity detected by MTT in all the cell lines, whereas in B16 and D4M (mouse cell lines), it increased that detected by the clonogenic assay. IL loading increased TMZ cell toxicity in all the cell lines, even if in D4M and A2058 a less pronounced effect was detected by the MTT compared to the clonogenic assay. IL loading of MIX increased the cell toxicity detected by the clonogenic assay in all the cell lines, except in M14, where it showed no effect; while, with MTT, it increased cell toxicity only in M14, displaying the opposite effect in the other cells. In the MTT assay, an additive effect between IL SOR and IL TMZ could be hypothesized for IL MIX on M14 cells, since this is the only cell line where IL SOR exerts a relevant cytotoxic effect.
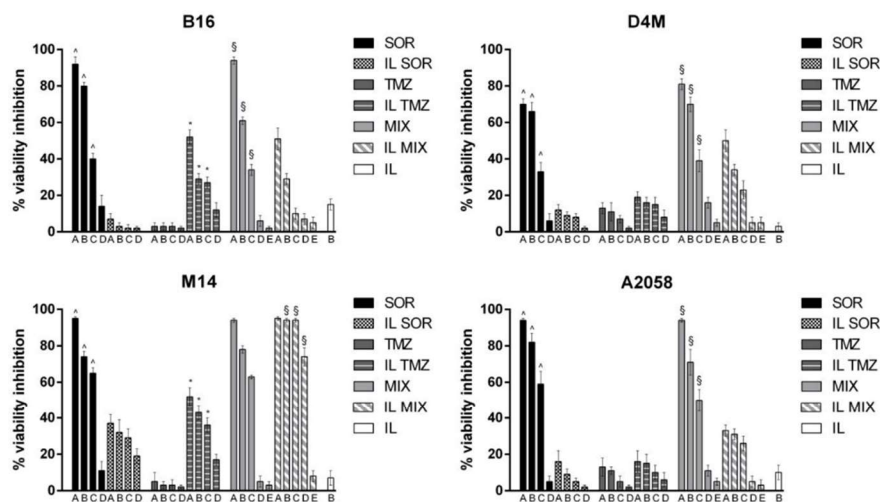
Figure 3. MTT assay performed after 72 h of incubation with the formulations under study. B16 cells: upper left panel; D4M cells: upper right panel; M14 cells: lower left panel; A2058 cells: lower right panel. Abbreviations: IL: Intralipid® 10%; SOR: sorafenib; TMZ: temozolomide; MIX: drug combination (temozolomide dodecyl ester, sorafenib, ICOS-Fc). Concentrations employed: SOR A = 16 μM; B = 10 μM; C = 8 μM; D = 4.5 μM; E = 0.8 μM. TMZ A = 48 μM; B = 32 μM; C = 24 μM; D = 16 μM; E = 2.4 μM. Statistical analysis: ˆ $p < 0.05$ SOR vs. IL SOR; * $p < 0.05$ TMZ vs. IL TMZ; § $p < 0.05$ MIX vs. IL MIX.

Figure 4. Clonogenic assay with B16 (upper left panel), D4M (upper right panel), M14 (lower left panel), and A2058 (lower right panel) melanoma cells. Abbreviations: IL: Intralipid® 10%; SOR: sorafenib; TMZ: temozolomide; MIX: drug combination (temozolomide dodecyl ester, sorafenib, ICOS-Fc). Cells were treated with the formulations under study for 3 h. Afterwards, the medium was changed, and cells were cultured in drug-free medium for an additional 7 days. Concentrations employed: SOR A = 16 μM; B = 10 μM; C = 8 μM; D = 4.5 μM; E = 0.8 μM. TMZ A = 48 μM; B = 32 μM; C = 24 μM; D = 16 μM; E = 2.4 μM. Statistical analysis: ˆ $p < 0.05$ SOR vs. IL SOR; * $p < 0.05$ TMZ vs. IL TMZ; § $p < 0.05$ MIX vs. IL MIX.
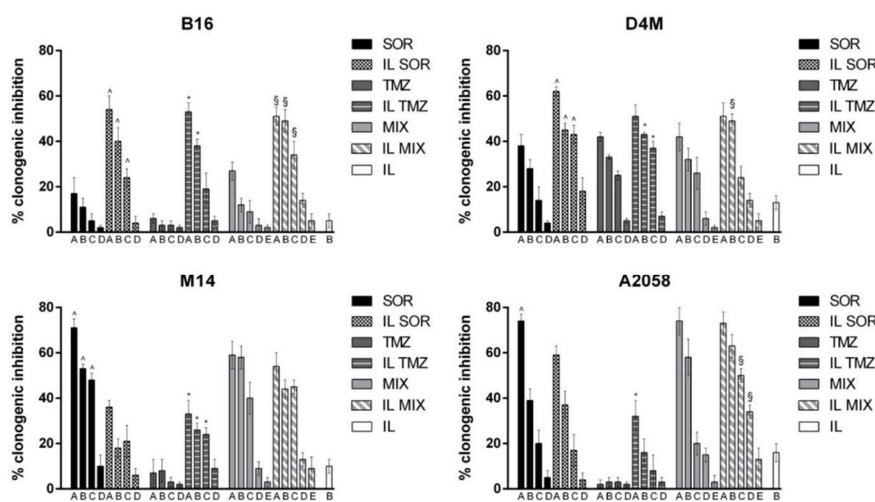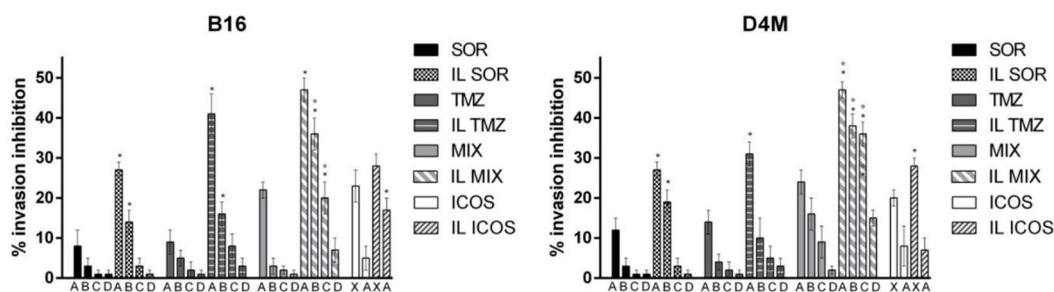
Figure 5. Migration assay with B16 (left panel) and D4M (right panel) melanoma cells. Abbreviations: IL: Intralipid® 10%; SOR: sorafenib; TMZ: temozolomide; MIX: drug combination (temozolomide dodecyl ester, sorafenib, ICOS-Fc). Concentrations employed: SOR A = 16 µM; B = 10 µM; C = 8 µM; D = 4.5 µM. TMZ A = 48 µM; B = 32 µM; C = 24 µM; D = 16 µM. ICOS X = 2 µg/mL; A = 0.5 µg/mL. Statistical analysis: * $p < 0.05$ IL-loaded vs. free; ° $p < 0.05$ additive effect between drugs.

Considering that interpreting the effect of IL MIX is complex, because it is influenced by the single drugs and the carrier, besides the cell phenotype, the most controversial results came from SOR-based formulations. This evidence further drove our investigations into the SOR mechanism of action. Release experiments in cell culture medium showed the unexpected profile that is depicted in Figure 6a. After an initial burst release, drug concentration decreased over time in the release medium. This cannot be ascribed to drug degradation, as the compound that was missing from the release medium was recovered in the lipid pellet obtained after centrifugation. Indeed, it appears that competition occurs between the release medium and the lipid matrix of IL. The internalization studies in melanoma cell lines (Figure 6b) showed that FCS strongly inhibited the internalization of free SOR, while it was ineffective on IL SOR. Moreover, IL SOR internalization was lower than that of free SOR, and this is probably because IL has an entry mechanism that is subject to saturation.

The mechanism depicted in Figure 6c may therefore be hypothesized. IL SOR internalization might be limited by a saturation-like effect, thus reducing the total SOR internalized within the cell, leading to reduced cytotoxic action (MTT assay), that is mediated exclusively by the inhibition of intracellular RAF kinases. On the other hand, extracellular SOR acts on receptor tyrosine kinases (RTK), which are located on the cell membrane and are responsible for angiogenesis and migration processes [28]. In the case of cell membrane-associated RTK, the availability of extracellular SOR in the culture medium is lowered by interactions with proteins, such as those of FCS [29,30]. When SOR is loaded into IL, competition is established between the lipid matrix and the culture medium, preventing SOR from protein sequestration and inactivation effects, thus resulting in more pronounced migration inhibition. The clonogenic assay, instead, entails the proliferation process, which is regulated, to various extents, by both RAF kinases and RTK, and this probably accounts for the variable results obtained among cell lines. In this case, the most striking differences were found between mouse (B16 and D4M) and human (M14 and A2058) cell lines, whose cellular targets (that is RAF kinases and RTK) could probably show different sensitivities to SOR.

These considerations suggest that the variable results obtained in the cell experiments with IL SOR may be ascribable to the experimental setting, rather than to the formulation itself.
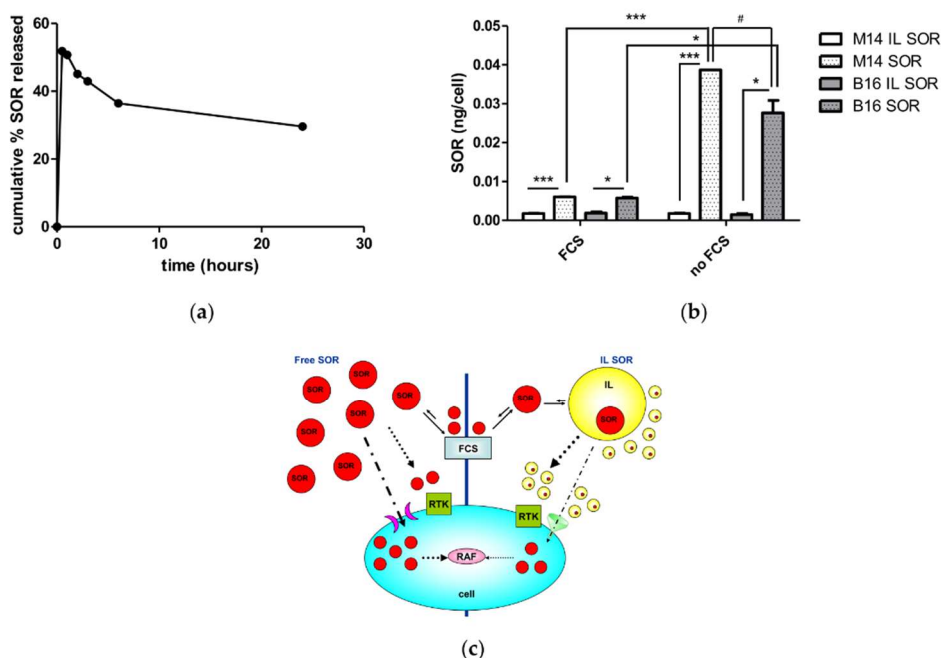
(a)

(b)

(c)

Figure 6. Hypothesized sorafenib (SOR) mechanism of action: (**a**) SOR release profile in culture medium, and (**b**) SOR internalization migration assay (B16, M14 melanoma cells): *** $p < 0.005$, * $p < 0.05$, # $p < 0.01$. (**c**) Hypothesized cellular pathways. Abbreviations: FCS: fetal calf serum; IL: Intralipid® 10%; RAF: rapidly accelerated fibrosarcoma kinases; RTK: receptor tyrosine kinases.

3.3. In Vivo Studies

Animal experiments were performed by comparing the growth inhibition of IL MIX and free MIX on the established subcutaneous B16-F10 melanoma mouse model. Moreover, an animal group treated with IL ICOS-Fc was also included to clarify the contribution of immunotherapy to the total therapeutic effect.

The results (Figure 7) show that only IL MIX was able to significantly reduce tumor volume and the mitotic index (Ki67), compared to the control animals. In contrast, tumor angiogenesis (CD31) was also decreased in animals treated with IL ICOS-Fc. Moreover, only treatment with IL MIX altered the cytokine expression pattern, inducing significant increases in IFN-γ, IL-1β, IL-6, and IL-10, while no effect on TNF-α was measured. No substantial toxicity was detected in analyses of the target organs, except for a slight increase in spleen weights for all the treated groups (Table 2).

Table 2. Animal experiments (I): organ weights (grams). Abbreviations: CTR: control; IL: Intralipid®; MIX: drug combination (temozolomide dodecyl ester, sorafenib, ICOS-Fc).

	Liver	Spleen	Kidneys	Lungs	Heart
CTR	1.07 ± 0.06	0.13 ± 0.01	0.25 ± 0.02	0.18 ± 0.03	0.14 ± 0.02
MIX	1.05 ± 0.08	0.25 ± 0.04	0.24 ± 0.00	0.15 ± 0.01	0.15 ± 0.03
IL MIX	0.91 ± 0.07	0.17 ± 0.05	0.22 ± 0.01	0.16 ± 0.01	0.12 ± 0.01
IL ICOS-Fc	1.00 ± 0.06	0.27 ± 0.04	0.22 ± 0.00	0.17 ± 0.01	0.15 ± 0.01

Figure 7. Animal experiments (I): (**a**) time course tumor volume, (**b**) endpoint tumor volume, (**c**) endpoint tumor weight, (**d**) tumor immunohistochemistry, and (**e**) tumor cytokines. Abbreviations: CD31: cluster of differentiation 31; CTR: control; IFN-γ: Interferon-γ; IL: Intralipid® 10%; IL-10: Interleukin-10; IL-1β: Interleukin-1β; IL-6: Interleukin-6; IL ICOS: Intralipid® 10% loaded with ICOS-Fc; IL MIX: Intralipid® 10% loaded with temozolomide dodecyl ester, sorafenib, and ICOS-Fc; Ki-67: Kiel original clone 67; MIX: free drug combination (temozolomide dodecyl ester, sorafenib, ICOS-Fc); TMD: tumor micro-vessel density; TNF-α: tumor necrosis factor-α. Days after B16-F10 cell subcutaneous injection (1×10^5 in 100 μL/mouse): T0 = 10 days; T1 = 14 days; T2 = 16 days; T3 = 19 days; T4 = 21 days; T5 = 23 days; T6 = 25 days; Tend = 28 days. T0: assignment to groups; T1 to T6: treatments; Tend: sacrifice. For this experiment, 20 mice were used (*n* = 5 each group). Statistical analysis *** = $p < 0.0001$; ** $p < 0.005$; * $p < 0.05$.

111

Further in vivo experiments were performed to investigate the therapeutic contribution of ICOS-Fc in the IL MIX, and to this aim, the effect of IL MIX was compared to that of IL MIX formulated without ICOS-Fc (Figure 8, Table 3). The removal of ICOS-Fc from IL MIX resulted in it having a lesser effect on tumor growth (mass, volume), cell proliferation (Ki67), and immune modulation, in terms of IL-1β, IL-6, and IL-10 expression. In contrast, no significant differences were detected in terms of angiogenesis (CD31) and IFN-γ expression.
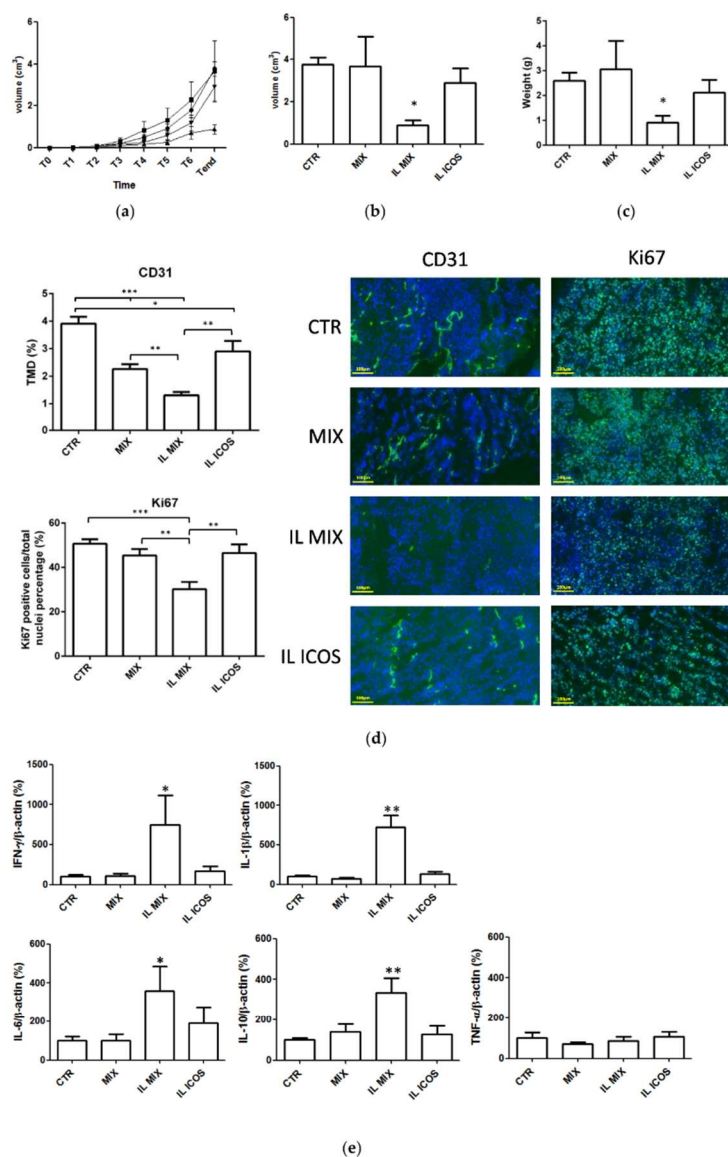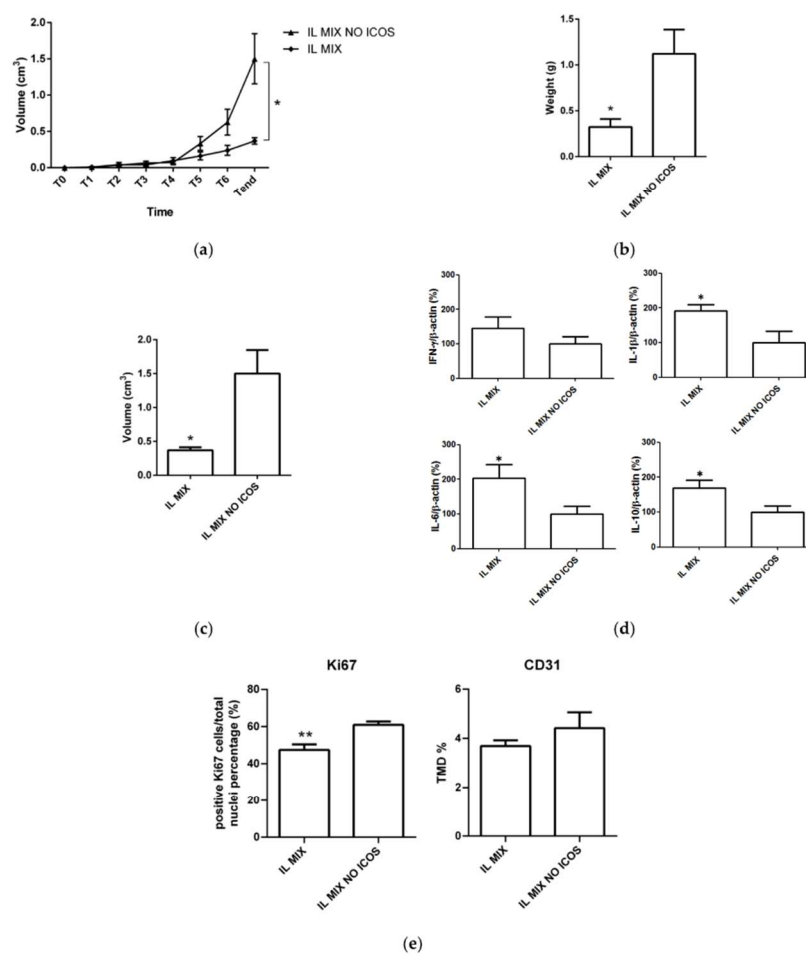

Figure 8. Animal experiments (II): (**a**) time-course tumor volume, (**b**) endpoint tumor volume, (**c**) endpoint tumor weight, (**d**) tumor cytokines, and (**e**) tumor immunohistochemistry. Abbreviations: IL: Intralipid® 10%; CD31: cluster of differentiation 31; IFN-γ: Interferon-γ; IL-10: Interleukin-10; IL-1β: Interleukin-1β; IL-6: Interleukin-6; IL MIX: Intralipid® 10% loaded with temozolomide dodecyl ester, sorafenib, and ICOS-Fc; IL MIX NO ICOS: Intralipid® 10% loaded with temozolomide dodecyl ester and sorafenib; Ki-67: Kiel original clone 67; TMD: tumor micro-vessel density. Days after B16-F10 cell subcutaneous injection (1×10^5 in 100 μL/mouse): T0 = 10 days; T1 = 14 days; T2 = 16 days; T3 = 19 days; T4 = 21 days; T5 = 23 days; T6 = 25 days; Tend = 28 days. T0: assignment to groups; T1 to T6: treatment; Tend: sacrifice. For this experiment, 10 mice were used (n = 5 each group). Statistical analysis ** $p < 0.005$; * $p < 0.05$.

Table 3. Animal experiments (II): organ weights (grams). Abbreviations: IL: Intralipid®; MIX: drug combination (temozolomide dodecyl ester, sorafenib, ICOS-Fc).

	Liver	Spleen	Kidneys	Lungs	Heart
IL MIX	0.86 ± 0.05	0.16 ± 0.04	0.20 ± 0.03	0.28 ± 0.14	0.13 ± 0.00
IL MIX NO ICOS-Fc	0.87 ± 0.06	0.18 ± 0.03	0.23 ± 0.01	0.16 ± 0.01	0.23 ± 0.08

4. Discussion

4.1. Challenges of Current Melanoma Chemotherapy

Targeted therapies and immunotherapies have allowed the improved therapeutic control of malignant melanoma to be achieved. However, several drawbacks (e.g., chemoresistance for targeted therapies, need for high mutational burden in immunotherapies) still limit the effectiveness of these approaches. It is worth noting that combinations of the two are currently under study and have provided promising results, despite the higher incidence of side effects [1]. This experimental study therefore proposes a multi-target approach that merges immunotherapy (ICOS-Fc), targeted therapy (SOR), and chemotherapy (TMZ) and evaluates it at a preclinical level. This approach targets three of the major factors driving melanoma growth, i.e., proliferation, angiogenesis, and the immune response. Using previous encouraging results that have been achieved by our research group [18], this combination was loaded into a biocompatible colloidal vehicle, namely the nanoemulsion for total parenteral nutrition. This formulation is already employed in marketed drug-delivery systems and is under evaluation for anti-cancer drug delivery because of its range of potential targeting mechanisms [31]. Indeed, passive targeting mechanisms are favored by both its nanometric size range and its high lipid content, which acts by saturating the reticuloendothelial system (RES) [32]. Moreover, recent findings showed that it can reduce blood viscosity, by interrupting the binding between fibrinogen and red blood cells, and thus increase the tumor blood flow, which plays a key role in passive targeting. Indeed, upregulation of fibrinogen has been reported in cancer, whereas fibrinogen-mediated clot formation is responsible for the reduced tumor blood flow, a major barrier to drug delivery to tumors [33].

4.2. Advantages of Merging Different Approches into One Biocompatible Lipid Vehicle

The variability of the data obtained, especially on cell toxicity in the case of SOR, is mainly a result of the experimental in vitro setting, which does not account for the in vivo fate of drug-loaded IL. Indeed, the in vivo results indicate that IL MIX has promising therapeutic efficacy, while no relevant signs of toxicity were detected due to the sub-therapeutic doses employed for each compound: in our experiments, TMZ 1.5 mg/kg, SOR 1.25 mg/kg, and ICOS-Fc 1.25 mg/kg were co-administered, while in the literature TMZ 40.0 mg/kg, SOR 9.0 mg/kg, and ICOS-Fc 5.0 mg/kg were employed [4,18,34,35]. It is worth noting that the in vivo experiments demonstrated the efficacy of the proposed approach as such (IL MIX), since the administration of free MIX, IL ICOS-Fc, and IL MIX without ICOS-Fc failed to provide substantial therapeutic effects in terms of tumor growth, angiogenesis inhibition, and immunomodulation. The inefficacy of IL ICOS-Fc is in apparent conflict with the previously documented efficacy of ICOS-Fc-loaded PLGA and cyclodextrin nanoparticles in the same tumor model [4]. This discrepancy can be ascribed to the ICOS-Fc dose, which, in IL, was only 25% of that used in the other nanoparticles. However, the effect of ICOS-Fc in the IL MIX is highlighted by the significant loss of the anti-tumor effects displayed in the IL MIX that lacked ICOS-Fc. The main effect of IL MIX appears to be its action against angiogenesis, which may take advantage of the ability of SOR and ICOS-Fc to inhibit VEGF and OPN induction, respectively.

4.3. The Role of Immune Modulation

It is noteworthy that multi-functional nanomedicines able to act as both immunomodulators and drug carriers have been suggested, including autologous microparticles [36].

Within this context, IL MIX also displayed substantial effects in terms of immune modulation, as detected by the increased expression of IFNγ, IL-1, IL-6, and IL-10. Intriguingly, the increase of IL-1, IL-6, and IL-10 was mostly dependent on the whole IL MIX drug combination, since these cytokines were not increased in mice treated with free MIX or IL ICOS and were significantly lower in mice treated with IL MIX without ICOS than in those treated with the whole IL MIX. In contrast, the increase of IFN-γ was independent from the presence of ICOS-Fc, since it was increased at similar levels in mice treated either with IL MIX or IL MIX without ICOS, while it was not increased in mice treated with free MIX or IL ICOS. The increased expression of IL-10 was unexpected since IL-10 usually works as an anti-inflammatory and pro-oncogenic agent because it is associated with regulatory T lymphocytes and the M2 polarization of tumor-associated macrophages. Conversely, IFN-γ is produced by lymphocytes with anti-tumor and pro-inflammatory activity, such as T helper type 1 lymphocytes, cytotoxic T lymphocytes, and natural killer (NK) cells [37]. Moreover, it is well-known that IL promotes the polarization of macrophages to the anti-cancer M1-like phenotype after i.v. administration [33]. However, the effect of IL-10 may vary depending on the tissue context as it can even trigger IFN-γ secretion and increase cytotoxic anti-tumor lymphocytes and tumor rejection [38]. Previous evidence that we have accrued [18,27] suggests that the increase in IL-10 may be mediated by the activation of P38 mitogen-activated protein kinase (MAPK) in B lymphocytes, as induced by cytostatic agents such as TMZ [39,40] (Figure 9). In contrast, the involvement of ICOS-Fc in this mechanism is unlikely, since our previous work has shown that ICOS-Fc decreases IL-10 expression in the tumor mass when loaded into cyclodextrin nanosponges, but not in PLGA nanoparticles. In this scenario, it is also noteworthy that, of the cytokines involved in acute inflammation, the expression of IL-6 and IL-1 was increased, but that of TNF-α was not.
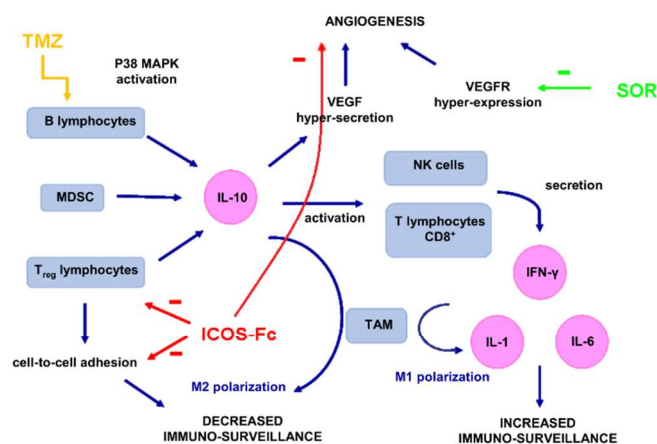
Figure 9. Scheme of immunologic pathways involved in polychemotherapy (MIX). Abbreviations: CD8: cluster of differentiation 8; IFN-γ: interferon-γ; IL-1: interleukin 1; IL-6: interleukin 6; IL-10: interleukin 10; MAPK: mitogen-activated protein kinase; MDSC: myeloid-derived suppressor cells; NK: natural killer; SOR: sorafenib; TAM: tumor-associated macrophages; TMZ: temozolomide; T$_{reg}$: lymphocytes T regulators; VEGF: vascular endothelial growth factor; VEGFR: VEGF receptor.

However, the immunological context can vary with the mouse model employed. Indeed, the immunocompetent B16-F10 model in this experimental work was selected because it expresses a large amount of ICOS-L (data not shown). Nonetheless, it is not a BRAF-mutated model. Therefore, we will also assess our approach in BRAF-mutated models in future studies to take advantage of the promising in vitro results obtained in genetically modified BRAF-mutated D4M cells. In this case, selective BRAF inhibitors

(such as vemurafenib) could be included in the drug combination to provide the necessary advantages.

5. Conclusions

Despite the relevant advances in the pharmacological therapy of high-grade melanoma obtained in recent years, this disease still represents a serious threat. This research work therefore presented a combination therapy that has been engineered to include ICOS-Fc as the immuno-stimulating agent, a cytostatic agent (TMZ), and a kinase inhibitor (SOR) for loading into a nanoemulsion used for total parenteral nutrition. Results showed that this therapy was effective in inhibiting the growth of mouse melanoma in vivo by exerting a potent anti-angiogenic effect and complex immuno-regulatory activity. This is the first attempt to introduce an immunotherapeutic drug working in the ICOS/ICOS-L axis in a polychemotherapy approach, and the results showed that this approach allows to substantially decrease the drug dose needed to obtain a therapeutic effect. Use of ICOS-Fc is innovative since it works as both an immunostimulatory and antiangiogenic agent, and therefore would be optimally synergistic with the other drugs loaded in the nanoparticles. Tumor growth inhibition was obtained without any sign of systemic toxicity. Indeed, sub-therapeutic drug doses were most probably effective because of the hypothesized targeting properties of IL. This approach might represent a potential future tool that can merge immunotherapy, targeted therapy, and chemotherapy into one safe delivery vehicle to improve therapeutic efficacy, without increasing the incidence of the adverse side effects that are typical of combination therapies.

6. Patents

PCT IB/2019/050154.

Author Contributions: C.D., L.B. and U.D. conceived and designed the experiments; I.S., C.M., C.D., L.C., C.F., N.C. and E.B. performed the experiments; C.L.G. performed data analysis; A.B., G.M. and S.P. provided technical support and corrections to the manuscript; L.B. wrote the manuscript. All authors have read and agreed to the published version of the manuscript.

Data Availability Statement: Not applicable.

Conflicts of Interest: A patent application has been submitted for the use of ICOS-L ligands loaded into nanoparticles in tumor treatment (PCT IB/2019/050154).

References

1. Battaglia, L.; Scomparin, A.; Dianzani, C.; Milla, P.; Muntoni, E.; Arpicco, S.; Cavalli, R. Nanotechnology Addresing Cutaneous Melanoma: The Italian Landscape. *Pharmaceutics* **2021**, *13*, 1617. [CrossRef] [PubMed]
2. Velho, T.R. Metastatic Melanoma—A Review of Current and Future Drugs. *Drugs Context* **2012**, *2012*, 212242. [CrossRef]
3. Passarelli, A.; Tucci, M.; Mannavola, F.; Felici, C.; Silvestris, F. The metabolic milieu in melanoma: Role of immune suppression by CD73/adenosine. *Tumour Biol.* **2019**, *41*, 1010428319837138. [CrossRef]
4. Clemente, N.; Boggio, E.; Gigliotti, L.C.; Raineri, D.; Ferrara, B.; Miglio, G.; Argenziano, M.; Chiocchetti, A.; Cappellano, G.; Trotta, F.; et al. Immunotherapy of experimental melanoma with ICOS-Fc loaded in biocompatible and biodegradable nanoparticles. *J. Control. Release* **2020**, *320*, 112–124. [CrossRef] [PubMed]
5. Redoglia, V.; Dianzani, U.; Rojo, J.M.; Portolés, P.; Bragardo, M.; Wolff, H.; Buonfiglio, D.; Bonissoni, S.; Janeway, C.A. Characterization of H4: A Mouse T Lymphocyte Activation Molecule Functionally Associated with the CD3/T Cell Receptor. *Eur. J. Immunol.* **1996**, *26*, 2781–2789. [CrossRef] [PubMed]

6. Buonfiglio, D.; Bragardo, M.; Bonissoni, S.; Redoglia, V.; Cauda, R.; Zupo, S.; Burgio, V.L.; Wolff, H.; Franssila, K.; Gaidano, G.; et al. Characterization of a Novel Human Surface Molecule Selectively Expressed by Mature Thymocytes, Activated T Cells and Subsets of T Cell Lymphomas. *Eur. J. Immunol.* **1999**, *29*, 2863–2874. [CrossRef]

7. Hutloff, A.; Dittrich, A.M.; Beier, K.C.; Eljaschewitsch, B.; Kraft, R.; Anagnostopoulos, I.; Kroczek, R.A. ICOS Is an Inducible T-Cell Co-Stimulator Structurally and Functionally Related to CD28. *Nature* **1999**, *397*, 263–266. [CrossRef]

8. Mesturini, R.; Nicola, S.; Chiocchetti, A.; Bernardone, I.S.; Castelli, L.; Bensi, T.; Ferretti, M.; Comi, C.; Dong, C.; Rojo, J.M.; et al. ICOS Cooperates with CD28, IL-2, and IFN-γ and Modulates Activation of Human Naïve CD4+ T Cells. *Eur. J. Immunol.* **2006**, *36*, 2601–2612. [CrossRef]

9. Yong, P.F.K.; Salzer, U.; Grimbacher, B. The Role of Costimulation in Antibody Deficiencies: ICOS and Common Variable Immunodeficiency. *Immunol. Rev.* **2009**, *229*, 101–113. [CrossRef]

10. Occhipinti, S.; Dianzani, C.; Chiocchetti, A.; Boggio, E.; Clemente, N.; Gigliotti, C.L.; Soluri, M.F.; Minelli, R.; Fantozzi, R.; Yagi, J.; et al. Triggering of B7h by the ICOS Modulates Maturation and Migration of Monocyte-Derived Dendritic Cells. *J. Immunol.* **2013**, *190*, 1125–1134. [CrossRef]

11. Hedl, M.; Lahiri, A.; Ning, K.; Cho, J.H.; Abraham, C. Pattern Recognition Receptor Signaling in Human Dendritic Cells Is Enhanced by ICOS Ligand and Modulated by the Crohn's Disease ICOSLG Risk Allele. *Immunity* **2014**, *40*, 734–746. [CrossRef]

12. Raineri, D.; Dianzani, C.; Cappellano, G.; Maione, F.; Baldanzi, G.; Iacobucci, I.; Clemente, N.; Baldone, G.; Boggio, E.; Gigliotti, C.L.; et al. Osteopontin Binds ICOSL Promoting Tumour Metastasis. *Commun. Biol.* **2020**, *3*, 615. [CrossRef]

13. Fu, T.; He, Q.; Sharma, P. The ICOS/ICOSL Pathway Is Required for Optimal Antitumour Responses Mediated by Anti–CTLA-4 Therapy. *Cancer Res.* **2011**, *71*, 5445–5454. [CrossRef]

14. Sun, J.; Carr, M.J.; Khushalani, N.I. Principles of Targeted Therapy for Melanoma. *Surg. Clin. N. Am.* **2020**, *100*, 175–188. [CrossRef]

15. Snyder, A.; Makarov, V.; Merghoub, T.; Yuan, J.; Zaretsky, J.M.; Desrichard, A.; Walsh, L.A.; Postow, M.A.; Wong, P.; Ho, T.S.; et al. Genetic Basis for Clinical Response to CTLA-4 Blockade in Melanoma A BS TR AC T. *N. Engl. J. Med.* **2014**, *371*, 2189–2199. [CrossRef]

16. Hugo, W.; Zaretsky, J.M.; Sun, L.; Song, C.; Moreno, B.H.; Hu-Lieskovan, S.; Berent-Maoz, B.; Pang, J.; Chmielowski, B.; Cherry, G.; et al. Genomic and Transcriptomic Features of Response to Anti-PD-1 Therapy in Metastatic Melanoma. *Cell* **2016**, *165*, 35–44. [CrossRef]

17. Riaz, N.; Havel, J.J.; Makarov, V.; Desrichard, A.; Urba, W.J.; Sims, J.S.; Hodi, F.S.; Martín-Algarra, S.; Mandal, R.; Sharfman, W.H.; et al. Tumour and Microenvironment Evolution during Immunotherapy with Nivolumab. *Cell* **2017**, *171*, 934–949. [CrossRef] [PubMed]

18. Dianzani, C.; Monge, C.; Miglio, G.; Serpe, L.; Martina, K.; Cangemi, L.; Ferraris, C.; Mioletti, S.; Osella, S.; Gigliotti, C.L.; et al. Nanoemulsions as Delivery Systems for Poly-Chemotherapy Aiming at Melanoma Treatment. *Cancers* **2020**, *12*, 1198. [CrossRef] [PubMed]

19. Amaravadi, R.K.; Schuchter, L.M.; McDermott, D.F.; Kramer, A.; Giles, L.; Gramlich, K.; Carberry, M.; Troxel, A.B.; Letrero, R.; Nathanson, K.L.; et al. Phase II Trial of Temozolomide and Sorafenib in Advanced Melanoma Patients with or without Brain Metastases. *Clin. Cancer Res.* **2009**, *15*, 7711–7718. [CrossRef] [PubMed]

20. Xiong, Y.-Q.; Sun, H.-C.; Zhang, W.; Zhu, X.-D.; Zhuang, P.-Y.; Zhang, J.-B.; Wang, L.; Wu, W.; Qin, L.-X.; Tang, Z.-Y. Human Hepatocellular Carcinoma Tumour–Derived Endothelial Cells Manifest Increased Angiogenesis Capability and Drug Resistance Compared with Normal Endothelial Cells. *Clin. Cancer Res.* **2009**, *15*, 4838–4846. [CrossRef] [PubMed]

21. Cao, M.; Xu, Y.; Youn, J.; Cabrera, R.; Zhang, X.; Gabrilovich, D.; Nelson, D.R.; Liu, C. Kinase Inhibitor Sorafenib Modulates Immunosuppressive Cell Populations in a Murine Liver Cancer Model. *Lab. Investig.* **2011**, *91*, 598–608. [CrossRef]

22. Suppasansatorn, P.; Wang, G.; Conway, B.R.; Wang, W.; Wang, Y. Skin Delivery Potency and Antitumour Activities of Temozolomide Ester Prodrugs. *Cancer Lett.* **2006**, *244*, 42–52. [CrossRef] [PubMed]

23. Annovazzi, L.; Schiffer, D.; Mellai, M.; Gallarate, M.; Battaglia, L.; Chirio, D.; Peira, E.; Muntoni, E.; Chegaev, K.; Barge, A.; et al. Solid Lipid Nanoparticles Loaded with Antitumour Lipophilic Prodrugs Aimed to Glioblastoma Treatment: Preliminary Studies on Cultured Cells. *J. Nanosci. Nanotechnol.* **2017**, *17*, 3606–3614. [CrossRef]

24. Battaglia, L.; Gallarate, M.; Peira, E.; Chirio, D.; Solazzi, I.; Giordano, S.M.A.; Gigliotti, C.L.; Riganti, C. Dianzani Bevacizumab loaded solid lipid nanoparticles prepared by the coacervation technique: Preliminary in vitro studies. *Nanotechnology* **2015**, *26*, 255102. [CrossRef]

25. Ganta, S.; Paxton, J.W.; Baguley, B.C.; Garg, S. Pharmacokinetics and pharmacodynamics of chlorambucil delivered in parenteral emulsion. *Int. J. Pharm.* **2008**, *360*, 115–121. [CrossRef]

26. Navas, N.; Herrera, A.; Martínez-Ortega, A.; Salmerón-García, A.; Cabeza, J.; Cuadros-Rodríguez, L. Quantification of an Intact Monoclonal Antibody, Rituximab, by (RP)HPLC/DAD in Compliance with ICH Guidelines. *Anal. Bioanal. Chem.* **2013**, *405*, 9351–9363. [CrossRef] [PubMed]

27. Clemente, N.; Ferrara, B.; Gigliotti, C.; Boggio, E.; Capucchio, M.; Biasibetti, E.; Schiffer, D.; Mellai, M.; Annovazzi, L.; Cangemi, L.; et al. Solid Lipid Nanoparticles Carrying Temozolomide for Melanoma Treatment. Preliminary In Vitro and In Vivo Studies. *Int. J. Mol. Sci.* **2018**, *19*, 255. [CrossRef] [PubMed]

28. Wilhelm, S.M.; Adnane, L.; Newell, P.; Villanueva, A.; Llovet, J.M.; Lynch, M. Preclinical Overview of Sorafenib, a Multikinase Inhibitor That Targets Both Raf and VEGF and PDGF Receptor Tyrosine Kinase Signaling. *Mol. Cancer Ther.* **2008**, *7*, 3129–3140. [CrossRef]

29. Villarroel, M.C.; Pratz, K.W.; Xu, L.; Wright, J.J.; Smith, B.D.; Rudek, M.A. Plasma Protein Binding of Sorafenib, a Multi Kinase Inhibitor: In Vitro and in Cancer Patients. *Investig. New Drugs* **2012**, *30*, 2096–2102. [CrossRef]

30. Kanno, S.-I.; Itoh, K.; Suzuki, N.; Tomizawa, A.; Yomogida, S.; Ishikawa, M. Exogenous Albumin Inhibits Sorafenib-Induced Cytotoxicity in Human Cancer Cell Lines. *Mol. Clin. Oncol.* **2013**, *1*, 29–34. [CrossRef]

31. Hippalgaonkar, K.; Majumdar, S.; Kansara, V. Injectable Lipid Emulsions—Advancements, Opportunities and Challenges. *AAPS PharmSciTech* **2010**, *11*, 1526–1540. [CrossRef] [PubMed]

32. Islam, R.; Gao, S.; Islam, W.; Šubr, V.; Zhou, J.-R.; Yokomizo, K.; Etrych, T.; Maeda, H.; Fang, J. Unraveling the Role of Intralipid in Suppressing Off-Target Delivery and Augmenting the Therapeutic Effects of Anticancer Nanomedicines. *Acta Biomater.* **2021**, *126*, 372–383. [CrossRef] [PubMed]

33. Liu, L.; Ho, C. Using Intralipid to Improve Delivery of Anti-Cancer Nanodrugs: Effects on RES Clearance and Toxicity, EPR, and Immune Modulation. *J. Nanotechnol. Nanomater.* **2021**, *2*, 76–82.

34. Zhang, N.; Zhang, B.; Gong, X.; Wang, T.; Liu, Y.; Yang, S. In Vivo Biodistribution, Biocompatibility, and Efficacy of Sorafenib-Loaded Lipid-Based Nanosuspensions Evaluated Experimentally in Cancer. *Int. J. Nanomed.* **2016**, *11*, 2329. [CrossRef]

35. Mathieu, V.; Le Mercier, M.; De Neve, N.; Sauvage, S.; Gras, T.; Roland, I.; Lefranc, F.; Kiss, R. Galectin-1 Knockdown Increases Sensitivity to Temozolomide in a B16F10 Mouse Metastatic Melanoma Model. *J. Investig. Dermatol.* **2007**, *127*, 2399–2410. [CrossRef]

36. Yin, B.; Ni, J.; Witherel, C.E.; Yang, M.; Burdick, J.A.; Wen, C.; Wong, S.H.D. Harnessing Tissue-derived Extracellular Vesicles for Osteoarthritis Theranostics. *Theranostics* **2022**, *12*, 207–231. [CrossRef]

37. Conciatori, F.; Bazzichetto, C.; Falcone, I.; Pilotto, S.; Bria, E.; Cognetti, F.; Milella, M.; Ciuffreda, L. Molecular Sciences Role of MTOR Signaling in Tumour Microenvironment: An Overview. *Int. J. Mol. Sci.* **2018**, *19*, 2453. [CrossRef]

38. Oft, M. IL-10: Master Switch from Tumour-Promoting Inflammation to Antitumour Immunity. *Cancer Immunol. Res.* **2014**, *2*, 194–199. [CrossRef]

39. Lu, L.; Yoshimoto, K.; Morita, A.; Kameda, H.; Takeuchi, T. AB0074 Alkylating Agents Enhance Interleukin-10 Secretion from B Cells via P38 MAP Kinase Activation. *Ann. Rheum. Dis.* **2014**, *73*, 828. [CrossRef]

40. Lu, L.; Yoshimoto, K.; Morita, A.; Kameda, H.; Takeuchi, T. Bendamustine Increases Interleukin-10 Secretion from B Cells via P38 MAP Kinase Activation. *Int. Immunopharmacol.* **2016**, *39*, 273–279. [CrossRef]

4.3.2   ICOS-Fc in combined immuno chemotherapy for pancreatic cancer

4.3.2.1   Introduction

Pancreatic cancer incidence is rising both in Europe (Partyka et al., 2023) and in USA (Siegel et al., 2023), with the lowest 5-year relative survival rate (12%) among all cancer types. In particular, pancreatic ductal adenocarcinoma (PDAC), the prevalent type of pancreatic cancer, is one of the deadliest cancers, as WHO reported that 90% of PDAC patients die within a year of diagnosis (C. Li et al., 2020). The disease is asymptomatic during its early stages, patients are often diagnosed with metastasized stage IV with no option for surgery (Lev et al., 2017). Moreover, the standard-of-care treatments, which mainly consist in gemcitabine (GEM) and FOLFIRINOX (a combination of folinic acid (leucovorin calcium), fluorouracil, irinotecan, and oxaliplatin) display often poor efficacy and/or tolerability(Conroy et al., 2018).

GEM hydrochloride was approved by FDA in 1996 for the treatment of unresectable and metastatic PDAC, despite a modest improvement on survival compared to 5-FU (Frezza et al., 2008). Nevertheless, GEM suffers of poor penetration in the stiff desmoplastic pancreatic tumor stroma, and of several mechanisms of chemoresistance, that range from the downregulation of the transporter of GEM to the impairment of enzymatic functions involved in the metabolism of the drug (Amrutkar & Gladhaug, 2017).

The major transporter of GEM into cells is the human concentrative nucleoside transporter 1, (hCNT1), and its overexpression is considered a predictive survival marker of PDAC patients following the treatment with the oligonucleoside (Giovannetti et al., 2006). Nevertheless, cancer cells often downregulate this transporter in response to oxidative stress (Randazzo et al., 2020), and this shortcoming diminish the response to GEM treatment (Khan et al., 2019).

In the last decades, nanosized drug delivery systems have been proposed as a solution to overcome the poor efficacy and resistance issues correlated with GEM, including liposomes (Tamam et al., 2019), polymeric nanoparticles and solid lipid nanoparticles (Cai et al., 2021). Furthermore, nanomedicines represent a valid technology for combination therapy, allowing for a more efficient treatment, able to counteract different mechanisms of cancer progression and resistance (Alshememry et al., 2022). In the clinical practice, GEM is often administered with albumin-bound paclitaxel (nab-paclitaxel) (Von Hoff et al., 2013), in order to improve its efficacy, but several other combinations are evaluated in clinical and preclinical studies; additionally novel mechanisms to

overcome resistance are constantly investigated (Lei et al., 2019; Z. Zhang et al., 2022). For instance, the overexpression of a mutated KRAS oncogene is registered in 90% of pancreatic cancer, and it is a very appealing target for novel drugs (K. Yang et al., 2018). Nevertheless, many strategies blocking the activated KRAS and the RAF/MEK/ERK pathway did not show the expected efficacy. The use of an antibody, RT11-i, which directly targets the intracellularly activated GTP-bound form of RAS, is able to sensitize pancreatic cancer cells to GEM, reducing cell growth (K. Yang et al., 2018). The KRAS mutation is also correlated with the overexpression of the Nuclear factor erythroid 2-related factor 2 (Nrf2) in pancreatic cancer, and therefore Nrf2 is an interesting target for the development of anticancer drugs (Hayes et al., 2015). Indeed, downregulating the Nrf2 and yes-associated protein 1 (YAP) protein at the post-translational level, and increasing the oxidative stress level in cancer cells, reduced the chemoresistance to traditional chemotherapeutic agent (Barrera et al., 2021; Grattarola et al., 2021).

Another major player in the GEM chemoresistance mechanisms is represented by the tumor-related glycoprotein HAb18G/CD147. The overregulation of HAb18G/CD147 is correlated with the activation of the EGFR-pSTAT3 signaling, acting as pancreatic cancer cells self-defense mechanism against GEM treatment. Indeed, following treatment with GEM, pancreatic cancer cells overexpress the HAb18G/CD147 and are more prone to invade and metastasize, in response to the genotoxic stress induced by the drug (Xu et al., 2016a).

So far, the most successful example of targeted-therapy for PDAC is represented by the poly (ADP-ribose) polymerase (PARP) inhibitors. PARP is critical enzyme for single-stranded DNA repair, which is upregulated in cancer with BRCA1 or BRCA2 mutations. The inhibition of this enzyme is correlated to extended PFS in PDAC patients, and the PARP inhibitor Olaparib has been approved by FDA as maintenance therapy of BRCA1 or BRCA2 mutated, platinum-sensitive metastatic PDAC (Hosein et al., 2022).

Furthermore, a peculiar feature of pancreatic cancer is the presence of an immunosuppressive microenvironment (Falcomatà et al., 2023). In fact, less than 1% of PDAC patients result sensitive to immune-checkpoint blockade via the PD-1/PD-L1 pathway (Le et al., 2015), due to the low mutational burden reported in the vast majority of the cases (Imamura et al., 2023). The mechanisms of immune suppression in PDAC have different origins, such as the desmoplastic stroma that produce a hypoxic environment that inhibits the CD8+ T-cell, and the infiltration of immune suppressor cells (mainly myeloid-derived suppressor cells and tumor-promoting M2-polarized Tumor-associated Macrophages) (Ullman et al., 2022). To date, several immunotherapeutic

approaches have been tested in pre-clinical and clinical studies, including immune-checkpoint modulators, chimeric antigen receptor CAR-T cells and cancer vaccines (Yoon et al., 2021). Nevertheless, all the efforts in developing novel immunotherapies, did not lead to a major breakthrough for PDAC patients, and leave open the need of investigating alternative strategies.

ICOS/ICOSL involvement in cancer progression has been already reported, several evidence documented ICOSL triggering via ICOS-Fc promising anti-neoplastic effects, when administered alone, loaded into nanodelivery system or co-administered with other drugs in a polychemotherapy strategy. It inhibited ECs and tumor cells line adhesion *in vitro* experiments, cancer cells metastatization *in vivo* cancer models and, when loaded into suitable nanocarriers, it was able also to inhibit tumour growth (Dianzani et al., 2014; Clemente et al., 2020; Monge et al., 2022).

Moreover, its immunostimulatory and antiangiogenic activity stood out when it was included into a polychemotherapy association (Monge et al., 2022). The cytokine immunomodulation detected supported its potential role in favoring a resumption of the anti-tumour response.

4.3.2.2   MIVO technology

One of the major issues in the development of novel therapies, including nanomedicines for PDAC treatment, is the lack of clinically relevant animal models of the disease. PDAC is a type of tumor characterized by high inter- and intra-tumoral heterogeneity, high stromal component and infiltration of immunosuppressive cells. These features are very difficult to be represented by preclinical models consisting of human or murine cell lines, patient-derived cells or genetically engineered mouse models (GEMMs) (Yu et al., 2021).

Substantial differences between 2D cultures and real tumours cell behavior lie in their different interactions with the microenviroment. The unequal nutrient concentration to which cells are exposed represents an example: if 2D cultures cells are uniformly exposed to nutrients, the *in vivo* concentration of nutrients is characterized by spatial gradients, which play a key role in biological differentiation, organ development, determination of cell fate and signal transduction. Furthermore, it was well documented how mechanical interactions with the surrounding microenvironment regulate several cancer development crucial steps, such as metastasis process and tissue organization, cell motility and proliferation (Lo et al., 2000; Cavo et al., 2018).

Organoids and spheroids have been shown to resemble many physiological aspects better than cells grown in monolayers, but they are still quite far from recapitulating the whole *in vivo* scenario, since

they do not resemble the fluid-dynamic stimuli at the cancer microenvironment level, and, consequently, the drug transport mechanisms across the vascular endothelium structure (Marrella A, 2021). Therefore, in the last years gained increasingly attention the new advanced *in vitro* models represented by a fluidic culture system set in an innovative organ on chip technologies. On one side, they keep important advantages belonging to the 2D models, such as the better control of the experimental conditions, the relatively easy manipulation and analysis, with a species-specificity feature. However, their main advantage stands in the possibility to reproduce the physiological blood flow element, which can affect cells survival and metastatic propension, alongside a reliable drug distribution, thus putting the model closer to the *in vivo* physiology (Hoarau-Véchot et al., 2018; Trujillo-de Santiago et al., 2019). According to the complexity of this model, compared to a 2D culture, it offers the opportunity to evaluate more in-depth cell behavior and to perform different investigation, such as dynamic migration assay, anti-proliferative assay, 3D cancer model immune cells infiltration, resemble skin or gastrointestinal drugs absorption assay (Cavo et al., 2018; Marrella et al., 2020; Marrella A, 2021; Pulsoni et al., 2022).

To better reproduce the *in vivo* cancer context, the 3D scaffold-based cancer models were often displayed in a dynamic *in vitro* system. They are able to resemble the tumor-associated stromal ECM, which is an important component of the TME, playing crucial roles in cancer progression and invasion (Dutta & Dutta, 2009; Marrella A, 2021). Different polymeric materials are used as artificial ECM, alginate hydrogels are the mainly chosen because suitable for 3D gel-like structure stable over a prolonged time, which can be easily tuned via calcium ions-mediated crosslinking. This defines them suitable for *in vitro* pharmacological tests. On the other side Matrigel has been taken into account to evaluate more aggressive cancer model, due to its capability to enhance cell biological events and cells expressing feature of inner malignancy. Unfortunately, its structural weakness limits its application in short-term analysis, or in monolayer or thin gel conformations. Cavo et al. (2018) suggested a promising compromise 3D cells-scaffold made by 50%:50% Alginate: Matrigel gels, showing it as a valid matrix to reproduce metastatic cancer model.

Among all the organ on chip technology emerging, we used a MULTI-ORGAN single flow device (MIVO®), commercialized by React4life company (S.r.l., Genova, IT). This advanced *in vitro* model was used to perform a dynamic migration assay (Cavo et al., 2018).

4.3.2.3 Aim

The aim of this work was proposing a β-cyclodextrin based nanosponges (NS) loaded with GEM and functionalized with ICOS-Fc as an innovative combination therapy, potentially suitable to overcome drug resistance in pancreatic cancer.

It is well known how NS have been widely engineered for cancer therapy and drug delivery purpose (Iravani & Varma, 2022), due to their high specificity, biocompatibility, degradability and prologued released behavior. Additionally, they were depicted as safe and biodegradable material with negligible toxicity on cell cultures and are well-tolerated after injection in mice (Trotta et al., 2012). We firstly evaluated how the encapsulation of GEM into the NS is able to enhance its viability and proliferation inhibition on 2D and 3D pancreatic cancer model. Moreover, the ICOS-Fc nanocarrier functionalization represents an additional innovative aspect of the co-delivery system proposed. ICOS-Fc NPs encapsulation and its involvement in polychemotherapy strategy were already investigated and promising anti-neoplastic and immunostimulatory activities were detected. However, this is the first time ICOS-Fc is displayed on the NS surface, as a targeting agent for ICOSL expressing pancreatic cancer cells, with a key anti-invasion contribution in the synergistic effect of the chemoimmunotherapy association. In this regard, the MIVO technology was exploited to confirm the 2D anti-invasion effect rising up the complexity of the system and achieving evidence closer to the *in vivo* scenario.

The project was performed in collaboration with Prof. Roberta Cavalli research group, which provide the synthesis of the NS system, and Prof. Guiot research groups, which collaborated through the MIVO technology purchase.

4.3.2.4 Material and Method

Materials

Dimethyl sulfoxide (DMSO), 3-(4,5-dimethyl thiazol-2-yl)-2,5-diphenyltetrazolium bromide (MTT), ultra-low 96-well plates, crystal violet, methanol, acetic acid were from Merk Life Science S.r.l. (Milan, Italy). Dulbeccos Modified Eagle Medium (DMEM) high glucose, RPMI1640 medium, Fetal Bovine Serum (FBS), penicillin, streptomycin, and trypsin were from Euroclone (Pero, Milan, Italy). Transwell Boyden Chamber and Matrigel, were from BD Biosciences (Milan, Italy). MIVO® device commercialized by React4life (S.r.l., Genova, IT). PE-conjugated anti-ICOSL mAb (R&DSystems,

Minneapolis, MN). Gemcitabine was purchased from Lilly France S.A. (Fegersheim, France) and ICOS-Fc was obtained from Novaicos (Novara, Italy). All the other reagents not specified were purchased from Sigma-Aldrich (Missouri, USA).

Cell culture

CFPAC-1 and MIA PaCa-2 human pancreatic cancer cells were purchased from the American Type Culture Collection (ATCC; Manassas, VA, USA). PANC-02 murine pancreatic cancer cells are a kind gift from Dr. Jose Courty, Université Paris EST France.

CFPAC-1 and MIA PaCa-2 cells were cultured in DMEM, while PANC-02 in RPMI1640 medium. All cultures were supplemented with 10% FBS, 100 U/mL penicillin, 100 U/mL streptomycin. PANC-02 and MIA PaCa-2 were also supplemented with 1% sodium pyruvate. Cell lines were cultured in a 5% CO_2, 37 °C incubator.

MTT Assay

Pancreatic cells (1 x 10^3/well) were seeded in 96 well plates for 24h, then they were treated with GEM free form, NSGEM or NS (empty) using 0.04-10µM as the concentration range used. MTT assay was performed to assess viability of both GEM sensitive (CFPAC-1 and PANC-02) and GEM resistant (MIA PaCa-2) pancreatic cells after 72h of treatment. The cell proliferation reagent MTT was used, as described by the manufacturer's protocol. Cells that had received no drug, as control, were normalized to 100%, and the readings from treated cells were expressed as percent of viability inhibition. Four replicates were used to determine each data point, the results are expressed as mean ± SEM (n=6).

To evaluate cell viability at the time used in the invasion test (6h), the Crystal Violet Assay was used. Cells (8×10^3/well) were seeded into 96 well plates and treated for 6h with the compounds (with GEM free form, NSGEM or NS used at the concentration range of 0.04-10 µM) under study. Cell viability was assessed using the Crystal Violet Assay (Merck Life Science S.R.L., Roma, Italy)(Dianzani et al., 2020b).

Clonogenic Assay

The pancreatic cells lines (1 x 10^3/well) were seeded into 6 well plates. The treatment (0.04-10 µM with GEM free form, NSGEM or NS) was performed after 24h from seeding and the different formulation were left on cell monolayer for only 3h. Afterwards, the medium was replaced with drug-free medium and the cells were cultured at 37 °C and 5% CO_2 for 7 days more. The Clonogenic

Assay was then performed fixing and staining the cells with a solution of 80% crystal violet (Sigma-Aldrich, St. Louis, MO, USA) and 20% methanol. In order to reach a quantitative data, the crystal violet colonies were dissolved using a solution of 30% v/v acetic acid prepared in milliQ water. Absorbance signal was recorded at 595 nm by a 96 well plate ELISA reader. The results are expressed as mean ± SEM (n=5).

Spheroid Formation of PANC2 Cells

PANC-02 cells, cultured in standard 2D condition, were dissociated with trypsin-EDTA into single-cell suspensions. The cells were then seeded on ultra-low attachment (ULA) 96-well flat-bottom plates (Sigma-Aldrich, St. Louis, MO, USA). Optimal seeding densities were established such that PANC-02 3D spheroids fell within a size range of 200 to 500 μm in diameter on day 8, considering appropriate for initiating experimental studies.

3D viability assay

The cytotoxic effect of GEM, NSGEM or NS on PANC-02 3D spheroids was determined by using the 2-(4-iodophenyl)-3-(4-nitrophenyl)-5-(2,4-disulfophenyl)-2H-tetrazolium (WST-1) reagent (Roche, Italy). Cells were seeded (0.8 – 1.5 ×10^3 cells/well) in 100 μl of serum-supplemented medium and treated with different concentrations of GEM, NSGEM or NS. After 72h, the drug was removed and the WST-1 assay was performed. The optical density (OD) of treated and untreated cells was determined at a wavelength of 450 nm with a microplate reader after 4h of incubation. Controls were normalized to 100%, and the readings from treated cells were expressed as % of viability inhibition. Eight replicates were used to determine each data point (n=5).

3D spheroid reconstructions were obtained by using ReViSP, http://sourceforge.net/p/revisp/, while the spheroid volumes were obtained by using AnaSP, https://sourceforge.net/projects/anasp/. The results are expressed as % inhibition of control and are the mean ± SEM (n=3).

Boyden Chamber Assay

The Boyden chamber is made up of two portions, basal and apical series of wells, separated by a Matrigel (BD Biosciences, San Jose, CA, USA) coated filtered membrane (8.2 mm diameter and 0.5 μm pore size), through which is evaluated the cells migration behavior.

In the apical compartment, over a 50μg/mL Matrigel coated filter (8.2mm diameter and 0.5μm pore size), were placed 1 x 10^3 cells/well in serum-free medium, with or without treatments under

testing. In the basal compartment was displayed medium containing FCS 20% acting as a chemo-attractant. Then, the Boyden Chamber was incubated at 37 °C under 5% CO2. After 6h, the cells on the apical side were wiped off with Q-tips. The lower side of the filtered membrane was stained with methanol-crystal-violet and the cells there migrated and attached were counted with an inverted microscope (magnification 40x). The results are expressed as the % vs control of migrated cells from all the wells of each quadruplicate filter ± SEM (n=5). The control migration was 55 ± 4 and 61 ± 5 cells for CFPAC-1 and MIA PaCa-2, respectively.

ICOSL expression in tumour cell lines

The cell-surface phenotypes were assessed via direct immunofluorescence and flow cytometry using the appropriate PE-conjugated anti-ICOSL mAb. The mean fluorescence intensity ratio (MFI-R) was calculated considering all of the alive cells according to the following formula: MFI of the ICOSL-stained sample histogram (arbitrary units)/MFI of the control histogram (arbitrary units) (Dianzani et al., 2014).
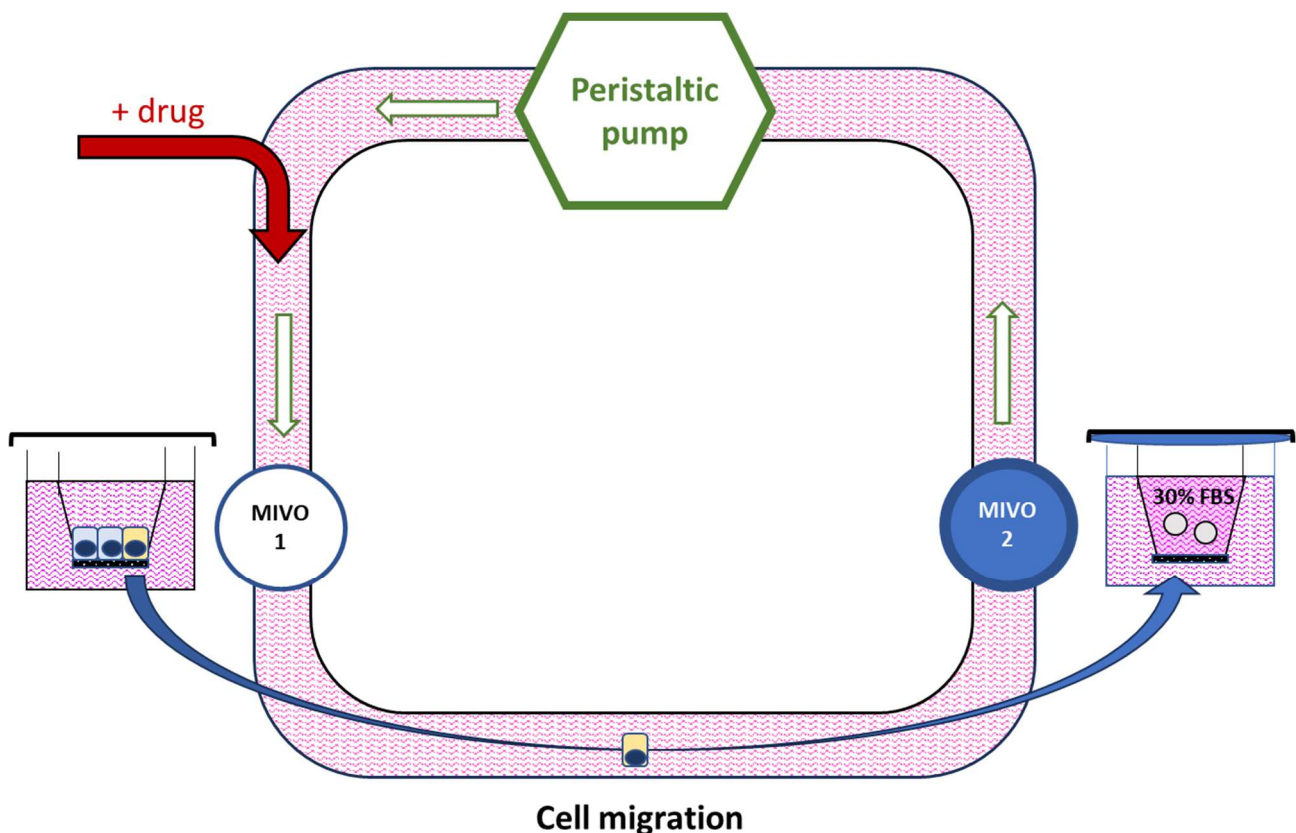
Dynamic culture

Figure 2: MIVO experimental model scheme

In vitro drug efficacy tests were performed using a MULTI-ORGAN single flow device (MIVO®) consisting of two chambers placed in a closed circuit in which a peristaltic pump set an internal flow rate. The system design is shown schematically in Figure 2.

In each chamber it was placed a 3 µm pore size TW insert and we chose to call MIVO1 the chamber which stands for the primary tumour site, consisting of a confluent MIA PaCa-2 cells monolayer placed in complete cell culture medium, and MIVO2 the chamber which stands for new tumour metastasis sites, consisting of two alginate hydrogels prepared with 30% FBS cell culture medium and placed in 30% cell culture medium. This second chamber works as a chemo-attractant factor for the cell migration.

The nanoformulations were prepared in complete cell culture medium (10% FBS), in the amount necessary to fill in all the circuit and apical MIVO1 chamber (around 6ml).

In each experiment three different circuits were built in parallel: CTR (untreated), GEM+ICOS-Fc in free form and NS[GEM+ICOS-Fc].

We set a flow rate of 20rpm using 2mm diameter tubes (this setting corresponds of a velocity of 0.64mm/sec below the TW and a flow rate of 4.28ml/min). This is the lowest flow rate that keeps cells into the circuit and prevent cell deposition on the bottom of the MIVO chambers, the direction of the flow rate is set from MIVO1 to MIVO2.

Once placed both chambers, displayed the chemo-attractant in MIVO2 chamber, filled the apical MIVO1 and the circuit with the nanoformulation treatment, the micro-fluidic system was connected to the peristaltic pump and moved into the incubator for 48h (37 °C and 5% CO2).

Analysis of drug antimetastatic effect in dynamic culture

In order to evaluate the antimetastatic effect of the different treatments, after 48h both TW were removed from the MIVO chambers and both TW membranes were fixed and stained with a solution of methanol-crystal-violet solution. The cells were counted at the microscope and the data collected were expressed as number of cells attached on the respectively MIVO1 or MIVO2 membranes. The results are expressed as mean of cells counting ± SEM (n=3). Only on MIVO2 membrane photos were taken at the microscope (magnification 10x).

To study if the cells, detached from the MIVO1 and MIVO2 membranes, kept their viability and proliferation ability in the static system and once they reached the circulation flow, the apical volume of MIVO1 chamber and the one displayed in the circuit tubes were moved into petri dishes. They

were kept in incubator at 37 °C and 5% CO_2 for 24h before replacing cell culture medium with fresh one. The cells were kept in complete medium (10% FBS) for 14d more and monitored looking to their ability to attach to the petri dish and grow (The analysis steps are shortly depicted in Fig 3.). The cell clones grew in each petri dish were counted at the microscope and the data collected were expressed as number of cells attached. The results are expressed as mean ± SEM (n=3). Representative photos of apical MIVO1 cells clones grew in petri dishes were taken at the microscope (magnification 10x).

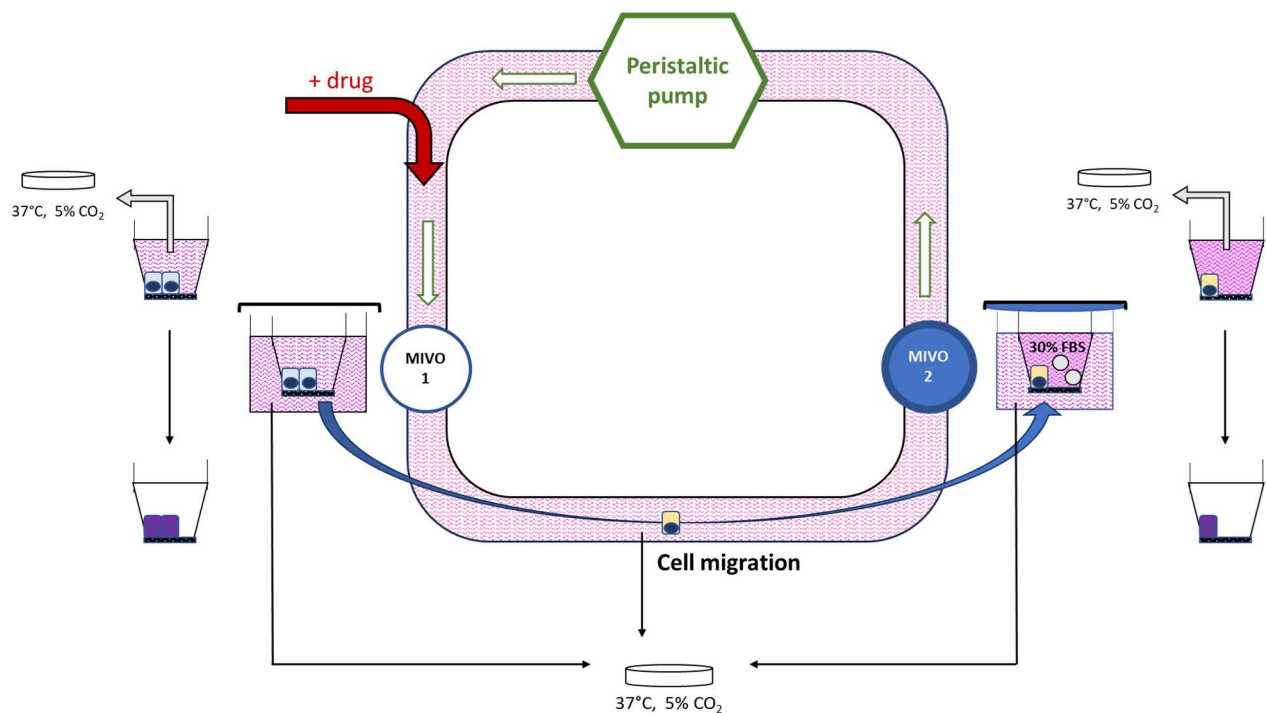**Figure 3.** Scheme of analysis of drug antimetastatic effect in dynamic culture

Statistics

The statistical significance was evaluated by one-way ANOVA followed by the multiple comparison post-test Bonferroni (GraphPad InStat software (San Diego, CA, USA). Data are expressed as mean and standard error of the mean (SEM) and the statistical significance was set up at *$p < 0.05$ and **$p < 0.01$.

4.3.2.5   Results

Viability: MTT Assay

Fig 4. showed the cytotoxicity results towards both GEM sensitive (CFPAC-1 and PANC-02) and GEM resistant (MIA PaCa-2) pancreatic cell lines.

After 72h of treatment in CFPAC-1 and PANC-02 cell lines there were a small but significant difference in cell viability inhibition, when GEM is administered encapsulated in NS compared to the free form (range of concentrations used for GEM sensitive cell lines: 0.4-200 nM). Differently, there is no significant difference between free or encapsulated GEM in MIA PaCa-2 treated cells (range of concentrations used for GEM resistant cell lines: 0.04-10μM). No viability inhibition was detected on cells treated with empty NS.
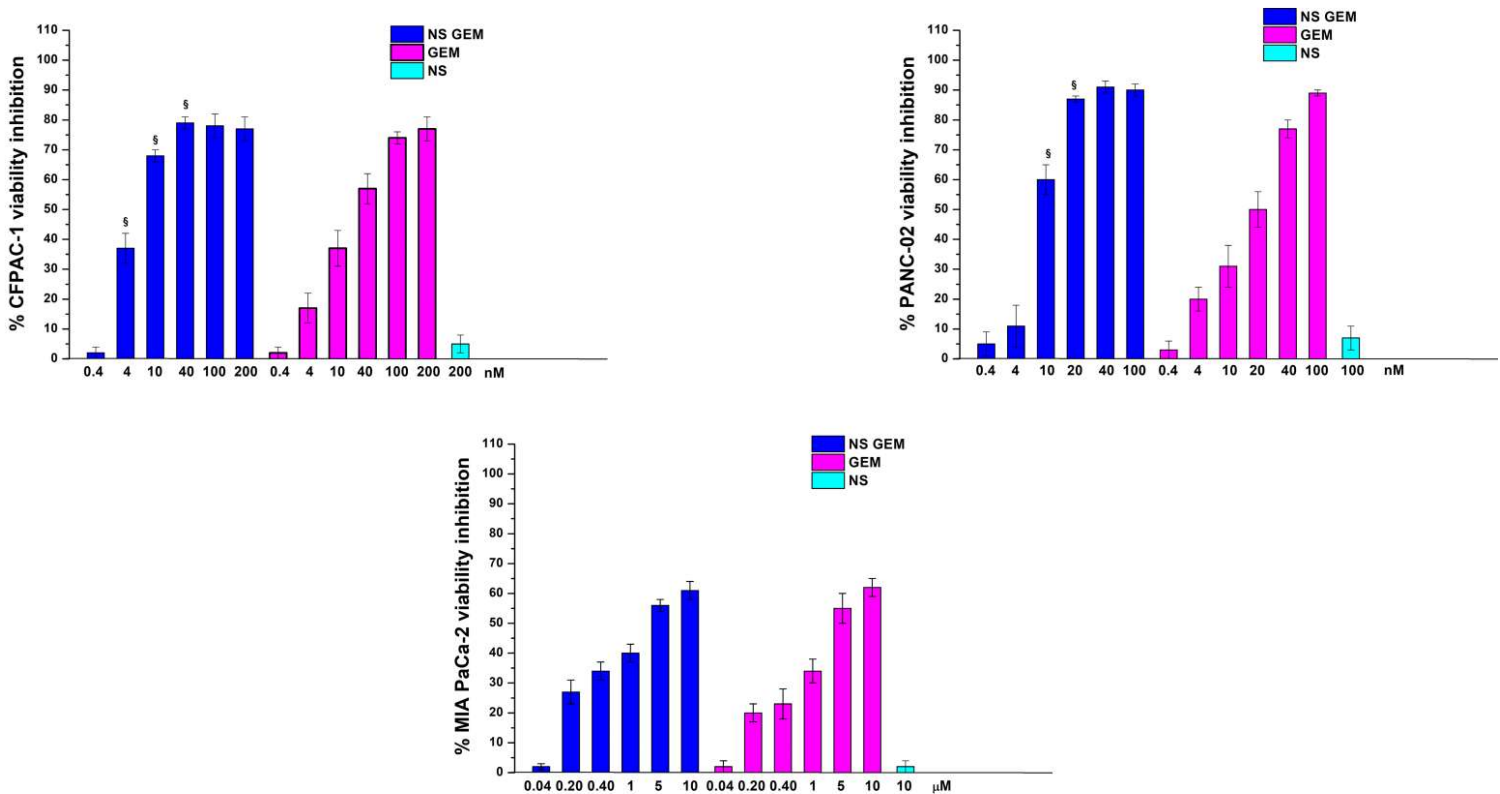

Figure 4: Viability (MTT assay) in CFPAC-1, PANC-02 and MIA PaCa-2 untreated or exposed to GEM, NSGEM or NS at the indicated concentrations 72h after the treatment. Results are expressed as a percentage of viability inhibition vs control. The data are mean ± SEM (n=6). §$p < 0.05$ NSGEM vs GEM.

Proliferation: Clonogenic Assay

The methodology of colony forming assay used in these experiments is able to give information about how fast the nanoformulation is uptaken by cancer cells and consequently how could be effective on cell proliferation. Indeed, the cells were incubated only for 3h with the different drug nanoformulations (range of concentrations used for GEM sensitive cell lines were 4-200nM in CFPAC-1 and 2-200nM in PANC-02; range of concentrations used for GEM resistant cell lines: 0.04-10μM). Then, cells were washed and incubated with free medium for 7d more.

CFPAC-1 cells Clonogenic Assay shows that the internalization of NSGEM was more efficient than that of GEM administered in free form. Indeed, clonogenic inhibition is approximately 80% for the highest concentration of NSGEM, while only 60% for GEM free (Fig. 5). The different speedy of internalization is even more evident in PANC-02 cells. Very interesting is the results obtained using MIA PaCa-2 cells. Indeed, Clonogenic Assay revealed that cells treated with NSGEM were first internalized and more inhibited in the proliferation capacity (Fig. 5).
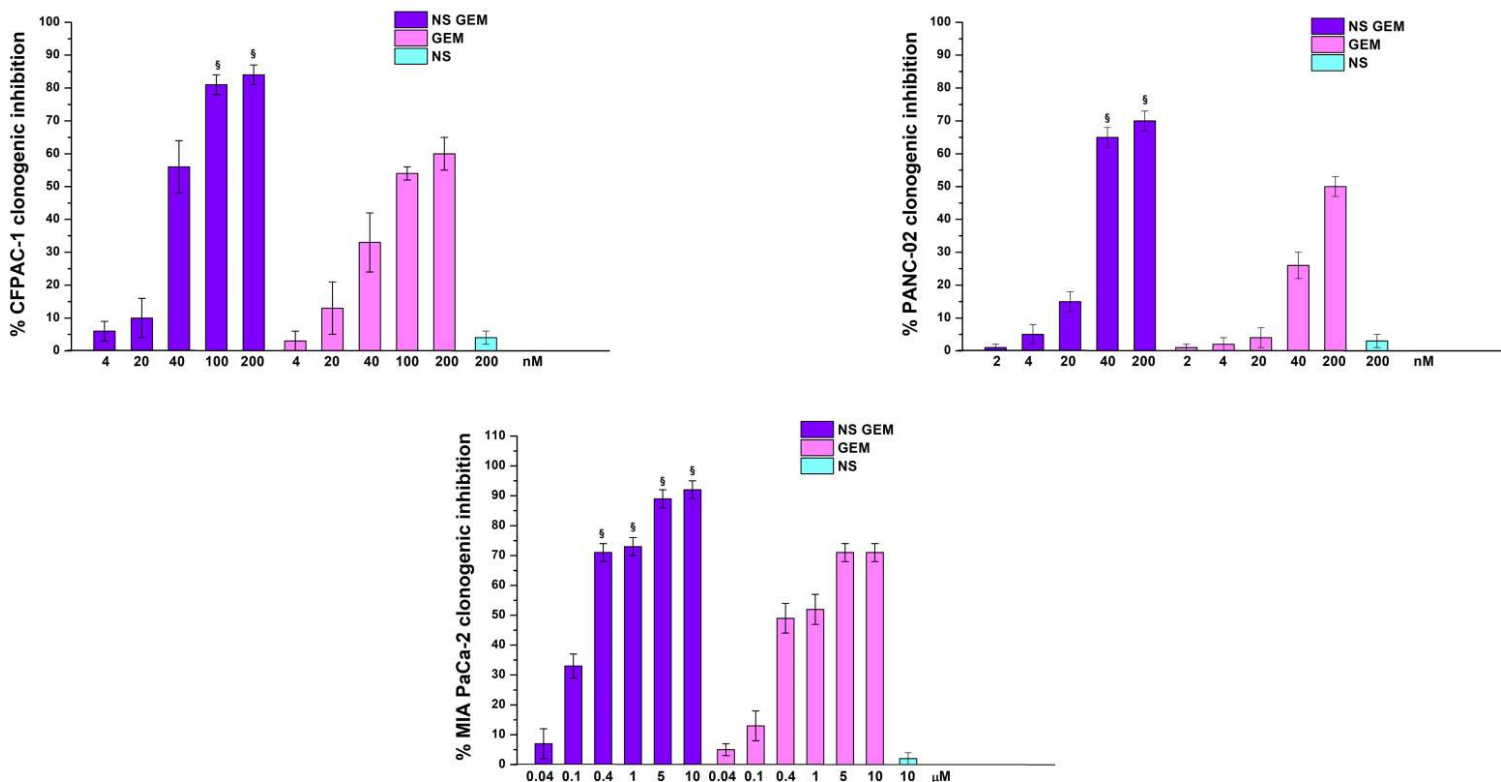

Figure 5: Clonogenic Assay in CFPAC-1, PANC-02 and MIA-PaCa-2 untreated or exposed to GEM, NSGEM or NS at the indicated concentrations. Cells were treated for 3h, then exposed with free medium for 7 days. Results are expressed as a percentage of clonogenic inhibition vs control. The data are mean ± SEM (n=5). §p < 0.05 NSGEM vs GEM.

3D viability assay

Naturally, in 2D cell cultures cells are grown in monolayer on a well, being very different from *in vivo* condition. 3D cell cultures allow predict drugs treatment efficacy more accurately; this model leave cells growing and interacting with surrounding extracellular framework in three dimensions better representing *in vivo* tissue condition.

Therefore, it is very important to verify if also in these conditions NS formulation could be better internalized and efficient than free drug.

To perform this viability assay PANC-02 cells were chosen, among all the others used, because the most suitable for being cultured in 3D models. The results demonstrated that NSGEM induced a significant and concentration-response volume reduction compared to the GEM free treatment. Spheroids representative images are placed in Fig 6. In panel A; spheroids 3D volume images. In panel B; the 3D spheroid reconstructions and quantitative data of % spheroids volume in graph C. The graph D shows the WST-1 assay data collected after 72h of treatment. The cell viability results confirmed that NSGEM can be internalized better and can slowly release GEM, being significantly more efficient than in the GEM free form condition tested.
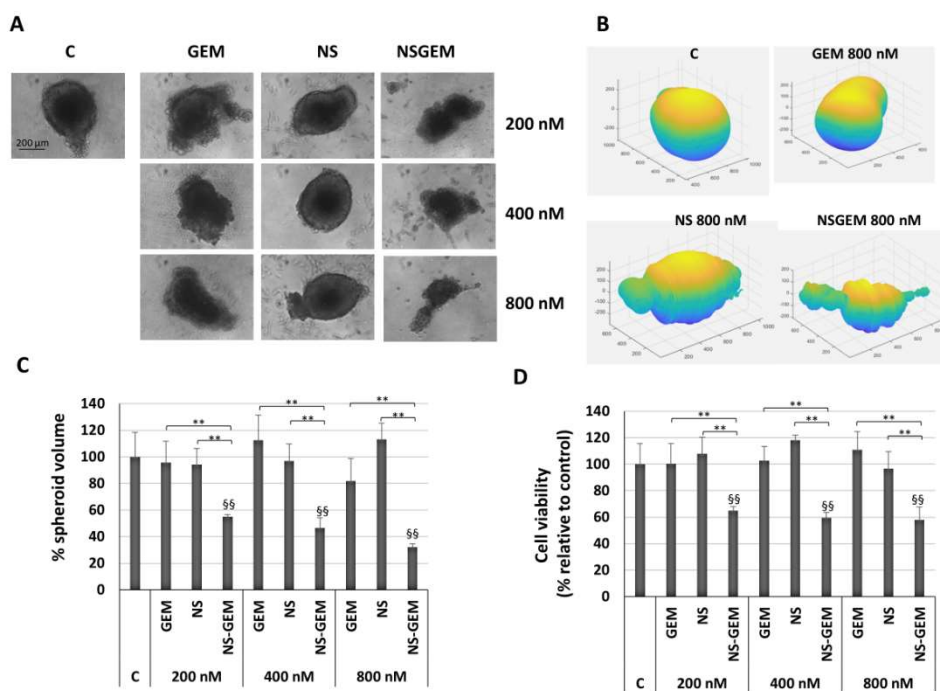

Figure 6: PANC02 spheroids untreated (C, control) or treated with GEM, NS, or NSGEM at 200, 400, or 800nM for 72h. Panel B: 3D spheroid reconstructions corresponding to C, GEM 800nM, NS 800nM, NSGEM 800nM were obtained by using ReViSP, http://sourceforge.net/p/revisp/. Panel C: Spheroid

volumes obtained by using AnaSP, https://sourceforge.net/projects/anasp/. The results are expressed as % inhibition of control and are the mean ± SEM (n=3). §§p < 0.01 *vs* control: **p < 0.01. Panel D: cell viability of 3D PANC02 spheroids treated as reported above. The results are expressed as % inhibition of control and are the mean ± SEM (n=3). §§p < 0.01 *vs* control: **p < 0.01

Invasion: Boyden Chamber Assay

It has been previously reported by many authors Arora et al., 2013; Gingis-Velitski et al., 2011; Hasnis et al., 2014; Xu et al., 2016b) that GEM can stimulate cell invasion *in vitro* and could be associated to an accelerated metastasis diffusion in mice pancreatic cancer models *in vivo*. Therefore, we wanted to check how our formulation behaved and whether they were able to interfere with the metastatic process. So, we tested them for *in vitro* inhibition of pancreatic cells invasion, which are initial step of the metastatization process.

In our experiments, GEM sensible and GEM resistant pancreatic cancer cells showed different invasion behaviors. Indeed, as showed from literature in GEM sensible cells, in the range of concentration tested (0.4-5µg/ml) GEM was unable to both induce or inhibit cell invasion. Really interesting were the NSGEM effect showed, since it was able to inhibit in a concentration-dependent manner CFPAC-1 invasion. On MIA PaCa-2 GEM resistant cells the results were even more striking because GEM induced cell invasion, while NSGEM inhibited it (Fig.7).
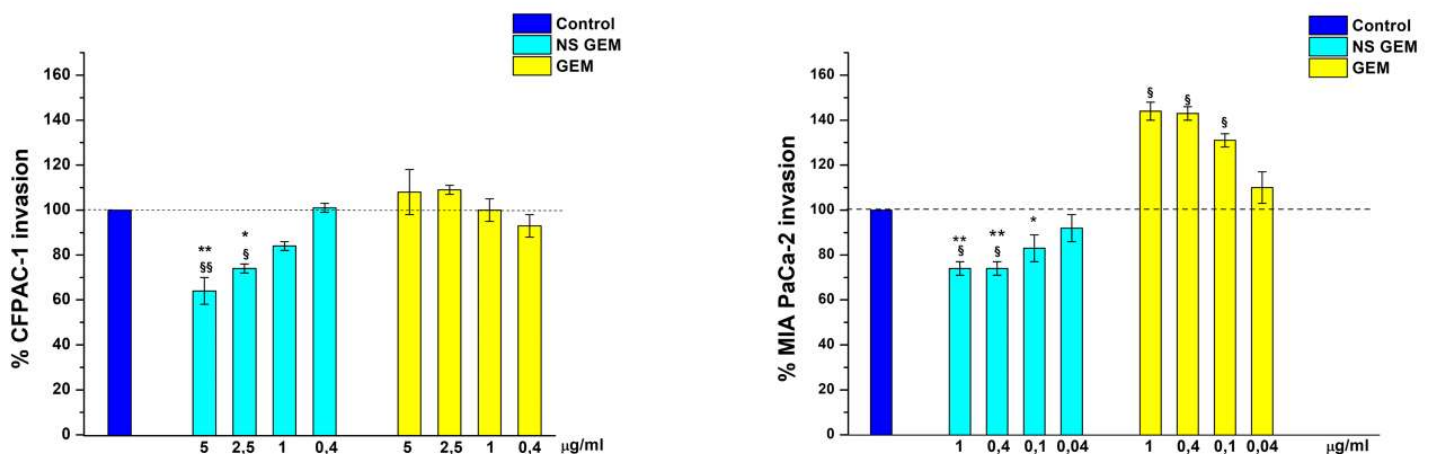

Figure 7: Invasion assay in CFPAC-1 and MIA PaCa-2 untreated or exposed to GEM, NSGEM or NS at the indicated concentrations. Cells were treated for 6h in a Boyden chamber. Results are expressed as a percent of invasion inhibition vs control. The data are mean ± SEM (n=6). §p < 0.05 NSGEM or GEM vs control; §§p < 0.01 NSGEM vs control; *p < 0.05 NSGEM vs GEM; **p < 0.01 NSGEM vs GEM.

ICOSL expression in tumour cell lines

To induce or increase an antimetastatic effect on pancreatic resistant cells, we decided to use NS decorated with ICOS-Fc, known for its ability to inhibit cell invasion, already reported when administered in free form, loaded into nanodelivery system and co-delivered with other drugs in a polychemotherapy strategy. Moreover, it was well documented how this effect was built on the ICOSL triggering (Clemente et al., 2020; Dianzani et al., 2010, 2014; Monge et al., 2022). For this reason, we checked the ICOSL expression level of the pancreatic cancer cells used in the biological test. Fig 8. shows that MIA PaCa-2, GEM resistant cell line, are the highest ICOSL expressing cells. They were suitably chosen to evaluate if NSGEM tailored with ICOS-Fc would be able to improve invasion inhibition induced by NSGEM.
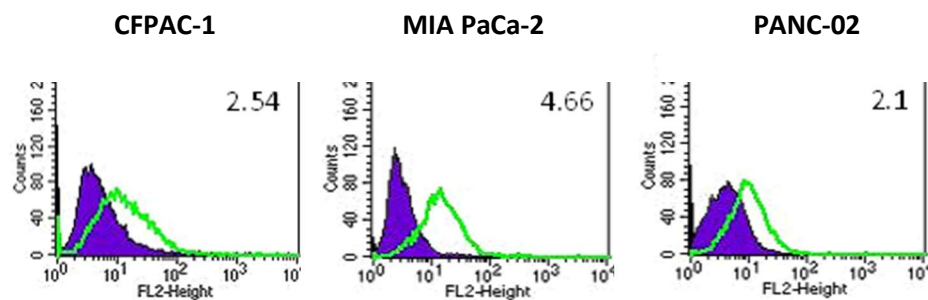
Figure 8: Flow cytometry data showing ICOSL expression in pancreatic cancer cells CFPAC-1, MIA PaCa-2 and PANC-02. The numbers in each panel indicate the MFI-R; the cutoff between the ICOSL[high] and ICOSL^{low} cells was set at MFI-R = 2.

First of all, it was necessary to fix the ICOS-Fc suitable concentration to functionalize the system, since it was the first time ICOS-Fc was displayed on the nanocarrier surface and not loaded into it. We started using the same ICOS-Fc loading concentration used in previous projects, realizing from the data collected that was too much high because responsible to counteract a functional ICOSL interaction, probably due to a steric obstacle reason. Using lower concentrations NSICOS-Fc were able not only to inhibit MIA PaCa-2 invasion in a concentration dependent manner, but also were 20 times more active than the free form (Fig. 9a).

To study the anti-invasion effect of the nanodelivery system here proposed, we chose a good proportion ratio of both components, such that allows to load GEM (0.4μM) and ICOS-Fc (0.2μg/ml) at concentrations which respectively are able to induce and significantly inhibit MIA PaCa-2 cell migration.

As it was showed before, GEM free 0.4μM induced cells invasion and ICOS-Fc free, 0.2μg/ml has no inhibition effect, while NSGEM 0.4μM and NSICOS-Fc 0.2μg/ml inhibited cancer cell invasion. When they are administered together (0.4μM GEM and 0.2μg/ml ICOS-Fc), both in free form, no reduction was observed, because that low dose of free ICOS-Fc was not effective. While, when both components are combined together, the cells invasion was counteracted with higher inhibition effect than all the other formulation (NSGEM+ICOS-Fc > NSGEM ≥ NSICOS-Fc) (Fig. 9b).
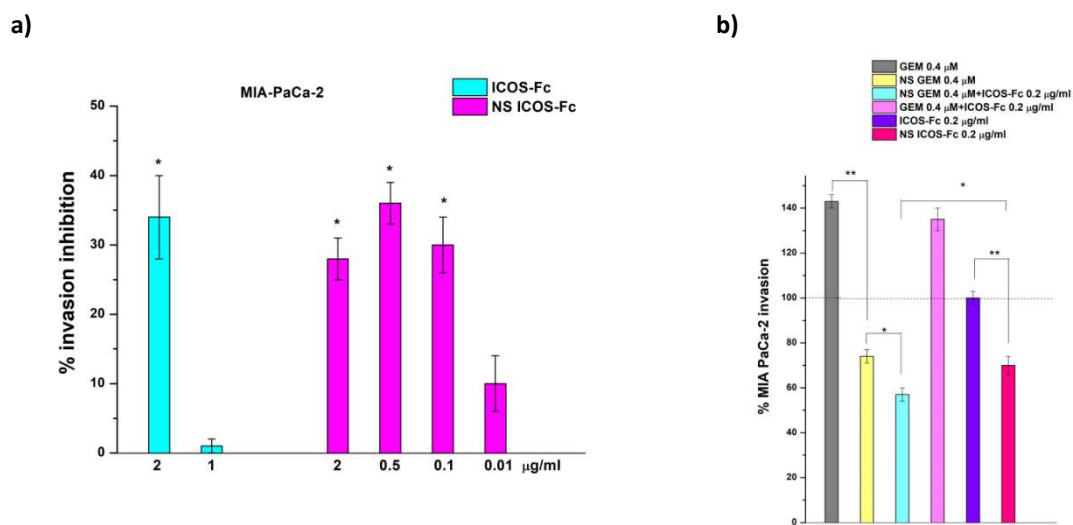
Figure 9: The graph a) reports the invasion assay results of in MIA PaCa-2 cell line exposed to ICOS-Fc in free form or loaded into NS at the indicated concentrations. The graph b) shows the invasion results collected after exposing MIA PaCa-2 cells with GEM free 0.4 μM, or ICOS-Fc free (0.2μg/ml), NSGEM (0.4μM) and NSICOS-Fc (0.2μg/ml), and with NS [GEM+ICOS-Fc] (0.4μM GEM and 0.2μg/ml ICOS-Fc). Cells were treated for 6h in a Boyden chamber. Results are expressed as a percent of invasion inhibition vs control. The data are mean ± SEM (n=6). *p < 0.05; **p < 0.01.

Migration: MIVO micro-fluid systems

We have recently developed a dynamic *in vitro* cancer model for testing anti-invasion drug effect. Among the arising new organ-on-chip technology we used a MULTI-ORGAN single flow device (MIVO®), commercialized by React4life, which consists in the realization of dynamic cell cultures, placed in different cellular compartments which can cross-communicate through channels interconnection, and/or porous membranes (Maulana et al., 2021). The MIVO® Migration Assay was performed using two chambers placed in a closed circuit in which a peristaltic pump set an internal flow rate. The primary tumor site was reproduced by a confluent cancer cells monolayer placed in

MIVO1 chamber, while the chemo-attractant factor displayed in MIVO2 chamber works on cells migration and stands for new tumor metastasis site.

This experiment was performed in order to evaluate the anti-invasion ability of NS [GEM+ICOS-Fc] in dynamic condition. Thus, we chose the concentrations that have primary an anti-invasion effect 0.4μM NSGEM with 0.2μg/ml NSICOS-Fc, using GEM+ICOS-Fc free form and no treated cells as control.

After 48h of dynamic condition cells attached to the TW membranes were counted. Cell counting values are similar among all three conditions tested in MIVO1 chamber, while the MIVO2 membranes showed very interesting trend (Fig. 10a).

MIVO2 cell counting values clearly showed the dominate GEM effect in the GEM+ICOS-Fc free form association treatment, explained by a higher number of MIA PaCa-2 cells migrated compared to the untreated condition (Fig. 10a). On the other side, NSGEM functionalized with ICOS-Fc significantly counteracted MIA PaCa-2 metastatic dissemination, being cells attached to MIVO2 membrane lower then both control and GEM+ICOS-Fc conditions (Fig. 10a).
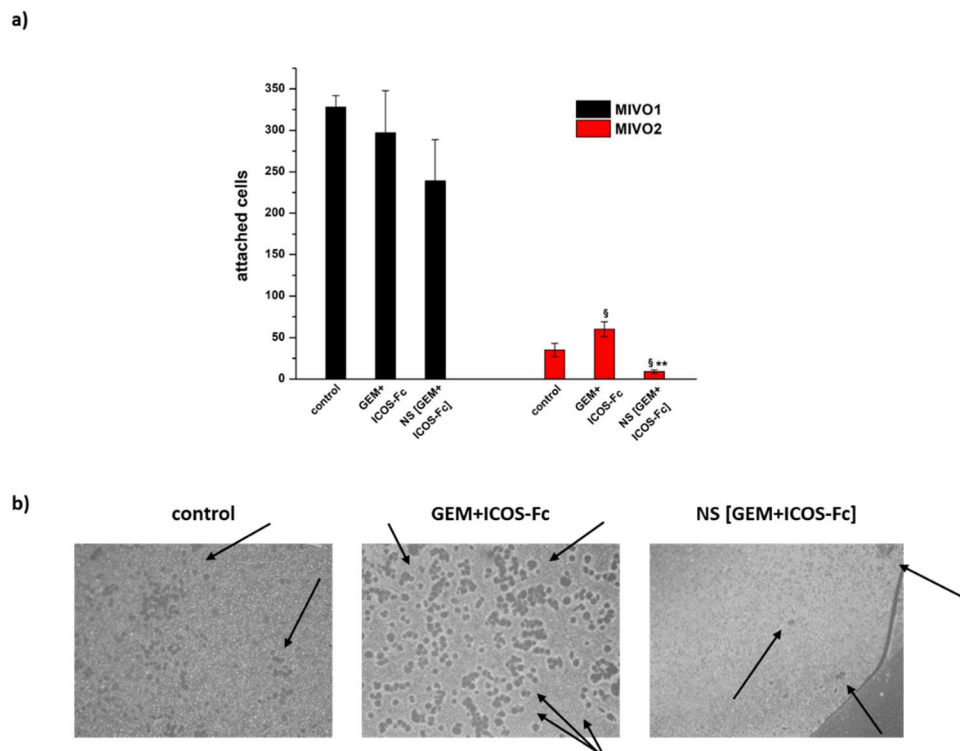

Figure 10: Counting cell values detected on MIVO1 and MIVO2 membrane after 48h of exposure to GEM+ICOS-Fc or NS [GEM+ICOS-Fc], used at the concentration indicated, in dynamic condition (10a) and representative images of all three conditions tested of MIA PaCa-2 cells attached on MIVO2 membrane. Fig 10b depicted the representative images of cells attached on MIVO2 membranes of

all three conditions tested. Results are expressed as mean of counting cell values ± SEM (n=3); *p < 0.05 GEM+ICOS-Fc vs control; ##p < 0.01 NS [GEM+ICOS-Fc] vs GEM+ICOS-Fc; °p<0.05 NS [GEM+ICOS-Fc] vs control.

Then we have collected the fluctuant cells in apical chambers MIVO1 and those circulating in the microfluid system to see if they were still alive and able to adhere to wells and grow. So, they were placed in petri dishes for one day, then culture medium was replaced with fresh one without any treatment and monitored for 14d.

Figure 11 shows the untreated condition counting cells values, which reports a very high number of cells clones in the apical MIVO1, increased from 7d (>50 clones) to 14d (>200 clones) of culturing at 37 °C and 5% CO_2. Representative images of cells collected from apical MIVO1 and cultured in complete medium for 14d are reported in panel b.

A significant increase of cells clones was found also in the dishes harvesting the circuit volumes, showing alive cells able to migrate and form metastasis.

The data related to the treated conditions (GEM+ICOS-Fc in free form or NS [GEM+ICOS-FC]) are reported in the 11c and 11d images, showing the MIVO1 and circuit counting cells respectively. In the MIVO1 supernatant treated with GEM+ICOS-Fc, the cells detached from the monolayer were still alive and able to grow in clones over time, while in the NS[GEM+ICOS-Fc] condition any clones were formed (Fig. 11c). Those evidence showed a better cells internalization of NS [GEM+ICOS-Fc] compared to the drugs administered in the free form, which leads to counteract the cells migration from MIVO1 to MIVO2. Indeed, NS [GEM+ICOS-Fc] can also inhibit the viability of the cells detached, being GEM slowly released by the NS.

Same trend was highlighted considering the cells collected in the circuit volume, the NS [GEM+ICOS-Fc] showed its ability to significantly counteract MIA PaCa-2 migration and proliferation over time, compared to GEM+ICOS-Fc treatment condition (Fig. 11d). Even though in the GEM+ICOS-Fc condition the cells collected from the circuit were much lesser than those detected in MIVO1 chamber, the counting cells values highlighted an increasing in number of cells clones depicting a treatment condition allowing metastasis cancer dissemination. On the other side, the NS [GEM+ICOS-Fc] treatment was able to counteract cell clones proliferation in both cells collected from MIVO1 chamber and those harvested from the circuit.
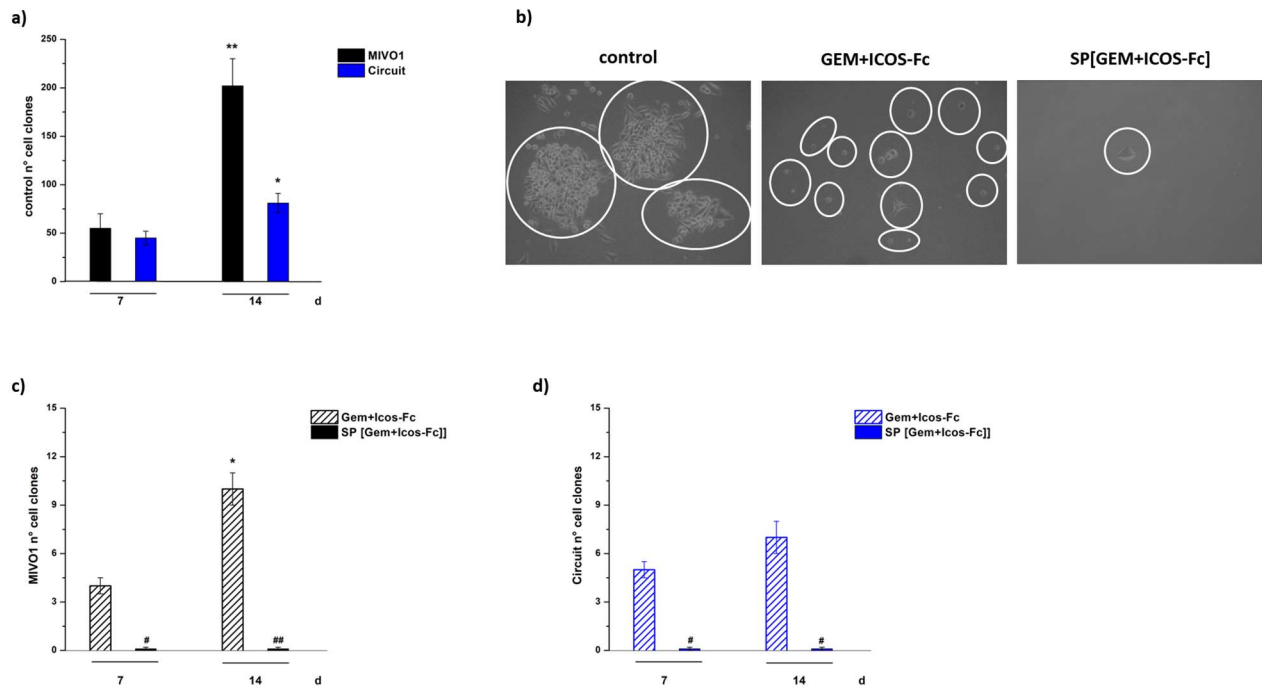
Figure 11: Counting cell values detected after 7-14d of culturing of cells harvested from MIVO1 or circuit compartment (kept in dynamic condition for 48h). The graph 11a reported the untreated condition of cells collected from both MIVO1 and circuit, the GEM+ICOS-Fc compared to NS [GEM+ICOS-Fc] treatment is displayed in the panels below, 11c reporting the MIVO1 data and 11d is referred to the circuit one. Panel 11b depicts representative images of MIA PaCa-2 cell line harvested from the MIVO1 apical chamber and cultured for 14d in complete medium.

4.3.2.6   Discussion

For this cancer, whose patients show a very poor outcome, compared to other resected solid tumours, very few alternative treatments are available next to gold standard one GEM. Most of the alternative clinical failure are due to the MDR, both intrinsic (innate) and acquired (in response to drug therapy), characterized by the higher expression of drug efflux pump and a very dense stromal environment tackling drug cancer permeation. Moreover, crucial role in promoting cancer aggressiveness and drug resistance phenomena is exerted by the TME, which includes the ECM and different kinds of cells, such as a variety of immune cells contributing for the immunosuppressive additional therapeutic challenge (Alshememry et al., 2022).

This work showed the β-cyclodextrin based NS loaded with GEM and functionalized with ICOS-Fc as a promising strategy to overcome pancreatic cancer drug resistance. The encapsulation of GEM showed in both GEM sensitive and GEM resistant cells a quicker internalization and a significantly higher efficacy of NSGEM compared to GEM administered in free form. Those high differences detected through colony forming assay were only slightly significant in MTT results correlated to GEM sensitive cells, and no marked at all in MTT data of GEM resistant cells. This suggest the NSGEM better internalization aspect, which is evident in the shorter time setting of the colony forming assay, while totally hidden in the 72h of MTT protocol. However, even if the 2D models offer a first step of *in vitro* investigation, since their static condition they are much far from representing what happen in reality.

In order to investigate the permeation capability of NSGEM in a pancreatic tumour mass, we developed a 3D cell culture system in collaboration with Prof.ssa Stefania Pizzimenti laboratory. Compared to 2D models, in which the forced planar morphology acquired by the cells is potentially responsible to alter several aspects of their behavior, cells that grow in a 3D environment are more likely to develop shapes and phenotypes observed in an *in vivo* TME. It was well documented how in a more complex system, allowing cell-cell contacts in all directions and cell-matrix interactions, 3D cancer cells models display higher aggressiveness, overexpress pro-angiogenic growth factors and acquire drug resistance (Leung et al., 2010; Lhuissier et al., 2017; Affoué Dit Faute et al., 2002).

The 3D model was performed using PANC-02 cell line, since identified as the most suitable one to be cultured in 3D model and, because of their murine origin, potentially exploited in a planned *in vivo* model. The viability assay shows that the spheroids volumes was significantly reduced when treated with NSGEM, compared to GEM administered in free form. The higher NSGEM efficacy was

137

confirmed through the WST-1 quantitative data, supporting much more how NSGEM are better uptaken, thus how the GEM encapsulation ameliorates the drug permeation into the 3D pancreatic cell structure.

According to literature migration experiments, GEM showed an induced-invasion effect on GEM resistant pancreatic cancer cell, while no effect on GEM sensitive one. Moreover, it was documented how this effect may be correlated to an induced overexpression of HAb18G/CD147, which acts as a novel upstream activator of STAT3-mediated signaling in pancreatic cancer (Xu et al., 2016c).

The HAb18G/CD147 belongs to the CD147 family, multifunctional surface transmembrane glycoproteins, found expressed by several malignant human cancers, including MIA PaCa-2 one (Biswas Chitra et al., 1995; Riethdorf et al., 2006; Schnelderhan et al., 2007). It was documented responsible to increase tumor invasion and metastasis, by inducing matrix metalloproteinases (MMPs) secretion, and MDR (Pan et al., 2012; Xu et al., 2016c). Moreover, the lowered response to GEM treatment could be related to the reduced GEM cell uptake, which is caused by the downregulation of hCNT1 transporter in response to oxidative stress (Giovannetti et al., 2006; Khan et al., 2019).

We performed a Boyden chamber assay to further demonstrate that GEM encapsulation in NS can promote an anti-invasion effect on pancreatic cancer cells, avoiding of hCNT1 transporter intake and HAb18G/CD147 GEM activation, especially on GEM-resistant one. Indeed, in our experiments we didn't find any changes in the expression of this transporter for all conditions tested (data not shown).

The different CFPAC-1 and MIA PaCa-2 cells behaviors confirmed the GEM-mediated invasion induced on MIA PaCa-2 cells and any correlated anti/induced invasion effects on CFPAC-1. However, the more striking results are correlated to the significantly anti-invasion effect promoted by NSGEM treatment. This evidence gained more weight particularly looking to MIA PaCa-2 GEM resistant cell, on which the GEM administered in free form mediates the completely opposite effect. This results could be due to the fact that the NS are internalized by endocytosis, avoiding the hCNT1-mediated intake. Furthermore, It is well documented how NS ability to be taken up via active mechanisms and circumvent the efflux drug pump depicts their reducing drug resistance properties (Daga et al., 2020.)

Step forward was proceeding with the evaluation of the anti-invasion effect of the co-delivery system proposed. In this regard, the ICOS-Fc choice lies on the several and promising evidence supporting its anti-neoplastic, immunostimulant, antiangiogenic effects. According to all data published, it was

documented how ICOSL triggering via ICOS-Fc significantly inhibit cancer cells migration in both *in vitro* and in *vivo* mouse models, when administered alone or encapsulated into nanodelivery system or nanodelivered with other drugs (Dianzani et al., 2010, 2014; Clemente et al., 2020; Monge et al., 2022). Since ICOSL triggering was found essential to exert any ICOS-Fc effects, the highest ICOSL level detected on MIA PaCa-2 cell line led to suitably use them to evaluate the anti-invasion effect of the combine therapy proposed. The good proportion ratio of both components was reached starting with the evaluation of the most suitable ICOS-Fc concentration to use, since instead of loaded it was displayed on the nanocarrier surface. Preliminary experiments didn't show any anti-invasion effects because the concentration of ICOS-Fc, used to decorate the NS, was the same already exploited to deliver ICOS-Fc loaded into PLGA/CDNS (data not shown). The significant anti-invasion effect was detected only using lower concentration of ICOS-Fc, suggesting how a too much high ICOS-Fc NS-decoration may counteract functional ICOSL interaction, necessary to exert any resulting effect. The ICOS-Fc decorated NS showed a statistically higher invasion inhibition till a concentration 20 times lower than ICOS-Fc administered in free form. Considering all this evidence and the loading-stability features of the NS carrier, GEM and ICOS-Fc were chosen to be administered at concentrations that for the first was able to induce cancer cells invasion and for the other was able to significantly inhibit it. According to the Boyden chamber *in vitro* results, the GEM+ICOS-Fc association administered through NS carrier exerted the maximum anti-invasion effect, compared to all other treatment condition tested (drugs alone or combine and administered in free form; drug nanodelivered alone). The next project step would have been proceeding with the *in vivo* evaluation of NS [GEM+ICOS-Fc] efficacy, but some challenges hindered to smoothly achieve a suitable pancreatic mouse model. In this regard, the best cancer cells choice should express high level of ICOSL and have murine origin, so that can be injected in immunocompetent mice. Unfortunately, if on one side MIA PaCa-2 were the highest ICOSL expressing cells, because of their human origin they would be injectable only in immunodeficient mice, hampering the possibility to evaluate any ICOS-Fc mediated effect. Thanks to Prof.ssa Caterina Guiot collaboration in this project we were able to buy and use an advanced dynamic organ-on-chip technology for testing NS [GEM+ICOS-Fc] anti-invasion effect (MIVO®).

This novel technology is emerging between the 2D cells cultures and *in vivo* animal models traditionally used by cancer biology researchers. It is well known how much these two categories differ, considering the microenvironment surrounding cells and consequently the different interactions to which cells are subjected if displayed in a 2D or 3D model (Goliwas et al., 2016). Many clinical failures are due to the too simplifying pre-clinical *in vitro* and *in vivo* tumor models, which

are also expensive and associated with ethical issues (Marrella et al., 2019). This explained how in the last years novel 3D *in vitro* culture systems gained more attention as an alternative to animal tests, a suitable and reliable compromise between traditional 2D culture and *in vivo* models (Hoarau-Véchot et al., 2018; Marrella et al., 2019). In this project we performed a dynamic migration assay using a MULTI-ORGAN single flow device (MIVO®), able to resemble primary and metastasis tumour sites connected together in a micro-fluidic system. This more complex *in vitro* setting allows to investigate NS [GEM+ICOS-Fc] efficacy on cells migration, investigating also how the treatment counteracts it on more fronts. In this regard, we evaluated if NS [GEM+ICOS-Fc] was able to affect viability of both cells just detached from the primary tumour (MIVO1) and the one already flouting in the circulation and ready to develop new metastasis spots (circuit). These are important physio-pathological steps towards the metastatic onset (Cavo et al., 2016).

The counting cells values detected on MIVO2 membrane clearly showed the dominate induced-invasion effect of GEM in the GEM+ICOS-Fc association treatment, which was reported by the substantial higher number of MIA PaCa-2 cells migrated. More strictly results were correlated to NS [GEM+ICOS-Fc] condition, which significantly counteract GEM resistant cells migration, compared to both GEM+ICOS-Fc and control conditions.

Likewise, amazing results showed how 48h of treatment with NS [GEM+ICOS-Fc] was able to counteract cell clones proliferation in both cells collected from MIVO1 and circuit. This effect was significantly markable compared to GEM+ICOS-Fc one, which allowed cells clones proliferation over time in both compartment sampled.

Thanks to a multidisciplinary approach, involving pharmacological, technological, pharmaceutical and immunological fields, we proposed the innovative β-cyclodextrin based NS decorated with ICOS-Fc as a valid strategy to improve GEM efficacy in pancreatic cancer treatment (Paper in submission).

5. BIBLIOGRAPHY

Acharya, S., & Sahoo, S. K. (2011). PLGA nanoparticles containing various anticancer agents and tumour delivery by EPR effect. In *Advanced Drug Delivery Reviews* (Vol. 63, Issue 3, pp. 170–183). https://doi.org/10.1016/j.addr.2010.10.008

Affoué Dit Faute, M., Laurent, L., Ploton, D., Poupon, M.-F., Jardillier, J.-C., & Héì Ene Bobichon, &. (2002). Distinctive alterations of invasiveness, drug resistance and cell-cell organization in 3D-cultures of MCF-7, a human breast cancer cell line, and its multidrug resistant variant. In *Clinical & Experimental Metastasis* (Vol. 19).

Alshememry, A. K., Alsaleh, N. B., Alkhudair, N., Alzhrani, R., & Alshamsan, A. (2022). Recent nanotechnology advancements to treat multidrug-resistance pancreatic cancer: Pre-clinical and clinical overview. In *Frontiers in Pharmacology* (Vol. 13). Frontiers Media S.A. https://doi.org/10.3389/fphar.2022.933457

Alves, G. F., Stoppa, I., Aimaretti, E., Monge, C., Mastrocola, R., Porchietto, E., Einaudi, G., Collotta, D., Bertocchi, I., Boggio, E., Gigliotti, C. L., Clemente, N., Aragno, M., Fernandes, D., Cifani, C., Thiemermann, C., Dianzani, C., Dianzani, U., & Collino, M. (2022). ICOS-Fc as innovative immunomodulatory approach to counteract inflammation and organ injury in sepsis. *Frontiers in Immunology*, *13*. https://doi.org/10.3389/fimmu.2022.992614

Amaravadi, R. K., Schuchter, L. M., McDermott, D. F., Kramer, A., Giles, L., Gramlich, K., Carberry, M., Troxel, A. B., Letrero, R., Nathanson, K. L., Atkins, M. B., O'Dwyer, P. J., & Flaherty, K. T. (2009). Phase II trial of temozolomide and sorafenib in advanced melanoma patients with or without brain metastases. *Clinical Cancer Research*, *15*(24), 7711–7718. https://doi.org/10.1158/1078-0432.CCR-09-2074

Amrutkar, M., & Gladhaug, I. P. (2017). Pancreatic cancer chemoresistance to gemcitabine. In *Cancers* (Vol. 9, Issue 11). MDPI AG. https://doi.org/10.3390/cancers9110157

Arora, S., Bhardwaj, A., Singh, S., Srivastava, S. K., McClellan, S., Nirodi, C. S., Piazza, G. A., Grizzle, W. E., Owen, L. B., & Singh, A. P. (2013). An undesired effect of chemotherapy: Gemcitabine promotes pancreatic cancer cell invasiveness through reactive oxygen species-dependent, nuclear factorκb- and hypoxia-inducible factor 1α-mediated up-regulation of CXCR4. *Journal of Biological Chemistry*, *288*(29), 21197–21207. https://doi.org/10.1074/jbc.M113.484576

Assaraf, Y. G., Leamon, C. P., & Reddy, J. A. (2014). The folate receptor as a rational therapeutic target for personalized cancer treatment. In *Drug Resistance Updates* (Vol. 17, Issues 4–6, pp. 89–95). Churchill Livingstone. https://doi.org/10.1016/j.drup.2014.10.002

Atkinson, V. (2017). Recent advances in malignant melanoma. In *Internal Medicine Journal* (Vol. 47, Issue 10, pp. 1114–1121). Blackwell Publishing. https://doi.org/10.1111/imj.13574

Banchereau, J., Briere, F., Caux, C., Davoust, J., Lebecque, S., Liu, Y.-J., Pulendran, B., & Palucka, K. (2000). IMMUNOBIOLOGY OF DENDRITIC CELLS. In *Annu. Rev. Immunol* (Vol. 18). www.annualreviews.org

Barrera, G., Cucci, M. A., Grattarola, M., Dianzani, C., Muzio, G., & Pizzimenti, S. (2021). Control of oxidative stress in cancer chemoresistance: spotlight on Nrf2 role. In *Antioxidants* (Vol. 10, Issue 4). MDPI. https://doi.org/10.3390/antiox10040510

Battaglia, L., Gallarate, M., Peira, E., Chirio, D., Solazzi, I., Giordano, S. M. A., Gigliotti, C. L., Riganti, C., & Dianzani, C. (2015). Bevacizumab loaded solid lipid nanoparticles prepared by the coacervation

technique: Preliminary in vitro studies. *Nanotechnology*, *26*(25). https://doi.org/10.1088/0957-4484/26/25/255102

Bazak, R., Houri, M., El Achy, S., Kamel, S., & Refaat, T. (2015). Cancer active targeting by nanoparticles: a comprehensive review of literature. In *Journal of Cancer Research and Clinical Oncology* (Vol. 141, Issue 5, pp. 769–784). Springer Verlag. https://doi.org/10.1007/s00432-014-1767-3

Bernstein, Z. S., Kim, E. B., & Raje, N. (2022). Bone Disease in Multiple Myeloma: Biologic and Clinical Implications. In *Cells* (Vol. 11, Issue 15). MDPI. https://doi.org/10.3390/cells11152308

Bhattacharjee, S. (2022). Craft of Co-encapsulation in Nanomedicine: A Struggle to Achieve Synergy through Reciprocity. In *ACS Pharmacology and Translational Science*. American Chemical Society. https://doi.org/10.1021/acsptsci.2c00033

Bird, S. A., & Boyd, K. (2019). Multiple myeloma: an overview of management. In *Palliative Care and Social Practice* (Vol. 13). SAGE Publications Ltd. https://doi.org/10.1177/1178224219868235

Biswas Chitra, Zhang Ying, DeCastro Rosana, Guo Huiming, Nakamura Toshiya, Kataoka Hiroaki, & Nabeshima Kazuki. (1995). The Human Tumor Cell-derived Collagenase Stimulatory Factor (Renamed EMMPRIN) Is a Member of the Immunoglobulin Superfamily. *Cancer Research*, *55*, 434–439.

Boggio, E., Dianzani, C., Gigliotti, C. L., Soluri, M. F., Clemente, N., Cappellano, G., Toth, E., Raineri, D., Ferrara, B., Comi, C., Dianzani, U., & Chiocchetti, A. (2016). Thrombin Cleavage of Osteopontin Modulates Its Activities in Human Cells In Vitro and Mouse Experimental Autoimmune Encephalomyelitis In Vivo. *Journal of Immunology Research*, *2016*. https://doi.org/10.1155/2016/9345495

Boggio, E., Gigliotti, C. L., Moia, R., Scotta, A., Crespi, I., Boggione, P., De Paoli, L., Deambrogi, C., Garzaro, M., Vidali, M., Chiocchetti, A., Stoppa, I., Rolla, R., Dianzani, C., Monge, C., Clemente, N., Gaidano, G., & Dianzani, U. (2021). Inducible T-cell co-stimulator (ICOS) and ICOS ligand are novel players in the multiple-myeloma microenvironment. *British Journal of Haematology*, *196*(6), 1369–1380. https://doi.org/10.1111/bjh.17968

Boggio, E., Gigliotti, C. L., Stoppa, I., Pantham, D., Sacchetti, S., Rolla, R., Grattarola, M., Monge, C., Pizzimenti, S., Dianzani, U., Dianzani, C., & Battaglia, L. (2023). Exploiting Nanomedicine for Cancer Polychemotherapy: Recent Advances and Clinical Applications. In *Pharmaceutics* (Vol. 15, Issue 3). MDPI. https://doi.org/10.3390/pharmaceutics15030937

Boomer, J. S., To, K., Chang, K. C., Takasu, O., Osborne, D. F., Walton, A. H., Bricker, T. L., Jarman, S. D., Kreisel, D., Krupnick, A. S., Srivastava, A., Swanson, P. E., Green, J. M., & Hotchkiss, R. S. (2011). Immunosuppression in patients who die of sepsis and multiple organ failure. *JAMA*, *306*(23), 2594–2605. https://doi.org/10.1001/jama.2011.1829

Bossaller, L., Burger, J., Draeger, R., Grimbacher, B., Knoth, R., Plebani, A., Durandy, A., Baumann, U., Schlesier, M., Welcher, A. A., Peter, H. H., & Warnatz, K. (2006). ICOS Deficiency Is Associated with a Severe Reduction of CXCR5+CD4 Germinal Center Th Cells. *The Journal of Immunology*, *177*(7), 4927–4932. https://doi.org/10.4049/jimmunol.177.7.4927

Brancato, S. K., & Albina, J. E. (2011). Wound macrophages as key regulators of repair: Origin, phenotype, and function. In *American Journal of Pathology* (Vol. 178, Issue 1, pp. 19–25). Elsevier Inc. https://doi.org/10.1016/j.ajpath.2010.08.003

Brimnes, M. K., Vangsted, A. J., Knudsen, L. M., Gimsing, P., Gang, A. O., Johnsen, H. E., & Svane, I. M. (2010). Increased level of both CD4+FOXP3+ Regulatory t Cells and CD14+HLA-DR-/low myeloid-

derived suppressor cells and decreased level of dendritic cells in patients with multiple myeloma. *Scandinavian Journal of Immunology*, *72*(6), 540–547. https://doi.org/10.1111/j.1365-3083.2010.02463.x

Brown, A. (2012). Osteopontin: A key link between immunity, inflammation and the central nervous system. *Translational Neuroscience*, *3*(3), 288–293. https://doi.org/10.2478/s13380-012-0028-7

Cai, H., Wang, R., Guo, X., Song, M., Yan, F., Ji, B., & Liu, Y. (2021). Combining Gemcitabine-Loaded Macrophage-like Nanoparticles and Erlotinib for Pancreatic Cancer Therapy. *Molecular Pharmaceutics*, *18*(7), 2495–2506. https://doi.org/10.1021/acs.molpharmaceut.0c01225

Cao, M., Xu, Y., Youn, J. I., Cabrera, R., Zhang, X., Gabrilovich, D., Nelson, D. R., & Liu, C. (2011). Kinase inhibitor Sorafenib modulates immunosuppressive cell populations in a murine liver cancer model. *Laboratory Investigation*, *91*(4), 598–608. https://doi.org/10.1038/labinvest.2010.205

Carthon, B., Wolchok, J. D., Yuan, J., Kamat, A., Ng Tang, D. S., Sun, J., Ku, G., Troncoso, P., Logothetis, C. J., Allison, J. P., & Sharma, P. (2010). *Published as: Clin Cancer Res* (Vol. 16, Issue 10).

Castello, L. M., Raineri, D., Salmi, L., Clemente, N., Vaschetto, R., Quaglia, M., Garzaro, M., Gentilli, S., Navalesi, P., Cantaluppi, V., Dianzani, U., Aspesi, A., & Chiocchetti, A. (2017). Osteopontin at the Crossroads of Inflammation and Tumor Progression. In *Mediators of Inflammation* (Vol. 2017). Hindawi Limited. https://doi.org/10.1155/2017/4049098

Cavo, M., Caria, M., Pulsoni, I., Beltrame, F., Fato, M., & Scaglione, S. (2018). A new cell-laden 3D Alginate-Matrigel hydrogel resembles human breast cancer cell malignant morphology, spread and invasion capability observed 'in vivo'. *Scientific Reports*, *8*(1). https://doi.org/10.1038/s41598-018-23250-4

Cavo, M., Fato, M., Peñuela, L., Beltrame, F., Raiteri, R., & Scaglione, S. (2016). Microenvironment complexity and matrix stiffness regulate breast cancer cell activity in a 3D in vitro model. *Scientific Reports*, *6*. https://doi.org/10.1038/srep35367

Chen, L., Deng, H., Cui, H., Fang, J., Zuo, Z., Deng, J., Li, Y., Wang, X., & Zhao, L. (2018). Oncotarget 7204 www.impactjournals.com/oncotarget Inflammatory responses and inflammation-associated diseases in organs. In *Oncotarget* (Vol. 9, Issue 6). www.impactjournals.com/oncotarget/

Chen, L., Ke, H., Zhang, Y., Jin, P., Liu, X., Hong, G., Zhao, G., Lu, Z., & Wu, B. (2022). Orai1 overexpression improves sepsis-induced T-lymphocyte immunosuppression and acute organ dysfunction in mice. *Heliyon*, *8*(12). https://doi.org/10.1016/j.heliyon.2022.e12082

Chen, Z. S., & Tiwari, A. K. (2011). Multidrug resistance proteins (MRPs/ABCCs) in cancer chemotherapy and genetic diseases. In *FEBS Journal* (Vol. 278, Issue 18, pp. 3226–3245). https://doi.org/10.1111/j.1742-4658.2011.08235.x

Choudhury, S. R., Ordaz, J., Lo, C. L., Damayanti, N. P., Zhou, F., & Irudayaraj, J. (2017). Zinc oxide nanoparticles-induced reactive oxygen species promotes multimodal cyto- and epigenetic toxicity. *Toxicological Sciences*, *156*(1), 261–274. https://doi.org/10.1093/toxsci/kfw252

Clemente, N., Boggio, E., Gigliotti, L. C., Raineri, D., Ferrara, B., Miglio, G., Argenziano, M., Chiocchetti, A., Cappellano, G., Trotta, F., Caldera, F., Capucchio, M. T., Yagi, J., Rojo, M. J., Renò, F., Cavalli, R., Dianzani, C., & Dianzani, U. (2020). Immunotherapy of experimental melanoma with ICOS-Fc loaded in biocompatible and biodegradable nanoparticles. *Journal of Controlled Release*, *320*, 112–124. https://doi.org/10.1016/j.jconrel.2020.01.030

Colombo, N., Dubot, C., Lorusso, D., Caceres, M. V., Hasegawa, K., Shapira-Frommer, R., Tewari, K. S., Salman, P., Hoyos Usta, E., Yañez, E., Gümüş, M., Olivera Hurtado de Mendoza, M., Samouëlian, V., Castonguay, V., Arkhipov, A., Toker, S., Li, K., Keefe, S. M., & Monk, B. J. (2021). Pembrolizumab for Persistent, Recurrent, or Metastatic Cervical Cancer. *New England Journal of Medicine*, *385*(20), 1856–1867. https://doi.org/10.1056/nejmoa2112435

Conciatori, F., Bazzichetto, C., Falcone, I., Pilotto, S., Bria, E., Cognetti, F., Milella, M., & Ciuffreda, L. (2018). Role of mTOR signaling in tumor microenvironment: An overview. In *International Journal of Molecular Sciences* (Vol. 19, Issue 8). MDPI AG. https://doi.org/10.3390/ijms19082453

Conroy, T., Hammel, P., Hebbar, M., Ben Abdelghani, M., Wei, A. C., Raoul, J.-L., Choné, L., Francois, E., Artru, P., Biagi, J. J., Lecomte, T., Assenat, E., Faroux, R., Ychou, M., Volet, J., Sauvanet, A., Breysacher, G., Di Fiore, F., Cripps, C., … Bachet, J.-B. (2018). FOLFIRINOX or Gemcitabine as Adjuvant Therapy for Pancreatic Cancer. *New England Journal of Medicine*, *379*(25), 2395–2406. https://doi.org/10.1056/nejmoa1809775

Constantinidou, A., Alifieris, C., & Trafalis, D. T. (2019). Targeting Programmed Cell Death -1 (PD-1) and Ligand (PD-L1): A new era in cancer active immunotherapy. In *Pharmacology and Therapeutics* (Vol. 194, pp. 84–106). Elsevier Inc. https://doi.org/10.1016/j.pharmthera.2018.09.008

Cote, B., Carlson, L. J., Rao, D. A., & Alani, A. W. G. (2015). Combinatorial resveratrol and quercetin polymeric micelles mitigate doxorubicin induced cardiotoxicity in vitro and in vivo. *Journal of Controlled Release*, *213*, 128–133. https://doi.org/10.1016/j.jconrel.2015.06.040

Cucci, M. A., Grattarola, M., Monge, C., Roetto, A., Barrera, G., Caputo, E., Dianzani, C., & Pizzimenti, S. (2023). Nrf2 as a Therapeutic Target in the Resistance to Targeted Therapies in Melanoma. *Antioxidants*, *12*(6). https://doi.org/10.3390/antiox12061313

Daga, M., de Graaf, I. A. M., Argenziano, M., Barranco, A. S. M., Loeck, M., Al-Adwi, Y., Cucci, M. A., Caldera, F., Trotta, F., Barrera, G., Casini, A., Cavalli, R., & Pizzimenti, S. (2020). Glutathione-responsive cyclodextrin-nanosponges as drug delivery systems for doxorubicin: Evaluation of toxicity and transport mechanisms in the liver. *Toxicology in Vitro*, *65*. https://doi.org/10.1016/j.tiv.2020.104800

Danon, D., Kowatcht, M. A., & Rotht, G. S. (1989). Promotion of wound repair in old mice by local injection of macrophages. In *Medical Sciences* (Vol. 86).

Dianzani, C., Minelli, R., Gigliotti, C. L., Occhipinti, S., Giovarelli, M., Conti, L., Boggio, E., Shivakumar, Y., Baldanzi, G., Malacarne, V., Orilieri, E., Cappellano, G., Fantozzi, R., Sblattero, D., Yagi, J., Rojo, J. M., Chiocchetti, A., & Dianzani, U. (2014). B7h Triggering Inhibits the Migration of Tumor Cell Lines. *The Journal of Immunology*, *192*, 4921–4931. https://doi.org/10.4049/jimmunol.1300587

Dianzani, C., Minelli, R., Mesturini, R., Chiocchetti, A., Barrera, G., Boscolo, S., Sarasso, C., Gigliotti, C. L., Sblattero, D., Yagi, J., Rojo, J. M., Fantozzi, R., & Dianzani, U. (2010). B7h Triggering Inhibits Umbilical Vascular Endothelial Cell Adhesiveness to Tumor Cell Lines and Polymorphonuclear Cells. *The Journal of Immunology*, *185*, 3970–3979. https://doi.org/10.4049/jimmunol.0903269

Dianzani, C., Monge, C., Miglio, G., Serpe, L., Martina, K., Cangemi, L., Ferraris, C., Mioletti, S., Osella, S., Gigliotti, C. L., Boggio, E., Clemente, N., Dianzani, U., & Battaglia, L. (2020a). Nanoemulsions as delivery systems for poly-chemotherapy aiming at melanoma treatment. *Cancers*, *12*(5). https://doi.org/10.3390/cancers12051198

Dianzani, C., Monge, C., Miglio, G., Serpe, L., Martina, K., Cangemi, L., Ferraris, C., Mioletti, S., Osella, S., Gigliotti, C. L., Boggio, E., Clemente, N., Dianzani, U., & Battaglia, L. (2020b). Nanoemulsions as delivery

systems for poly-chemotherapy aiming at melanoma treatment. *Cancers*, *12*(5). https://doi.org/10.3390/cancers12051198

Dronca, R. S., Allred, J. B., Perez, D. G., Nevala, W. K., Lieser, E. A. T., Thompson, M., Maples, W. J., Creagan, E. T., Pockaj, B. A., Kaur, J. S., Moore, T. D., Marchello, B. T., & Markovic, S. N. (2014). Phase II study of temozolomide (TMZ) and everolimus (RAD001) therapy for metastatic melanoma: A north central cancer treatment group study, N0675. *American Journal of Clinical Oncology: Cancer Clinical Trials*, *37*(4), 369–376. https://doi.org/10.1097/COC.0b013e31827b45d4

Dutta, R. C., & Dutta, A. K. (2009). Cell-interactive 3D-scaffold; advances and applications. In *Biotechnology Advances* (Vol. 27, Issue 4, pp. 334–339). https://doi.org/10.1016/j.biotechadv.2009.02.002

Edner, N. M., Carlesso, G., Rush, J. S., & Walker, L. S. K. (2020). Targeting co-stimulatory molecules in autoimmune disease. In *Nature Reviews Drug Discovery* (Vol. 19, Issue 12, pp. 860–883). Nature Research. https://doi.org/10.1038/s41573-020-0081-9

Fairfield Heather, Falank Carolyne, Avery Lindsey, & Reagan Michaela. (2016). Multiple myeloma in the marrow: pathogenesis and treatments. *Ann N T Acad Sci*, *1364*(1), 32–51.

Falcomatà, C., Bärthel, S., Schneider, G., Rad, R., Schmidt-Supprian, M., & Saur, D. (2023). Context-Specific Determinants of the Immunosuppressive Tumor Microenvironment in Pancreatic Cancer. In *Cancer Discovery* (Vol. 13, Issue 2, pp. 278–297). American Association for Cancer Research Inc. https://doi.org/10.1158/2159-8290.CD-22-0876

Farkona, S., Diamandis, E. P., & Blasutig, I. M. (2016). Cancer immunotherapy: The beginning of the end of cancer? In *BMC Medicine* (Vol. 14, Issue 1). BioMed Central Ltd. https://doi.org/10.1186/s12916-016-0623-5

Felice, B., Prabhakaran, M. P., Rodríguez, A. P., & Ramakrishna, S. (2014). Drug delivery vehicles on a nano-engineering perspective. In *Materials Science and Engineering C* (Vol. 41, pp. 178–195). Elsevier BV. https://doi.org/10.1016/j.msec.2014.04.049

Fleischmann-Struzek, C., & Rudd, K. (2023). Challenges of assessing the burden of sepsis. *Medizinische Klinik, Intensivmedizin Und Notfallmedizin*. https://doi.org/10.1007/s00063-023-01088-7

Fortis, S., Khadaroo, R. G., Haitsma, J. J., & Zhang, H. (2015). Osteopontin is associated with inflammation and mortality in a mouse model of polymicrobial sepsis. *Acta Anaesthesiologica Scandinavica*, *59*(2), 170–175. https://doi.org/10.1111/aas.12422

Frezza, E. E., Wachtel, M. S., Xu, K. T., Zhang, Y., & Chiriva-Internati, M. (2008). Pancreas Cancer Survival in the Gemcitabine Era. In *Clinical Medicine: Oncology* (Vol. 2).

Fu, T., He, Q., & Sharma, P. (2011). The ICOS/ICOSL pathway is required for optimal antitumor responses mediated by anti-CTLA-4 therapy. *Cancer Research*, *71*(16), 5445–5454. https://doi.org/10.1158/0008-5472.CAN-11-1138

Gandhi, L., Rodríguez-Abreu, D., Gadgeel, S., Esteban, E., Felip, E., De Angelis, F., Domine, M., Clingan, P., Hochmair, M. J., Powell, S. F., Cheng, S. Y.-S., Bischoff, H. G., Peled, N., Grossi, F., Jennens, R. R., Reck, M., Hui, R., Garon, E. B., Boyer, M., … Garassino, M. C. (2018). Pembrolizumab plus Chemotherapy in Metastatic Non–Small-Cell Lung Cancer. *New England Journal of Medicine*, *378*(22), 2078–2092. https://doi.org/10.1056/nejmoa1801005

Gao, X., Song, Y., Du, P., Yang, S., Cui, H., Lu, S., Hu, L., Liu, L., Jia, S., & Zhao, M. (2022). Administration of a microRNA-21 inhibitor improves the lupus-like phenotype in MRL/lpr mice by repressing Tfh cell-

mediated autoimmune responses. *International Immunopharmacology*, *106*. https://doi.org/10.1016/j.intimp.2022.108578

Ghahremanloo, A., Soltani, A., Modaresi, S. M. S., & Hashemy, S. I. (2019). Recent advances in the clinical development of immune checkpoint blockade therapy. In *Cellular Oncology* (Vol. 42, Issue 5, pp. 609–626). Springer Netherlands. https://doi.org/10.1007/s13402-019-00456-w

Ghasemi-Chaleshtari, M., Kiaie, S. H., Irandoust, M., Karami, H., Nabi Afjadi, M., Ghani, S., Aghaei Vanda, N., Ghaderi Sede, M. J., Ahmadi, A., Masjedi, A., Hassannia, H., Atyabi, F., Hojjat-Farsangi, M., Namdar, A., Ghalamfarsa, G., & Jadidi-Niaragh, F. (2020). Concomitant blockade of A2AR and CTLA-4 by siRNA-loaded polyethylene glycol-chitosan-alginate nanoparticles synergistically enhances antitumor T-cell responses. *Journal of Cellular Physiology*, *235*(12), 10068–10080. https://doi.org/10.1002/jcp.29822

Gigliotti, C. L., Boggio, E., Clemente, N., Shivakumar, Y., Toth, E., Sblattero, D., D'Amelio, P., Isaia, G. C., Dianzani, C., Yagi, J., Rojo, J. M., Chiocchetti, A., Boldorini, R., Bosetti, M., & Dianzani, U. (2016). ICOS-Ligand Triggering Impairs Osteoclast Differentiation and Function In Vitro and In Vivo. *The Journal of Immunology*, *197*, 3905–3916. https://doi.org/10.4049/jimmunol.1600424

Gigliotti, C. L., Dianzani, C., Stoppa, I., Monge, C., Sutti, S., Sblattero, D., Puricelli, C., Rolla, R., Dianzani, U., & Boggio, E. (2023). Differential Modulation of Human M1 and M2 Macrophage Activity by ICOS-Mediated ICOSL Triggering. *International Journal of Molecular Sciences*, *24*(3). https://doi.org/10.3390/ijms24032953

Gigoux, M., Shang, J., Pak, Y., Xu, M., Choe, J., Mak, T. W., & Suh, W.-K. (2009). *Inducible costimulator promotes helper T-cell differentiation through phosphoinositide 3-kinase*. www.pnas.orgcgidoi10.1073pnas.0911573106

Gingis-Velitski, S., Loven, D., Benayoun, L., Munster, M., Bril, R., Voloshin, T., Alishekevitz, D., Bertolini, F., & Shaked, Y. (2011). Host response to short-term, single-agent chemotherapy induces matrix metalloproteinase-9 expression and accelerates metastasis in mice. *Cancer Research*, *71*(22), 6986–6996. https://doi.org/10.1158/0008-5472.CAN-11-0629

Giovannetti, E., Del Tacca, M., Mey, V., Funel, N., Nannizzi, S., Ricci, S., Orlandini, C., Boggi, U., Campani, D., Del Chiaro, M., Iannopollo, M., Bevilacqua, G., Mosca, F., & Danesi, R. (2006). Transcription analysis of human equilibrative nucleoside transporter-1 predicts survival in pancreas cancer patients treated with gemcitabine. *Cancer Research*, *66*(7), 3928–3935. https://doi.org/10.1158/0008-5472.CAN-05-4203

Grattarola, M., Cucci, M. A., Roetto, A., Dianzani, C., Barrera, G., & Pizzimenti, S. (2021). Post-translational down-regulation of Nrf2 and YAP proteins, by targeting deubiquitinases, reduces growth and chemoresistance in pancreatic cancer cells. *Free Radical Biology and Medicine*, *174*, 202–210. https://doi.org/10.1016/j.freeradbiomed.2021.08.006

Greenwald, R. J., Freeman, G. J., & Sharpe, A. H. (2005). The B7 family revisited. In *Annual Review of Immunology* (Vol. 23, pp. 515–548). https://doi.org/10.1146/annurev.immunol.23.021704.115611

Grimbacher, B., Hutloff, A., Schlesier, M., Glocker, E., Warnatz, K., Dräger, R., Eibel, H., Fischer, B., Schäffer, A. A., Mages, H. W., Kroczek, R. A., & Peter, H. H. (2003). Homozygous loss of ICOS is associated with adult-onset common variable immunodeficiency. *Nature Immunology*, *4*(3), 261–268. https://doi.org/10.1038/ni902

Guo, S., & DiPietro, L. A. (2010). Critical review in oral biology & medicine: Factors affecting wound healing. *Journal of Dental Research*, *89*(3), 219–229. https://doi.org/10.1177/0022034509359125

Hainsworth, J. D., Infante, J. R., Spigel, D. R., Peyton, J. D., Thompson, D. S., Lane, C. M., Clark, B. L., Rubin, M. S., Trent, D. F., & Burris, H. A. (2010). Bevacizumab and everolimus in the treatment of patients with metastatic melanoma: A phase 2 trial of the Sarah Cannon Oncology Research Consortium. *Cancer*, *116*(17), 4122–4129. https://doi.org/10.1002/cncr.25320

Hani, U., Gowda, B. H. J., Haider, N., Ramesh, K., Paul, K., Ashique, S., Ahmed, M. G., Narayana, S., Mohanto, S., & Kesharwani, P. (2023). Nanoparticle-Based Approaches for Treatment of Hematological Malignancies: a Comprehensive Review. *AAPS PharmSciTech*, *24*(8). https://doi.org/10.1208/s12249-023-02670-0

Hasnis, E., Alishekevitz, D., Gingis-Veltski, S., Bril, R., Fremder, E., Voloshin, T., Raviv, Z., Karban, A., & Shaked, Y. (2014). Anti-Bv8 Antibody and Metronomic Gemcitabine Improve Pancreatic Adenocarcinoma Treatment Outcome Following Weekly Gemcitabine Therapy. *Neoplasia (United States)*, *16*(6), 501–510. https://doi.org/10.1016/j.neo.2014.05.011

Hayes, A. J., Skouras, C., Haugk, B., & Charnley, R. M. (2015). Keap1-Nrf2 signalling in pancreatic cancer. In *International Journal of Biochemistry and Cell Biology* (Vol. 65, pp. 288–299). Elsevier Ltd. https://doi.org/10.1016/j.biocel.2015.06.017

Hess, K. L., Medintz, I. L., & Jewell, C. M. (2019). Designing inorganic nanomaterials for vaccines and immunotherapies. In *Nano Today* (Vol. 27, pp. 73–98). Elsevier B.V. https://doi.org/10.1016/j.nantod.2019.04.005

Higgins, C. F. (2007). Multiple molecular mechanisms for multidrug resistance transporters. In *Nature* (Vol. 446, Issue 7137, pp. 749–757). Nature Publishing Group. https://doi.org/10.1038/nature05630

Hippalgaonkar, K., Majumdar, S., & Kansara, V. (2010). Injectable lipid emulsions-advancements, opportunities and challenges. In *AAPS PharmSciTech* (Vol. 11, Issue 4, pp. 1526–1540). https://doi.org/10.1208/s12249-010-9526-5

Hoang, B., Zhu, L., Shi, Y., Frost, P., Yan, H., Sharma, S., Sharma, S., Goodglick, L., Dubinett, S., & Lichtenstein, A. (2006). Oncogenic RAS mutations in myeloma cells selectively induce cox-2 expression, which participates in enhanced adhesion to fibronectin and chemoresistance. *Blood*, *107*(11), 4484–4490. https://doi.org/10.1182/blood-2005-09-3926

Hoarau-Véchot, J., Rafii, A., Touboul, C., & Pasquier, J. (2018). Halfway between 2D and animal models: Are 3D cultures the ideal tool to study cancer-microenvironment interactions? In *International Journal of Molecular Sciences* (Vol. 19, Issue 1). MDPI AG. https://doi.org/10.3390/ijms19010181

Hosein, A. N., Dougan, S. K., Aguirre, A. J., & Maitra, A. (2022). Translational advances in pancreatic ductal adenocarcinoma therapy. In *Nature Cancer* (Vol. 3, Issue 3, pp. 272–286). Nature Research. https://doi.org/10.1038/s43018-022-00349-2

Hotchkiss, R. S., Monneret, G., & Payen, D. (2013). Sepsis-induced immunosuppression: From cellular dysfunctions to immunotherapy. In *Nature Reviews Immunology* (Vol. 13, Issue 12, pp. 862–874). https://doi.org/10.1038/nri3552

Hutloff, A., Dittrich, A. M., Beier, K. C., Eljaschewitsch, B., Kraft, R., Anagnostopoulos, I., & Kroczek, R. A. (1999). ICOS is an inducible T-cell co-stimulator structurally and functionally related to CD28. *Nature*, *397*, 263–266. https://doi.org/10.1038/16717

Imamura, T., Ashida, R., Ohshima, K., Uesaka, K., Sugiura, T., Ohgi, K., Yamada, M., Otsuka, S., Hatakeyama, K., Nagashima, T., Sugino, T., Urakami, K., Akiyama, Y., & Yamaguchi, K. (2023). Characterization of

pancreatic cancer with ultra-low tumor mutational burden. *Scientific Reports*, *13*(1). https://doi.org/10.1038/s41598-023-31579-8

Iravani, S., & Varma, R. S. (2022). Nanosponges for Drug Delivery and Cancer Therapy: Recent Advances. In *Nanomaterials* (Vol. 12, Issue 14). MDPI. https://doi.org/10.3390/nano12142440

Jang, S. G., Lee, J., Hong, S. M., Song, Y. S., Kim, M. J., Kwok, S. K., Cho, M. La, & Park, S. H. (2021). Niclosamide suppresses the expansion of follicular helper T cells and alleviates disease severity in two murine models of lupus via STAT3. *Journal of Translational Medicine*, *19*(1). https://doi.org/10.1186/s12967-021-02760-2

Jenkins, R. W., Barbie, D. A., & Flaherty, K. T. (2018). Mechanisms of resistance to immune checkpoint inhibitors. *British Journal of Cancer*, *118*(1), 9–16. https://doi.org/10.1038/bjc.2017.434

Johnson, B. Z., Stevenson, A. W., Prêle, C. M., Fear, M. W., & Wood, F. M. (2020). The role of IL-6 in skin fibrosis and cutaneous wound healing. *Biomedicines*, *8*(5). https://doi.org/10.3390/BIOMEDICINES8050101

Jovanović, K. K., Escure, G., Demonchy, J., Willaume, A., Van De Wyngaert, Z., Farhat, M., Chauvet, P., Facon, T., Quesnel, B., & Manier, S. (2019). Deregulation and targeting of TP53 pathway in multiple myeloma. In *Frontiers in Oncology* (Vol. 9, Issue JAN). Frontiers Media S.A. https://doi.org/10.3389/fonc.2018.00665

Kenefeck, R., Wang, C. J., Kapadi, T., Wardzinski, L., Attridge, K., Clough, L. E., Heuts, F., Kogimtzis, A., Patel, S., Rosenthal, M., Ono, M., Sansom, D. M., Narendran, P., & Walker, L. S. K. (2015). Follicular helper T cell signature in type 1 diabetes. *Journal of Clinical Investigation*, *125*(1), 292–303. https://doi.org/10.1172/JCI76238

Khan, S., Setua, S., Kumari, S., Dan, N., Massey, A., Hafeez, B. Bin, Yallapu, M. M., Stiles, Z. E., Alabkaa, A., Yue, J., Ganju, A., Behrman, S., Jaggi, M., & Chauhan, S. C. (2019). Superparamagnetic iron oxide nanoparticles of curcumin enhance gemcitabine therapeutic response in pancreatic cancer. *Biomaterials*, *208*, 83–97. https://doi.org/10.1016/j.biomaterials.2019.04.005

Khayyamian, S., Hutloff, A., Bü, K., Grä, M., Henn, V., Kroczek, R. A., & Mages, H. W. (2002). *ICOS-ligand, expressed on human endothelial cells, costimulates Th1 and Th2 cytokine secretion by memory CD4 T cells*. https://doi.org/10.1073/pnas.092576699

Khongsti, K., & Das, B. (2021). Osteopontin and breast cancer metastasis: Possible role of genistein on the regulation of osteopontin. In *Phytomedicine Plus* (Vol. 1, Issue 4). Elsevier B.V. https://doi.org/10.1016/j.phyplu.2021.100138

Khosravi, N., Mokhtarzadeh, A., Baghbanzadeh, A., Hajiasgharzadeh, K., Shahgoli, V. K., Hemmat, N., Safarzadeh, E., & Baradaran, B. (2020). Immune checkpoints in tumor microenvironment and their relevance to the development of cancer stem cells. In *Life Sciences* (Vol. 256). Elsevier Inc. https://doi.org/10.1016/j.lfs.2020.118005

Kiaie, S. H., Salehi-Shadkami, H., Sanaei, M. J., Azizi, M., Shokrollahi Barough, M., Nasr, M. S., & Sheibani, M. (2023). Nano-immunotherapy: overcoming delivery challenge of immune checkpoint therapy. In *Journal of Nanobiotechnology* (Vol. 21, Issue 1). BioMed Central Ltd. https://doi.org/10.1186/s12951-023-02083-y

Kondo, T., & Ishida, Y. (2010). Molecular pathology of wound healing. *Forensic Science International*, *203*(1–3), 93–98. https://doi.org/10.1016/j.forsciint.2010.07.004

Krauss, A. C., Gao, X., Li, L., Manning, M. L., Patel, P., Fu, W., Janoria, K. G., Gieser, G., Bateman, D. A., Przepiorka, D., Shen, Y. L., Shord, S. S., Sheth, C. M., Banerjee, A., Liu, J., Goldberg, K. B., Farrell, A. T., Blumenthal, G. M., & Pazdur, R. (2019). FDA approval summary: (daunorubicin and cytarabine) liposome for injection for the treatment of adults with high-risk acute myeloid leukemia. *Clinical Cancer Research*, *25*(9), 2685–2690. https://doi.org/10.1158/1078-0432.CCR-18-2990

Kravchenko, J., Corsini, E., Williams, M. A., Decker, W., Manjili, M. H., Otsuki, T., Singh, N., Al-Mulla, F., Al-Temaimi, R., Amedei, A., Colacci, A. M., Vaccari, M., Mondello, C., Ivana Scovassi, A., Raju, J., Hamid, R. A., Memeo, L., Forte, S., Roy, R., … Kim Lyerly, H. (2015). Chemical compounds from anthropogenic environment and immune evasion mechanisms: Potential interactions. In *Carcinogenesis* (Vol. 36, pp. S111–S127). Oxford University Press. https://doi.org/10.1093/carcin/bgv033

Kroemer, G., Galassi, C., Zitvogel, L., & Galluzzi, L. (2022). Immunogenic cell stress and death. In *Nature Immunology* (Vol. 23, Issue 4, pp. 487–500). Nature Research. https://doi.org/10.1038/s41590-022-01132-2

Kuo, J. C., Han, X., Hsiao, C. Te, Yates, J. R., & Waterman, C. M. (2011). Analysis of the myosin-II-responsive focal adhesion proteome reveals a role for β-Pix in negative regulation of focal adhesion maturation. *Nature Cell Biology*, *13*(4), 383–395. https://doi.org/10.1038/ncb2216

Kurosawa, S., Saito, K., Wagatsuma, T., Toyama, H., Ejima, Y., Hoshi, K., Shibusawa, M., & Kato, M. (2008). Sepsis is Characterized by the Increases in Percentages of Circulating CD4 + CD25 + Regulatory T Cells and Plasma Levels of Soluble CD25. In *Tohoku J. Exp. Med* (Vol. 216, Issue 1).

Kurzbach, D., Platzer, G., Schwarz, T. C., Henen, M. A., Konrat, R., & Hinderberger, D. (2013). Cooperative unfolding of compact conformations of the intrinsically disordered protein osteopontin. *Biochemistry*, *52*(31), 5167–5175. https://doi.org/10.1021/bi400502c

Larkin, J., Chiarion-Sileni, V., Gonzalez, R., Grob, J.-J., Rutkowski, P., Lao, C. D., Cowey, C. L., Schadendorf, D., Wagstaff, J., Dummer, R., Ferrucci, P. F., Smylie, M., Hogg, D., Hill, A., Márquez-Rodas, I., Haanen, J., Guidoboni, M., Maio, M., Schöffski, P., … Wolchok, J. D. (2019). Five-Year Survival with Combined Nivolumab and Ipilimumab in Advanced Melanoma. *New England Journal of Medicine*, *381*(16), 1535–1546. https://doi.org/10.1056/nejmoa1910836

Larouche, J., Sheoran, S., Maruyama, K., & Martino, M. M. (2018). Immune regulation of skin wound healing: Mechanisms and novel therapeutic targets. *Advances in Wound Care*, *7*(7), 209–231. https://doi.org/10.1089/wound.2017.0761

Le, D. T., Uram, J. N., Wang, H., Bartlett, B. R., Kemberling, H., Eyring, A. D., Skora, A. D., Luber, B. S., Azad, N. S., Laheru, D., Biedrzycki, B., Donehower, R. C., Zaheer, A., Fisher, G. A., Crocenzi, T. S., Lee, J. J., Duffy, S. M., Goldberg, R. M., de la Chapelle, A., … Diaz, L. A. (2015). PD-1 Blockade in Tumors with Mismatch-Repair Deficiency. *New England Journal of Medicine*, *372*(26), 2509–2520. https://doi.org/10.1056/nejmoa1500596

Lei, F., Xi, X., Batra, S. K., & Bronich, T. K. (2019). Combination therapies and drug delivery platforms in combating pancreatic cancer. In *Journal of Pharmacology and Experimental Therapeutics* (Vol. 370, Issue 3, pp. 682–694). American Society for Pharmacology and Experimental Therapy. https://doi.org/10.1124/jpet.118.255786

Leng, F. Y., Liu, J. L., Liu, Z. J., Yin, J. Y., & Qu, H. P. (2013). Increased proportion of CD4+CD25+Foxp3+ regulatory T cells during early-stage sepsis in ICU patients. *Journal of Microbiology, Immunology and Infection*, *46*(5), 338–344. https://doi.org/10.1016/j.jmii.2012.06.012

Leonardi, G. C., Falzone, L., Salemi, R., Zanghì, A., Spandidos, D. A., Mccubrey, J. A., Candido, S., & Libra, M. (2018). Cutaneous melanoma: From pathogenesis to therapy (Review). In *International Journal of Oncology* (Vol. 52, Issue 4, pp. 1071–1080). Spandidos Publications. https://doi.org/10.3892/ijo.2018.4287

Leung, M., Kievit, F. M., Florczyk, S. J., Veiseh, O., Wu, J., Park, J. O., & Zhang, M. (2010). Chitosan-alginate scaffold culture system for hepatocellular carcinoma increases malignancy and drug resistance. *Pharmaceutical Research*, *27*(9), 1939–1948. https://doi.org/10.1007/s11095-010-0198-3

Lev, A., Lulla, A. R., Wagner, J., Ralff, M. D., Kiehl, J. B., Zhou, Y., Benes, C. H., Prabhu, V. V, Oster, W., Astsaturov, I., Dicker, D. T., & El-Deiry, W. S. (2017). Anti-pancreatic cancer activity of ONC212 involves the unfolded protein response (UPR) and is reduced by IGF1-R and GRP78/ BIP. In *Oncotarget* (Vol. 8, Issue 47). www.impactjournals.com/oncotarget/

Lhuissier, E., Bazille, C., Aury-Landas, J., Girard, N., Pontin, J., Boittin, M., Boumediene, K., & Baugé, C. (2017). Identification of an easy to use 3D culture model to investigate invasion and anticancer drug response in chondrosarcomas. *BMC Cancer*, *17*(1). https://doi.org/10.1186/s12885-017-3478-z

Li, C., Ren, Z., Han, D., Wang, H., Xu, F., Zheng, S., & Lyu, J. (2020). A prognostic nomogram for pancreatic ductal adenocarcinoma patients' all-cause survival in a Surveillance, Epidemiology, and End Results analysis. *Translational Cancer Research*, *9*(5), 3586–3599. https://doi.org/10.21037/tcr-19-2962

Li, D. Y., & Xiong, X. Z. (2020a). ICOS+ Tregs: A Functional Subset of Tregs in Immune Diseases. In *Frontiers in Immunology* (Vol. 11). Frontiers Media S.A. https://doi.org/10.3389/fimmu.2020.02104

Li, D. Y., & Xiong, X. Z. (2020b). ICOS+ Tregs: A Functional Subset of Tregs in Immune Diseases. In *Frontiers in Immunology* (Vol. 11). Frontiers Media S.A. https://doi.org/10.3389/fimmu.2020.02104

Li, P., Jin, Y., Zhao, R., Xue, Z., & Ji, J. (2022). Expression of ICOS in the salivary glands of patients with primary Sjogren's syndrome and its molecular mechanism. *Molecular Medicine Reports*, *26*(5). https://doi.org/10.3892/mmr.2022.12864

Liu Jie, Liu Qishen, Zhao Zhigang, Yu Honggang, Luo Hesheng, & Tang Zhongzhi. (2014). Osteopontin promotes the progression of gastric cancer through the NF-κB pathway regulated by the MAPK and PI3K. *International Journal of Oncology*, *45*, 282–290.

Liu, P., Chen, J., Zhao, L., Hollebecque, A., Kepp, O., Zitvogel, L., & Kroemer, G. (2022). PD-1 blockade synergizes with oxaliplatin-based, but not cisplatin-based, chemotherapy of gastric cancer. *OncoImmunology*, *11*(1). https://doi.org/10.1080/2162402X.2022.2093518

Liu, Z., & Huang, Y. (2014). Advantages of proteins being disordered. In *Protein Science* (Vol. 23, Issue 5, pp. 539–550). Blackwell Publishing Ltd. https://doi.org/10.1002/pro.2443

Lo, C.-M., Wang, H.-B., Dembo, M., & Wang, Y.-L. (2000). *Cell Movement Is Guided by the Rigidity of the Substrate*.

Lu, J., Wu, J., Xia, X., Peng, H., & Wang, S. (2021). Follicular helper T cells: potential therapeutic targets in rheumatoid arthritis. In *Cellular and Molecular Life Sciences* (Vol. 78, Issue 12, pp. 5095–5106). Springer Science and Business Media Deutschland GmbH. https://doi.org/10.1007/s00018-021-03839-1

Maeda, S., Fujimoto, M., Matsushita, T., Hamaguchi, Y., Takehara, K., & Hasegawa, M. (2011). Inducible costimulator (ICOS) and ICOS ligand signaling has pivotal roles in skin wound healing via cytokine production. *American Journal of Pathology*. https://doi.org/10.1016/j.ajpath.2011.07.048

Mak, T. W., Shahinian, A., Yoshinaga, S. K., Wakeham, A., Boucher, L. M., Pintilie, M., Duncan, G., Gajewska, B. U., Gronski, M., Eriksson, U., Odermatt, B., Ho, A., Bouchard, D., Whorisky, J. S., Jordana, M., Ohashi, P. S., Pawson, T., Bladt, F., & Tafuri, A. (2003). Costimulation through the inducible costimulator ligand is essential for both T helper and B cell functions in T cell-dependent B cell responses. *Nature Immunology*. https://doi.org/10.1038/ni947

Manoussakis, M. N., & Moutsopoulos, H. M. (2000). Sjogren's syndrome: Autoimmune epithelitis. *Bailliere's Best Practice and Research in Clinical Rheumatology*, *14*(1), 73–95. https://doi.org/10.1053/berh.1999.0078

Mao, W., Wu, F., Lee, R. J., Lu, W., & Wang, J. (2019). Development of a stable single-vial liposomal formulation for vincristine. *International Journal of Nanomedicine*, *14*, 4461–4474. https://doi.org/10.2147/IJN.S205276

Marrella, A., Buratti, P., Markus, J., Firpo, G., Pesenti, M., Landry, T., Ayehunie, S., Scaglione, S., Kandarova, H., & Aiello, M. (2020). In vitro demonstration of intestinal absorption mechanisms of different sugars using 3d organotypic tissues in a fluidic device. *Altex*, *37*(2), 255–264. https://doi.org/10.14573/altex.1908311

Marrella, A., Dondero, A., Aiello, M., Casu, B., Olive, D., Regis, S., Bottino, C., Pende, D., Meazza, R., Caluori, G., Castriconi, R., & Scaglione, S. (2019). Cell-laden hydrogel as a clinical-relevant 3D model for analyzing neuroblastoma growth, immunophenotype, and susceptibility to therapies. *Frontiers in Immunology*, *10*(AUG). https://doi.org/10.3389/fimmu.2019.01876

Marrella A, V. G. A. M. V. I. V. C. M. M. D. C. S. S. (2021). Marrella_2021. *ALTEX*, *38*(1), 82–94. https://doi.org/10.14573/altex.2003131

Martin, P. (1997). *Wound Healing-Aiming for Perfect Skin Regeneration*. https://www.science.org

Maulana, T. I., Kromidas, E., Wallstabe, L., Cipriano, M., Alb, M., Zaupa, C., Hudecek, M., Fogal, B., & Loskill, P. (2021). Immunocompetent cancer-on-chip models to assess immuno-oncology therapy. In *Advanced Drug Delivery Reviews* (Vol. 173, pp. 281–305). Elsevier B.V. https://doi.org/10.1016/j.addr.2021.03.015

Menéndez, R., Méndez, R., Almansa, R., Ortega, A., Alonso, R., Suescun, M., Ferrando, A., Feced, L., & Bermejo-Martin, J. F. (2019). Simultaneous depression of immunological synapse and endothelial injury is associated with organ dysfunction in community-acquired pneumonia. *Journal of Clinical Medicine*, *8*(9). https://doi.org/10.3390/jcm8091404

Meng, H., Mai, W. X., Zhang, H., Xue, M., Xia, T., Lin, S., Wang, X., Zhao, Y., Ji, Z., Zink, J. I., & Nel, A. E. (2013). Codelivery of an optimal drug/siRNA combination using mesoporous silica nanoparticles to overcome drug resistance in breast cancer in vitro and in vivo. *ACS Nano*, *7*(2), 994–1005. https://doi.org/10.1021/nn3044066

Meszaros, A. J., Reichner, J. S., & Albina, J. E. (2000). Macrophage-Induced Neutrophil Apoptosis. *The Journal of Immunology*, *165*(1), 435–441. https://doi.org/10.4049/jimmunol.165.1.435

Michels, T. C., & Petersen, K. E. (2017). *Multiple Myeloma: Diagnosis and Treatment* (Vol. 95, Issue 6). www.aafp.org/afp

Mishra, P., Nayak, B., & Dey, R. K. (2016). PEGylation in anti-cancer therapy: An overview. In *Asian Journal of Pharmaceutical Sciences* (Vol. 11, Issue 3, pp. 337–348). Shenyang Pharmaceutical University. https://doi.org/10.1016/j.ajps.2015.08.011

Monge, C., Stoppa, I., Ferraris, C., Bozza, A., Battaglia, L., Cangemi, L., Miglio, G., Pizzimenti, S., Clemente, N., Gigliotti, C. L., Boggio, E., Dianzani, U., & Dianzani, C. (2022). Parenteral Nanoemulsions Loaded with Combined Immuno- and Chemo-Therapy for Melanoma Treatment. *Nanomaterials*, *12*(23). https://doi.org/10.3390/nano12234233

Morè, S., Corvatta, L., Manieri, V. M., Morsia, E., Poloni, A., & Offidani, M. (2023). Novel Immunotherapies and Combinations: The Future Landscape of Multiple Myeloma Treatment. *Pharmaceuticals*, *16*(11), 1628. https://doi.org/10.3390/ph16111628

Morton, S. W., Lee, M. J., Deng, Z. J., Dreaden, E. C., Siouve, E., Shopsowitz, K. E., Shah, N. J., Yaffe, M. B., & Hammond, P. T. (2014). A nanoparticle-based combination chemotherapy delivery system for enhanced tumor killing by dynamic rewiring of signaling pathways. *Science Signaling*, *7*(325). https://doi.org/10.1126/scisignal.2005261

Mosser, D. M., & Edwards, J. P. (2008). Exploring the full spectrum of macrophage activation. In *Nature Reviews Immunology* (Vol. 8, Issue 12, pp. 958–969). https://doi.org/10.1038/nri2448

Ni, J., Miao, T., Su, M., Khan, N. U., Ju, X., Chen, H., Liu, F., & Han, L. (2021). PSMA-targeted nanoparticles for specific penetration of blood-brain tumor barrier and combined therapy of brain metastases. *Journal of Controlled Release*, *329*, 934–947. https://doi.org/10.1016/j.jconrel.2020.10.023

Nurieva, R. I. (2005). Regulation of immune and autoimmune responses by ICOS-B7h interaction. *Clinical Immunology*, *115*(1 SPEC. ISS.), 19–25. https://doi.org/10.1016/j.clim.2005.02.010

Occhipinti, S., Dianzani, C., Chiocchetti, A., Boggio, E., Clemente, N., Gigliotti, C. L., Soluri, M. F., Minelli, R., Fantozzi, R., Yagi, J., Rojo, J. M., Sblattero, D., Giovarelli, M., & Dianzani, U. (2013). Triggering of B7h by the ICOS Modulates Maturation and Migration of Monocyte-Derived Dendritic Cells. *The Journal of Immunology*, *190*, 1125–1134. https://doi.org/10.4049/jimmunol.1201816

O'Dwyer, R., Kovaleva, M., Zhang, J., Steven, J., Cummins, E., Luxenberg, D., Darmanin-Sheehan, A., Carvalho, M. F., Whitters, M., Saunders, K., & Barelle, C. J. (2018). Anti-ICOSL new antigen receptor domains inhibit T cell proliferation and reduce the development of inflammation in the collagen-induced mouse model of rheumatoid arthritis. *Journal of Immunology Research*, *2018*. https://doi.org/10.1155/2018/4089459

Pan, Y., He, B., Song, G., Bao, Q., Tang, Z., Tian, F., & Wang, S. (2012). CD147 silencing via RNA interference reduces tumor cell invasion, metastasis and increases chemosensitivity in pancreatic cancer cells. *Oncology Reports*, *27*(6), 2003–2009. https://doi.org/10.3892/or.2012.1729

Parhizkar, M., Reardon, P. J. T., Harker, A. H., Browning, R. J., Stride, E., Pedley, R. B., Knowles, J. C., & Edirisinghe, M. (2020). Enhanced efficacy in drug-resistant cancer cells through synergistic nanoparticle mediated delivery of cisplatin and decitabine. *Nanoscale Advances*, *2*(3), 1177–1186. https://doi.org/10.1039/c9na00684b

Park, H., Li, Z., Yang, X. O., Chang, S. H., Nurieva, R., Wang, Y.-H., Wang, Y., Hood, L., Zhu, Z., Tian, Q., & Dong, C. (2005). *A distinct lineage of CD4 T cells regulates tissue inflammation by producing interleukin 17*. http://npg.nature.com/reprintsandpermissions/

Partyka, O., Pajewska, M., Kwaśniewska, D., Czerw, A., Deptała, A., Budzik, M., Cipora, E., Gąska, I., Gazdowicz, L., Mielnik, A., Sygit, K., Sygit, M., Krzych-Fałta, E., Schneider-Matyka, D., Grochans, S., Cybulska, A. M., Drobnik, J., Bandurska, E., Ciećko, W., … Kozłowski, R. (2023). Overview of Pancreatic Cancer Epidemiology in Europe and Recommendations for Screening in High-Risk Populations. In

Cancers (Vol. 15, Issue 14). Multidisciplinary Digital Publishing Institute (MDPI). https://doi.org/10.3390/cancers15143634

Paz-Ares, L., Luft, A., Vicente, D., Tafreshi, A., Gümüş, M., Mazières, J., Hermes, B., Çay Şenler, F., Csőszi, T., Fülöp, A., Rodríguez-Cid, J., Wilson, J., Sugawara, S., Kato, T., Lee, K. H., Cheng, Y., Novello, S., Halmos, B., Li, X., … Kowalski, D. M. (2018). Pembrolizumab plus Chemotherapy for Squamous Non–Small-Cell Lung Cancer. *New England Journal of Medicine*, *379*(21), 2040–2051. https://doi.org/10.1056/nejmoa1810865

Peng, Y., Huang, J., Xiao, H., Wu, T., & Shuai, X. (2018). Codelivery of temozolomide and siRNA with polymeric nanocarrier for effective glioma treatment. *International Journal of Nanomedicine*, *13*, 3467–3480. https://doi.org/10.2147/IJN.S164611

Pol, J., Vacchelli, E., Aranda, F., Castoldi, F., Eggermont, A., Cremer, I., Sautès-Fridman, C., Fucikova, J., Galon, J., Spisek, R., Tartour, E., Zitvogel, L., Kroemer, G., & Galluzzi, L. (2015). Trial Watch: Immunogenic cell death inducers for anticancer chemotherapy. *OncoImmunology*, *4*(4). https://doi.org/10.1080/2162402X.2015.1008866

Pourmadadi, M., Ghaemi, A., Shamsabadipour, A., Rajabzadeh-Khosroshahi, M., Shaghaghi, M., Rahdar, A., & Pandey, S. (2023). Nanoparticles loaded with Daunorubicin as an advanced tool for cancer therapy. In *European Journal of Medicinal Chemistry* (Vol. 258). Elsevier Masson s.r.l. https://doi.org/10.1016/j.ejmech.2023.115547

Prasad, P., Shuhendler, A., Cai, P., Rauth, A. M., & Wu, X. Y. (2013). Doxorubicin and mitomycin C co-loaded polymer-lipid hybrid nanoparticles inhibit growth of sensitive and multidrug resistant human mammary tumor xenografts. *Cancer Letters*, *334*, 263–273.

Pulsoni, I., Lubda, M., Aiello, M., Fedi, A., Marzagalli, M., Hagen, J. von, & Scaglione, S. (2022). Comparison Between Franz Diffusion Cell and a novel Micro-physiological System for In Vitro Penetration Assay Using Different Skin Models. *SLAS Technology*, *27*(3), 161–171. https://doi.org/10.1016/j.slast.2021.12.006

Rafae, A., van Rhee, F., & Al Hadidi, S. (2023). Perspectives on the Treatment of Multiple Myeloma. *The Oncologist*. https://doi.org/10.1093/oncolo/oyad306

Raineri, D., Cappellano, G., Vilardo, B., Maione, F., Clemente, N., Canciani, E., Boggio, E., Gigliotti, C. L., Monge, C., Dianzani, C., Boldorini, R., Dianzani, U., & Chiocchetti, A. (2022). Inducible t-cell costimulator ligand plays a dual role in melanoma metastasis upon binding to osteopontin or inducible t-cell costimulator. *Biomedicines*, *10*(1). https://doi.org/10.3390/biomedicines10010051

Raineri, D., Dianzani, C., Cappellano, G., Maione, F., Baldanzi, G., Iacobucci, I., Clemente, N., Baldone, G., Boggio, E., Gigliotti, C. L., Boldorini, R., Rojo, J. M., Monti, M., Birolo, L., Dianzani, U., & Chiocchetti, A. (2020). Osteopontin binds ICOSL promoting tumor metastasis. *Communications Biology*, *3*(1). https://doi.org/10.1038/s42003-020-01333-1

Rajkumar, S. V. (2022). Multiple myeloma: 2022 update on diagnosis, risk stratification, and management. *American Journal of Hematology*, *97*(8), 1086–1107. https://doi.org/10.1002/ajh.26590

Ramavath, N. N., Gadipudi, L. L., Provera, A., Gigliotti, L. C., Boggio, E., Bozzola, C., Albano, E., Dianzani, U., & Sutti, S. (2021). Inducible T-Cell Costimulator Mediates Lymphocyte/Macrophage Interactions During Liver Repair. *Frontiers in Immunology*, *12*. https://doi.org/10.3389/fimmu.2021.786680

Randazzo, O., Papini, F., Mantini, G., Gregori, A., Parrino, B., Liu, D. S. K., Cascioferro, S., Carbone, D., Peters, G. J., Frampton, A. E., Garajova, I., & Giovannetti, E. (2020). "Open sesame?": Biomarker status of the

human equilibrative nucleoside transporter-1 and molecular mechanisms influencing its expression and activity in the uptake and cytotoxicity of gemcitabine in pancreatic cancer. *Cancers*, *12*(11), 1–20. https://doi.org/10.3390/cancers12113206

Remiker, A., Bolling, K., & Verbsky, J. (2023). Common Variable Immunodeficiency. In *Medical Clinics of North America*. W.B. Saunders. https://doi.org/10.1016/j.mcna.2023.06.012

Riethdorf, S., Reimers, N., Assmann, V., Kornfeld, J. W., Terracciano, L., Sauter, G., & Pantel, K. (2006). High incidence of EMMPRIN expression in human tumors. *International Journal of Cancer*, *119*(8), 1800–1810. https://doi.org/10.1002/ijc.22062

Robert, C., Karaszewska, B., Schachter, J., Rutkowski, P., Mackiewicz, A., Stroiakovski, D., Lichinitser, M., Dummer, R., Grange, F., Mortier, L., Chiarion-Sileni, V., Drucis, K., Krajsova, I., Hauschild, A., Lorigan, P., Wolter, P., Long, G. V., Flaherty, K., Nathan, P., … Schadendorf, D. (2015). Improved Overall Survival in Melanoma with Combined Dabrafenib and Trametinib. *New England Journal of Medicine*, *372*(1), 30–39. https://doi.org/10.1056/nejmoa1412690

Robert Caroline, Schachter Jacob, Long Georgina V., Arance Ana, Grob Jean Jacques, Mortier Laurent, Daud Adil, Carlino Matteo S., McNeil Catriona, Lotem Michal, Larkin, J., Lorigan, P., Neyns, B., Blank, C. U., Hamid, O., Mateus, C., Shapira-Frommer, R., Kosh, M., Zhou, H., … Ribas, A. (2015). Pembrolizumab versus Ipilimumab in Advanced Melanoma. *New England Journal of Medicine*, *372*(26), 2521–2532. https://doi.org/10.1056/nejmoa1503093

Roodman, G. D. (2011). Osteoblast function in myeloma. In *Bone* (Vol. 48, Issue 1, pp. 135–140). https://doi.org/10.1016/j.bone.2010.06.016

Rudd, K. E., Johnson, S. C., Agesa, K. M., Shackelford, K. A., Tsoi, D., Kievlan, D. R., Colombara, D. V., Ikuta, K. S., Kissoon, N., Finfer, S., Fleischmann-Struzek, C., Machado, F. R., Reinhart, K. K., Rowan, K., Seymour, C. W., Watson, R. S., West, T. E., Marinho, F., Hay, S. I., … Naghavi, M. (2020). Global, regional, and national sepsis incidence and mortality, 1990–2017: analysis for the Global Burden of Disease Study. *The Lancet*, *395*(10219), 200–211. https://doi.org/10.1016/S0140-6736(19)32989-7

Salzer, U., Maul-Pavicic, A., Cunningham-Rundles, C., Urschel, S., Belohradsky, B. H., Litzman, J., Holm, A., Franco, J. L., Plebani, A., Hammarstrom, L., Skrabl, A., Schwinger, W., & Grimbacher, B. (2004). ICOS deficiency in patients with common variable immunodeficiency. *Clinical Immunology*, *113*(3), 234–240. https://doi.org/10.1016/j.clim.2004.07.002

Schinke, C., Poos, A. M., Bauer, M., John, L., Johnson, S., Deshpande, S., Carrillo, L., Alapat, D., Rasche, L., Thanendrarajan, S., Zangari, M., Al Hadidi, S., van Rhee, F., Davies, F., Raab, M. S., Morgan, G., & Weinhold, N. (2022). Characterizing the role of the immune microenvironment in multiple myeloma progression at a single-cell level. *Blood Advances*, *6*(22), 5873–5883. https://doi.org/10.1182/bloodadvances.2022007217

Schnelderhan, W., Diaz, F., Fundel, M., Zhou, S., Siech, M., Hasel, C., Möller, P., Gschwend, J. E., Seufferlein, T., Gress, T., Adler, G., & Bachem, M. G. (2007). Pancreatic stellate cells are an important source of MMP-2 in human pancreatic cancer and accelerate tumor progression in a murine xenograft model and CAM assay. *Journal of Cell Science*, *120*(3), 512–519. https://doi.org/10.1242/jcs.03347

Seidel, J. A., Otsuka, A., & Kabashima, K. (2018). Anti-PD-1 and anti-CTLA-4 therapies in cancer: Mechanisms of action, efficacy, and limitations. In *Frontiers in Oncology* (Vol. 8, Issue MAR). Frontiers Media S.A. https://doi.org/10.3389/fonc.2018.00086

Seidu, T. A., Kutoka, P. T., Asante, D. O., Farooq, M. A., Alolga, R. N., & Bo, W. (2022). Functionalization of Nanoparticulate Drug Delivery Systems and Its Influence in Cancer Therapy. In *Pharmaceutics* (Vol. 14, Issue 5). MDPI. https://doi.org/10.3390/pharmaceutics14051113

Sharpe, A. H., & Freeman, G. J. (2002). The B7-CD28 superfamily. In *Nature Reviews Immunology* (Vol. 2, Issue 2, pp. 116–126). European Association for Cardio-Thoracic Surgery. https://doi.org/10.1038/nri727

Shuhendler, A. J., Cheung, R. Y., Manias, J., Connor, A., Rauth, A. M., & Wu, X. Y. (2010). A novel doxorubicin-mitomycin C co-encapsulated nanoparticle formulation exhibits anti-cancer synergy in multidrug resistant human breast cancer cells. *Breast Cancer Research and Treatment*, *119*(2), 255–269. https://doi.org/10.1007/s10549-008-0271-3

Siegel, R. L., Miller, K. D., Wagle, N. S., & Jemal, A. (2023). Cancer statistics, 2023. *CA: A Cancer Journal for Clinicians*, *73*(1), 17–48. https://doi.org/10.3322/caac.21763

Singampalli, K. L., Balaji, S., Wang, X., Parikh, U. M., Kaul, A., Gilley, J., Birla, R. K., Bollyky, P. L., & Keswani, S. G. (2020). The Role of an IL-10/Hyaluronan Axis in Dermal Wound Healing. In *Frontiers in Cell and Developmental Biology* (Vol. 8). Frontiers Media S.A. https://doi.org/10.3389/fcell.2020.00636

Singh Akash, Afshan Noor, Singh Anshuman, Singh Suraj Kumar, Yadav Sudhanshu, Kumar Manoj, Sarma Devojit Kumar, & Verma Vinod. (2023). Recent trends and advances in type 1 diabetes therapeutics: A comprehensive review. *European Journal of Cell Biology*, *102*, 1–12.

Socinski, M. A., Jotte, R. M., Cappuzzo, F., Orlandi, F., Stroyakovskiy, D., Nogami, N., Rodríguez-Abreu, D., Moro-Sibilot, D., Thomas, C. A., Barlesi, F., Finley, G., Kelsch, C., Lee, A., Coleman, S., Deng, Y., Shen, Y., Kowanetz, M., Lopez-Chavez, A., Sandler, A., & Reck, M. (2018). Atezolizumab for First-Line Treatment of Metastatic Nonsquamous NSCLC. *New England Journal of Medicine*, *378*(24), 2288–2301. https://doi.org/10.1056/nejmoa1716948

Solinas, C., Gu-Trantien, C., & Willard-Gallo, K. (2020). The rationale behind targeting the ICOS-ICOS ligand costimulatory pathway in cancer immunotherapy. In *ESMO Open* (Vol. 5, Issue 1). BMJ Publishing Group. https://doi.org/10.1136/esmoopen-2019-000544

Son, H., & Moon, A. (2010). Epithelial-mesenchymal Transition and Cell Invasion. In *Toxicol. Res* (Vol. 26, Issue 4).

Sordo-Bahamonde, C., Lorenzo-Herrero, S., Gonzalez-Rodriguez, A. P., Martínez-Pérez, A., Rodrigo, J. P., García-Pedrero, J. M., & Gonzalez, S. (2023). Chemo-Immunotherapy: A New Trend in Cancer Treatment. In *Cancers* (Vol. 15, Issue 11). MDPI. https://doi.org/10.3390/cancers15112912

Stoppa, I., Gigliotti, C. L., Clemente, N., Pantham, D., Dianzani, C., Monge, C., Puricelli, C., Rolla, R., Sutti, S., Renò, F., Boldorini, R., Boggio, E., & Dianzani, U. (2022). ICOSL Stimulation by ICOS-Fc Accelerates Cutaneous Wound Healing In Vivo. *International Journal of Molecular Sciences*, *23*(13). https://doi.org/10.3390/ijms23137363

Su, Z., Li, L., Hao, F., Zhao, J., Li, M., Zhao, X., & Zhao, D. (2023). A Stable Irinotecan Liposome with Enhanced Antitumor Activity in a Range of Tumor Models. *Pharmaceutical Research*. https://doi.org/10.1007/s11095-023-03622-w

Sung, H., Ferlay, J., Siegel, R. L., Laversanne, M., Soerjomataram, I., Jemal, A., & Bray, F. (2021). Global Cancer Statistics 2020: GLOBOCAN Estimates of Incidence and Mortality Worldwide for 36 Cancers in 185 Countries. *CA: A Cancer Journal for Clinicians*, *71*(3), 209–249. https://doi.org/10.3322/caac.21660

Tamam, H., Park, J., Gadalla, H. H., Masters, A. R., Abdel-Aleem, J. A., Abdelrahman, S. I., Abdelrahman, A. A., Lyle, L. T., & Yeo, Y. (2019). Development of Liposomal Gemcitabine with High Drug Loading Capacity. *Molecular Pharmaceutics*. https://doi.org/10.1021/acs.molpharmaceut.8b01284

Tang, G., Qin, Q., Zhang, P., Wang, G., Liu, M., Ding, Q., Qin, Y., & Shen, Q. (2009). Reverse signaling using an inducible costimulator to enhance immunogenic function of dendritic cells. *Cellular and Molecular Life Sciences*, *66*(18), 3067–3080. https://doi.org/10.1007/s00018-009-0090-7

Tomasson, M. H., Ali, M., De Oliveira, V., Xiao, Q., Jethava, Y., Zhan, F., Fitzsimmons, A. M., & Bates, M. L. (2018). Prevention is the best treatment: The case for understanding the transition from monoclonal gammopathy of undetermined significance to myeloma. In *International Journal of Molecular Sciences* (Vol. 19, Issue 11). MDPI AG. https://doi.org/10.3390/ijms19113621

Trédan, O., Galmarini, C. M., Patel, K., & Tannock, I. F. (2007). Drug resistance and the solid tumor microenvironment. In *Journal of the National Cancer Institute* (Vol. 99, Issue 19, pp. 1441–1454). https://doi.org/10.1093/jnci/djm135

Trotta, F., Zanetti, M., & Cavalli, R. (2012). Cyclodextrin-based nanosponges as drug carriers. In *Beilstein Journal of Organic Chemistry* (Vol. 8, pp. 2091–2099). https://doi.org/10.3762/bjoc.8.235

Trujillo-de Santiago, G., Flores-Garza, B. G., Tavares-Negrete, J. A., Lara-Mayorga, I. M., González-Gamboa, I., Zhang, Y. S., Rojas-Martínez, A., Ortiz-López, R., & Álvarez, M. M. (2019). The tumor-on-chip: Recent advances in the development of microfluidic systems to recapitulate the physiology of solid tumors. In *Materials* (Vol. 12, Issue 18). MDPI AG. https://doi.org/10.3390/ma12182945

Tsai, H. F., & Hsu, P. N. (2017). Cancer immunotherapy by targeting immune checkpoints: Mechanism of T cell dysfunction in cancer immunity and new therapeutic targets John T Kung. In *Journal of Biomedical Science* (Vol. 24, Issue 1). BioMed Central Ltd. https://doi.org/10.1186/s12929-017-0341-0

Tzogani, K., Penttilä, K., Lapveteläinen, T., Hemmings, R., Koenig, J., Freire, J., Márcia, S., Cole, S., Coppola, P., Flores, B., Barbachano, Y., Roige, S. D., & Pignatti, F. (2020). EMA Review of Daunorubicin and Cytarabine Encapsulated in Liposomes (Vyxeos, CPX-351) for the Treatment of Adults with Newly Diagnosed, Therapy-Related Acute Myeloid Leukemia or Acute Myeloid Leukemia with Myelodysplasia-Related Changes. *The Oncologist*, *25*(9), e1414–e1420. https://doi.org/10.1634/theoncologist.2019-0785

Ullman, N. A., Burchard, P. R., Dunne, R. F., & Linehan, D. C. (2022). SPECIAL SERIES: PRECISION MEDICINE AND IMMUNOTHERAPY IN GI MALIGNANCIES review articles Immunologic Strategies in Pancreatic Cancer: Making Cold Tumors Hot. In *J Clin Oncol* (Vol. 40). https://doi.org/10.

Valković, T., Babarović, E., Lučin, K., Štifter, S., Aralica, M., Pećanić, S., Seili-Bekafigo, I., Duletić-Načinović, A., Nemet, D., & Jonjić, N. (2014). Plasma levels of osteopontin and vascular endothelial growth factor in association with clinical features and parameters of tumor burden in patients with multiple myeloma. *BioMed Research International*, *2014*. https://doi.org/10.1155/2014/513170

van Berkel, M. E. A. T., & Oosterwegel, M. A. (2006). CD28 and ICOS: Similar or separate costimulators of T cells? In *Immunology Letters* (Vol. 105, Issue 2, pp. 115–122). https://doi.org/10.1016/j.imlet.2006.02.007

Vega-Vásquez, P., Mosier, N. S., & Irudayaraj, J. (2020). Nanoscale Drug Delivery Systems: From Medicine to Agriculture. In *Frontiers in Bioengineering and Biotechnology* (Vol. 8). Frontiers Media S.A. https://doi.org/10.3389/fbioe.2020.00079

Verhoef, J. J. F., Carpenter, J. F., Anchordoquy, T. J., & Schellekens, H. (2014). Potential induction of anti-PEG antibodies and complement activation toward PEGylated therapeutics. In *Drug Discovery Today* (Vol. 19, Issue 12, pp. 1945–1952). Elsevier Ltd. https://doi.org/10.1016/j.drudis.2014.08.015

Veronese, F. M., & Pasut, G. (2005). PEGylation, successful approach to drug delivery. In *Drug Discovery Today* (Vol. 10, Issue 21, pp. 1451–1458). https://doi.org/10.1016/S1359-6446(05)03575-0

Von Hoff, D. D., Ervin, T., Arena, F. P., Chiorean, E. G., Infante, J., Moore, M., Seay, T., Tjulandin, S. A., Ma, W. W., Saleh, M. N., Harris, M., Reni, M., Dowden, S., Laheru, D., Bahary, N., Ramanathan, R. K., Tabernero, J., Hidalgo, M., Goldstein, D., … Renschler, M. F. (2013). Increased Survival in Pancreatic Cancer with nab-Paclitaxel plus Gemcitabine. *New England Journal of Medicine*, *369*(18), 1691–1703. https://doi.org/10.1056/nejmoa1304369

Wang, H., & Huang, Y. (2020). Combination therapy based on nano codelivery for overcoming cancer drug resistance. *Medicine in Drug Discovery*, *6*, 100024. https://doi.org/10.1016/j.medidd.2020.100024

Wang, X., Chen, Y., Dahmani, F. Z., Yin, L., Zhou, J., & Yao, J. (2014). Amphiphilic carboxymethyl chitosan-quercetin conjugate with P-gp inhibitory properties for oral delivery of paclitaxel. *Biomaterials*, *35*(26), 7654–7665. https://doi.org/10.1016/j.biomaterials.2014.05.053

Warnatz, K., Bossaller, L., Salzer, U., Skrabl-Baumgartner, A., Schwinger, W., Van Der Burg, M., Van Dongen, J. J. M., Orlowska-Volk, M., Knoth, R., Durandy, A., Draeger, R., Schlesier, M., Peter, H. H., & Grimbacher, B. (2006). *Human ICOS deficiency abrogates the germinal center reaction and provides a monogenic model for common variable immunodeficiency*. https://doi.org/10.1182/blood-2005-07

Wei, R., Wong, J. P. C., & Kwok, H. F. (2017). Osteopontin - A promising biomarker for cancer therapy. In *Journal of Cancer* (Vol. 8, Issue 12, pp. 2173–2183). Ivyspring International Publisher. https://doi.org/10.7150/jca.20480

Weis, S. M., & Cheresh, D. A. (2011). Tumor angiogenesis: Molecular pathways and therapeutic targets. In *Nature Medicine* (Vol. 17, Issue 11, pp. 1359–1370). https://doi.org/10.1038/nm.2537

Weyand, C. M., & Goronzy, J. J. (2021). The immunology of rheumatoid arthritis. In *Nature Immunology* (Vol. 22, Issue 1, pp. 10–18). Nature Research. https://doi.org/10.1038/s41590-020-00816-x

Wong, H. L., Bendayan, R., Rauth, A. M., & Wu, X. Y. (2006). Simultaneous delivery of doxorubicin and GG918 (Elacridar) by new Polymer-Lipid Hybrid Nanoparticles (PLN) for enhanced treatment of multidrug-resistant breast cancer. *Journal of Controlled Release*, *116*(3), 275–284. https://doi.org/10.1016/j.jconrel.2006.09.007

Wong, H. L., Rauth, A. M., Bendayan, R., Manias, J. L., Ramaswamy, M., Liu, Z., Erhan, S. Z., & Wu, X. Y. (2006). A new polymer-lipid hybrid nanoparticle system increases cytotoxicity of doxorubicin against multidrug-resistant human breast cancer cells. *Pharmaceutical Research*, *23*(7), 1574–1585. https://doi.org/10.1007/s11095-006-0282-x

Wong, M. Y., & Chiu, G. N. C. (2011). Liposome formulation of co-encapsulated vincristine and quercetin enhanced antitumor activity in a trastuzumab-insensitive breast tumor xenograft model. *Nanomedicine: Nanotechnology, Biology, and Medicine*, *7*(6), 834–840. https://doi.org/10.1016/j.nano.2011.02.001

Xia, H., Wang, F., Wang, M., Wang, J., Sun, S., Chen, M., Huang, S., Chen, X., & Yao, S. (2020). Maresin1 ameliorates acute lung injury induced by sepsis through regulating Th17/Treg balance. *Life Sciences*, *254*. https://doi.org/10.1016/j.lfs.2020.117773

Xin Yu, J., Hubbard-Lucey, V. M., & Tang, J. (2019). Immuno-oncology drug development goes global. In *Nature Reviews Drug Discovery* (Vol. 18, Issue 12, pp. 899–900). Nature Research. https://doi.org/10.1038/d41573-019-00167-9

Xiong, W., Wu, X., Starnes, S., Johnson, S. K., Haessler, J., Wang, S., Chen, L., Barlogie, B., Shaughnessy, J. D., & Zhan, F. (2008). *An analysis of the clinical and biologic significance of TP53 loss and the identification of potential novel transcriptional targets of TP53 in multiple myeloma*. https://doi.org/10.1182/blood-2007-10

Xiong, Y. Q., Sun, H. C., Zhang, W., Zhu, X. D., Zhuang, P. Y., Zhang, J. B., Wang, L., Wu, W. Z., Qin, L. X., & Tang, Z. Y. (2009). Human hepatocellular carcinoma tumor-derived endothelial cells manifest increased angiogenesis capability and drug resistance compared with normal endothelial cells. *Clinical Cancer Research*, *15*(15), 4838–4846. https://doi.org/10.1158/1078-0432.CCR-08-2780

Xu, B.-Q., Fu, Z.-G., Meng, Y., Wu, X.-Q., Wu, B., Xu, L., Jiang, J.-L., Li, L., & Chen, Z.-N. (2016a). *Gemcitabine enhances cell invasion via activating HAb18G/ CD147-EGFR-pSTAT3 signaling*. www.impactjournals.com/oncotarget

Xu, B.-Q., Fu, Z.-G., Meng, Y., Wu, X.-Q., Wu, B., Xu, L., Jiang, J.-L., Li, L., & Chen, Z.-N. (2016b). *Gemcitabine enhances cell invasion via activating HAb18G/ CD147-EGFR-pSTAT3 signaling*. www.impactjournals.com/oncotarget

Xu, B.-Q., Fu, Z.-G., Meng, Y., Wu, X.-Q., Wu, B., Xu, L., Jiang, J.-L., Li, L., & Chen, Z.-N. (2016c). *Gemcitabine enhances cell invasion via activating HAb18G/ CD147-EGFR-pSTAT3 signaling*. www.impactjournals.com/oncotarget

Yang, K., Li, Y., Lian, G., Lin, H., Shang, C., Zeng, L., Chen, S., Li, J., Huang, C., Huang, K., & Chen, Y. (2018). KRAS promotes tumor metastasis and chemoresistance by repressing RKIP via the MAPK–ERK pathway in pancreatic cancer. *International Journal of Cancer*, *142*(11), 2323–2334. https://doi.org/10.1002/ijc.31248

Yang, Y., Bolomsky, A., Oellerich, T., Chen, P., Ceribelli, M., Häupl, B., Wright, G. W., Phelan, J. D., Huang, D. W., Lord, J. W., Van Winkle, C. K., Yu, X., Wisniewski, J., Wang, J. Q., Tosto, F. A., Beck, E., Wilson, K., McKnight, C., Travers, J., … Young, R. M. (2022). Oncogenic RAS commandeers amino acid sensing machinery to aberrantly activate mTORC1 in multiple myeloma. *Nature Communications*, *13*(1). https://doi.org/10.1038/s41467-022-33142-x

Yong, P. F. K., Salzer, U., & Grimbacher, B. (2009). The role of costimulation in antibody deficiencies: ICOS and common variable immunodeficiency. In *Immunological Reviews* (Vol. 229, Issue 1, pp. 101–113). https://doi.org/10.1111/j.1600-065X.2009.00764.x

Yoon, J. H., Jung, Y. J., & Moon, S. H. (2021). Immunotherapy for pancreatic cancer. *World Journal of Clinical Cases*, *9*(13), 2969–2982. https://doi.org/10.12998/wjcc.v9.i13.2969

Yoshinaga Steven K., Whoriskey John S., Khare Sanjay D., Sarmiento Ulla, Guo Jane, Horan Tom, Shih Grace, Zhang Ming, Coccia Marco A., Kohno Tadahiko, Tafuri-Bladt Anna, Brankow David, Campbell Pauline, Chang David, Chiu Laura, Dai Tianang, Duncan Gordon, Elliott Gary S., Hui Ariela, … Senaldi Giorgio. (1999). Steven K. Yoshinaga_et al 1999. *Nature*, *402*, 827–832.

Yu, Y., Yang, G., Huang, H., Fu, Z., Cao, Z., Zheng, L., You, L., & Zhang, T. (2021). Preclinical models of pancreatic ductal adenocarcinoma: challenges and opportunities in the era of precision medicine. In *Journal of Experimental and Clinical Cancer Research* (Vol. 40, Issue 1). BioMed Central Ltd. https://doi.org/10.1186/s13046-020-01787-5

Zeng, L., Gowda, B. H. J., Ahmed, M. G., Abourehab, M. A. S., Chen, Z. S., Zhang, C., Li, J., & Kesharwani, P. (2023). Advancements in nanoparticle-based treatment approaches for skin cancer therapy. In *Molecular Cancer* (Vol. 22, Issue 1). BioMed Central Ltd. https://doi.org/10.1186/s12943-022-01708-4

Zhang, M., Liu, E., Cui, Y., & Huang, Y. (2017). Nanotechnology-based combination therapy for overcoming multidrug-resistant cancer. In *Cancer Biology and Medicine* (Vol. 14, Issue 3, pp. 212–227). Cancer Biology and Medicine. https://doi.org/10.20892/j.issn.2095-3941.2017.0054

Zhang, Y., Luo, Y., Qin, S. L., Mu, Y. F., Qi, Y., Yu, M. H., & Zhong, M. (2016). The clinical impact of ICOS signal in colorectal cancer patients. *OncoImmunology*, *5*(5). https://doi.org/10.1080/2162402X.2016.1141857

Zhang, Z., He, S., Wang, P., & Zhou, Y. (2022). The efficacy and safety of gemcitabine-based combination therapy vs. gemcitabine alone for the treatment of advanced pancreatic cancer: A systematic review and meta-analysis. *Journal of Gastrointestinal Oncology*, *13*(4), 1967–1980. https://doi.org/10.21037/jgo-22-624

Zhang, Z., Xu, S., Wang, Y., Yu, Y., Li, F., Zhu, H., Shen, Y., Huang, S., & Guo, S. (2018). Near-infrared triggered co-delivery of doxorubicin and quercetin by using gold nanocages with tetradecanol to maximize anti-tumor effects on MCF-7/ADR cells. *Journal of Colloid and Interface Science*, *509*, 47–57. https://doi.org/10.1016/j.jcis.2017.08.097

Zhao, J., & Guan, J. L. (2009). Signal transduction by focal adhesion kinase in cancer. In *Cancer and Metastasis Reviews* (Vol. 28, Issues 1–2, pp. 35–49). https://doi.org/10.1007/s10555-008-9165-4

Zhao, X., Liu, D., Gong, W., Zhao, G., Liu, L., Yang, L., & Hou, Y. (2014). The toll-like receptor 3 Ligand, Poly(I:C), improves immunosuppressive function and therapeutic effect of mesenchymal stem cells on sepsis via inhibiting MiR-143. *Stem Cells*, *32*(2), 521–533. https://doi.org/10.1002/stem.1543

Zhu, S., Zhang, T., Zheng, L., Liu, H., Song, W., Liu, D., Li, Z., & Pan, C. xian. (2021). Combination strategies to maximize the benefits of cancer immunotherapy. In *Journal of Hematology and Oncology* (Vol. 14, Issue 1). BioMed Central Ltd. https://doi.org/10.1186/s13045-021-01164-5

Zitvogel, L., Pitt, J. M., Daillère, R., Smyth, M. J., & Kroemer, G. (2016). Mouse models in oncoimmunology. In *Nature Reviews Cancer* (Vol. 16, Issue 12, pp. 759–773). Nature Publishing Group. https://doi.org/10.1038/nrc.2016.91